DEDICATED TO 65th ANNIVERSARY OF THE ESTABLISHMENT OF
MONGOLIAN UNIVERSITY OF SCIENCE AND TECHNOLOGY

geomine.must.edu.mn

GEOMINE24

ADVANCING GEOLOGY AND MINING

FOR A GREENER FUTURE

GEOMINE2024

BIANNUAL CONFERENCE ON GEOLOGY AND MINING

Proceedings

OCTOBER 09-10
Ulaanbaatar
MONGOLIA

DEDICATED TO 65th ANNIVERSARY OF THE ESTABLISHMENT OF
MONGOLIAN UNIVERSITY OF SCIENCE AND TECHNOLOGY

PROCEEDINGS OF THE GEOMINE2024 BIANNUAL INTERNATIONAL CONFERENCE ON GEOLOGY AND MINING

Ulaanbaatar, Mongolia
2024

Dedicated to 65th Anniversary of the Establishment of Mongolian University of Science and Technology

+ 976 11 312291
+ 976 9909 6452

geomine@must.edu.mn
https://geomine.must.edu.mn/

School of Geology and Mining Engineering
Mongolian University of Science and Technology
8th khoroo, Baga toiruu 34, Sukhbaatar district
Ulaanbaatar 46/520, MONGOLIA 14191

CO-ORGANIZER AND PARTNERS:

WUHAN UNIVERSITY OF TECHNOLOGY

M-JEED 1000 ENGINEERS

TrigTeQ More Efficient

KOREA UNIVERSITY

MUST

МОНГОЛ УЛСЫН ШИНЖЛЭХ УХААН ТЕХНОЛОГИЙН ИХ СУРГУУЛЬ

MONGOLIAN UNIVERSITY OF SCIENCE AND TECHNOLOGY

Dedicated to 65th Anniversary of the Establishment of Mongolian University of Science and Technology

GEO MINE 24

BIANNUAL INTERNATIONAL CONFERENCE ON GEOLOGY AND MINING

Sustainable Solutions:

ADVANCING GEOLOGY AND MINING FOR A GREENER FUTURE

CONFERENCE: OCTOBER 09-10th, 2024
PRE & POST CONFERENCE EVENTS: OCTOBER 01 – 15th, 2024
THE CHINGGIS KHAAN HOTEL, ULAANBAATAR, MONGOLIA

DIAMOND TIER SPONSOR:

ERDENET MINING CORPORATION SOE

EMERALD ELITE SPONSOR: badrakh energy, ЭРДЭНЭС ТАВАНТОЛГОЙ ETT

RUBY ROYALE SPONSOR: MN JOIN LLC, MAJOR Drilling

SAPPHIRE SPONSOR: TELMEN RESOURCE, BLAST COMPANY

QUARTZ CONTRIBUTOR: TERRA ENERGY, GOparts.mn, GLOGEX Geology & Mining Consulting Services

SUPPORTING ORGANIZATION: CHANDMANI MONGOLIA, CHANDMANI MONGOLIA LLC, CHINGGIS KHAAN HOTEL, NOMAD TOYS STUDIO, SOM SOUND OF MONGOLIA

CONFERENCE ORGANIZING CORE COMMITTEE

President of MUST	Namnan Tumurpurev
Chair:	Tsolmonbaatar Danjkhuu
Vice-Chair:	Khavalbolot Kyelgyenbai
Vice-Chair:	Shenxu Bao
Secretary General:	Munkhtsetseg Oidov
Secretary:	Ulziisaikhan Ganbold
Finance Committee:	Khavalbolot Kyelgyenbai
	Bayar-Erdene Lkhagvasuren
	Javkhlan Ganidbazar
	Chinzorig Bavuu
	Buyanjargal Narmandakh
	Dagva Myagmarsuren
Scientific Program Committee:	Munkhtsengel Baatar
	Batkhishig Bayaraa
	Orkhontuul Borya
	Oyuntugs Magsar
Publication Technical Committee:	Munkhtsetseg Oidov
	Narantsetseg Buyanbat
	Suvd-Erdene Damdin
	Enkhbayar Dandar
Logistics Committee:	Munkhtsetseg Oidov
	Ganzorig Erdenenemekh
	Odontuya Tumurchudur
	Buyanjargal Narmandakh
	Nandintsetseg Sosorbaram
	Suvd-Erdene Damdin
Exhibition Coordinator:	Suvd-Erdene Damdin
	Odontuya Tumurchudur
Technology and AV Committee:	Ganzorig Erdenenemekh
	Binderya Taivan
Post-Conference Evaluation:	Nandintsetseg Sosorbaram
Pre & Post event Committee:	Uranbaigal Gundsambuu
	Altanzul Baasandorj
	Orkhon Erdenebaatar
Press Committee:	Gerelt-Od Dolgor
	Enkhjargal Galbadrakh

Layout: Munkhtsetseg Oidov; Suvd-Erdene Damdin

Printed in MUST Press, Ulaanbaatar, Mongolia.
ISBN: 978-9919-506-81-0

Proceedings of the Geomine2024 Biannual International Conference on Geology and Mining

CONTENTS

FACIES AND STRATIGRAPHY OF PALAEOZOIC ROCKS IN SOUTHERN MONGOLIA AND IMPLICATIONS FOR REGIONAL GEOLOGY 1

PALEONTOLOGY IN MONGOLIA: LOOKING FORWARD TO NEW DISCOVERIES 2

TECTONIC FACTOR OF POST-FORMATION CHANGES IN COAL-BEARING MASSIFS OF THE DONETS BASIN, UKRAINE 4

THE PRELIMINARY RESULT OF OPHIOLITE AND OPHIOLITIC MÉLANGE IN THE KHAN-KHUKHEY MOUNTAINS, WESTERN MONGOLIA 8

CONTRASTING EARLY PERMIAN PLUTONISM IN THE TRANS-ALTAI ZONE, SW MONGOLIA 8

A LONG-LIVED SLAB-MELT-ORIGIN ADAKITIC MAGMATISM AT THE PERMIAN–TRIASSIC SIBERIAN CONTINENTAL MARGIN 9

LITHIUM-FLORINE GRANITES IN THE MONGOL-OKHOTSK OROGENIC BELT: PETROLOGY, GECHEMISTRY AND ASSOCIATED MINERALIZATION 13

PETROLOGICAL CHARACTERISTICS AND ORIGINS OF CARBONATITES FROM THE YONGHWA AND HONGCHEON COMPLEXES, SOUTH KOREA 14

GEOLOGY AND MINERALOGY OF THE NEW PORPHYRY COPPER MINERALIZATION OCCURENCE IN THE EASTERN BALKHASH REGION (KAZAKHSTAN) 14

HFSE MOBILITY IN SUBDUCTION ZONE: EVIDENCE FROM HP METAMORPHIC ROCK IN THE ZAVKHAN TERRANE, WESTERN MONGOLIA 18

AGE OF HADAASAN METAMORPHIC CORE COMPLEX 19

A COALBED METHANE RESERVOIR STUDY OF NARYN SUKHAIT COAL DEPOSIT, MONGOLIA 20

IMPACT OF ENGINEERING PARAMETERS ON MARCELLUS SHALE GAS PRODUCTION: A DATA ANALYTICS APPROACH 21

DETERMINATION OF THE HEAT BALANCE DURING THE FORMATION OF ASPHALTENE, PARAFFIN SEDIMENTS 28

TOWARD A SUSTAINABLE SUPPLY OF MINERAL RESOURCES - COPPER AS A CASE STUDY 36

THE INVESTIGATION OF CRITICAL METALS AND RARE EARTH ELEMENTS ENRICHMENT MECHANISMS USING HIGH-RESOLUTION INTEGRATED ANALYSIS 41

CHARACTERIZATION OF A GIANT SANGDONG W–MO SKARN DEPOSIT, SOUTH KOREA 46

THE MYEONSAN FE-TI PALEO-PLACER DEPOSIT IN SOUTH KOREA: MINERALOGICAL AND GEOCHEMICAL PROPERTIES WITH MICROSCOPIC OBSERVATION 46

ESTIMATING SOIL HYDRAULIC PARAMETERS BASED ON GROUND PENETRATING RADAR WAVEFORM INVERSION 47

AIRBORNE GEOPHYSICS IN MONGOLIA – A NEW APPROACH 47

PROBABILISTIC SEISMIC HAZARD ASSESSMENT OF HAZARA DIVISION, PAKISTAN 49

INVESTIGATION OF SOIL POLLUTION IN THE TERRITORY OF THE OIL FIELDS OF MONGOLIA (TAMSAG BULAG AND DZUNBAYAN) BY REMOTE SENSING METHODS 50

FROM ASEISMIC TO ACTIVE: SEISMIC PATTERNS IN EASTERN MONGOLIA'S PETROLEUM FIELDS 54

INVESTIGATING THE IMPACT OF WILDFIRES ON CLIMATE CHANGE AND PUBLIC HEALTH: FROM LABORATORY EXPERIMENTS TO FIELD CAMPAIGNS .. 55

NATURAL FLOW REGIME AND WATER VARIABILITY IN THE ORKHON RIVER, MONGOLIA 56

FORMATION AND DISTRIBUTION OF GROUNDWATER IN THE DORNOGOBI BASIN: HYDROGEOLOGICAL STUDIES OF DULAAN UUL AND ZOOVCH OVOO ROLL-FRONT-TYPE URANIUM DEPOSIT IN ZUUNBAYAN AND UNEGT SUB BASIN 56

COMPREHENSIVE MULTI-METAL ISOTOPIC MODEL FOR REGIONAL-SCALE ENVIRONMENTAL MANAGEMENT IN ERDENET MINE 57

LATE ORDOVICIAN MAGMATIC EVENT IN THE WESTERN GOBI ALTAI ZONE, SW MONGOLIA 58

PETROGENESIS OF THE KHAN BOGD RHYOLITES AND GRANITES IN THE SOUTH MONGOLIA 58

NEW ASSEMBLAGE OF SMALL SHELLY FOSSILS (CAMBRIAN STAGE 3) FROM THE LAKE ZONE OF WESTERN MONGOLIA 59

PALAEOGEOGRAPHIC MODELS OF PRECAMBRIAN-CAMBRIAN TERRAINS: TESTED BY SMALL SHELLY FOSSIL BIOPROVINCE ASSIGNMENTS 59

AUTOMATED QUANTITATIVE MINERAL CHARACTERIZATION OF PRIMARY ORE TYPES FROM THE ERDENETIIN OVOO CU-MO PORPHYRY DEPOSIT, MONGOLIA 60

CHRONOLOGY OF THE EDIACARAN-CAMBRIAN BOUNDARY: DISCUSSION WITH NEW DATA FROM AKSU AREA OF XINJIANG PROVINCE, CHINA 61

SUGGESTED METHODS OF EVALUATING GROUND REINFORCEMENT TENDON INTEGRITY IN ENVIRONMENTALLY CHALLENGING GROUND IN TUNNELLING AND MILIJIE GUOING 63

CROWN PILLAR OPTIMIZATION FOR FLUORITE MINE IN MOGOLIA -TANSFER FROM OPEN PIT TO UNDERGROUND- 76

EXPRESS - METHOD FOR DETERMINING PARAMETERS OF HEAVING OF WATER-SATURATED ROCKS TAKEN INTO ACCOUNT OF PRESSURE IN THE PORE FLUID 83

NUMERICAL RESEARCH ON THE IMPACT OF RAINFALL ON THE SLOPE STABILITY OF OPEN-PIT MINES 84

NON-CONVENTIONAL SOURCES AND METHODS OF MINERAL EXTRACTION – CHALLENGES AND OPPORTUNITIES 84

USE OF AI/ MACHINE LEARNING AND GIS – CASE STUDY EVALUATION OF DUMP STABILITY 85

INVESTIGATION OF REUSED PREPARATORY WORKINGS DEFORMATIONS OF AS A RESULT OF CLEANING OPERATIONS 85

MODELING THE PROCESS OF DYNAMIC DEVELOPMENT OF CRACKS IN THE EXPLOSION OF ADJACENT CYLINDRICAL CHARGES FOR DIRECTED DESTRUCTION 86

RESEARCH PROGRESS, TRENDS, AND INNOVATIONS OF DEVELOPMENT ON MINING BACKFILL TECHNOLOGY OF UNDERGROUND METALLIFEROUS MINE . 89

OPTIMIZING UNDERGROUND DEVELOPMENT CYCLES AND GROUT QUALITY WITH PERFORMANCE MINE GROUTS 105

OYU TOLGOI GEOTECHNICAL MONITORING SYSTEM: LEVERAGING TECHNOLOGY FOR ENABLING INFORMED DECISION MAKING 106

THE METHODS AND PRACTICES OF DEMOLISHING BUILDINGS AND STRUCTURES WITH USE OF BLASTING TECHNIQUES IN VARIOUS COUNTRIES 106

INSIGHT INTO IN-SITU MODIFICATION OF WHITE CARBON BLACK WITH SURFACTANT/SILANE COUPLING AGENT VIA SURFACE GRAFTING AND ITS PERFORMANCE 112

ALTERNATIVE METHODS FOR RECOVERY OF VALUABLE METALS FROM WASTE PRINTED CIRCUIT BOARDS 112

CORRELATION BETWEEN ROCK FORMING MINERALOGICAL COMPOSITION AT DIFFERENT DEPTHS AND BOND WORK INDEX FOR THE ERDENETIIN OVOO CU-MO PORPHYRY DEPOSIT, MONGOLIA 113

PREPARATION AND PERFORMANCE RESEARCH OF THERMAL INSULATION MATERIALS FROM IRON AND COPPER COMPOSITE TAILINGS 114

OPTIMIZATION AND CONTINUOUS IMPROVEMENT OF THE OYU TOLGOI CONCENTRATOR 114

THE VALUE-ADDED UTILIZATION OF COPPER SMELTER AND REFINERY WASTES 115

CONCEPT OF ECONOMIC POLICY OF A MINING COMPANY IN MODERN CONDITIONS 118

INNOVATION CHALLENGES IN THE MONGOLIAN MINING INDUSTRY 119

WATER GOVERNANCE IN THE CONTEXT OF MINING 120

APPLICATION OF ROLLING ROCK-CUTTING ELEMENTS IN PDC DRILL BITS 120

ENHANCING POWER GRID RELIABILITY FOR MINING INDUSTRY 122

RESEARCH ON DETERMINING THE SPEED OF HAUL TRUCKS DEPENDING ON MINING TECHNICAL FACTORS 128

ABILITY TO CALCULATE THE OPTIMAL OPERATING TIME OF THE OPEN-PIT DRILLING MACHINE BASED ON THE SDM 128

STUDY OF OPTIMAL BLASTING PARAMETERS FOR IN-PIT CRUSHING AND CONVEYING SYSTEMS 129

EFFECT OF MINERAL PHYSICAL PROPERTIES ON BENEFICIATION OF COPPER MOLYBDENUM SULFIDE ORES 134

STRATEGIC STUDY OF TECHNOLOGY FOR THE DEVELOPMENT OF MINING-METALLURGY COMPLEX (AS AN EXAMPLE OF THE POLICY OF COMPREHENSIVE EXPLOITATION OF IRON ORE DEPOSIT) 138

THE CURRENT STATE OF E-LEARNING, FUTURE TREND, WAYS TO MAKE IT SOPHISTICATED AND PERFECT, ITS SIGNIFICANCE AND RECOMMENDATIONS 148

CAPITAL AND OPERATIONAL COST ESTIMATION ON ISR PROCESS ON THE EXAMPLE OF ZUUVCH OVOO DEPOSIT 148

METHODOLOGICAL RESEARCH OF RISK ASSESSMENT OF MINING PROJECTS 150

STUDY ON THE TECHNOLOGY FOR SEPARATING COPPER-MOLYBDENUM-PYRITE CONCENTRATES 156

RESULTS OF TERRESTRIAL LASER SCANNING FOR CROSS PENETRATION LENGTHS AND VOLUMES IN UNDERGROUND MINING 162

VOLTAGE FLUCTUATIONS IN THE MINING POWER SUPPLY SYSTEM 163

RESEARCH ON INCREASING THE LEVEL OF COAL PROCESSING AND REDUCING THE COST OF PRODUCTS 164

DIESEL FUEL CONSUMPTION AND IMPACT ON AIR POLLUTION 170

THE REPUTATION OF THE MINING INDUSTRY IN TO THE MONGOLIAN PUBLIC AND THE NEED TO CHANGE PERCEPTIONS 171

FACIES AND STRATIGRAPHY OF PALAEOZOIC ROCKS IN SOUTHERN MONGOLIA AND IMPLICATIONS FOR REGIONAL GEOLOGY

Peter Königshof[1*], Johnny A. Waters[2], Sarah K. Carmichael[2], Sersmaa Gonchigdorj[3], Ariuntogos Munkhjargal[1, 3]

[1] Senckenberg Research Institute and Natural History Museum Frankfurt, Senckenberganlage 25, 60325 Frankfurt am Main, GERMANY
[2] Department of Geological and Environmental Sciences, Appalachian State University, Boone, NC 28608, U.S.A.
[3] Mongolian University of Science and Technology, 14191 Ulaanbaatar, MONGOLIA
*Corresponding author: peter.koenigshof@senckenberg.de

Palaeozoic rocks south of the Main Mongolian Lineament are subdivided into different zones (terranes) and blocks and exhibit less metamorphism in comparison to the northern part of the lineament. Nevertheless, rocks underwent thrusting and faulting and are partially recrystallized. Although a number of structural studies were conducted, detailed sedimentological and stratigraphical data are rare. Those studies are necessary to reconstruct the complex depositional and tectonic history, and to decipher regional relationships with adjacent tectonic blocks.

Facies development and new biostratigraphic data from a section in the Shine Jinst region and coeval successions from the Bayankhoshuu Ruins section with a focus on Devonian to Mississippian rocks are presented. Based on detailed sampling during field expeditions of the last years, we achieved a much better overview on the overall facies developments in both areas. Whereas facies differences in both regions are obvious in Ordovician and Silurian successions, a number of similarities occur in Devonian to Mississippian rocks. Massive cobble conglomerates, which are interpreted to represent braided fluvial or fan-delta to shallow fully marine deposits occur in both regions. Furthermore, thick limestone successions are characteristic in both areas, whereas pure sandstones are rare. Whether the Lower Devonian limestones represent real reefs is questionable. At least the section in the Shine Jinst area represents a biostromal limestone. Although reef organisms such as corals and stromatoporoids occur they never accumulated enough to build real reefs. A tectonic event led to a profound change of reef communities in the late Early Devonian. Reef organisms grew as scattered colonies forming less densely populated biostromes. Diversity of reef builders is low. Volcanic activity increased during the Eifelian and Frasnian, which is documented by thick-bedded submarine and subaerial volcanic deposits in both regions. Facies data are supported by new biostratigraphic results based on conodonts, which provided the background, and we could also pinpoint Devonian events in Mongolia for the first time, such as the Choteč Event, the Dasberg Crisis and the Hangenberg Crisis. The talk will focus on facies development and new stratigraphic data within a highly mobile depositional setting in southern Mongolia with respect to the complex tectonic frame.

Keywords: Facies, stratigraphy, Conodonts, Southern Mongolia, Events

PALEONTOLOGY IN MONGOLIA: LOOKING FORWARD TO NEW DISCOVERIES

Johnny A. Waters[1*], Sersmaa Gonchigdorj[2], Peter Königshof[3], Sarah K. Carmichael[1], Ariuntogos Munkhjargal[2, 3]

[1] Department of Geological and Environmental Sciences, Appalachian State University, Boone, NC 28608, U.S.A
[2] Mongolian University of Science and Technology, 14191 Ulaanbaatar, MONGOLIA
[3] Senckenberg Research Institute and Natural History Museum Frankfurt, Senckenberganlage 25, 60325 Frankfurt am Main, GERMANY
*Corresponding author: watersja@appstate.edu

Abstract

Mongolia has a very long and complex geologic history from the Archean to present times. It also has a very well-known paleontological heritage, at least in the context of its dinosaurs. The dinosaurs of Mongolia are not only a paleontological heritage, they are part of the country's national heritage known to virtually every citizen in the country. However, the tapestry of life is more robust and interesting than the age of the dinosaurs and Mongolia's paleontological heritage likewise is much broader. This "other" paleontological heritage is not known to most of Mongolia's citizens, nor is it necessarily well known by professional geologists and paleontologists, whether foreign or from Mongolia. The goal of this paper is to summarize some of the most significant contributions in Mongolia to our understanding of the history of life in general not just dinosaurs and to look forward to future successes.

Keywords: Paleontology, Ediacaran, Devonian

Paleontology in Mongolia

The history of life is punctuated with major ecological and evolutionary advances and major extinctions and reorganizations of ecosystems. The evolution of life itself, the transition from anaerobic to aerobic respiration, from single-celled to multi-celled organisms, from invertebrates to vertebrates, from jawless to jawed organisms, from aquatic to terrestrial ecosystems are but a few of the events that have given us life on earth as we know it and Mongolia has an exceptional natural history in this regard.

The dinosaurs and Tertiary mammals from Mongolia have been intensively studied for more than 100 years. From the early successes of the Central Asiatic Expedition of the American Museum of Natural History led by Roy Chapman Andrews and the geological expeditions of the Academy of Sciences of the USSR led by I.P. Rachkovskii to today, the vertebrates from Mongolia are known globally. Kurochkin and Barsbold (2000) present a comprehensive history of early Russian vertebrate expeditions in Mongolia. Other expeditions are well documented in a variety of readily available sources and are ongoing and well publicized. Other paleontological studies in Mongolia do not involve subjects as charismatic as dinosaurs and the largest land mammal ever found, but they provide essential information on critical events in the history of life.

The Ediacaran marks the relatively sudden evolutionary radiation of complex multicellular organisms following the global glaciation known as the Snowball Earth. Rare phosphatized Doushantuo-type multicellular embryos and possible multicellular life have been found in the Ediacaran of Mongolia. Although the soft bodied Ediacaran Fauna has not been found in Mongolia, reports of Burgess Shale type deposits of macroscopic algae confirm the presence of exceptional preservation in Ediacaran deposits. The discovery of complex penetrative trace fossils from the late Ediacaran of Mongolia demonstrates that the "agronomic revolution" when complex bilaterian animals increased the depth and intensity of bioturbation started earlier than previously considered. Exceptionally well-preserved Early Cambrian fossil eggs, embryos and microscopic bilaterian post-embryonic developmental stages from Mongolia provide critical insights into the early evolution of fundamental animal body plans. One of the

authors has been deeply involved in the discovery of Ediacaran fossils in Mongolia. Calcimicrobial reefs from Mongolia are the earliest known Cambrian reefs providing critical insight into the evolution of biomineralization and a fundamental habitat in marine ecosystems.

Devonian fish fossils from Mongolia are providing key data on fundamental developments in vertebrates such as the origin of jaws and teeth and the evolution of bony versus cartilaginous skeletons. The Devonian Period was a time of fundamental change in the atmosphere, the oceans and the biosphere. The major fish groups evolved and one group invaded land to form the first terrestrial vertebrate faunas. Plants completed their colonization of land and formed the first multi-story forests by the end of the period. Stromatoporoid coral reefs reached the maximum geographic extent in the Middle Devonian and likely covered ten times the geographic area they did today.

The Devonian was also a time of fundamental upheaval in earth history. The early Devonian greenhouse climate changed to an end Devonian icehouse earth as carbon dioxide concentrations in the atmosphere plummeted. These changes in atmospheric chemistry resulted in dynamic climate change as global temperatures declined significantly. Devonian oceans suffered many anoxic events as increased nutrient loading from terrestrial runoff upset geochemical equilibrium. Tropical marine ecosystems were severely impacted. Four of the eleven most severe ecological disruptions in the past 500,000,000 years occurred in the Devonian. Four of the top ten most severe extinction events occurred in the Devonian. Unlike other major extinction events which happened relatively rapidly by volcanic and / or extraterrestrial impacts, the Devonian extinctions occurred over tens of millions of years and were climate driven. Coral-stromatoporoid reefs collapsed in the Late Devonian losing 99% of their areal extent. The “reef gap” lasted for more than 30,000,000 years before reefs slowly recovered in the Carboniferous.

Mongolia is part of the Central Asian Orogenic belt (CAOB). Our research group has been conducting field-based research in Mongolia for more than a decade and in other parts of the CAOB for much longer. The results thus far indicate that Mongolia and the entire CAOB will play a pivotal role in understanding this tumultuous time in earth history. In the Devonian the CAOB was a series of open oceanic island arcs and microcontinents. Faunas from the Central Asian Orogenic Belt (CAOB) demonstrate that central Asia acted as a refugium for marine organisms after the Late Devonian extinction events, became a diversity hotspot in the Famennian, and a center of radiation for marine life prominent in the Mississippian. The most significant fauna is from the Hongguleleng Formation in the Xinjiang Autonomous Region of China with a diversity of more than 198 genera and 285 species. Recent collections from the Devonian terranes in Mongolia support the hypothesis that the Famennian diversity hotspot extended beyond the arc complexes in Xinjiang Province. Sparse collections from Shine Jinst document the presence of survivor Famennian echinoderm communities. The Hushoot Shiveetiin Gol locality in Baruunhuurai Terrane yielded a relatively abundant and diverse Famennian echinoderm community that has many genera in common with localities in Xinjiang, but endemic genera as well.

Lower Devonian coral stromatoporoid and bivalve biostromes are present at Shine Jinst in the Gobi-Altai Terrane. These biostromes are part of the great expanse of Lower Devonian reefs, although local volcanic activity limited their geographic and stratigraphic success. Relatively diverse echinoderm communities in the same section document their presence in Mongolia prior to the Middle and Late Devonian extinction events. These are the northernmost Lower Devonian echinoderm faunas known to date.

The variety and significance of paleontological resources in Mongolia extends far beyond its famous dinosaurs and mammals. Importantly, these other paleontological studies are in their infancy and are being pursued by small research groups compared to well-funded dinosaur expeditions. Many occur in geologically frontier regions with sparse data beyond basic geologic mapping. Often, basic stratigraphy and biostratigraphy have to be established prior to in depth faunal analyses. Many of these areas are tectonically complex.

Based on the results we have seen in a relatively small period of time, we are optimistic that many paleontological success stories will come out of Mongolia in the future with appropriate investments in local researchers and financial support for fieldwork and

subsequent laboratory studies. It is important to note that most of active research groups working in Mongolia are led by Mongolian geologists.

References

Kurochkin, E.N. and Barsbold, R., 2000. The Russian-Mongolian expeditions and research in vertebrate paleontology. The age of dinosaurs in Russia and Mongolia, pp.235-255.

TECTONIC FACTOR OF POST-FORMATION CHANGES IN COAL-BEARING MASSIFS OF THE DONETS BASIN, UKRAINE

Nataliia Vergelska[1]*, Valentyn Verkhovtsev[2], Ihor Skopychenko[1], Viktoriia Vergelska[1, 2]

[1] State Institution «Scientific Center of Mining Geology, Geoecology and Infrastructure Development of the National Academy of Sciences of Ukraine», Akademik Vernadskyi Blvd, 34b, Kyiv, 03142, UKRAINE
[2] State Institution «The Institute of Environmental Geochemistry of National Academy of Sciences of Ukraine», Palladin Ave., 34a, Kyiv, 03142, UKRAINE
*Corresponding author: vergelskanv@gmail.com

Abstract

The coal rock massif of the Krasnoarmiysk coalmine district of Donets basin is represented by Mississippian and Pennsylvanian strata of Carboniferous period. The investigation of tectonic processes impact on natural gas content of coal seams due to post-sedimentary transformations during Hercynian (partly), Cimmerian and Alpine stages of tectono-magmatic reactivations is of top priority fundamental and practical issue for conducting safe mining operations.

This study is based on analysis of the coals and host rocks sampled in the mines of SE CC Krasnolymanska during 2007–2022, studied plans of mining works and sections of coal massifs.

Most of the tectonic faults were formed during the Hercynian and Cimmerian stages of formation of the modern structure. The tectonic faults identified during exploration are confirmed in the mining operations. The faults with offsets, fracture zones, and the transition of host rocks and coal seams that are clearly visible in the l_3 seam are leveled or completely absent in the m_4^2 seam located above it. Considerable fracturing of the coal rock mass testifies to reorganization of the coal seam l rock massif followed by considerably quiet tectonic regime. Due to re-structuring of the existed coal rock massif the hydrocarbon content and zonation is also changed. When studying the residual gas content in coal seams, it was established that the volume and variety of gases increases in the direction of fault planes and fractured zones. Gas saturation of coal seams in the studied area does not correlate with depth in tectonically disturbed zones.

Keywords: Donets basin, Krasnoarmiysk coalmine district, tectonic, coal, faults

Introduction

The sections of the coal-bearing massifs of the Donets basin have been studied in detail for many decades. The Carboniferous coal-bearing formations of the Hercynian structural and stratigraphic complex were formed in the sedimentogenesis mode of the period of active tectono-magmatic (tectono-volcanic) processes and changed in the post-sedimentation stages under the influence of Cimmerian and Alpine tectono-magmatic activations.

The coal rock massif of the Krasnoarmiysk coalmine district of Donets basin is represented by Mississippian and Pennsylvanian strata of Carboniferous period. At the Krasnoarmiysk coalmine district there are three coal-bearing suites under production as follows: Kamenska (C_2^5, coal seam *k*), Almazna (C_2^6, coal seam *l*), and Gorlivska (C_2^7, coal seam *m*) which are developed at SE CC Krasnolymanska. The coal seams m_4^2 and l_3 have as similar as different

features that can be referred to the accumulation time (sedimentation) and overprinting (post-sedimentary) processes (Vergelska, Pravotorova, 2008; Vergelska et al., 2011).

The possibilities to reveal a dependence of the coal rock massifs gas potential on deep-seated structures in the Krasnoarmiysk coalmine district are steadily increasing due to the move of coal mine working faces towards tectonically complicated peripheral parts of mine fields coupled with increasing depth of the mining as well. The investigation of tectonic processes impact on natural gas content of coal seams due to post-sedimentary transformations during Hercynian (partly), Cimmerian and Alpine stages of tectono-magmatic reactivations is of top priority fundamental and practical issue for conducting safe mining operations (Vergelska et al., 2022).

Research materials and methods

This study is based on analysis of the coals and host rocks sampled in the mines of SE CC Krasnolymanska during 2007–2022. During this period it was conducted macro- and micropetrographic studies of coals from seams m_4^2, l_1^c, l_2, l_3, l_4^a and k_5, host rocks and inclusions and measured residual gas content in coal samples. Also, it was made generalization and analysis of previosly collected data. Recognition of stadial (of different level) dislocations within the coal seams m_4^2 and l_3 under production of the North-Rodinska-2 license permit allow prediction of local zones containing gas accumulations within the studied area of SE CC Krasnolymanska.

Presentation of the research material

The sedimentary rock stratum of the Krasnoarmiysk coal mining district lies on Precambrian formations, which is the oldest structural floor. Coal deposits are widespread everywhere, their strike is northwest and dip is northeast. The main part of the study area is occupied by the southwestern wing of the Kalmius-Toretsk depression, which is called the Krasnoarmiysk monocline. Coal deposits occur mainly at angles of 8-12º, while in the southern part of the area the rocks occur at angles of 2-6º.

The studied area is located within the hanging wall of the major Central thrust in the Krasnoarmiysk coalmine district. The Carboniferous rocks form a monocline dipping to the east and northeast at angle 3°-14°. At the central part of the area studied it is observed a gentle dipping flexure with elevated northwest flank. The host rocks strikes northwest on the flanks and proximal to meridional one within the fold closure. Vertical height of the flexural bend is about 100 m. The stratal inclination at the flanks and the closure is practically unchanged. The occurrence of rocks is complicated by disjunctive faults (fourteen normal ones and seven up thrusts). During coal extraction it had been documented that these faults split into subordinate branches or have staircase array in l_3 and m_4^2 coal seams governing poulation density of fractures and gas content of those seams.

In the direction of the central part of the Kalmius-Toretsk depression, the rocks are generally uplifted. Against the general background of monoclinal occurrence of Carboniferous rocks, there are faults such as thrusts. Thrusts have amplitudes from 50 to 400 m and divide the area into a number of large blocks. Enveloping faults are developed mostly in the hanging wings of the thrusts. The thrusts and flexures are located in groups and have steeply falling offsets with predominant amplitudes of 5-20 m, sometimes 50-80 m. Mining operations in the mines identify and record faults with an amplitude of 0.15-3.0 m, sometimes up to 25 m.

The third structural level consists of Triassic and Jurassic sediments, which lie with angular and stratigraphic unconformity on the eroded surface of Carboniferous rocks. They have been preserved only in the northwestern part of the district. The Mesozoic sediments forming a series of brachy-syncline and brachy-anticline folds have dip

angles of 0-2º, rarely 4-5º. Thrusts and thrusts commonly break up and displace these deposits. A series of thrusts disrupts not only Paleogene-Neogene, but even Quaternary sediments.

Most of the tectonic faults were formed during the Hercynian and Cimmerian stages of formation of the modern structure. The faults were formed in tensile zones at the boundaries of crystalline basement blocks, and the wing movements were subvertical. A clear zone of block movement (with an amplitude of about 25 m and a width of 0.20-0.75 m) was found in the overburden zone of the l_3 seam in the workings of the SE CC Krasnolymanska. The thrusts are also confined to the boundaries of the blocks formed as a result of compressive subhorizontal stresses arising from the block movement of sediments of the Krasnoarmiysk monocline as a whole and its individual blocks relative to the main part of the Kalmius-Toretsk depression. Compressive stresses led to the disruption of sediments in the upper horizons during the transition of the Carboniferous rocks from large to smaller dip angles.

Within the mine field of the SE CC Krasnolymanska, the identified tectonic faults are represented by the Hlybokoyarsky, Fedorivsky, Hrushevsky, Grachivsky, Bezymenny faults and much smaller thrusts 2, 3, 5, 9. One of the largest disturbances is the Central thrust. These faults were also recorded by seismic surveys at deep horizons. Other faults detected by seismic surveys are short in length and are likely to be small-amplitude faults (up to 1-3 m) (Tirkel et al., 2008).

The tectonic disturbances are accompanied by active fracture zones up to 30 m wide, fractures of the seams with and without displacement with an amplitude of 1.0-15.0 m. There are zones of fractures and faults in the k_5 seam (within 5-10-20 m), and slip mirrors are clearly visible in the contact zone between the host rocks and the coal seam (0.2-0.75 m wide).

The tectonic faults identified during exploration are confirmed in the mining operations. It should be noted that the structure of the m_4^2 seam (-545 m horizon) differs significantly in terms of faults, their size and distribution from the l_3 seam (-843 m horizon). Most of the faults with offsets, fracture zones, and the transition of host rocks and coal seams that are clearly visible in the l_3 seam are leveled or completely absent in the m_4^2 seam located above it. Most likely, the differences are related to the period of formation of the Hrachivsky fault, which can be traced in the workings of the l_3 seam, and by the time the m_4^2 seam was accumulated, the formation of most dumps and thrusts was almost complete. Despite the smaller number of faults, the Hlybokoyarsky and Fedorovsky faults are clearly visible in the m_4^2 coal seam.

Intense tectonic changes in the coal bed and individual seams are also indicated by dissemination and cleavage textural elements, often in contact with coal seams, such as slip mirrors and plastic deformation textures.

The dynamics of the tectonic-sedimentaryl regime of the coal rock massif within the license area mine of SE CC Krasnolymanska emphasizes recurrent splitting of the coal seams and changing of their thickness (towards the Central thrust) as well as abundant erosion gaps and pinch-outs.

Considerable fracturing of the coal rock mass testifies to reorganization of the coal seam l rock massif followed by considerably quiet tectonic regime. Inherited faults typical for the Almazna and Gorlivka suites, for example Hlybokoyarsky or Fedorivsky normal ones have different influence on dislocation of the coal seams and formation of fractures. The Hlybokoyarsky fault is inherited from older tectonic disturbance and distinctly traced in the seams l_3 and m_4^2. At the same time the amplitude of the Fedorivsky fault (25 m) taken upon seam l_3 almost completely attenuates in m_4^2 seam.

The coal seams of that area are characterized as low gas-bearing ones up to 16.3 m^3/t of gas content (Kravtsov, 1979). Coal samples selected for the analysis of the residual gas component (Vergelska, Pravotorova, 2008; Vergelska et al., 2011; Vergelska et al., 2022) testifies that their component composition changes depending on the distance from fault plane. Methane is characteristic constituent for all of residual gas samples varying from 22.22 to 77.4 vol.%. Hydrogene is also typical for all coal samples (the highest concentration is about $3.97x10^{-2}$ vol.%, the lowest is $1.21x10^{-3}$ vol. %). The unsaturated hydrocarbons are represented by ethylene (the highest is about $0.845x10^{-3}$ vol. %, and the lowest one is $2.7x10^{-6}$ vol.%) and propylene (traces). Their concentrations increase while approaching the fault plane.

The gas content of the sandstones (host rock) at favorable conditions range from 0.01 to 0.27 m^3/t and closely related to the presence of dissolved gas in formation waters. The sandstones have different permeability (Kravtsov, 1979; Tirkel et al., 2008). Higher permeability of sandstones is caused by weak metamorphism of the rock massif and stipulates active degassing of coal seams and even accumulation of gas in them at favorable conditions (Kravtsov, 1979; Vergelska et al., 2011). It is identified helium in those samples besides of methane homologues and hydrogen. This may point out at present-day gas inflow from deeper sources viathe damage zones to the coal rock massif.

The gas potential of the Almazna and Gorlivska coal-bearing suites is different. The highest gas content is characteristic of Almazna formation (C_2^6), which is confirmed by previous, exploration studies, observations at the mine and gas saturation of the collected samples (Vergelska, Pravotorova, 2008; Vergelska et al., 2011; Vergelska et al., 2022).

Conclusions

Due to re-structuring of the existed coal rock massif the hydrocarbon content and zonation is also changed.

When studying the residual gas content in coal seams, it was established that the volume and variety of gases increases in the direction of fault planes and fractured zones. Gas saturation of coal seams in the studied area does not correlate with depth in tectonically disturbed zones.

When developing a coal seam in tectonically disturbed areas, it is advisable to monitor the gas mixture to prevent gas-dynamic phenomena in the mining operations.

References

Kravtsov A. I. (Ed.). 1979. Coal basins and fields of the European part of USSR. – In: Gas-bearingness of USSR coal basins and fields, vol. 1. Nedra, Moscow, 628 p. (in Russian).

Radzivill A. Ya. 2001. On the issue of methane concentration changes with depth in the coal formation of the Folded Donbas. Inst. Fundamental Res. Treatises. Kiev: Znannya Publ., 105–110 (in Ukrainian).

Tirkel M. G., V. A. Antsiferov, A. A. Glukhov. 2008. Research on gas-bearing potential of the coal formation. Donetsk: VEBER Publ., 208 p. (in Ukrainian).

Vergelska N. V., O. V. Pravotorova, I. O. Nazarova. 2011. On peculiarities of coal gas content in the tectonic active zone: Case study for North-Rodinska-2 SE Krasnolimanska Coal Co. Lease. UkrNDMI NAS Ukarine Treatises, Donetsk, 9, 2, 440–450 (in Ukrainian).

Vergelska N. V., O. V. Pravotorova. 2008. Peculiarities of geological structure of some coal seams the Karsnoarmiysk coalmine district: Krasnolimanska coal mine case study. Tectonics and Stratigraphy, 36, 85–91 (in Ukrainian).

Vergelska N.V., Pymonenko L.I., Skopychenko I.M. 2022. Mining and geological features of forecasting dynamic phenomena in coal mines. Mining geology and geoecology. No1 (4). P. 5 -15. DOI:https://doi.org/10.59911/mgg.2786-7994.2022.1(4).273777. (in Ukrainian).

THE PRELIMINARY RESULT OF OPHIOLITE AND OPHIOLITIC MÉLANGE IN THE KHAN-KHUKHEY MOUNTAINS, WESTERN MONGOLIA

Ulambadrakh Khukhuudei

Research Center of Geology and Mineral Resources, School of Arts and Sciences, National University of Mongolia, Ulaanbaatar 14000, Mongolia
ulambadrakh@num.edu.mn

The Khan-Khukhey ophiolite is located in the same named ridge, which is a specific latitudinal and asymmetric horst in western Mongolia. The composition and structure of this ophiolite has not been well studied. We define it as a complete ophiolite, based on the field survey and original map report, which were the only sources, interpreting as an intrusive rock.

The Khan-Khukhey ophiolite is up to 4 km wide and extends for several km. The ophiolite is more than 50 km^2 in separate, and comprises a section from serpentinized ultramafic rocks (ophiolite) to deep-water chert, shale and siltstone (OPS) of the Ediacaran - Lower Cambrian Khan-Khukhey Formation (middle Cambrian Icheet Formation?).

Structurally, W-E-striking ophiolite is composed of imbricated mélange, thrusted nappe sheets and olistostrome. The nappe sheets contain an ultramafic-mafic complex with layers of serpentinized dunite, peridotite and pyroxenite, isotrope gabbro and layered gabbro. The volcanogenic sedimentary formation overlying the ophiolite is widespread. The basaltic rocks with siliceous sediments and limestone–chert–basalt are dominantly by the main unit. Massive basalt and weakly pillow lavas are alternated with thin chert, siliceous siltstone, shale and sandstone, and thick limestone.

Structural feature of the Khan-Khukhey Ridge is not well known. The ophiolitic mélange is strongly serpentinized and foliated, and contains rounded and lens-shaped ultramafic fragments as block-in-matrix. The general structure is similar to many mélange zones that were thrust together with OPS and ophiolitic complex in many accretionary orogens of various ages.

The Khan-Khukhey ophiolite in this study has in range of zircon age: ~718-824 Ma (SHRIMP age) for an isotrope gabbro.

Keywords: Khan-Khukhey, ophiolite, mélange, zircon age

CONTRASTING EARLY PERMIAN PLUTONISM IN THE TRANS-ALTAI ZONE, SW MONGOLIA

Pavel Hanžl[1]*, Vojtěch Janoušek[1], Battushig Altanbaatar[2], Karel Schulmann[1], Kristýna Hrdličková[1], Gerel Ochir[3], David Buriánek[1]

[1]Czech Geological Survey, Prague, CZECH REPUBLIC
[2] Takhi resources LLC, Ulaanbaatar, MONGOLIA
[3] School of Geology and Mining Engineering, MUST, Ulaanbaatar, MONGOLIA
*Corresponding author: pavel.hanzl@geology.cz

The Trans-Altai Zone (TAZ) in the southern tract of the Central Asian Orogenic Belt (CAOB) is formed by the Early Paleozoic oceanic crust covered by Carboniferous volcanosedimentary complexes and intruded by numerous Carboniferous to Permian plutons. Two contrasting belts of the Early Permian plutons stand out among them: (1) Gobi Tien Shan Intrusive Complex (GTSIC) in the south and (2) late- to post-tectonic plutons of noticeably oval shape distributed along the central and northern parts of the TAZ.

Petrologic and geochemical characteristics of the 310–290 Ma old GTSIC correlate with westerly magmatic belts in the Eastern Tien Shan and point to an active continental margin

setting. Voluminous arc-related granodiorites–diorites with well-preserved magma mingling textures come from deeper parts of the GTSIC, while granites with subvolcanic features represent relatively shallow intrusion levels of the Late Carboniferous–Early Permian volcanic arc.

The Aaj Bogd Pluton (ABP) is the largest among the Early Permian (300–280 Ma) plutons distributed in a belt spanning from the Dulate Arc in the Eastern Junggar through the Trans-Altai Zone to the Khan Bogd Pluton in the Southern Gobi. Whole-rock chemistry of the ABP points to an intra-plate geotectonic setting. The mafic rocks in the center of ABP are interpreted as having crystallized from melts derived from asthenospheric mantle domains unmodified by previous subduction-related metasomatism. These parental magmas further evolved by assimilation of pre-existing, arc-related metaigneous crust and fractional crystallization processes to yield the prevailing syenitic–granitic members of the Aaj Bogd Pluton.

The A-type magmatic activity in the Trans-Altai Zone and I-type, subduction-related magmatism in the southerly Gobi Tien Shan were temporally and spatially connected with the Late Carboniferous–Early Permian amalgamation of the Trans-Altai Zone to the northern parts of CAOB. During this process, GTSIC is thought to have originated in a continental arc developed over a retreating oceanic subduction zone. The back-arc rifting scenario for the contemporaneous A-type magmatism in TAZ assumes asthenosphere upwelling triggered by the collisional zone, probably related to the same subduction zone on which the GTSIC evolved far to the south. The linear arrangement of the A-type plutons over a distance of more than 1600 km can be explained through their association with major Permian strike-slip zones likely controlling the granite emplacement.

The research was supported by the project GAČR EXPRO 19-27682X and presented data were published in the Journal of Geosciences: http://doi.org/10.3190/jgeosci.366

A LONG-LIVED SLAB-MELT-ORIGIN ADAKITIC MAGMATISM AT THE PERMIAN–TRIASSIC SIBERIAN CONTINENTAL MARGIN

Kazuhiro Tsukada[1]*, Purevdulam Sukhbaatar[2]

[1] Nagoya University Museum, Nagoya 464-8601, JAPAN
[2] Graduate School of Environmental Studies, Nagoya University, Nagoya 464-8601, JAPAN
*Corresponding author: tsukada@num.nagoya-u.ac.jp

Abstract

The ages and geochemical features of the Selenge igneous rock complex, Mongolia, a huge igneous rock body, are compiled to examine the Late Permian–Late Triassic magmatism of the Siberian continental margin. About 200 geochemical data of the complex of ca. 260–210 Ma consistently show typical adakitic nature of subducted oceanic slab-melt-origin. This fact suggests that the large-scale adakitic igneous activity had continued for > 50 million years at that time, along the Siberian continental margin.

Keywords: Selenge igneous rock complex, adakitic rocks derived from slab-melt, Late Permian–Late Triassic, Siberian continental margin.

The geochemistry of the Permian–Triassic large-scale igneous rock body (Selenge igneous rock complex: SIC here) of northern Mongolia is a key factor in understanding the subduction-related magmatism at the margin of the “former Siberian continent” (Fig. 1). Several studies have been made in the SIC; however, its detailed magma genesis and tectonic significance remain unclear. In this presentation, the ages and geochemical features of the Upper Permian and Upper Triassic volcanic rocks and the Late Permian–Late Triassic plutonic

rocks of the SIC and Late Triassic intermediate dikes intruding into them are taken, and discusses the Late Permian–Late Triassic magmatism of the Siberian continental margin.

Mongolia is geologically divided into the northern and southern superblocks by the Mid Mongolian tectonic line (Tomurtogoo, 2014). The rocks of the northern superblock, former Siberian continental margin, composed mainly of the Khangai-Daur belt (Late Paleozoic accretionary complexes) and the Sayan-Baikal belt (continental basement). The Sayan-Baikal belt is covered/intruded by the Permian–Triassic volcanic/plutonic rocks of the SIC (Tomurtogoo, 2003; Onon and Tsukada, 2017) (Fig. 1).

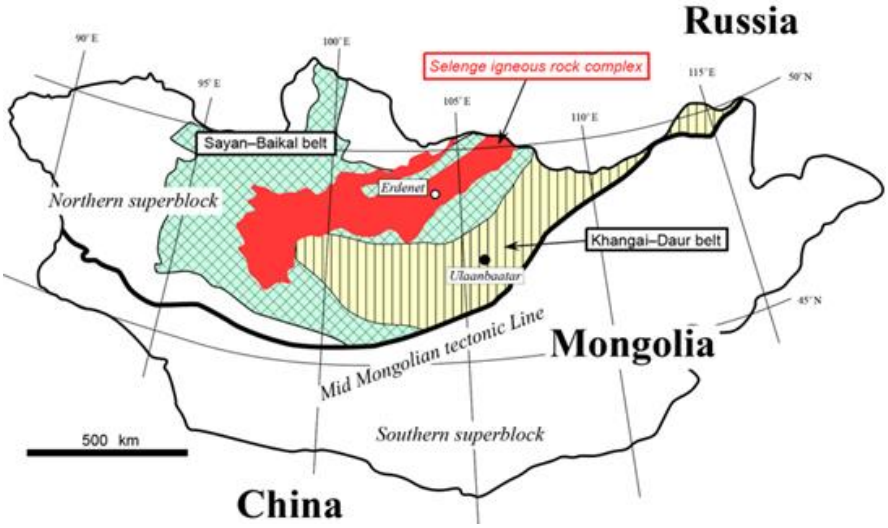

Fig. 1. Simplified tectonic division of northern Mongolia (modified from Tomurtogoo, 2003, 2014; Tsukada et al., 2021).

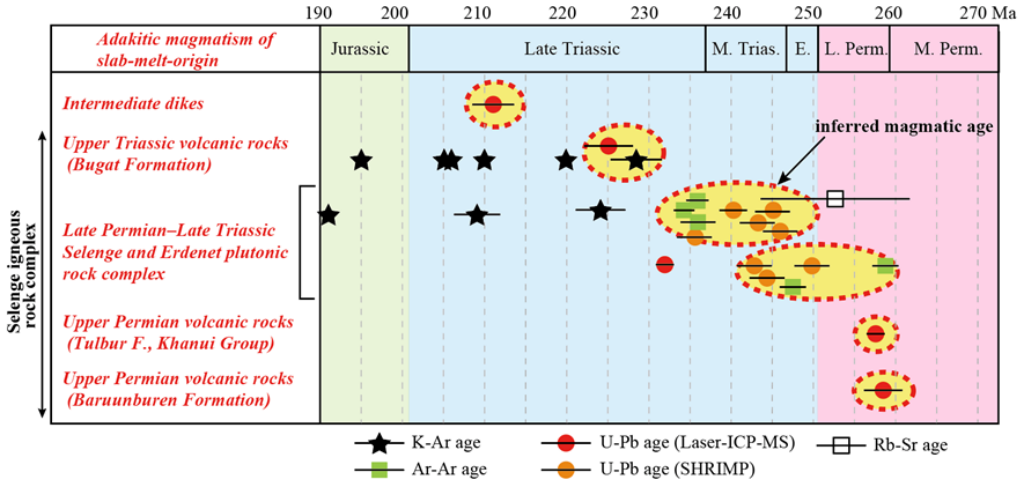

Fig. 2. Ages from the adakitic rocks of the Selenge igneous rock complex and intermediate dikes. Data were from Kepezhinskas and Luchitsky (1974), Sotnikov et al. (1995, 2005), Izawa and Ohsawa (2004), Gerel and Munkhtsengel (2005), Munkhtsengel et al. (2007), Berzina et al. (2009), Tsukada et al. (2018), Tsukada et al. (2021), Umeda et al. (2022), and this study. F.: Formation, E.: Early Triassic, M: Middle.

The Upper Permian volcanic rocks of the SIC give U-Pb age of ca. 258–257 Ma (Tsukada et al., 2018; Tsukada et al., 2021). The magmatic age of the Late Permian–Late Triassic plutonic rocks of the complex is considered to be ca. 253–236 Ma (Rb-Sr age, ^{39}Ar-^{40}Ar age, and SHRIMP U-Pb age) (Sotnicov, 2005; Berzina et al., 2009; Gerel and Munkhtsengel, 2005; Munkhtsengel et al., 2007). The Upper Triassic volcanic rocks show U-Pb age of ca. 225 Ma. And, U-Pb age of ca. 210 Ma were obtained from the intermediate dikes intruding into the above rocks (Fig. 2).

The chemical composition of all these rocks is nearly the same, characterized by low K_2O/Na_2O, high Sr/Y, high La/Yb, and high Sr/La ratios, which are the adakitic rocks of subducted oceanic slab (MORB)-melt origin. The samples are enriched in Cr and Ni and have

a high Mg# compared with the typical slab-melt. This is likely due to an interaction between the slab-melt and the overlying mantle peridotite during its ascent. The Nb/Ta variation of the samples points crustal contamination to the magma (Umeda et al., 2022).

Partial melting of the MORB requires particular condition of 2.0 GPa and 900–950 °C, and the adakitic magmatism is hardly caused at the usual thermal gradient in the subduction system (Defant and Drummond, 1990; Sen and Dunn,1994; Rapp and Watson, 1995; Tsuchiya et al., 2007). And, the “hot and young (< 5 Ma) slab subduction model” is considered to be the most reasonable explanation for the subducted slab-melting. However, the subducted oceanic plate beneath the Siberian continent in the Late Paleozoic time was estimated to be > 50 million years old when it reached the trench, and the “partial melting of hot and young slab model” is incompatible with this case (Kurihara et al., 2008; Umeda et al., 2022). Then, some possible scenarios explaining the Permian–Triassic slab-melting have been proposed such as heat supply from the superplume that caused the Siberian traps and oblique subduction of the Mongol-Okhotsk oceanic plate (Umeda et al., 2022) (Fig. 3). What caused the slab-melting at that time remains as a matter to be discussed further, but in any case, the wedge mantle there had certainly been in a peculiar thermal condition.

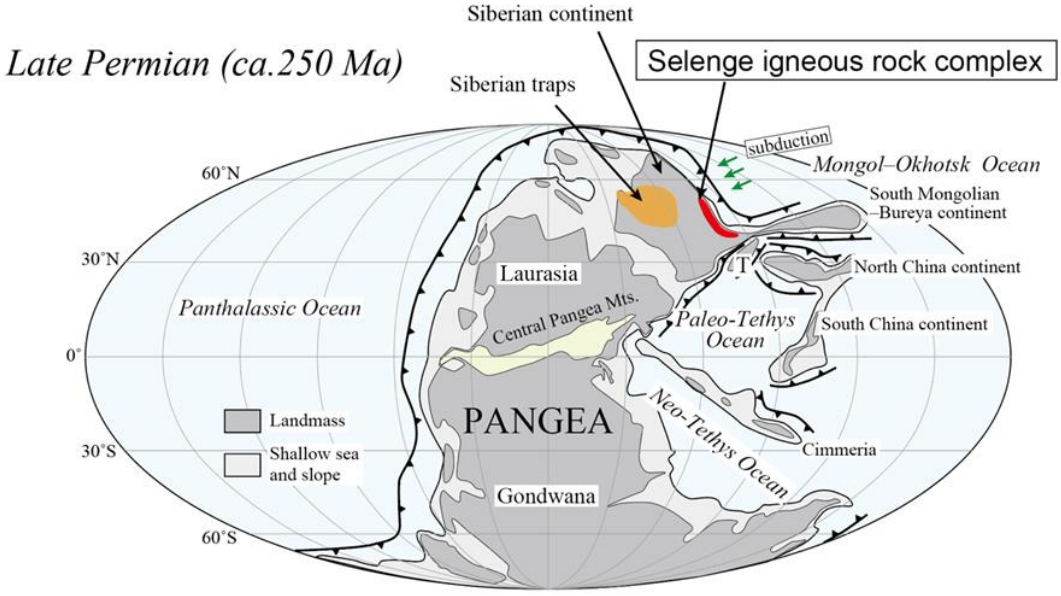

Fig. 3. Paleogeographic reconstruction for the Late Permian time (modified from Umeda et al., 2022). T: Tarim continent, Cimmeria: Cimmeria continent.

The paleolatitude of the Middle Triassic volcanic rocks were calculated to be 37.1˚ N based on thermal remanent magnetization (Pruner, 1987; Umeda et al., 2022) (Fig. 3). In summary, the large-scale adakitic igneous activity, caused by slab-melting of the subducted Mongol-Okhotsk oceanic plate, had probably been continued from Late Permian to Late Triassic and after, along the Siberian continental margin in the mid-latitudes of the Northern Hemisphere (Figs. 1, 2, 3). This means that an anomalous “hot” condition of the wedge mantle had continued for > about 50 million years, there.

References

Berzina, A. P., Gimon, V. O., Nikolaeva, I. V., Palesskii, S. V., and Travin, A. V. (2009) Basites of the polychromous magmatic center with the Erdenetiin Ovoo porphyry Cu-Mo deposit (northern Mongolia): petrogeochemistry, $^{40}Ar/^{39}Ar$ geochronology, geodynamic position, and related ore formation. *Russian Geology and Geophysics*, 50, 827–841.

Defant, M. J. and Drummond, M. S. (1990) Derivation of some modern arc magmas by melting of young subducted lithosphere. *Nature*, 347, 662–665.

Gerel, O. and Munkhtsengel, B. (2005) Erdenetiin Ovoo porphyry copper-molybdenum deposit in central Mongolia. Porter, T. M. (ed.), *Super Porphyry Copper & Gold Deposits –A Global Perspective*, 2, 525–543, PGC Publishing, Adelaide.

Izawa, T. and Ohsawa, H. (2004) Basic Research Report on the Cooperation for the Development of Resources Exploration in the Western Erdenet Area, Mongolia. Japan International Cooperation Agency and Japan Oil, Gas and Metals National Corporation, Tokyo, 213 p.

Kepezhinskas, B. B. and Luchitsky, I. B. (1974) Continental Volcanic Associations of Central Mongolia. Nauka, Moscow, 69 p.

Kurihara, T., Tsukada, K., Otoh, S., Kashiwagi, K., Minjin, C., Dorjsuren, B., Boijir, B., Sersmaa, G., Manchuk, N., Niwa, M., Tokiwa, T., Hikichi, G., and Kozuka, T. (2008) Upper Silurian and Devonian pelagic deep-water radiolarian chert from the Khangai- Khentei belt of Central Mongolia: Evidence for Middle Paleozoic subduction-accretion activity in the Central Asian Orogenic Belt. *Journal of Asian Earth Sciences*, 34, 209–225.

Munkhtsengel, B., Tsuchiya, N., Dan, D., and Gerel, O. (2007) SHRIMP U-Pb zircon age of the intrusive and host rocks in Erdenet district, and their relationship between ore mineralization age of Erdenetiin Ovoo deposit. *Mongolian Geoscientist*, 34, 120–125.

Onon, G. and Tsukada, K. (2017) Late Paleozoic low-angle southward-dipping thrust in the Züünharaa area, Mongolia: tectonic implications for the geological structures in the Sayan-Baikal and Hangai-Daur belts. *International Journal of Earth Science*, 106, 2549–2573.

Rapp, R. P. and Watson, E. B. (1995) Dehydration melting of metabasalt at 8–32 kbar: implications for continental growth and crust–mantle recycling. *Journal of Petrology*, 36, 891–931.

Sen, C. and Dunn, T. (1994) Dehydration melting of a basaltic composition amphibolite at 1.5 and 2.0 GPa: implications for the origin of adakites. *Contribution to Mineralogy and Petrology*, 117, 394–409.

Sotnikov, V. I., Ponomarchuk, V. A., Berzina, A. P., and Travin, A. V. (1995) Geochronological borders of magmatism of Cu-Mo-porphyry Erdenetuin-Obo deposit. *Russian Geology and Geophysics*, 36, 78–89.

Sotnikov, V. I., Ponomarchuk, V. A., Shevchenko, D. O., and Berzina, A. P. (2005) The Erdenetiyn-ovoo porphyry Cu-Mo deposit, northern Mongolia: $^{40}Ar/^{39}Ar$ geochronology and factors of large-scale mineralization. *Russian Geology and Geophysic*s, 46, 620–631.

Tomurtogoo, O. (2003) *Tectonic Map of Mongolia at the Scale of 1:1000000 and Tectonics of Mongolia (Brief Explanatory Notes of the Map)*. Mineral Resources Authority of Mongolia, Ulaanbaatar.

Tomurtogoo, O. (2014) Tectonics of Mongolia. Petrov, O. V., Leonov, Y. G., and Pospelov, I. I. (eds.), *Tectonics of Northern, Central and Eastern Asia. Explanatory Note to the Tectonic Map of Northern–Central–Eastern Asia and Adjacent Areas at Scale 1:2500000.* SPb. 110–126, VSEGEI Printing House, St. Petersburg.

Tsuchiya, N., Kimura, J. I., and Kagami, H. (2007) Petrogenesis of Early Cretaceous adakitic granites from the Kitakami Mountains, Japan. *Journal of Volcanology and Geothermal Research*, 167, 134–159.

Tsukada, K., Nuramkhaan, M., Purevsuren, N., Kabashima, T., Kondo, T., Gantumur, O., Hasegawa, H., and Yamamoto, K. (2018) Permian adakitic magmatism in the Khanui Group, Northern Mongolia – Late Paleozoic slab-melting of subducted oceanic plate beneath the “Siberian continent.” *Journal of Geodynamics*, 121, 49–63.

Tsukada, K., Umeda, K., Nadmid, B., Sodnom, K., and Nuramkhaan, M. (2021) Ages from the “Mogod Formation” of the Permian–Triassic igneous rocks in the Sayan-Baikal belt, northern Mongolia, *Bulletin of Nagoya University Museum*, 37, 1–12.

Umeda, L., Nemekhbayar P., Tsukada, K, Lodoidanzan A., Bayart N., Khishigsuren S., Manchuk N., Kabashima, T., and Kondo, T. (2022) Permian–Triassic adakitic igneous activity at Northern Mongolia: Implication for Permian–Triassic subduction system at the Siberian continental margin. *Journal of Geodynamics*, 151, https://doi.org/10.1016/j.jog.2022.101918.

LITHIUM-FLORINE GRANITES IN THE MONGOL-OKHOTSK OROGENIC BELT: PETROLOGY, GECHEMISTRY AND ASSOCIATED MINERALIZATION

Gerel Ochir[1*], Odgerel Dashdorjgochoo[2]

[1] Geoscience Center, MUST, Ulaanbaatar 14191, MONGOLIA
[2] Institute of Geology, MAS, Ulaanbaatar, MONGOLIA
*Corresponding author: gerel@must.edu.mn

Lithium-fluorine (Li-F) granites are highly fractionated, leucocratic, peraluminous granites that are rich in rare metals, including Li, Ta, Nb, Sn, and W. These granites are commonly associated with rare-metal pegmatites, greisen, and subvolcanic ongonites, which share similar mineralogy and geochemistry. Li-F granites are predominantly found in the Mongol-Okhotsk orogenic belt, which formed as a result of the continental collision and closure of the Mongol-Okhotsk Ocean. This tectonic event led to extensive Permian to Mesozoic magmatism and the formation of large Khangai and Khentei batholiths, composed of calc-alkaline to high-K calc-alkaline granitoid series. Surrounding these batholiths are shallower granite plutons characterized by higher alkalinity and a post-orogenic affinity. Li-F granites represent the latest stage of multiphase plutons and can occur either as the apical parts of plutons or as small one- to two-stage intrusions. Their composition is variable, but they mainly consist of quartz, albite, K-feldspar, Li-mica, and topaz, along with accessory minerals such as fluorite, zircon, monazite, columbite-tantalite, microlite, and cassiterite. A characteristic feature of Li-F granites is the presence of phenocrysts of euhedral to subhedral quartz set in a groundmass predominantly composed of albite. In the multistage pluton, the latest stage of Li-F granites includes microcline-albite, amazonite-albite, and lepidolite-albite varieties. These granites may be affected by late magmatic and post-magmatic processes and are crosscut by greisens (zwitters) and dikes of microcline-albite-fluorite and albitites, such as those found in some intrusions, which primarily occur at the periphery of the plutons. The subvolcanic equivalent of Li-F granites, aphanitic to porphyritic ongonites, appear as a dike swarm and have a similar composition. Topaz-lepidolite-albite pegmatites also share similar mineral assemblages with Li-F granites and ongonites but contain additional minerals like tourmaline and beryl. Li-F leucogranites are silica-rich (ranging from 70.5 to 75.6 wt.% SiO_2), peraluminous (A/CNK ranging from 1.17 to 1.32), and alkaline (with $Na_2O + K_2O$ ranging from 8.5 to 9.7 wt.% and A/NK ranging from 1.19 to 1.36). They are classified as A-type (A1) granites, plotted in the within-plate granite (WPG) field. These granites are significantly enriched in Rb, Cs, Ta, and Li while being strongly depleted in Sr, Ba, P, Ti, and Eu. Rare metal pegmatites of the LCT (Lithium, Cesium, Tantalum) type are high in F, Li, Rb, Cs, Nb, Ta, and Be but depleted in Sr, Ba, and Zr. Fluorine content is approximately 2% and can reach up to 4% in pegmatites and ongonites. The REE distribution, which shows a distinct tetrad effect, indicates relative enrichment in heavy rare earth elements (HREE). εNd varies from -3.1 to 3.4, and lead isotope data plot close to the orogenic curve and suggest that hydrothermal/metasomatic processes have not significantly modified the Pb isotopic system. Li-F granites and ongonites represent the final stage of highly fractionated, fluorine-rich granitic magma. The source of this granitic magma is inferred to be a biotite/phlogopite-bearing continental lithospheric source that contained a significant juvenile mantle-derived (basaltic) component enriched in incompatible trace elements. Late stage magmatic, water-rich fluids enriched in incompatible elements including Nb, Ta, Li, Sn, W and were responsible for the late- to post-magmatic alteration and associated mineralization.

Keywords: Lithium-fluorine granite, petrology, geochemistry, mineralization, Mongolia

PETROLOGICAL CHARACTERISTICS AND ORIGINS OF CARBONATITES FROM THE YONGHWA AND HONGCHEON COMPLEXES, SOUTH KOREA

Jieun Seo[1], Seon–Gyu Choi[1], Young Jae Lee[1*]

[1]Department of Earth and Environmental Sciences, Korea University, Seoul, 02841, KOREA

Carbonatite has been reported in two places, Yonghwa and Hongcheon in Korea. The Yonghwa phoscorite–carbonatite complex and Hongcheon carbonatite occur as an isolated individual body and dyke within the Precambrian gneiss in the northeastern part of Gyeonggi Massif. The phoscorite mainly consists of magnetite, olivine, apatite, carbonates, amphibole, and phlogopite. This phosphorite exhibits characteristics various assemblage from olivine-rich to apatite-rich types. The carbonatite composed of magnetite, apatite, monazite and various carbonate minerals such as calcite, dolomite, ankerite, and siderite. The $\delta^{13}C$ and $\delta^{18}O$ isotopic compositions respectively show −8.2 ~ −3.4‰ and 6.6 ~ 11.0‰ of carbonates in the Yonghwa phoscorite–carbonatite complex, indicative of a primary mantle source of the magmas. In addition, sulfur isotope compositions ($\delta^{34}S$ values of about 0.2 ~ 2.2‰) of the sulfides also indicates a mantle origin. Coexistence of silicate magma stage (phoscorite) and hydrothermal stage (carbonatite) are observed in Yonghwa, whereas carbonatite of the hydrothermal stage is solely observed in Hongcheon. Phlogopite by the fenitization shown ca. 193~195 Ma K–Ar ages in Yonghwa. Despite the Yonghwa phoscorite–carbonatite complex being relatively younger than the Hongcheon carbonatite, petrological, geochemical, and mineralogical evidence suggests a shared geological origin and formation period, indicating that both complexes represent similar intrusive processes.

GEOLOGY AND MINERALOGY OF THE NEW PORPHYRY COPPER MINERALIZATION OCCURENCE IN THE EASTERN BALKHASH REGION (KAZAKHSTAN)

Adilkhan Baibatsha[1]*, Daulet Muratkhanov[1], Bulegenov Kanat[1]

[1] Satbayev University, Geology and Oil-gas Business Institute named after K. Turyssov, 22 Satbaev str., Almaty 050013, KAZAKHSTAN
*Corresponding author: baibatsha48@mail.ru

Abstract

In Kazakhstan, the main porphyry copper deposits are located in the Balkhash region. The Konyrat, Aktogay, Aidarly, and Borly copper-porphyry deposits have been explored and exploited in this area. The main reserves of the country's copper raw materials are associated with these deposits. The Eastern Balkhash region is part of the North Balkhash ore zone. Previous studies on the Eastern Balkhash region focused on the Aktogay region and did not pay due attention to the southern part of the East Balkhash region, despite the fact that this region borders the Aktogay ore field and has prerequisites for the discovery of new ore sites. The geological structure of the area includes devonian and carboniferous terrigenous-effusive formations which are broken through by granitoid intrusions. Hydrothermal changes are widespread in the host rock and intrusive massifs. We have conducted cosmogeological studies and compiled a cosmogeological scheme of the territory with the allocation of ore-controlling annular and linear structures, the spread of areal bodies of intrusive rocks and metasomatic changes. According to the data of geological and cosmogeological studies, promising areas have been identified, within which geological and geophysical prospecting works have been carried out. According to the data of geophysical work, local anomalies have been identified for drilling mapping and prospecting wells. As a result of geological,

geophysical, drilling, mineralogical and petrographic studies in the buried intrusion of granitoids, a new promising sulfide copper-molybdenum mineralization was revealed.

Keywords: Kazakhstan, Prediction of ore deposits, Blind intrusion of granitoids, Porphyry copper deposits, Sulfide ores.

Introduction

In recent years, Kazakhstan has faced a growing shortage of mineral resources, including copper. The copper reserves in existing deposits are nearing depletion, and there are challenges in discovering new ones. This is largely because of the underdevelopment of methods for locating "blind deposits" in regions covered by sedimentary layers (Baibatsha et al., 2017).

The Eastern Balkhash region of Kazakhstan (Fig. 1) was not previously regarded as a promising area for copper ore exploration. However, there are known porphyry copper deposits, such as Aktogai and Aidarly, in its vicinity. Our scientific research, which involved developing a new theoretical framework and analyzing satellite imagery, has demonstrated that it is possible to identify potential areas for discovering new deposits in this previously overlooked region (Baibatsha and Muszynski, 2020), (Baibatsha et al., 2015). This paper outlines the geological characteristics of a newly identified porphyry copper occurrence.

Materials and Methods

We first analyzed satellite image data to clarify the structure of the area buried beneath the sedimentary cover and to plan prospecting activities. The initial remote sensing data were obtained from archived Landsat ETM+ and Aster satellite surveys, along with digital terrain models, including SRTM (2000y) and AsterGDEM (2011y). Following the interpretation of the satellite images, a geological structure map was created

Field geophysical surveys were conducted on magnetic anomalies. Mapping and exploratory wells were drilled at these geophysical anomalies, revealing a buried intrusive body of granitoids. Mineralogical analyses were performed on samples from borehole cores to investigate sulfide copper-molybdenum mineralization in hydrothermally altered granitoids.

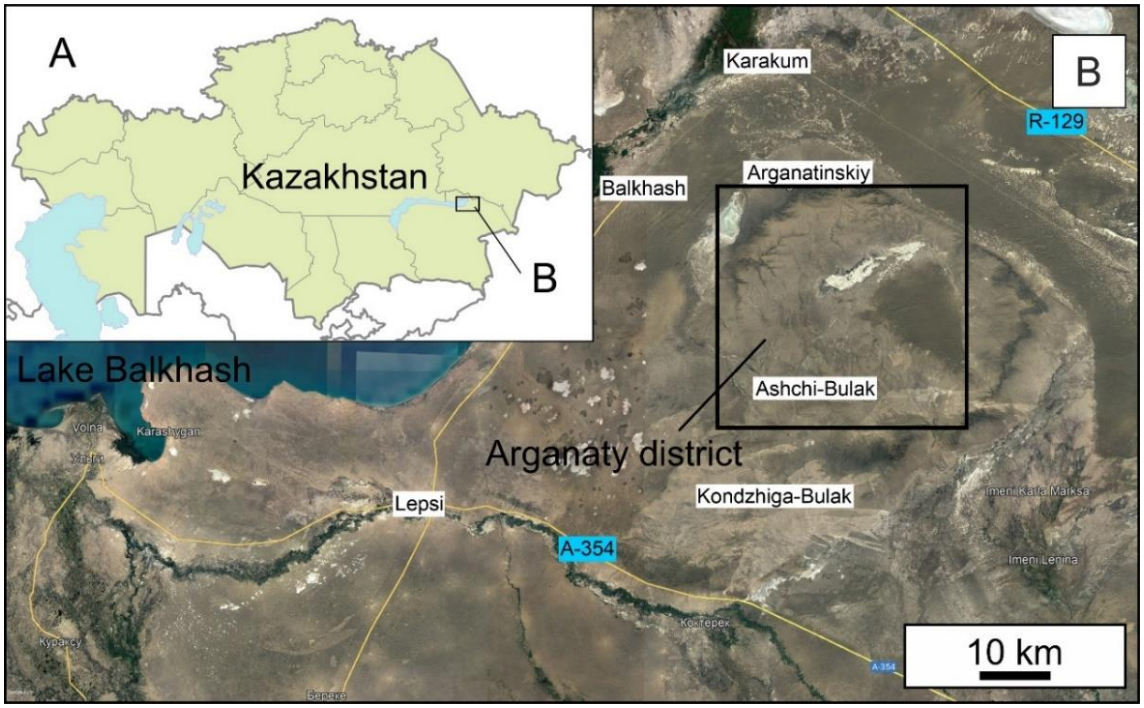

Fig. 1. A - Location of the Eastern Balkhash region on Kazakhstan map;
B – Borders of the Arganaty district

Results

The ore-controlling factors for the localization of mineralization within the studied area include ring structures, particularly their arc segments, and areas where these segments intersect with multidirectional faults. Other key factors are buried intrusive bodies, zones showing evidence of contact-metamorphic effects on the host rocks (such as skarns and hornfels), and areas displaying signs of hydrothermal-metasomatic alterations. Drilling at the II-5 site revealed a buried intrusive body, whose boundaries were delineated solely by geophysical data (Fig. 2). This felsic intrusive body is mapped in the central part of the area, and geological samples were collected from the borehole cores.

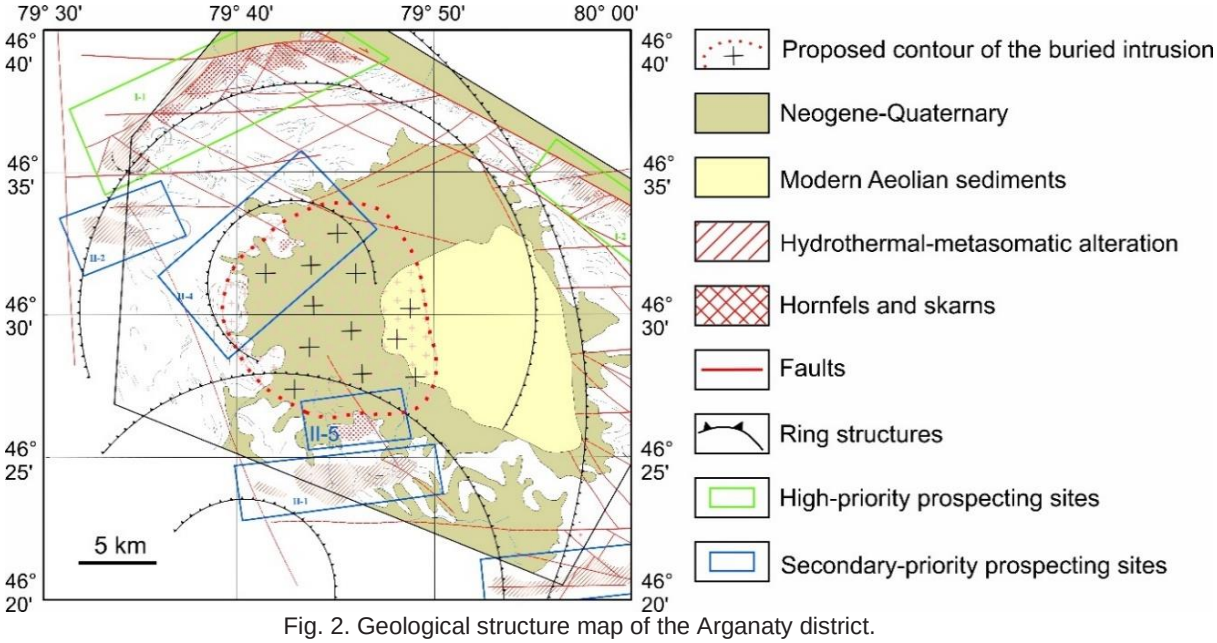

Fig. 2. Geological structure map of the Arganaty district.

A petrographic analysis of the core samples revealed that their composition is predominantly porphyritic biotite granodiorites, which are light-colored and exhibit varying degrees of silicification and metasomatism. Compared to the well-known Aktogai porphyry copper deposit, where K-feldspathization is common, albitization is observed in this area. Ore sulfide mineralization is associated with silicification, while molybdenum mineralization is linked to late vein quartz, overlying silicified and variably metasomatised light-colored porphyritic granodiorites. (Figs. 3, 4).

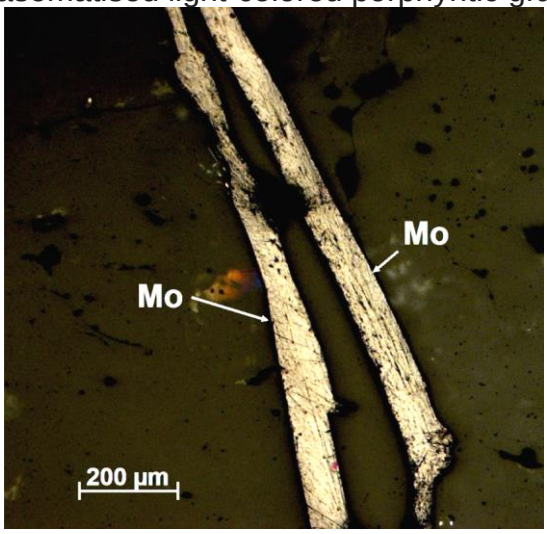

Fig. 3. Plates of molybdenite (Mo) in quartz

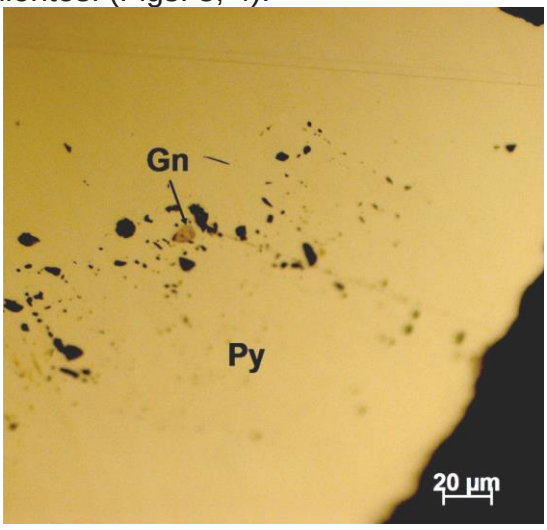

Fig. 4. Plates of molybdenite (Mo) in quartz, inclusions of galena (Gn) in pyrite (Py).

Discussion

There are certain similarities between the Arganaty site and the Aktogai ore district. Like the Aktogai group of fields, the area is located in the zone of a deep fault of the first internal ring structure (Fig. 5) (Baibatsha, 2017), (Baibatsha, 2022), (Baibatsha, 2020). The intru-sive massif of the Arganaty site, like the Aktogai deposit, is a blind intrusion. Both areas contain intermediate to felsic intrusions, many linear and ring structures and faults, and the rocks underwent hydrothermal alteration.

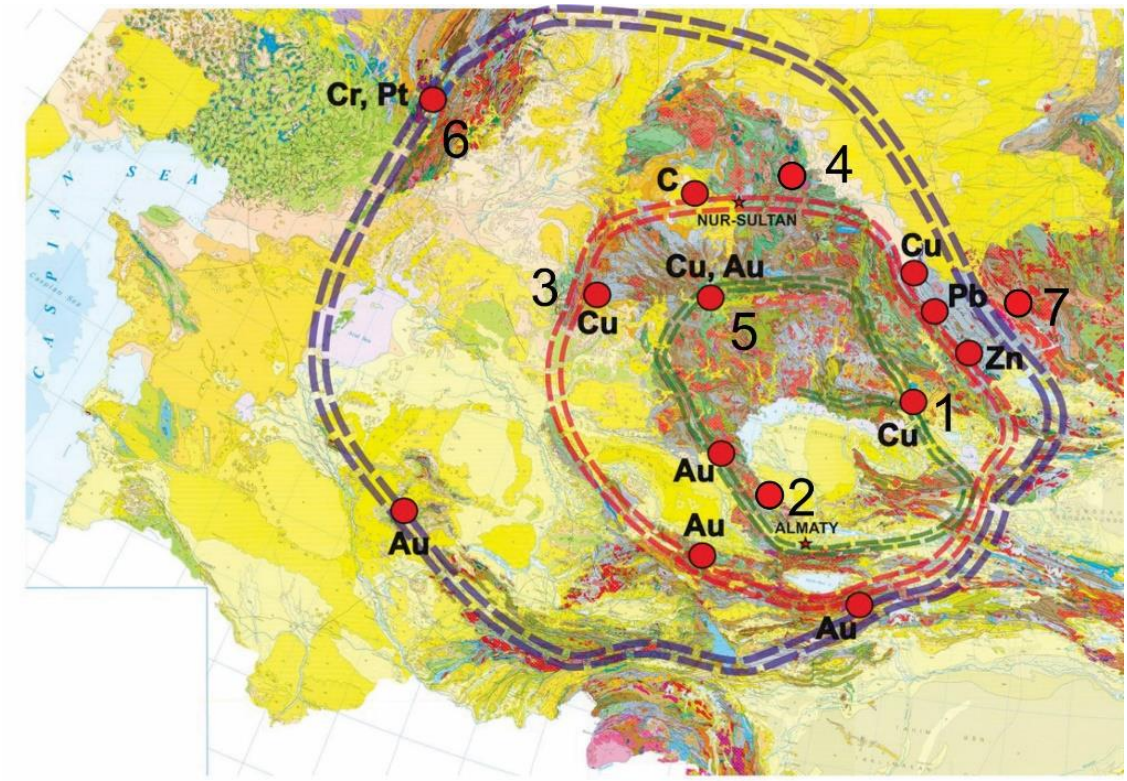

Fig. 5. The location of metallogenic zones of copper deposits (according to A.B. Baybatsha, 2017 with additions and changes by the authors). The numbers indicate the deposits: 1 – Aktogai, 2 – Nizhne-Ili, 3 – Zhezkazgan, 4 – Bozshakol, 5 – Samar, 6 – deposits of the Mugalzhar type, 7 – deposits of the Rudny Altai type (modified after Baibatsha, 2020)

Conclusion

Given the similarities to the Aktogai ore district, it is plausible that the mineralization in the Arganaty district is related to intrusive magmatism. Evidence of this includes a singular stock, magmatic ring structures, and zones of thermal impact on the host rocks within the region. It is anticipated that ores of copper, gold, molybdenum, zinc, lead, tungsten, and tin may be present. It is recommended to carry out prospecting in this area using ground geophysical surveys, drilling, and mapping of prospecting wells.

Acknowledgment(s)

This research was funded by the Science Committee of the Ministry of Science and Higher Education of the Republic of Kazakhstan under the grant project AP14870909.

References

Baibatsha, A., Arshamov, Y., Bekbotayeva, A., Baratov, R. Geology of the main industrial types of copper ore deposits in Kazakhstan. In: International Multidisciplinary Scientific GeoConference Surveying Geology and Mining Ecology Management, SGEM 2017, vol. 17/issue 1.1, pp. 231-238, Bulgary (2017).

Baibatsha, A.B., Muszynski, A. Geological-geophysical prospecting indicators of the Arganaty district predictive blocks (Eastern Balkhash). News of the National Academy of Sciences of the Republic of Kazakhstan, Series of Geology and Technical Sciences 2 (140), 31-39 (2020).

Baibatsha, A.B., Bekbotayeva, A.A., Mamanov, E. Detection of deep ore-controlling structure using remote sensing. In: International Multidisciplinary Scientific GeoConference Surveying Geology and Mining Ecology Management, SGEM 2015, pp. 113-118. Bulgary (2015).

Baibatsha, A.B. Geotectonics and Geodynamics of Kazakhstan Paleozoides from the Plume Tectonics Position (Kazakhstan), Advances in Science, Technology and Innovation, pp. 573–575 (2022)

Baibatsha, A. Relationship of paleozoides and mineral deposits of Kazakhstan with the paleozoic superplume. In: International Multidisciplinary Scientific GeoConference Surveying Geology and Mining Ecology Management, SGEM 2017, vol. 17/issue 11, pp. 479-486, Bulgary (2017).

Baibatsha A. Geotectonics and geodynamics of paleozoic structures from the perspective of plume tectonics: a case of Kazakhstan. International Journal of GEOMATE, July, 2020, Vol.19, Issue 71, pp. 194-202. ISSN: 2186-2982 (P), 2186-2990 (O), Japan, DOI: https://doi.org/10.21660/2020.71.31100. Geotechnique, Construction Materials and Environment.

HFSE MOBILITY IN SUBDUCTION ZONE: EVIDENCE FROM HP METAMORPHIC ROCK IN THE ZAVKHAN TERRANE, WESTERN MONGOLIA

Manzshir Bayarbold[1, 2], Atsushi Okamoto[1], Masaoki Uno[1], Otgonbayar Dandar[1, 2], Mayuko Fukuyama[3], Geri Agroli[1], Noriyoshi Tsuchiya[1, 4]*

[1] Graduate School of Environmental Studies, Tohoku University, Sendai, JAPAN
[2] Geoscience Center, MUST, Ulaanbaatar, MONGOLIA
[3] Graduate School of Engineering Science, Akita University, Akita 010-8502, JAPAN
[4] National Institute of Technology, Hachinohe College, Hachinohe, Aomori 039-1192, JAPAN

The subduction processes are pivotal in the cycling of numerous elements (e.g., Cl, B, large ion lithophile elements, Pb, Sr, U, S, and light rare earth elements) and some volatiles (H_2O and CO_2). High-pressure (HP) and ultrahigh-pressure (UHP) metamorphic rocks serve as critical natural laboratories for understanding element transport processes in deep subduction zones. High field strength element (HFSE; Ti, Nb, Zr, and Hf) mobilization has been recorded from HP and UHP metamorphic rocks due to multi-compound fluid rock interaction, which is presented by rutile (Rt) daughter crystal in fluid inclusion, Rt-bearing HP veins, differences in TiO_2 concentrations in bulk rock, and HFSE zonation in Rt. Moreover, experimental works aimed at deciphering the mobility of HFSE based on Rt under varying pressure and temperature condition have established that HFSE mobility increases in the order of salinity concentration in fluid. This research reports on the distribution of garnet and Ti-bearing minerals from the Khungui eclogite of the Zavkhan Terrane in Western Mongolia. The eclogite facies mineral assemblage in the Khungui eclogite featuring inclusions within the high–Ca rim composed of garnet, omphacite, barroisite, phengite, rutile, epidote, and quartz. The peak pressure estimated for the eclogite stage of the Khungui eclogite was 2.1–2.2 GPa and 580–610°C, with the *P*–*T* conditions of the decompression stage estimated at approximately 0.1–0.5 GPa and 575–635°C (Bayarbold et al., 2022). Garnet and quartz in the eclogite contain abundant primary fluid inclusions of varying salinities; H_2O-dominated saline fluids (13–16 wt.% NaCl eq.) during early eclogite stage, H_2O–CO_2-dominated hypersaline fluid (~32 wt.% NaCl eq., 7.3 wt.% CO_2 with variable solute components Fe, Mg, Ca, and K) at later eclogite stage, and H_2O-dominated saline fluid (12.5–16.3 wt.% NaCl eq.) throughout the exhumation stage (Bayarbold et al., 2023).

Within the eclogite sample, two types of garnet were identified, featuring dissimilar microstructures and compositional zoning: aggregate-type garnet with asymmetric zoning (Grt1) and euhedral garnet with symmetric zoning (Grt2). Grt1 and Ti-bearing minerals are closely associated with each other. The characteristics of major, trace elements, and microtextures of Grt1 and Ti-bearing minerals suggest that the nucleation of titanite and garnet was simultaneously accelerated by the destabilization of Ti-augite during pre-eclogite metamorphism, creating the aggregation textures of Ti-bearing minerals and Grt1 in the

Khungui eclogite. Based on major divalent elemental composition zoning and trace element characteristics, both Grt1 and Grt2 in the Khungui eclogite are formed simultaneously from the pre-eclogite to eclogite stages. The cores of Grt1 and Grt2 are attributed to Rayleigh fractionation or a diffusion-limited uptake process. In contrast, the growth mechanisms of the Grt1 rim and Grt2 rim are distinct during eclogite stage. The Grt1 rim is explained by a dissolution–reprecipitation, which resulted in the atoll texture observed in Grt1. For the Grt2 rim, it grew through a mechanism consistent with that of the Grt2 core. The major and trace element zonings of these garnets provide insights into element mobility related to Ti-bearing minerals and infiltration of high salinity fluids at different stages: (1) the mobilization of Ti and V increased under eclogite facies conditions (growth stage of garnet) compared to the pre-eclogite stage, with the mobility of Ti, Nb, Ta elements being pronounced under the exhumation stage (Rt–Ilm–Ttn2), possibly because of the infiltration of high-saline fluids and an increase in temperature, and (2) post-growth compositional modification of Grt1 was induced by a localized transport of Fe, Mg, Mn, and Ca elements in response to the replacement of ilmenite by titanite during decompression (0.1–0.5 GPa and 421–534°C). The contrasting zoning of garnet in Khungui eclogite indicates dissimilar scales of element mobility under eclogite facies conditions (over a thin section scale) and during decompression (up to several centimeters or beyond).

Keywords: HFSE mobility, Ti-bearing minerals, Garnet, Eclogite

AGE OF HADAASAN METAMORPHIC CORE COMPLEX

Javkhlanbold Dorjsuren[1], Chuluun Danzan[2]

[1]Mintores Co ltd.,
[2]Mongolian University of Science and Technology

Closing of the Mongol-Okhotsk ocean generated Khangay-Hentey fold-and-thrust belt at Permian-Jurassic. This arch-like orogen belt has been segmented and offset by major and minor transverse faults with right lateral strike slip component. Also, some extensional basins resulted formation in behind Permo-Triassic convergent suture zone. The Hadaasan metamorphic core complex is located along the one of major transverse fault at the outer middle part of Mongol-Okhotsk belt. Researchers reported that the metamorphic core complexes (MCCs) along the mostly outer rim of Mongol-Okhotsk belt in Transbaikalia and northern Mongolia has been formed in late Mesozoic time. 235U/238U and 207Pb/206Pb were measured in 2 samples (8801, 8802) from syn-tectonic sill formed aplitic dykes parallel to a foliation plane for the analysis of isotope ratios of Pb and U respectively, also geochemical characteristic determined in 12 samples. A total of about 150 zircon grains from samples 8801, 8802 were prepared for analysis and total 24-30 zircon grains were measured based on internal structure and texture comparison. Evaporation of zircon grains yielded a mean 207Pb/206Pb age of 269.2±1.4 (8801) and 270.7±1.6(8802) Ma that we consider to reflect the time of protolith emplacement. Also, coeval distribution determined in sample 8802 as 174.3±2.7 (172-205Ma), that we assumed exhumation age of metamorphic core complex.

The Hadaasan metamorphic core complex exhumed to the surface most likely due to NW-SE directed opening of a pull-apart basin occupying a dilatational stepover bridging the Tarna and Bad right-lateral strike-slip faults. The transtensional basin forming at the Tarna-Bad releasing bend took the form of rotating “domino” blocks bounded by synthetic normal faults resulting in a rolling-hinge style deformation. As a result, unmetamorphosed cover sediments are sliced and attenuated by copious arrays of moderate- to low-angle normal faults. Coeval with the onset of the exhumation of the Hadaasan metamorphic core complex, magma generated at greater depths by partial melting advected rather rapidly in order to restore isostatic equilibrium. Moreover, the residual fluids of the magmatic melts were emplaced along fracture networks and tectonic foliations forming pegmatite, aplite, and quartz veins that are largely concordant with tectonic foliations and often discordant with veins of preceding phases.

Such veins also commonly appear to have been folded in harmony with their host rocks (i.e. migmatite, gneiss, schist), boudinaged.

A COALBED METHANE RESERVOIR STUDY OF NARYN SUKHAIT COAL DEPOSIT, MONGOLIA

O.Javkhlan[1]*, P.Purev-Ochir[1], Ts.Sandagdorj[1], T.Delgerjargal[1], B.Badamgerel[1], N.Purevtogtokh[1], B.Dulguun[1], E.Tamir[1], V.Ganzorig[1, 2], B.Stats[2], Z.Tsetsen[1, 2]

[1]Telmen Resource LLC, Ulaanbaatar 13336, Mongolia
[2] TMK Energy Limited, Perth 6005, Western Australia
*Corresponding author: jotgonkhuu@tmkenergy.com.au

Mongolia has abundant coal resources and is exploring the potential for coal seam gas as a source of energy. Coal seam gas (also known as coalbed methane) is a type of natural gas that is found in coal seams.

The coal seam gas (CSG) exploration project is taking place in the South Gobi basin, which is a largest coal mining basin in Southern Mongolia. Main coal resource is hosted in Upper Permian, and Triassic-Jurassic sedimentary rocks.

Our project area (Gurvantes-XXXV) located in the western part of South Gobi basin. The Gurvantes-XXXV project area has a geologic history of continental accretion and basin and range-style crustal extension followed by compressional folding and faulting. The project area is dominated by elongate, east-west trending mountain ranges and intervening basins, which comprise sedimentary rocks of Late Cretaceous to Permian age, overlain a relatively thin Quaternary gravel layer or thin aeolian deposits.

The coal beds occur in the Late Permian Delinshand Formation, the Triassic Noyon Soum Formation and the Middle Jurassic Orgilokhbulag Formation.

Mountain ranges between the basins comprise mostly bimodal volcano-terrigenous rocks dominated by intermediate to high angle faults that show evidence for both compressional and extensional movement.

The coal-bearing Permo-Triassic-Jurassic sequences strike east west and in general dip to the south at about 15 to 30 degrees, although a number of localised synclinal and anticlinal structures are observed. Individual stratigraphic units can be mapped over a distance of 160km.

The existing coal mining and exploration projects within the Project area provide a large amount of detail on the coal quantities and depths. The low to medium ash, high volatile bituminous coking coals generally have an ash content of 7.0% to 19.8%, inherent moisture of 1.0% to 2.8% and density of 1.4g/cc to 1.7g/cc. The coal is comprised predominantly of vitrinite (bright coal) and has vitrinite reflectance (thermal maturity) ranging from VRo of 0.62% in the west to VRo of 1.49% in the east. This thermal maturity is more than sufficient to generate significant quantities of gas.

Our team have been conducted CSG study in the Naryn Sukhait coal deposit which is situated in the western part of the project area. The most prominent feature relating to the Naryn Sukhait coal deposit is the arcuate shape, which occurs along the east-west trending Naryn Sukhait fault. The coal-bearing section, interpreted to be Middle Jurassic in age, is primarily exposed in a window adjacent to this fault.

The coal occurs in three zones, unofficially termed an upper zone, a lower zone and a lowermost zone in the Naryn Sukhait coal deposit area. The gas content of the Naryn Sukhait area is 5.0-13.2 m3/t. Ash yield (dry basis [db]) ranges from 3.04% to 72.19% while volatile matter (dry, ash free basis [daf]) ranges from 34.73% to 55.89%.

In all upper, lower and lowermost coal zone gas contents increase with depth. Moreover, gas content increase with decreasing ash yield, this seems to be the main controlling factor on gas volume. Based on volatile matter data, the coal rank increases from the upper zone to

the lower zone, whereas the coal rank decreases from the lower to the lowermost coal zone. The average methane content ranged from 92% to 99%, with some variations of CO and C_2H_6 observed between the upper and lower seams.

All coal samples are rich in vitrinite, low in liptinite with moderate inertinite. Vitrinite reflectance (mean maximum on telovitrinite [Romax]) has an ranges of 0.85% to 0.99%.

Gas saturation in the upper coal seams ranges from 67% to 99%, while in the lower seams, it ranges from 37% to 83%. A decrease in vitrinite reflectance with increasing gas saturation was observed in the upper seams of some holes. An increase in the inertinite component and a decrease in the liptinite component from the upper to lower seams were observed.

The permeability of the upper coal zone ranges from 20 mD to 56 mD (millidarcies), which is relatively high for coal. On the other hand, the permeability of the lower coal zone is determined to be less than 0.1 mD, which is much lower than the upper coal zone.

The coals of Naryn Sukhait are characterized by having very low ash yield and high volatile matter compared to other coal deposits in the South Gobi basin. The coals of the South Gobi basin, in general, have lower moisture compared to those from other basins.

Contingent Resource estimate of 1.2 tcf, together with an updated Prospective Resource estimate of 5.3 tcf for the Nariin Sukhait coal deposit area completed by NSAI (2022). Three pilot wells drilled in the Naryn Sukhait area, and based on static and dynamic modeling conducted in 2022, it is estimated that these wells will produce a stable gas rate of approximately 1200 Msftd (million standard cubic feet per day) after 9 months of dewatering. Furthermore, the modeling suggests that the dewatering rate will decrease from approximately 4000 barrels of water per day (bwpd) to 1200 bwpd in the initial 36 months of production.

IMPACT OF ENGINEERING PARAMETERS ON MARCELLUS SHALE GAS PRODUCTION: A DATA ANALYTICS APPROACH

Md Mostafijul Karim[1], Jeremy M. Gernand[1], John Wang B[1]

[1] The Pennsylvania State University, University Park, PA 16802 U.S.A

Abstract

Recent advanced hydraulic fracturing practices in Marcellus shale have eased a significant growth in gas production. However, the effectiveness of hydraulic fracture stimulation in horizontal wells is not yet fully understood. Using data analytics, this study aims to identify factors influencing gas recovery by establishing correlations between gas production performance and various engineering parameters. A representative sample of 2311 gas-producing wells in Pennsylvania's northern zone of the Marcellus shale, selected from all active wells, provided complete datasets, including location, completion data, hydraulic fracture treatment data, and production data. The statistical analysis, including traditional regression and advanced statistical methods, explores the relationship between well performance and engineering attributes. Factors analyzed included number of hydraulic fracture stages, lateral length, measured depth, proppant weight, fracture fluid volume, and treatment rate. Engineering parameters evolution over time established this zone's shale gas development trend. From 2010 to 2021, lateral length increased from 3016 ft to 9759 ft, with a mean of 6734 ft and a standard deviation of 40%. During the same period, pounds of proppant increased from 4 million to 21 million pounds, with an average of 7 million pounds. The relationship between production and the stimulation and completion parameters provided a better understanding of production optimization. Pounds of proppant is identified as the most influential factor among the engineering parameters. Single parameter analysis indicates a strong relationship between proppant and production, and principal component analysis indicates it account for the highest variance, 22.82%. Additionally, number of stages and total fracture fluid volumes are also significant, as gray correlation analysis demonstrates that both are highly correlated with pounds of proppant. The findings give valuable insights into the

trends affecting well performance in the Marcellus Shale and provide a foundation for optimizing stimulation treatments and well completions in Marcellus shale development.

Introduction

Marcellus shale is a geological formation in the Appalachian Basin, covering parts of Pennsylvania, West Virginia, New York, Ohio, and Maryland. Marcellus shale is distinguished by its rich organic content and substantial thickness, ranging from 50 to 200 feet. The formation's depth varies between 4,000 and 8,500 feet below the surface, with the most productive areas in the northeastern United States. The shale's composition is predominantly clay, quartz, and organic material, with minor components such as pyrite and calcite. Organic matter, mainly Type II kerogen derived from algae and plankton, is crucial for its gas generation potential. Thermal maturity, typically measured by vitrinite reflectance (Ro), increases west to east within the Marcellus Shale, significantly influencing hydrocarbon generation. The vitrinite reflectance (Ro) value ranges from 0.8% to 2.5% [1]. Higher Ro values indicate greater thermal maturity with Ro values exceeding 1.0% considered mature for gas generation.

Marcellus Shale exhibits low porosity, typically between 0.5% and 5%, and low permeability, around 10^{-4} md. However, the induced fracture network from hydraulic fracturing, which intensely improves the shale's permeability, increases the potential for gas production. Stratigraphically, the Marcellus Shale sits above the Onondaga Limestone and beneath the Hamilton Shale Member of the Hamilton Group. It was deposited in a marine environment in the Middle Devonian period, where anoxic environment favored the preservation of organic matter. The formation is one of the most organic-rich shales in North America, with an average organic carbon content ranging from 3% to 14%. The sedimentary layers of the Marcellus Shale consist of black, fissile shale with occasional interbeds of limestone and dolostone. The formation's stratigraphy is divided into several members, with the lower Marcellus typically having higher organic content and better reservoir characteristics [2,3]. In Pennsylvania, Marcellus Shale's gas production is particularly prolific, and the northeastern part of the state is in a dry-gas window. Thick shale layers, high thermal maturity, and optimal geological conditions are favorable for gas accumulation in this region. The Ro value varies from 1.0% to 2.0%, making it highly productive for natural gas generation. The paper will consider this region for the analysis.

Previous studies have explored various aspects of data analysis techniques to investigate the relationship between engineering and geological parameters and shale gas production. Reference [4] proposed a method for predicting shale gas production by analyzing the relationship between various engineering parameters and gas production rates for 180 wells in the Fuling gas reservoir, China. Under the principal component analysis (PCA) and backpropagation neural-network context, the primary methodology involves standardizing the data, efficiency. They identified the number of stages, horizontal length, fluid volume, and cluster spacing as crucial factors, with the first two accounting for 64% of the total variance. Reference [5] integrated analytical modeling and data analysis to investigate the relationship between engineering parameters and shale oil and gas production. The process involves modeling production behavior under various conditions using the F.A.S.T. program and assessing how sensitive production is to these parameters. Key findings indicate that production rates increase with longer horizontal wells, closer fracture spacing, greater fracture half-length, and higher fracture conductivity. Moreover, there is an optimal value for each parameter beyond which additional increases do not significantly enhance production and may lead to higher operational costs. However, according to the analytical model, the parameters' impact on production rates is not the same as observed in real-field analysis, limiting the approach. Reference [6] analyzed data from 187 wells in the Marcellus Shale in West Virginia using data mining techniques to identify correlations between production rate and various completion and geological parameters. They categorized the geological settings into four subgroups and analyzed completion parameters such as the number of hydraulic fracture stages, lateral length, vertical depth, proppant, and fracture fluid volume through regression analysis. Using PCA and clustering methods, they identified the number of stages as the most

significant parameter, with fracture fluid volume and proppant mass being relatively important for more brittle lithologies. Reference [7] used a self-organizing mapping technique to evaluate the performance of different proppants and to correlate completion parameters and production performance, based on reservoir and completion data from the North Texas Barnett shale zone. Reference [8] used the same methodology to investigate hydraulic fracture efficiency by analyzing completion parameters and productivity. Multivariable regression analysis is also used to investigate the mutual relationship between the completion design, reservoir properties and production data [9]. However, a better understanding of the effectiveness of hydraulic fracturing is still challenging. This study aims to apply data analytics to establish a correlation between dry shale gas production performance and different engineering parameters, focusing on Marcellus shale. A representative sample of 2311 wells provided complete datasets, including location, completion, hydraulic fracture treatment, and production data. The study utilizes traditional regression and advanced statistical methods to analyze the factors including the number of hydraulic fracture stages, lateral length, vertical depth, proppant volume, fracture fluid volume, and treatment rate. In addition, evaluating different parameters over time establishes this zone's shale gas development trend.

Data and Methodology

A. Data Source and Quality

The study utilized data from four distinct sources: the U.S. Energy Information Administration (EIA), the Pennsylvania Department of Environmental Protection (DEP), the Pennsylvania Geological Survey's Exploration and Development Well Information Network (EDWIN), and Drillinginfo. The first two sources are publicly accessible and are updated regularly. EDWIN and Drillinginfo are comprehensive data repositories that contain an extensive array of well-related information utilized by industry professionals and researchers and are periodically reviewed and updated.

B. Data Processing

Data processing involves several key steps to compile and organize data from multiple sources into a comprehensive and consistent format. Monthly production data was obtained from the Pennsylvania Department of Environmental Protection (DEP). A MATLAB script was developed to reorganize the data into a chronological monthly format, using unique identifiers such as county, municipality, permit number, latitude, and longitude. These identifiers were used to integrate the dataset and represent distinct wells from 2010 to 2023. Permit numbers were converted to API14 format to reconcile production data with well information. Well information and production data were sourced from the Drillinginfo. The data was filtered based on parameters like sub-play and producing formation to select wells specific to the Marcellus region. Well completion and drilling data were compiled from the Exploration and Development Well Information Network (EDWIN). To create a comprehensive dataset, well information, production, completion, and drilling data were consolidated into a single sheet using another MATLAB script. This script merged data based on the unique API14 number, adding new entries if the API14 number from subsequent datasets did not match existing ones.

C. Data Analysis

Data screening process involves the identification and removal of outliers. In the Exploratory Data Analysis (EDA) phase, the distribution of each parameter is examined through histograms and probability density functions (PDFs). Key statistical measures such as mean, median, and variance are calculated to provide a comprehensive understanding of the data's characteristics. The study also includes a time evaluation component, where the temporal evolution of key parameters is investigated from 2010 to 2023. The analysis is utilized to identify trends, patterns, and changes over time, providing insights into the temporal dynamics of the dataset.

Assuming all the parameters are independent, the regression analysis is then conducted to model the relationships between production rates and various engineering parameters. Multiple linear regression techniques are employed, and model performance is evaluated using R-squared values and significance tests to ensure robustness and reliability. For multivariable analysis, the data are standardized considering their mutual relationship. Gray

correlation analysis identifies the highly correlated data, thus reducing the redundancy of the data. Finally, Principal Component Analysis (PCA) is applied for dimensionality reduction, identifying key components that explain the most variance in the dataset.

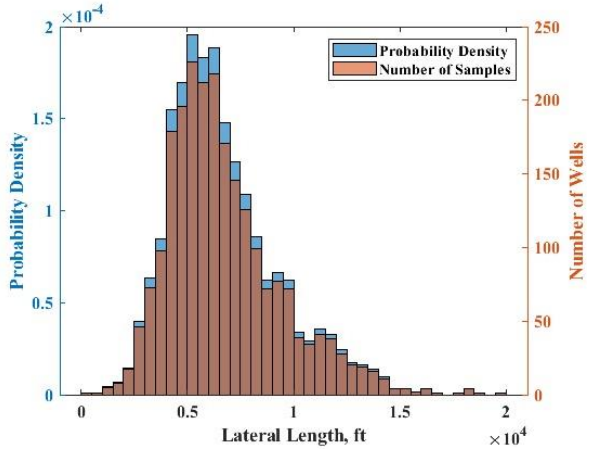

Fig. 1 Probability density and histogram of lateral length

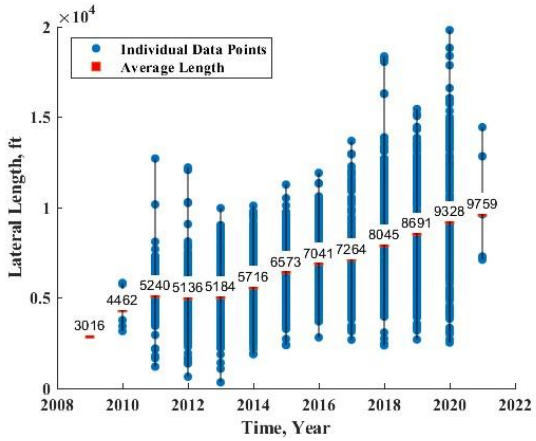

Fig. 2 Lateral length evolution from 2010 to 2021

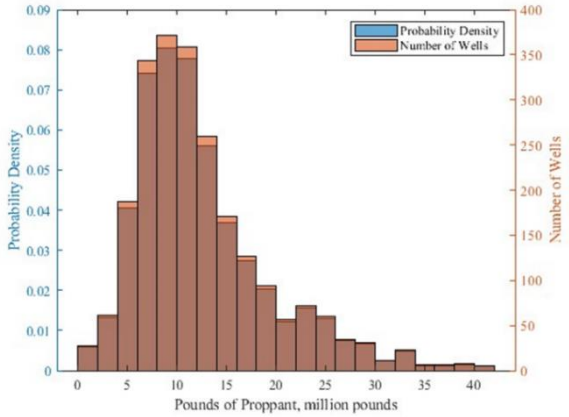

Fig. 3 Probability density and histogram of pounds of proppant

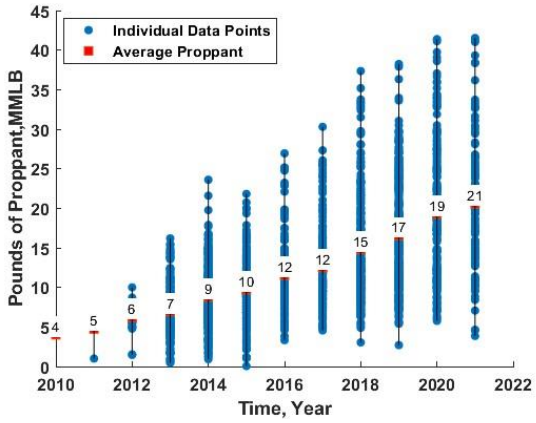

Fig. 4 Pounds of proppant evolution from 2010 to 2021

Results and Analysis

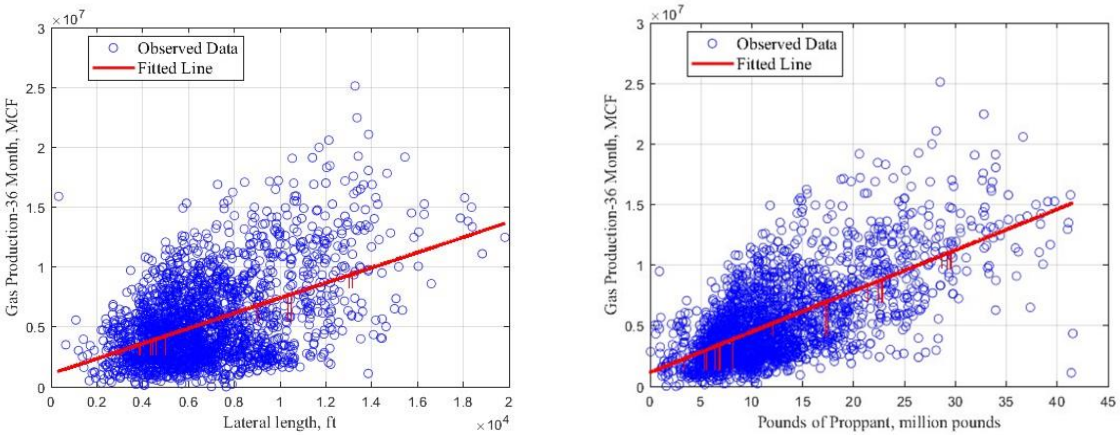

Fig. 5 Regression analysis of lateral length (top) and pounds of proppant (bottom)

A. Engineering Parameters

This study considered eleven engineering parameters, which are influencing the gas production in shale reservoirs. Number of stages refers to the total fracturing segments along the wellbore, while the lateral length denotes the length of the well drilled horizontally through

the shale formation. Cluster spacing is the distance between clusters within each stage. Treatment rate is the speed (BPM) at which fracturing fluids are injected into the well, impacting the creation of fractures. Treatment pressure, measured in psi, represents the inlet pressure during the treatment process. Pounds of proppant pertains to quantity of proppant used to prop open the fractures. Stage spacing is the mean length of each fracturing stage along the wellbore. Proppant concentration refers to the weight of proppant per unit of fracture fluid, measured in pound per gallon.

B. Exploratory Data Analysis

For the analysis, a histogram was generated, probability density was investigated, and time evolution was evaluated for all the parameters mentioned in previous section. In this section, we will detail the analysis results for lateral length and pounds of proppant. The remaining parameters will be summarized through a discussion on Table 1.

Table 1. Sumarry of analysis results

Parameter	Lateral Length	Total volume of fracture fluid	Pounds of Proppant	Treatment Rate	Treatment Pressure	Number of Stages	Proppant concentration	Fluid per Length	Measured Depth	Stage Spacing	Shots per Stage
	ft	thousand bbl	million pounds	BPM	psi		lb/gal	bbl/ft	ft		
Mean	6734	235	13	91	8147	31	1	35	14456	245	41
Standard Deviation	2671		7	11	824	16	0	13	2737	101	9
Median	6233	204	11	92	8129	28	1	35	14003	205	40
Kurtosis	1	3	2	3	0	2	4	7	1	2	3
Skewness	1	1	1	-1	0	1	1	1	1	2	-1
Range	19488	846	41	111	5811	116	4	136	19889	685	71
Maximum	19820	858	42	126	10637	124	4	139	26838	693	72
Confidence Level (95.0%)	109	5	0	0	34	1	0	1	112	4	0

Lateral length is the extent of the well drilled horizontally through the shale formation. A longer lateral section intersects more natural fractures and accesses a greater reservoir volume, increasing potential gas production. Reference [4] found that horizontal length contributes 21.4% to the total variance in gas production. The length of a horizontal well has been found to positively correlate with production [5]. Longer wells are associated with higher production, and cost. Fig. 1 shows the distribution of the lateral length in the Marcellus from 2010 to 2021, with a mean of 6734 ft and a standard deviation of 2669ft, indicating significant variability. 95% confidence intervals for the mean are 6625 ft to 6842 ft and standard deviation from 2595 ft to 2749 ft, highlight this spread. Kurtosis denotes whether extreme values are more common than expected in a typical normal distribution. Fig. 2 shows the lateral length evolution over time. From 2010 to 2021, lateral lengths in shale gas wells have shown a noticeable increase. The average length grew from around 4462 ft in 2010 to approximately 9759 ft in 2021. This reflects a double increase over eleven years. This was attributed to completion techniques and improved technology. Proppants ensure higher conductivity in hydraulic fracturing by providing stability to the aperture of the fracture. Fig. 3 shows the distribution of pounds of proppant with a mean value of 13 million pounds and standard deviation of 7, indicating considerable variability in the amount used across different wells. From 2010 to 2021, the pounds of proppant used in shale gas wells generally increased, as shown in Fig. 4. The average weight started at approximately 4 million pounds in 2010 and reached 21 million pounds in 2021.

Table 1 summarizes the analysis results of all parameters. In addition to usual statistical parameters, kurtosis measures the sharpness of the data distribution peak, with higher values indicating a higher outlier's existence. Skewness represents the symmetry of the data

distribution: a positive skewness indicates longer tails on right-side, while a negative indicates flatter shape in left side. Total volume of fracture fluid shows significant variability, with a large range and high standard deviation, indicating a broad spread in fluid volumes used. Treatment rate is relatively consistent with a small standard deviation and narrow range. A diverse treatment pressure is evident as it has notable variability with a wide range and moderate standard deviation. Number of stages displays moderate variability, but with a high mean and relatively low standard deviation, indicating a common range of stages considerable variance. Proppant concentration is highly consistent with minimal variation, reflecting a standard concentration across treatments. Fracture fluid volume per length shows very little variability, suggesting uniformity in fluid distribution relative to the length. Stage spacing exhibits a high degree of variability with a broad range, indicating diverse spacing practices. Shots per stage shows relatively low variability, suggesting a consistent approach in number of shots used per Stage. In summary, except for treatment rate, proppant concentration and shots per stage, all other parameters show considerable variance Fig. 5 presents the regression analysis results of 3-year gas production with lateral length and pounds of proppant. Both parameters exhibit a moderate linear correlation. Using the least squares method for curve fitting, the slope for lateral length indicates a change of 633 thousand cubic feet in gas production per unit change in length over 36 months of production.

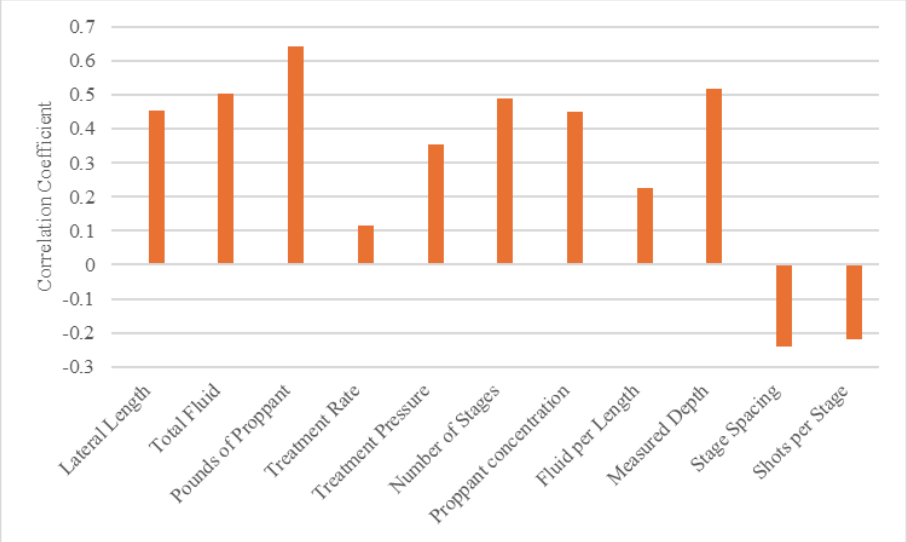

Fig. 6 Correlation coefficients of different engineering parameters

The relationship with proppant weight is stronger, with the calculated slope showing an increase of 337 thousand cubic feet per million pounds of proppant. Fig. 6 summarizes the results of the regression analysis. Pounds of proppant exhibit the highest correlation coefficient, indicating the most linear relationship with production among all parameters. Total volume of fracture fluid and measured depth show an equal degree of correlation with production. It is evident that stage spacing has an inverse relationship with production, as greater spacing suggests fewer perforations or a more limited fracture network. Conversely, the number of shots per stage also shows an inverse relationship, potentially due to densely perforated stages reducing the well's production potential. The time evolution of the correlation coefficient indicates that over longer periods, nearly all parameters demonstrate improved performance. For treatment rate, the correlation coefficient increased by 37% from 3 months to 3-years of production, while for total fracture fluid volume, the increase is 9%. The trends show a slight decrease at the six-month mark, which is attributed to the high initial production often observed in stimulated horizontal wells due to flowback effects.

Table 2. Principal component score coefficient

Parameters	PC1	PC2
Pounds of Proppant	0.52	0.023

Fracture fluid volume per length	0.178	0.22
Proppant concentration	-0.22	0.46
Stage spacing	0.50	-0.28
Lateral Length	-0.02	0.66
Shots per stage	0.25	0.47
Treatment rate	0.44	-0.013

Table 3. Total variance of interpretation

Parameters	Variance percentage	Cumulative percentage
Pounds of proppant	22.84	22.84
Lateral Length	17.04	39.88
Shots per stage	15.77	55.65
Fracture fluid volume per length	14.19	69.85
Proppant concentration	12.43	82.29
Stage spacing	9.54	91.836
Treatment rate	8.16	100

C. Multiple Variable Study

For multivariable analysis, we considered the inter-relationships between the parameters. Due to the varying units of these parameters, standardization was performed by scaling each parameter to its standard deviation, resulting in standardized values with a mean of zero and a standard deviation of one. Gray correlation analysis on these standardized values revealed that number of stages, pounds of proppant, and total fluid were highly correlated. Similarly, measured depth and lateral length formed another correlated pair. Based on these findings, the number of stages, total fluid, and measured depth were excluded from further analysis, leaving the remaining parameters as independent variables. Tables 2 and 3 present these independent variables' principal component analysis results. The component score coefficients identified two main pairs: pounds of proppant with average stage spacing, and lateral length with short per stage. Finally, the total variance showed that pounds of proppant had the highest variance (22.84%), indicating that this parameter is the primary factor influencing production performance in the dry gas zone of the Marcellus.

Conclusions

An efficient completion design is crucial for ensuring effective hydraulic fracturing, which leads to improved production performance. This research assessed the impact of engineering parameters on dry shale gas production from the Marcellus shale. Findings are as follows:

1.Probability density analysis and histogram indicate that most parameters show an increasing trend, attributed to longer well drilled using advanced technologies. Particularly, from 2010 to 2021, lateral length increased from 3,016 feet to 9,759 feet, with an average of 6,734 feet and a standard deviation of 2671 feet. Similarly, pounds of proppant rose from 4 million to 21 million pounds, with an average of 13 million pounds. The distribution variance reveals that proppant concentration and shots per stage remain consistent with current industry practices in the dry gas region.

2.Pounds of proppant exhibits the strongest correlation with production, followed by volume of fracture fluid, measured depth, number of stages, and lateral length.

3.The influence of pounds of proppant, lateral length, total fluid, and treatment rate becomes more significant over longer flow periods.

4.Principal component analysis reveals that pounds of proppant account for the highest variance at 22.82%, highlighting its impact as the most critical factor in the completion design for this dry gas region. Number of stages and total fracture fluid volumes are also significant, as gray correlation analysis shows a strong correlation between these factors and pounds of proppant. Lateral length and shots per stage rank second and third, respectively

References

Kissel, R. R., et al. (2014). Characterization of thermal maturity in the Marcellus Shale. AAPG Bulletin, 98(10), 2125-2147.

Harper, J. A. (2008). The Marcellus Shale—An Old "New" Gas Reservoir in Pennsylvania. Pennsylvania Geology, 38(1), 2-13.

Darrah, T. H., Jackson, R. B., Vengosh, A., Warner, N. R., Whyte, C. J., Walsh, T. B., ... & Poreda, R. J. (2015). The evolution of Devonian hydrocarbon gases in shallow aquifers of the northern Appalachian Basin: Insights from integrating noble gas and hydrocarbon geochemistry. Geochimica et Cosmochimica Acta, 170, 321-355.

Li, T., Tan, Y., Ahmad, F. A., & Liu, H. (2020). A new method to production prediction for the shale gas reservoir. Energy Sources, Part A: Recovery, Utilization, and Environmental Effects, 1-14.

Xu, B. X., Bai, Y. H., Chen, G. H., & Feng, R. Y. (2015). The impact of engineering parameters on shale oil and gas production: theory and practice, (2), 24-31.

Zhou, Q., Dilmore, R., Kleit, A., & Wang, J. Y. (2014). Evaluating gas production performances in marcellus using data mining technologies. Journal of Natural Gas Science and Engineering, 20, 109-120.

Soeder, D. J., & Borglum, S. J. (2019). The fossil fuel revolution: Shale gas and tight oil. Elsevier.

Mousavi, S. M., Lari, K., Salehi, G., & Torabi Azad, M. (2020). Technical, economic, and environmental assessment of flare gas recovery system: a case study. Energy Sources, Part A: Recovery, Utilization, and Environmental Effects, 1-13.

Lane, H. S., Lancaster, D. E., & Watson, A. T. (1991). Characterizing the role of desorption in gas production from Devonian shales. Energy Sources, 13(3), 337-359

DETERMINATION OF THE HEAT BALANCE DURING THE FORMATION OF ASPHALTENE, PARAFFIN SEDIMENTS

Oleksandr Pashchenko[1]*, Volodymyr Khomenko[1], Boranbay Ratov[2], Vitalii Petrenko[3], Ostap Fedick[4]

[1]Dnipro University of Technology, Department of Underground Mining, 19 Yavornytskoho Ave., 49005 Dnipro, UKRAINE
[2]Satbayev University, 22a Satpaeva str., 050013, Almaty, KAZAKHSTAN
[3]Ukrainian State University of Science and Technologies, Gagarina ave., 4, 49600, Dnipro, UKRAINE
[4]Drogobych Applied College of Oil and Gas, Hrushevsky St., 57, Drohobych, 82100, UKRAINE
*Corresponding author: pashchenko.o.a@nmu.one

Abstract

The article provides a analysis of the formation and prevention of asphalt-resin-paraffin sediments (ARPS) in oil production, transportation, and storage systems. ARPS, which includes components such as paraffins, asphaltenes, and resins, precipitates onto the inner surfaces of pipes and other equipment, leading to a significant reduction in oil flow efficiency and increasing operational costs. The article explores the various stages where ARPS occurs, from the oil reservoir to the surface pipelines and storage tanks. It highlights the key factors contributing to ARPS formation, including changes in pressure, temperature, gas release, and fluid velocity during oil extraction and transportation. Additionally, it discusses how the thermodynamic properties of oil, such as the saturation pressure and paraffin melting point, influence the sedimintation process. The paper introduces mathematical models and formulas to predict the conditions under which paraffin crystallization and sedimintation occur. Furthermore, the study examines three primary mechanisms of ARPS formation: crystallization on surfaces, sedimentation in the bulk of the oil, and a mixed mechanism combining both processes. The article concludes that preventive measures, such as thermal methods, are the most effective for controlling ARPS, although the optimal solution must be determined based on the specific conditions of each oil well. This paper serves as a valuable resource for understanding the challenges of ARPS and the methods used to manage it in the oil industry.

Keywords: asphalt-resin-paraffin sediments (ARPS), oil extraction, paraffin crystallization, pressure drop, temperature decrease, thermal resistance, oil well

Introduction

Formation of asphaltene-resin-paraffin sediments (ARPS) - components of oil that settle on the inner walls of pipes and other equipment and complicate its extraction, transfer and storage on the inner walls of oil production equipment (fig. 1) and their removal/prevention is one of the main problems of the oil producing industry. Asphalt-resin-paraffin sediments (ARPS) are found at all stages of oil production and transportation: in the productive formation, in production wells, in flow lines, in pipelines and in tanks. Formation of solid organic sediments in the bottomhole formation zone worsens the filtration-capacitive properties. Formations on the inner surface of lift pipes and pipelines lead to a decrease in the live cross-section, respectively, to a decrease in well productivity and pipeline throughput. Sedimentation of paraffin particles in product storage tanks contributes to the loss of useful volume (Kozhevnykov et al., 2020, Khomenko et al., 2023, Punase et al., 2023, Pashchenko et al., 2024).

The amount of ARPS may vary depending on the well depth, oil composition, and temperature. The melting point of paraffin, in turn, is directly proportional to the molecular weight. The density of paraffins in the solid state is within 865-940 kg/m^3, in the molten state - 777-790 kg/m^3. The key components of the sediments are paraffins, the content of which is 20-70% of the mass, and asphaltene -resinous compounds - 20-40% of the mass (Al-Yaari, 2011).

Figure 1 – Condition of pipes affected by ARPS complications

A number of conditions are of great importance for the formation of ARPS during oil production (Valiev et al., 2019, Khomenko et al. 2024):

- a decrease in the pressure at the bottomhole and the associated changes in the hydrodynamic equilibrium of the gas-liquid system;
- increased gas emission;
- reduction of temperature in the oil reservoir and well pipes;
- change in the flow rate of the liquid-gas mixture and its individual components;
- the composition of hydrocarbons in each phase of the gas-liquid system;
- the proportions of oil and water.

Process of the heavy oil sediments, asphaltene sedimentation

ARPS is formed at various depths, and the location of the deposit formation also depends on the operating mode of the oil well (fig. 2). The key thermodynamic factors influencing the formation of sediments are a decrease in pressure and temperature. Oil degassing also significantly affects the rate of the process paraffinization.

The rapid sedimentation of ARPS is facilitated or hindered by the following conditions (Chi et al. 2017, Belsky et al., 2018):

- the presence of high-molecular hydrocarbon compounds in oil;
- reduction of reservoir pressure to saturation pressure;
- reducing the flow temperature to values at which the solid phase is released from the oil;
- use of a low-temperature substrate on which crystals of high-molecular hydrocarbons are formed with sufficiently strong adhesion to the surface.

As the temperature drops and gas is released from the oil, its dissolving capacity in relation to paraffins decreases (fig. 3). The patterns of temperature change along the well depth depend on the transfer of thermal energy to the rocks surrounding the well by the liquid flowing through the well pipes. The difference in temperature between the liquid and the surrounding

rocks at a certain well depth increases the intensity of heat transfer. The increase in the rate of heat transfer is indicated by the thermal conductivity of the medium in the intertube space. According to experimental data [7], the temperature along the well is determined by such factors as heat transfer, and consequently, the well flow rate (El-Dalatony et al., 2019, Bissengaliev et al., 2022).

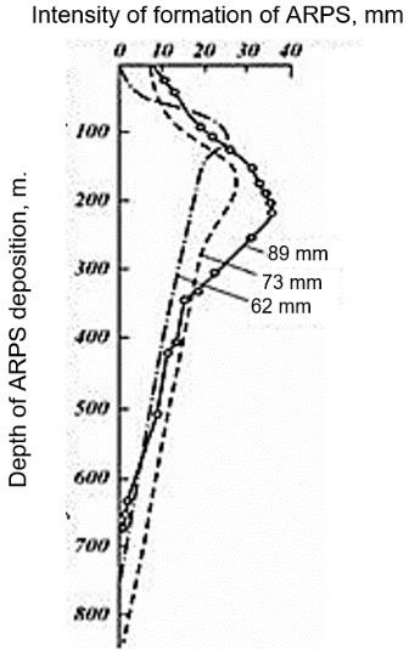

Figure 2 – Formation of sediment in a well

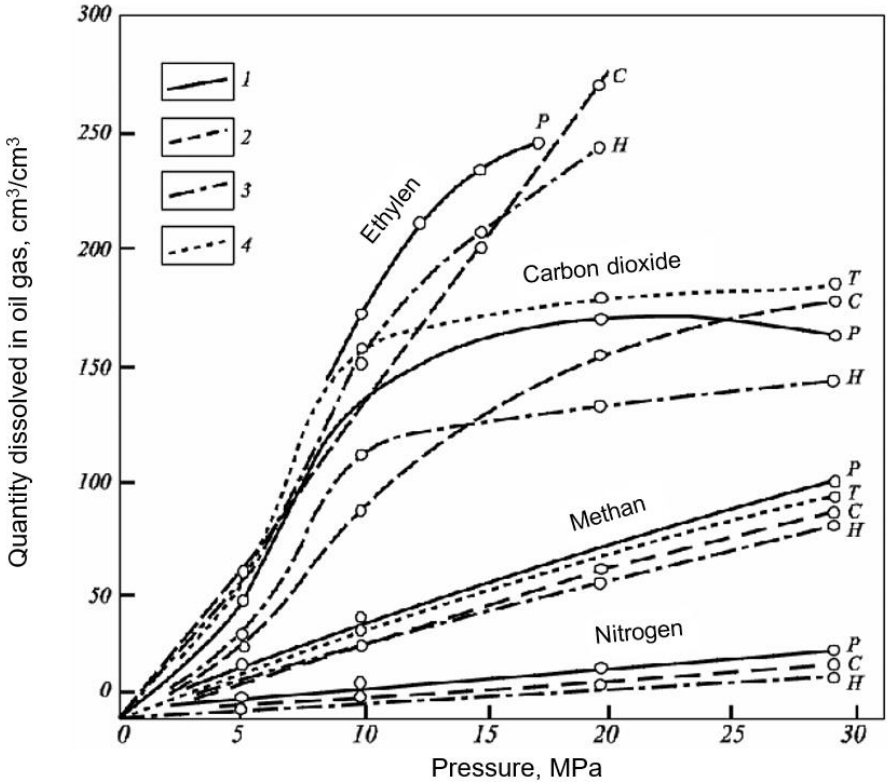

Figure 3 – Isotherms solubility gases at a temperature of 50° C in oils:
1 – Romashkinskaya (P); 2 – Surakhanskaya (C); 3 – Nebitdagskaya (H); 4 – Tuymazinskaya (T)

When the pressure decreases compared to the saturation pressure, gas and solid hydrocarbons are released from single-phase oil, the amount of which increases with distance from the point of equal pressure to the wellhead. Since gas moves faster than liquid, the

thermobaric conditions change rapidly along the length of the flow. Both the pressure and temperature in the flow of the produced formation fluid decrease (Togasheva et al., 2024, Wang et al., 2014, Souas et al., 2020, Rehan et al., 2016).

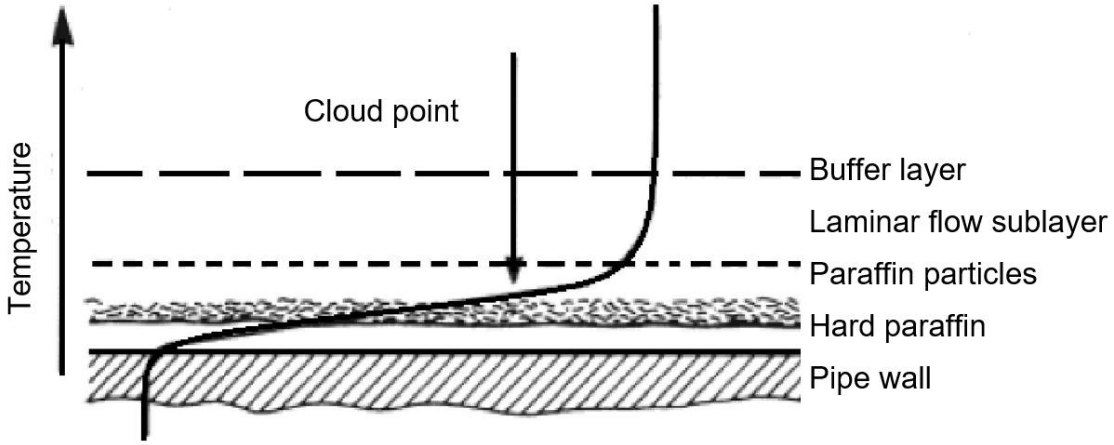

Figure 4 – Temperature profile in the longitudinal section of the pipe

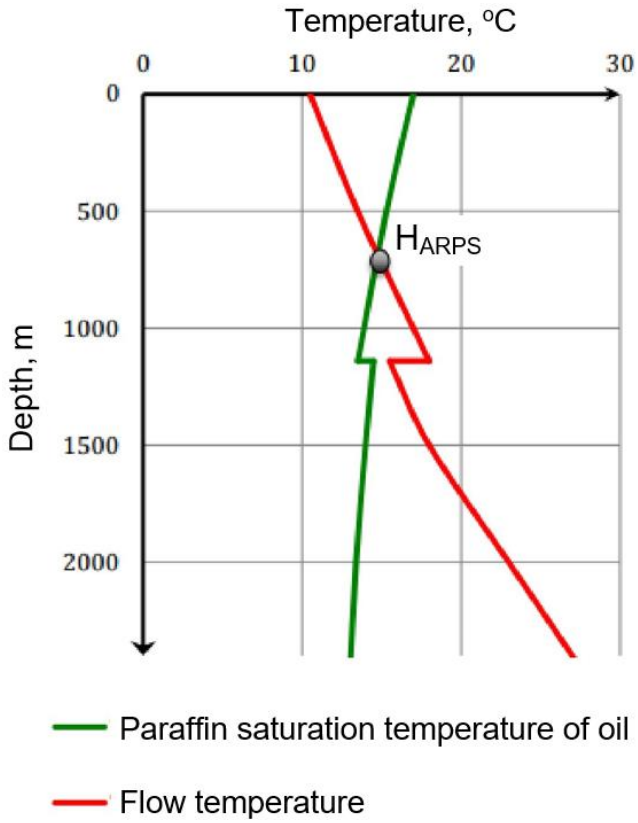

Figure 5 – Graphic data of the formation of the paraffin sedimentation point in the well

Wax sedimentation occurs primarily due to a sudden drop in crude oil temperature. When the paraffin-containing crude is cooled, nucleation occurs, and the wax begins to crystallize. The temperature at which crystallization begins is called the cloud point or crystallization temperature. Its value depends on the concentration of the wax in solution and its solubility. Pressure may also have some effect on the temperature because as pressure increases, the light fractions are compressed more than the heavy ones. A less obvious assumption is that the paraffins become less soluble. Thus, as pressure increases, the cloud point temperature will generally also increase. Paraffin has normal solubility and may be present in solution at higher temperatures.

Paraffin sedimentation occurs when the pipe wall temperature becomes lower than the liquid temperature and the crystallization onset temperature. Sediments can form only in

limited areas of pump and compressor pipes or pipelines. Before the deposit zone, the oil temperature exceeds the crystallization onset temperature, so there is no solid paraffin here. Downstream after the deposit zone, the paraffin cools down so much that it loses its adhesive properties. The onset of crystallization depends on the temperature distribution, which changes as the sediments grow. Initially, the crystallization onset temperature may occur at the pipe walls, and by the end it may move to the liquid-paraffin interface. When the pipe wall temperature becomes equal to the crystallization onset temperature, sediments form on the walls. If the oil flow temperature drops below the crystallization onset temperature, paraffin crystals nucleate in the laminar sublayer in the section with a temperature equal to the cloud point. These crystals then either move due to shear stresses into the main flow of liquid, where they dissolve, or move to cooler sections of the pipe and settle on its wall. (fig. 4) (Wenda et al., 2014, Veliyev, 2020, Ihnatov et al., 2022, Wang et al., 2024).

According to the data (Xu et al., 2020), the process of formation of ARPS on the internal surfaces of oilfield equipment can occur by three mechanisms (fig. 5). Firstly, the crystallization-surface layer is associated with the crystallization of hydrocarbons on the metal surface and the gradual accumulation of the solid phase of the sediment over time, due to replenishment from the oil system. Secondly, the sedimentary-volume mechanism, based on the fact that hydrocarbon crystals are formed in the volume of the oil disperse system and gradually settle on the internal surface of the equipment, forming a sedimentary layer of organic compounds. Thirdly, a mixed mechanism combining the features of the first two. Regardless of the mechanism, the process of formation (crystallization) of solid hydrocarbons is the determining condition for the formation of ARPS (Mcelfresh et al., 2012, Tiwari et al. 2014, Rashid et al., 2019, Zholbassarova et al., 2024).

Results and discussion

Let us consider a hypothesis based on the idea that paraffin crystallization occurs when the energy of the oil flow decreases to the melting point (crystallization) of the paraffin.

When rising, the volume of liquid dV in an elementary section of a pipe dh_w with a lateral surface $\pi D dh_w$ gives off heat through the pipe wall, the amount of which is equal to:

$$dQ = K[t_o - t_e]\pi D dh_w, \quad (1)$$

where K is the coefficient of heat transfer from the liquid to the environment, W/(m^2 K);

t_o - oil temperature in the area under consideration, K;

t_e - ambient temperature in the area under consideration, K;

D - internal pipe diameter, m.

It is obvious that, considering only heat transfer as the prevailing factor, crystallization of paraffin will occur at the release of such an amount of heat that will lead to the establishment of the crystallization temperature:

$$dQ = c(t_o - t_c)dm, \quad (2)$$

where c is the specific heat capacity of oil, J/(kg K);

dm – mass of an elementary volume of oil, kg;

t_c – the temperature at which wax crystallizes in oil is called the wax saturation temperature (WSTP). It can vary depending on the type of oil and production conditions but is usually in the range of 313 to 333 degrees Kelvin.

Then the condition for crystallization of paraffin in oil will be:

$$K[t_o - t_e]\pi D dh_w = cdm(t_o - t_c). \quad (3)$$

Because $dm = \rho_o \frac{\pi D^2}{4} dh_w$, (4)

where ρ_o is the density of oil, kg/m^3;

we get

$$K[t_o - t_e]\pi D dh_w = c\rho_o \frac{\pi D^2}{4} dh_w(t_o - t_c), \quad (5)$$

$$K[t_o - t_e] = c\rho_o D(t_o - t_c)/4. \quad (6)$$

Hence, to avoid crystallization, the oil temperature must not be lower than:

$$Kt_o - Kt_e = c\rho_o D(t_o - t_c)/4; \quad (7)$$

$4Kt_o - c\rho_o\, Dt_o = -c\rho_o\, Dt_c + 4Kt_e$; (8)

$t_o = \frac{4Kt_e - c\rho_o\, Dt_c}{4K - c\rho_o\, D}$. (9)

Let us consider this condition when the oil flow is moving. Considering the drop in oil temperature according to $\Delta t = c\rho_o v S_p c dt$ we get:

$K[t_o - t_e - \Delta t] = \frac{1}{4} c\rho_o\, D(t_o - t_c - \Delta t)$; (10)

$4K\left[t_o - t_e - c\rho_o v S_p c dt\right] = c\rho_o\, D(t_o - t_c - c\rho_o v S_p c dt)$; (11)

$4K[t_o - (t_e - wh)]\pi D dh = c\rho_o\, v S_p dt$, (12)

where K is the coefficient of heat transfer from the liquid to the environment;

t_o - temperature of the liquid in the elementary section, K;

D - internal diameter of the pipe, m;

c - specific heat capacity of liquid, J/(kg K);

ρ_o - liquid density, kg/m^3;

v - average speed of liquid flow, m^2/s;

S_p - cross-sectional area of the pipe, m^2;

dt - geothermal gradient, K/m;

t_o - formation temperature (temperature of the liquid at the bottom of the well), K;

h - the distance (vertically) from the face to the elementary section of the pipe under consideration, m;

t_e - ambient temperature (temperature of rocks at depth $\mathrm{H}_w - h$; H_w - well depth).

Considering that $vS_p = q$ (volume flow rate of liquid), solution equation (12) has the form:

$t_o = t_e - wh + \frac{c_o w \rho_o q}{K\pi D} - c_1 e^{\frac{K\pi Dh}{c_o \rho_o q}}$, or $t_o = t_e - wh + \frac{c_o w \rho_o q}{K\pi D}\left(1 - e^{\frac{K\pi Dh}{c_o \rho_o q}}\right)$, (13)

where c_1 is the integration constant, which is determined from the initial conditions: when $h = 0$ $t_o = t_e$, That's why $c_1 = \frac{c_o w \rho_o q}{K\pi D}$.

The heat transfer coefficient can be represented as $K = \frac{1}{\frac{1}{\alpha} + R}$, (14)

where α is the coefficient of heat transfer from the liquid to the inner wall of the pipe;

R - thermal resistance of pipe walls, annular spaces and the environment around the well (fig. 6).

The coefficient α can be determined from the dependencies [5] for turbulent flow:

$\alpha = 0{,}021 Re^{0.8} \cdot Pr^{0.43} \cdot \frac{\lambda_f}{D}$, (15)

for laminar flow

$a = 4 \cdot \frac{\lambda_f}{D}$, (16)

where $Re = \frac{4q\rho_o}{\mu_o \pi D}$ is the Reynolds number;

μ_o - coefficient of dynamic viscosity of liquid;

λ_f - thermal conductivity coefficient of the pipe material;

$Pr = \frac{c_o \mu_o}{\lambda_f}$ Prandtl number.

Thermal resistance R includes the resistance of the compressor pipe body, the medium filling the annular space, the body of the production string pipe, cement stone and rocks surrounding the well. Analytical determination of R is difficult (lack of information on the thermal properties of rocks surrounding the well, cement stone is not constant in thickness, pipes are not strictly centered in the production string, etc.) (fig.7).

When solving the inverse problem using formulas (14), (15) and (16) the actual thermogram, the thermal resistance R is determined.

Thermal resistance R can be determined using thermograms, which are constructed based on data obtained during well repair.

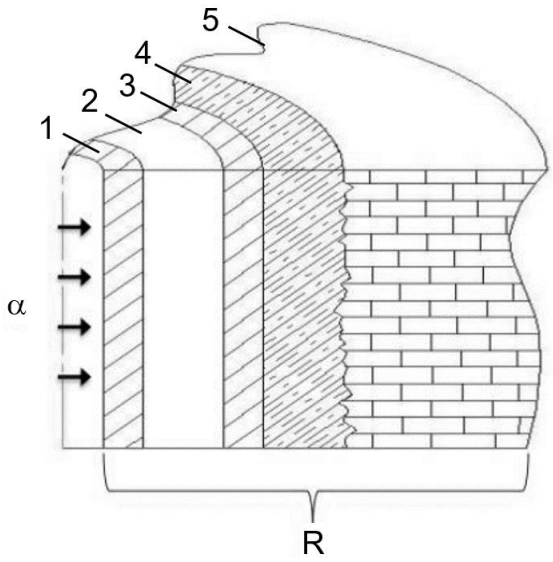

Figure 6 – Heat transfer diagram from liquid to well wall
1 – walls of the drill string; 2 – drilling fluid; 3 – walls of the casing string; 4 – cement layer behind the casing string; 5 – near-wellbore space.

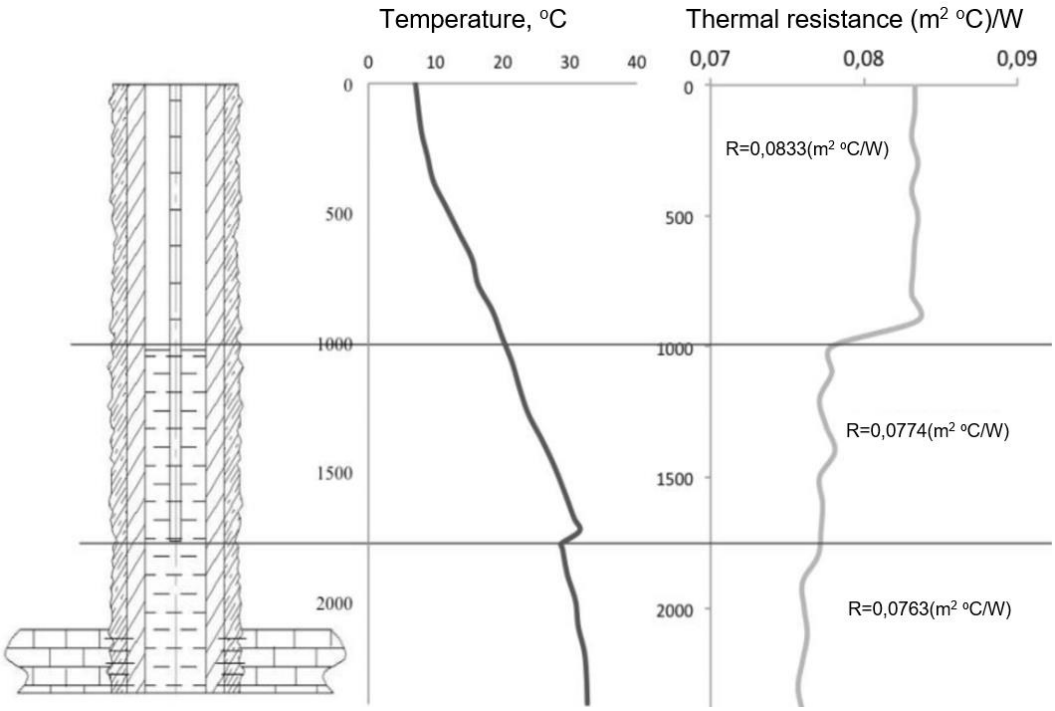

Figure 7 – Example of a well interval with dependence of temperature and thermal resistance R

Conclusions

Paraffin sedimentation occurs when the pipe wall temperature becomes lower than the liquid temperature and the crystallization onset temperature. Sediments can form only in limited areas of pump and compressor pipes or pipelines. Before the deposit zone, the oil temperature exceeds the crystallization onset temperature, so there is no solid paraffin here. Downstream after the deposit zone, the paraffin cools down so much that it loses its adhesive properties. The onset of crystallization depends on the temperature distribution, which

changes as the sediments grow. Initially, the crystallization onset temperature may occur near the pipe walls, and by the end it may move to the liquid-paraffin interface. When the pipe wall temperature becomes equal to the crystallization onset temperature, sediments form on the walls. If the oil flow temperature drops below the crystallization onset temperature, paraffin crystals nucleate in the laminar sublayer in a section with a temperature equal to the cloud point. These crystals then either move due to shear stresses into the main liquid flow, where they dissolve.

The formation of ARPS is associated with such factors as:

- the ratio of such elements in oil as gas/water/resins/paraffins;
- temperature of oil, surrounding rocks and paraffin crystallization;
- oil density, pressure;
- thermal resistance.

The formulas presented above can be used to calculate the point of formation of ARPS in wells.

Thermal resistance does not have a constant value across the depth of the well, and since at different intervals it consists of different components, when determining it, the well should be divided into separate sections.

Thus, the method of preventing or removing paraffin sediments is selected empirically individually for each well, but the priority method is the thermal method, since it is simple to implement and more effective.

References

Al-Yaari, M. (2011). Paraffin wax deposition: mitigation & removal techniques. SPE-155412-MS. In: SPE Saudi Arabia section Young Professionals Technical Symposium.

Belsky, A. A., Dobush, V. S., Morenov, V. A., Sandyga, M. S. (2018). The use of a wind-driven power unit for supplying the heating cable assembly of an oil well, complicated by the formation of asphalt-resin-paraffin deposits. Journal of Physics: Conference Series, 1111, 012052–012052.

Bissengaliev, M., Bayamirova, R., Togasheva, A., et al. (2022). Analysis of complications associated with the paraffinization of borehole equipment and measures to prevent them. News of the National Academy of Sciences of the Republic of Kazakhstan, Series of Geology and Technical Sciences, 3(453), 76–88.

Chi, Y., Daraboina, N., Sarica, C. (2017). Effect of the flow field on the wax deposition and performance of wax inhibitors: cold finger and flow loop testing. Energy & Fuels, 31(5), 4915–4924.

El-Dalatony, M., Jeon, B.-H., Salama, E.-S., et al. (2019). Occurrence and characterization of paraffin wax formed in developing wells and pipelines. Energies, 12(6), 967.

Ihnatov, A. O., Haddad, J., Stavychnyi, Ye. M., Plytus, M. M. (2022). Development and implementation of innovative approaches to fixing wells in difficult conditions. Journal of the Institution of Engineers (India): Series D.

Khomenko, V. L., Ratov, B. T., Pashchenko, O. A., Davydenko, O. M., & Borash, B. R. (2023). Justification of drilling parameters of a typical well in the conditions of the Samskoye field. In IOP Conference Series: Earth and Environmental Science (Vol. 1254, No. 1, p. 012052). IOP Publishing.

Khomenko, V., Pashchenko, O., Ratov, B., Kirin, R., Svitlychnyi, S., & Moskalenko, A. (2024). Optimization of the technology of hoisting operations when drilling oil and gas wells. In IOP Conference Series: Earth and Environmental Science (Vol. 1348, No. 1, p. 012008). IOP Publishing.

Kozhevnykov, A., Khomenko, V., Liu, B. C., Kamyshatskyi, O., & Pashchenko, O. (2020). The history of gas hydrates studies: From laboratory curiosity to a new fuel alternative. Key Engineering Materials, 844, 49-64.

Mcelfresh, P. M., Olguin, C., Ector, D. (2012). The application of nanoparticle dispersions to remove paraffin and polymer filter cake damage. SPE-151848-MS. In SPE International Symposium and Exhibition on Formation Damage Control. Society of Petroleum Engineers.

Pashchenko, O., Khomenko, V., Ishkov, V., Koroviaka, Y., Kirin, R., & Shypunov, S. (2024). Protection of drilling equipment against vibrations during drilling. In IOP Conference Series: Earth and Environmental Science (Vol. 1348, No. 1, p. 012004). IOP Publishing.

Punase, A., Smith, R., Burnett, W., Mutch, K. (2023). Impact of Waxphaltenes on Overall Stability of Asphaltenes, Paraffins, and Emulsion. 10.2118/216472-MS.

Rashid, Z., Wilfred, C. D., Gnanasundaram, N., et al. (2019). A comprehensive review on the recent advances on the petroleum asphaltene aggregation. Journal of Petroleum Science and Engineering, 176, 249–268.

Rehan, M., Nizami, A.-S., Taylan, O., et al. (2016). Determination of wax content in crude oil. Petroleum Science and Technology, 34(9), 799–804.

Souas, F., Safri, A., Benmounah, A. (2020). A review on the rheology of heavy crude oil for pipeline transportation. Petroleum Research, 6(2), 116–136.

Tiwari, S., Verma, S. K., Karthik, R., et al. (2014). In-situ heat generation for near wellbore asphaltene and wax remediation. In: IPTC 2014: International Petroleum Technology Conference, cp-395-00016.

Togasheva, A., Bayamirova, R., Sarbopeyeva, M., et al. (2024). Measures to prevent and combat complications in the operation of high-viscosity oils of Western Kazakhstan. News of the National Academy of Sciences of the Republic of Kazakhstan, Series of Geology and Technical Sciences, 1(463), 257–270.

Valiev, D., Kemalov, A., Gayfullin, A. (2019). Modeling of the Process of Formation and Prevention of Asphaltene Sediments. Journal of Computational and Theoretical Nanoscience. 16. 182-187. 10.1166/jctn.2019.7720.

Veliyev, E. F. (2020). Review of modern in-situ fluid diversion technologies. SOCAR Proceedings, 2, 50–66.

Wang, R., Du, T., Cao, J., Wang, G. (2024). The paraffin crystallization in emulsified waxy crude oil by dissipative particle dynamics. Frontiers in Heat and Mass Transfer, 22(1), 1–10.

Wang, W., Huang, Q. (2014). Prediction for wax deposition in oil pipelines validated by field pigging. Journal of the Energy Institute, 87(3), 196–207.

Wenda, W., Qiyu, H., Jun, H., et al. (2014). Study of paraffin wax deposition in seasonally pigged pipelines. Chemistry and Technology of Fuels and Oils, 50(1).

Xu, X., Bao, T. (2020). Research on the removal of near-well blockage caused by asphaltene deposition using sonochemical method. Ultrasonics Sonochemistry (Print), 64, 104918–104918.

Zholbassarova, A., Bayamirova, R., Ratov, B., Khomenko, V., Togasheva, A., et al. (2024). Development of technology for intensification of oil production using emulsion based on natural gasoline and solutions of nitrite compounds. SOCAR Proceedings, 2, 48–55. https://doi.org/10.5510/OGP20240200965.

TOWARD A SUSTAINABLE SUPPLY OF MINERAL RESOURCES - COPPER AS A CASE STUDY

Tsuyoshi Adachi[1]*

[1] Graduate School of International Resource Sciences, Akita University, Tegatagakuen-machi, Akita , JAPAN
*Corresponding author: adachi.t@gipc.akita-u.ac.jp

Abstract

This paper explores sustainable mineral resources supply, focusing on shifts in consumption patterns with economic growth, particularly for copper. Increasing consumption from emerging economies like China has a contrast with declining consumption in developed countries. Per capita copper consumption of China may reach to current whole world consumption according to relationship between consumption and GDP. The analysis realizes the challenges of maintaining resource supply amid rising demand, considering the transition to the carbon neutral society. This study emphasizes the need for sustainable resource management strategies to address the complex interaction between economic growth, resources consumption and environmental concerns.

Keywords: Mineral Supply, Sustainability, Copper, Consumption, Intensity of Use (IU)

Introduction

In recent years, various efforts have been undertaken to achieve a sustainable society as outlined in the Sustainable Development Goals (SDGs) in order to address global warming and climate change in particular, where a global consensus has been reached. Problems regarding “Resources” has been traditional topics of discussion and consideration, and the questions whether resources are going to be depleted and depletion timing are still essential.

These are fundamental questions unique to resources. Since the physical resources on earth are limited, the amount remaining will inevitably decrease as humans continue to consume them. Here, “resources” refers to underground resources, such as oil and minerals.

However, since the 2000s, discussions have been more focused on renewable energy, recycling, and the circular economy aspects of renewing and material cycles. Simultaneously, increased competition throughout the world for resources securing has accompanied the increase in consumption, especially in China. This situation has led to a significant rise in the prices of resources.

A further development is the accelerating trend toward renewable energy, batteries, and electrification with the aim of realizing a carbon-neutral society. Power generation and battery equipment associated with electrification require the use of a large amount of specific rare metals. These metals with high supply risks are called “Critical Metals”. Developed countries, including Japan, have started to conduct risk assessments and implement appropriate countermeasures throughout the supply chain.

Various factors are necessary for realizing a sustainable society; these include countermeasures against global warming, the eradication of poverty, and environmental protection. However, society will not be viable without an adequate supply of resources. The ability to maintain a sustainable supply thereof is a necessary condition. On the other hand, reducing the environmental impact of resource production and consumption to zero is impossible. A movement is underway to avoid petroleum and coal usage, which emit CO_2. Metals also emit CO_2 during the production process, and mining of metals may lead to some environmental damages. The future production of resources will undoubtedly need to be cleaner than ever before.

Herein, we consider copper, one of the most consumed and widely used nonferrous metals, to examine the production and consumption of mineral resources. The relationship between resource consumption and economic growth, and the conditions necessary for maintaining a sustainable supply of mineral resources are also examined. Though copper is discussed here, the main points can be applied to other mineral resources, including energy and various metals.

Trends in Resource Prices

Resource prices changed significantly after 2004. Figure 1 shows changes in the prices of copper, lead and zinc, the main base metals, from 2000 to 2023. The prices of all metals, as the figure shows, started to rise sharply in 2004. The price of crude oil exhibited a similar trend although not included in this figure. The reason for the rise in prices during this period was the increase in demand for resources in BRICS countries, especially increased consumption in China, and the influx of speculative funds into the resource market. Resource prices plummeted in 2008 as capital was pulled out because of the financial crisis (i.e., the Lehman shock) but recovered the following year and peaked again in 2011. Prices at this peak were about five times higher than they were at the beginning of 2000. Naturally, prices of raw materials in the manufacturing industry soared; thus, the struggle for resources became to the focus of global attention in that decade.

Although prices of raw materials have declined or kept a certain level since 2012, they have remained more than three times higher than they were before 2000. Since 2020, the impact of economic policies and investments due to the spread of the COVID-19 pandemic has led to an expansion of speculative funds into stocks and resources. Furthermore, with the added impact of Russia’s invasion of Ukraine, copper prices reached an all-time high in 2021.

Thus, resource price levels have been extremely high since 2004, and price volatility has become more intense than in the past. The magnitude of price volatility has become a major risk for the resource industry as well as other industries and households that utilize resources.

Resource Consumption

Next, we look at resource consumption aspect. Figure 2 illustrates the change in copper metal consumption from 1980 to 2021. The chart does not represent usage of copper metal in final products; rather, it illustrates consumption of copper metal ingot. The bars from bottom

to top for each year represent the consumption in China, G7 countries, and the rest of the world (except for China and G7).

The first thing to note is that consumption in China rose sharply around 2000. Since then, Chinese consumption has continued to grow, with the country accounting for 55% of global consumption in 2021. Conversely, direct usage of copper metal in developed countries, represented by the G7, continued to decline gradually while global consumption grew (i.e., their share dropped from 58% in 1980 to 18% in 2021). The rest of the world's share, excluding that of China and G7 countries, dropped from 40% to 26% and did not change significantly.

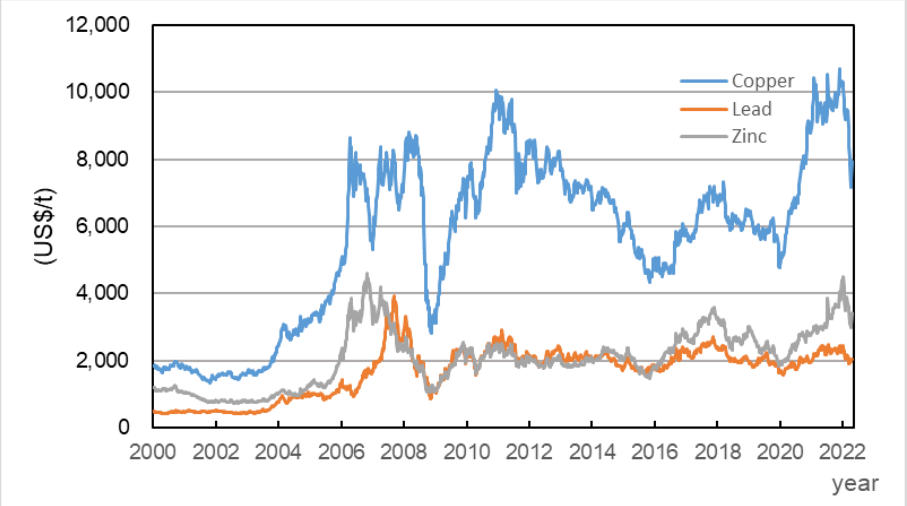

Source: London Metal Exchange (LME) (2000-2023) Cash

Figure 1. Trends in copper, lead, and zinc metal prices

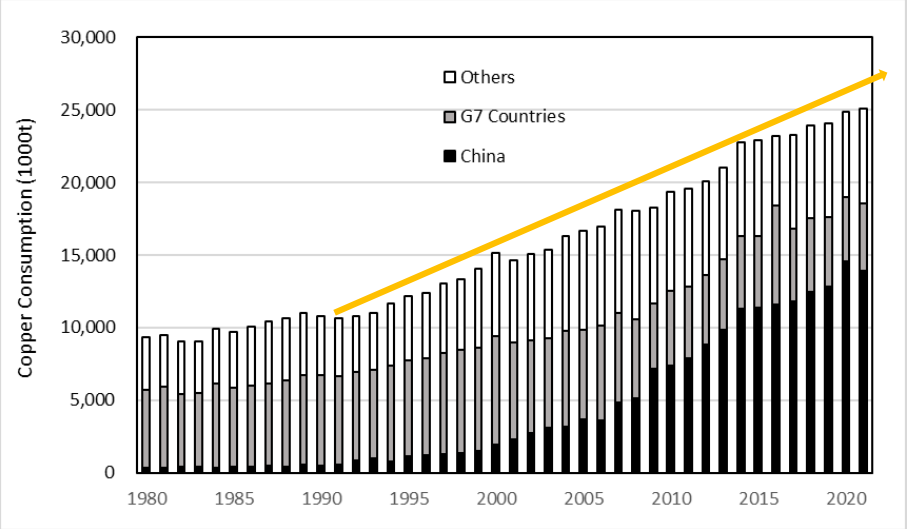

Source: World Bureau of Metal Statistics (1980-2022)

Figure 2. Changes in copper metal consumption by region

What is remarkable here is that, despite the significant shift from the G7 to China as the consumer country, the change in overall global consumption has been smooth. As the yellow line in Figure 2 illustrates, consumption has increased linearly since 1990, maintaining an approximate annual growth rate of 2.8% per year. Looking at the large price fluctuations described in Figure 1 and the previous section, the degree of involvement of price fluctuations due to changes in consumption is very low, suggesting that speculative investment has a significant impact to the prices.

Resource Consumption and Economic Growth

In this section, we focus on the evolution of the relationship between per capita resource consumption and per capita economic growth (GDP growth). The general view is that resource consumption increases with the country's economic growth, but as the previous section demonstrated, the amount of resources directly consumed in developed countries has tended

to decrease over time. In Figure 3, trends in per capita consumption and per capita GDP are illustrated to further clarify the relationship between resource consumption and economic growth.

First, developed countries, such as Japan, the US, and Germany, are on the right, showing a constant or downward trend in consumption (5–10 kg). Thus, as per capita GDP rises, per capita copper consumption declined. Conversely, China, accounting for 55% of the world's copper metal consumption, is at the bottom left of the graph. Although its per capita GDP is lower than that of developed countries, its copper consumption per capita is at the same level. India is at the lower left corner of the graph, with low indicator values for both GDP and consumption. Other developing countries are not included in the graph but would be located in the lower left side near India and China. Using UN terminology, China's economy and resource consumption are in a state of coupling between economic growth and resource usage, while those of developed countries are in a state of decoupling.

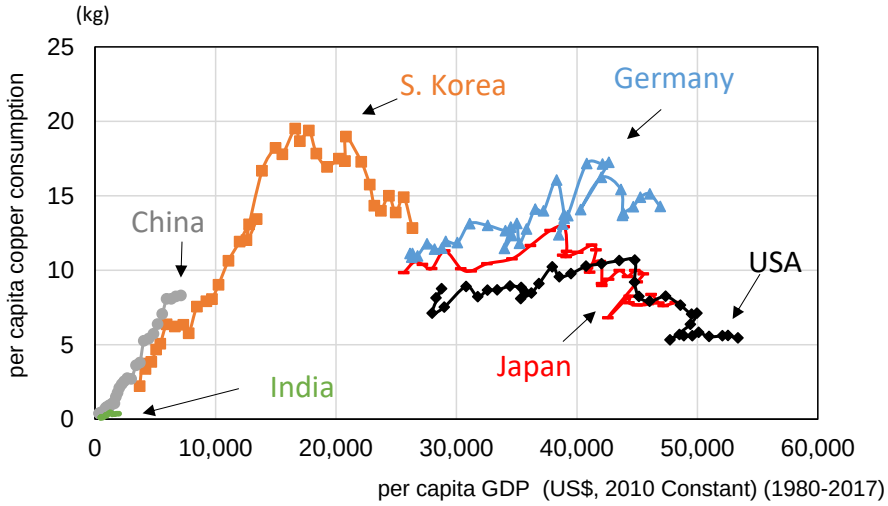

Source: World Bureau of Metal Statistics (1980-2022), World Bank (1980-2022)
Figure 3. Relationship between per capita GDP and per capita copper consumption by country

South Korea marks the shift between developing and developed countries. Korea's trend is mountain-shaped, rising from the lower left side to a peak at around per capita GDP of 18,000 US$ and per capita copper consumption at 20 kg before falling to the right. If we can assume that economic growth in other countries will follow a same transition pattern of resource consumption from developing to developed countries like Korea, China will continue to increase its copper consumption per capita as the economy grows, rising to 20 kg per capita. Assuming a constant population, China's consumption will continue to increase until it reaches 2.4 times its current consumption level. This means that China alone would account for more than the current total global consumption, an amount that is difficult to meet through the current mining and recycling supply system. Once China enters a downward trend, other large countries like India and Indonesia will follow, which suggests that global copper consumption will continue to increase in the future. This situation can be avoided through measures that would allow copper consumption to transition directly to the 10 kg level in developed countries without going through 20 kg per capita, but specific technologies and systems that could bring this about remain unclear.

Figure 4 shows the relationship between the global per capita GDP and copper consumption. Looking at the global total, a linear increase trend appears. Extrapolating this trend would be one basis for projecting future copper resource consumption in the world.

In mineral economics, the relationship between economic growth and resource consumption is measured with an index for the intensity of use of resources, which is often used to predict future demand. Intensity of use, or IU, is expressed as resource consumption (demand) (weight) divided by GDP (value), which herein means tons of copper consumed per million dollars of GDP, for example.

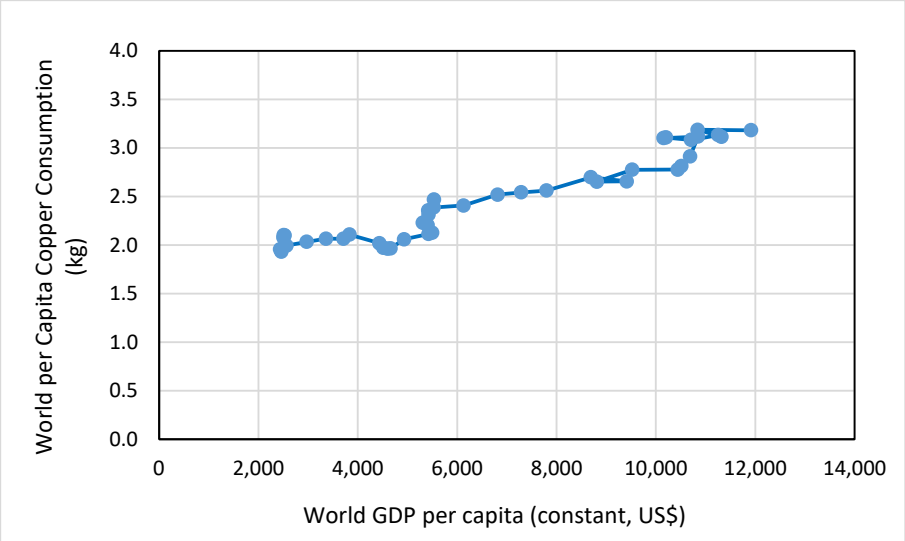

Source: IMF, World Bureau of Metal Statistics (1980-2022)
Figure 4. Relationship between per capita GDP and per capita copper consumption (World total)

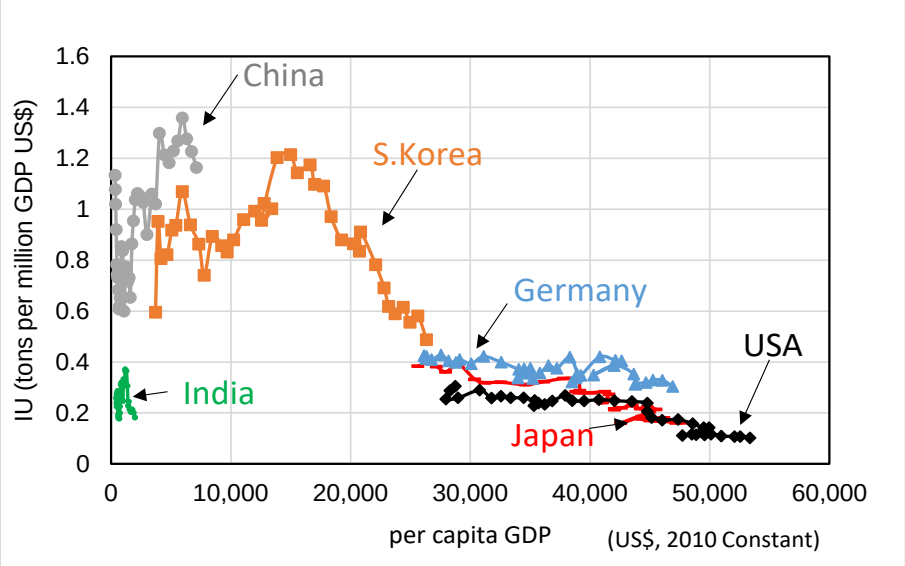

Source: World Bureau of Metal Statistics (1980-2022), World Bank (1980-2022)
Figure 5. Relationship between per capita GDP and IU (Intensity of Use)

Mineral economics theory states that IU follows an inverse U shape as an economy grows. When a country's per capita GDP is low, the main industry is the primary industry, which does not consume much resources, and the IU is low. As the secondary industry becomes the main industry, the next stage of economic development begins, and the IU rises with the usage in manufacturing industry and the development of domestic infrastructure. As the economy grows further and the value added by the tertiary industry makes up a significant part of the GDP, IU declines, as GDP can be increased without directly consuming resources (e.g., advanced countries moving their manufacturing production bases overseas).

Intensity of Use (IU) of Resource Consumption

Figure 5 plots the same countries examined previously and the relationship between GDP per capita and IU. While developed countries (e.g., Japan, the US, Germany), are located on the lower right side—denoting high per capita GDP and low IU—, many developing countries are on the lower left side, denoting low per capita GDP and IU. South Korea's transition bridges the two sides, with a per capita GDP of 15,000 US$ and a peak IU of 1.2t/MUS$, which then falls to IU 0.4t/MUS$ while the

GDP continues to rise. China has already exceeded South Korea's peak IU; thus, we must pay attention to the point in the future economic growth cycle when its IU will begin to decline.

Assuming how the IU will change helps us predict resource consumption based on the expected GDP value. Although the scope of this study did not include forecasting future consumption, the IU trend suggests that consumption in China will continue to rise, as will be followed by large economies' country like India's.

Conclusion

This paper presents a basic analysis that is based mainly on trends in copper consumption, with the aim of studying how consumption is expected to increase. Global copper consumption has increased linearly since 1990, and the analysis of per capita consumption and IU reveals that consumption in China is expected to continue to increase. China's consumption alone could equal the total amount consumed by the world today. This volume would require a supply so large that the current mine supply system would be unable to fulfill it. Excessive demand will cause resource prices to rise further, and price fluctuations will significantly increase resource risks. Substantially increasing supply through recycling and reducing per GDP or per capita resources consumption will be essential, but experience shows that this strategy will be difficult to actually implement.

In the future, if the use of renewable energy for electrification, including electrification in the automobile industry, is continued in order to realize a carbon-neutral society, the demand for copper and other metals will further increase for such applications as electric wires. The focus of this study was copper, and although other metal resources are affected by individual circumstances, we believe that the outlook for other metals will be similar to that for copper. It would not be exaggerating that the sustainable supply of mineral resources will be fraught with difficulties in the future.

References

London Metal Exchange (LME) (2000-2023) Historical Data
World Bureau of Metal Statistics (1980-2022) World Metal Statistics Yearbook
World Bank (1980-2022) World Development Indicators

THE INVESTIGATION OF CRITICAL METALS AND RARE EARTH ELEMENTS ENRICHMENT MECHANISMS USING HIGH-RESOLUTION INTEGRATED ANALYSIS

Seungyeol Lee[1]*, Daeyong Kim[1]

[1]Department of Earth and Environmental Sciences, Chungbuk National University, Chungbuk 28644, REPUBLIC OF KOREA
*Corresponding author: slee2@cbnu.ac.kr

Abstract

To gain a deeper understanding of how critical metals and rare earth elements are concentrated in ore deposits, we employed complementary methodologies, including synchrotron diffraction and scattering analysis intergrating with high-resolution electron microscopic techniques. In this study, we discuss three specific cases: (1) the enrichment of trace elements in ferromanganese nodules, (2) rare element enrichment in hydrogenetic ferromanganese crusts, and (3) the discovery of gold nanoparticles in Marcellus shale gas.

Firstly, in the case of trace element adsorption, we found that arsenates are preferentially adsorbed onto the surface of proto-goethite. Our study provides a direct view of the atomic positions of iron oxyhydroxides. The methodologies we used can be effectively applied to identify trace elements and heavy metals that have been adsorbed on the minerals in geological systems.

Secondly, we conducted a study on the hydrogenetic ferromanganese crust in the north-west Pacific Ocean. Our findings showed that rare-earth elements and phosphorus were

preferentially adsorbed onto the iron-rich vernadite. On the other hand, platinum-group elements, cobalt, and nickel were found to be enriched in the manganese-rich vernadite.

Thirdly, we found a high density of gold nanoparticles on the surfaces of opal nanospheres that coexist in kerogen-bearing shales from the Marcellus Formation. Our newly discovered textures suggest that these opal nanospheres may have played a role in facilitating the co-precipitation of pure gold nanoparticles in environments rich in organic matter and under reduced environment. Moreover, our TEM observations provide clear images of the initial phase of colloidal gold and silica. This could potentially contribute to the formation of gold deposits involving “invisible” gold, secondary supergene enrichments, or high-grade gold accumulations.

These case studies effectively illustrate how the combined approach can be a powerful tool for determining critical metals and rare earth elements in ore forming processes.

Keywords: Trace elements**,** rare-earth elements, gold nanoparticles, high-resolution electron microscopic techniques

Introduction

The study of critical metals and rare earth elements (REEs) in ore deposits is crucial for understanding their concentration mechanisms and potential economic value. Traditional analytical methods have often fallen short in providing detailed insights into the complex processes involved in the enrichment of these elements. This research aims to address this gap by employing a combination of advanced techniques, including synchrotron diffraction, scattering analysis, and high-resolution electron microscopy, to investigate three distinct cases of element enrichment in geological systems.

The first case examines the adsorption of trace elements, particularly arsenates, onto proto-goethite in ferromanganese nodules (Lee et al., 2016). This study provides unprecedented atomic-level observations of iron oxyhydroxides and their role in trace element sequestration. The second case focuses on the enrichment of rare elements in hydrogenetic ferromanganese crusts from the north-west Pacific Ocean, revealing preferential adsorption patterns of REEs, phosphorus, and platinum-group elements on different mineral phases (Lee et al., 2019). The third case presents a novel discovery of gold nanoparticles associated with opal nanospheres in Marcellus shale gas deposits, offering new insights into the formation of "invisible" gold and potential mechanisms for high-grade gold accumulations (Lee et al., 2021).

These case studies collectively demonstrate the power of integrating advanced analytical techniques in unraveling the complex processes governing the concentration of critical metals and REEs in various geological settings (Lee and Xu, 2020) . By providing detailed observations at the atomic and nanoscale levels, this research not only enhances our understanding of ore-forming processes but also opens new avenues for exploring and evaluating potential mineral resources. The findings from this study have significant implications for both theoretical geochemistry and practical applications in mineral exploration and resource assessment.

Case Studies

Trace element adsorption onto the surface of minerals

Trace element adsorption onto the surface of minerals is a critical process in geological systems, with particular interest in the adsorption mechanisms occurring on iron oxyhydroxide surfaces (Lee and Xu, 2016). This study investigates nanophase Fe-oxyhydroxides in freshwater ferromanganese nodules (FFN) from Green Bay, Lake Michigan, and the adsorbed arsenate on their surfaces. Advanced analytical techniques, including high-resolution transmission electron microscopy (HRTEM), Z-contrast imaging, and ab initio calculations using density functional theory (DFT), were employed to provide atomic-level insights into the adsorption processes. These methods allow for direct observation of mineral structures and the positions of adsorbed trace elements at the nanoscale, enabling an unprecedented understanding of adsorption mechanisms at the atomic level.

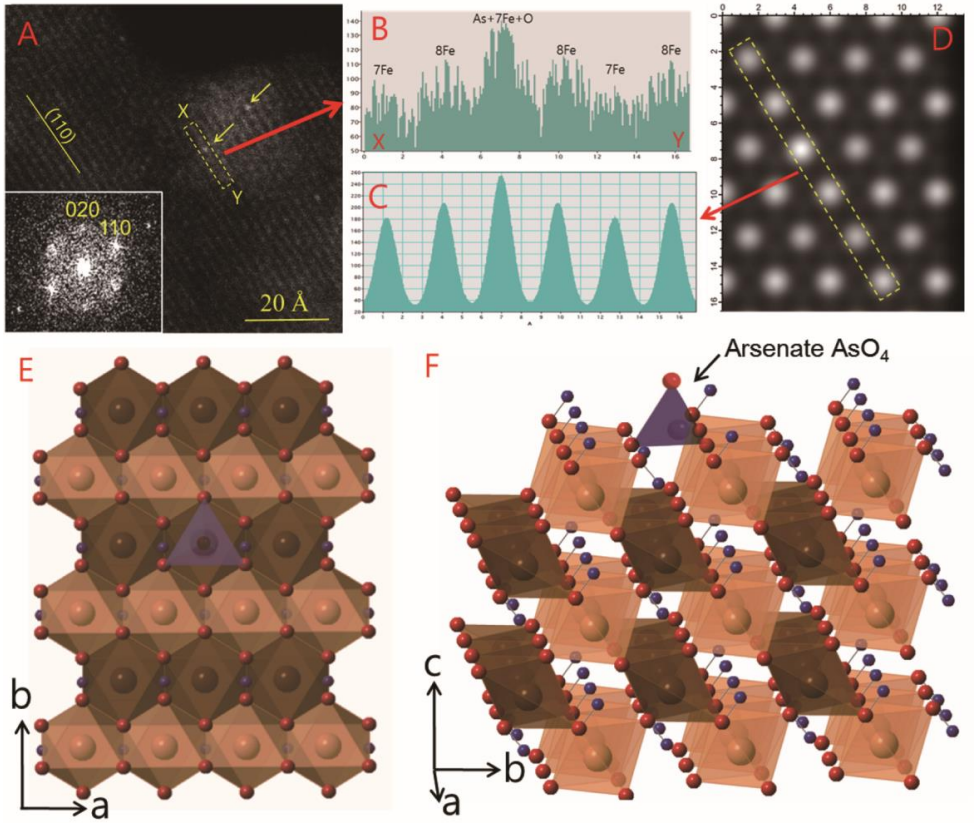

Fig. 1 The arsenate tetrahedra are preferentially adsorbed on the proto-goethite (001) surface via tridentate adsorption. Z-contrast image of proto-goethite; bright spots are positions of Fe atom columns. Very bright spots are As atoms on the surface right above Fe.

The research findings reveal that a nanophase FeOOH, termed "proto-goethite," plays a crucial role in arsenate adsorption. Z-contrast imaging demonstrates that arsenate tetrahedra are preferentially adsorbed on the proto-goethite (001) surface via tridentate adsorption (Fig. 1). This structural characteristic of proto-goethite not only favors arsenate adsorption but also suggests a preference for other tetrahedral ions such as SiO_4^{4-}, PO_4^{3-}, and SO_4^{2-}. These observations explain the higher arsenic concentrations in the immature outer layers of the nodules and highlight the importance of the crystallization degree of iron oxyhydroxides in their trace element adsorption capacity. Such insights contribute significantly to our understanding of contaminant transport and concentration processes in environmental systems, potentially informing strategies for water purification and pollution management.

Rare earth element enrichment in ferromangese crust

Rare earth element (REE) enrichment in ferromanganese crusts has been a subject of significant interest, particularly in the northwest Pacific Ocean (Lee et al., 2019). Recent studies on hydrogenetic ferromanganese crusts (HFMC) from the Magellan Seamount have provided valuable insights into the mechanisms of REE concentration. X-ray diffraction (XRD) and transmission electron microscopy (TEM) analyses reveal that HFMC primarily consists of low crystalline Fe-bearing vernadite. Chemical analyses of HFMC layers demonstrate a preferential adsorption of REEs and phosphorus on Fe-rich vernadite, while platinum-group elements (PGE), cobalt, and nickel show enrichment in Mn-rich vernadite.

The enrichment mechanism of REEs in HFMC appears to be closely associated with phosphate content (Fig. 2). A positive correlation between total REE (ΣREE) and phosphorus has been observed, suggesting that REEs are incorporated into the crust structure in association with phosphate. Furthermore, phosphate shows a positive correlation with iron in both electron probe microanalysis (EPMA) and TEM-EDS analysis, indicating that Fe-rich vernadite layers serve as hosts for phosphate incorporation, which in turn leads to localized REE enrichment. This elemental correlation is attributed to the chemical hardness and softness of metal cations and ligands, where REE cations, as hard Lewis acids, preferentially bind with hard bases like phosphate anions. The presence of phosphorus tetrahedra at the

Fe-bearing Mn-layer facilitates strong bonding with REE elements, playing a crucial role in the REE enrichment process in HFMC.

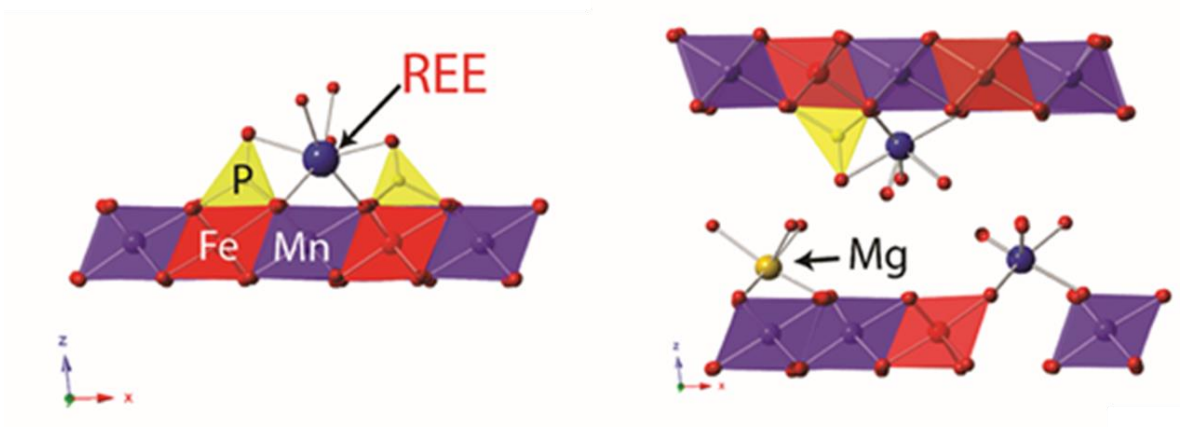

Fig. 2 The model of P REE enrichment of the vernadite structure The Mn octahedral sites are purple and the Fe octahedral sites are red.

Gold Nanoparticles in Marcellus natural gas

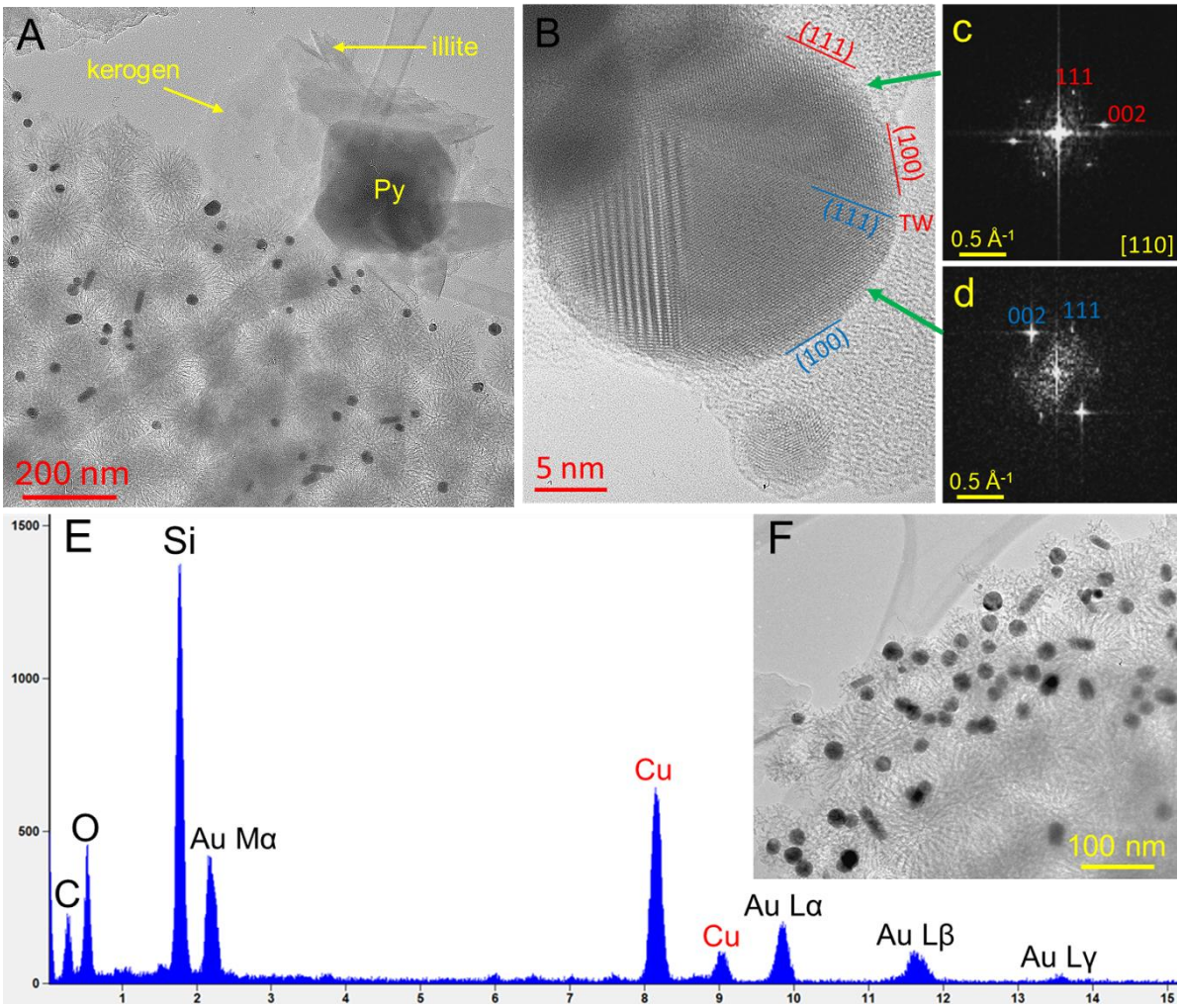

Fig.3 A series of TEM micrographs illustrating the coexistence of gold nanoparticles (black dots) with opal nanospheres (gray structures), kerogen, and illite. TEM images and X-ray EDS spectra from opal nanospheres and gold nanoparticles in host opal nanospheres

Gold nanoparticles in Marcellus natural gas deposits represent a novel and intriguing discovery in the field of geochemistry and mineral exploration. Recent studies have revealed

a high density of gold nanoparticles on the surfaces of opal nanospheres coexisting in kerogen-bearing shales from the Marcellus Formation (Lee et al., 2021; Lee et al., 2022). This finding introduces a new formation type of colloidal gold nanoparticles and identifies a unique kind of natural opal-A characterized by a mesoporous texture formed through oil-in-water emulsion processes. High-resolution transmission electron microscopy (TEM) combined with energy-dispersive X-ray spectroscopy has provided direct evidence of spherical gold nanoparticles and gold nanorods associated with these mesoporous opal nanospheres.

The discovery suggests that opal nanospheres may have facilitated the co-precipitation of pure gold nanoparticles in organic-rich, reduced environments. This observation provides insight into the initial phase of colloidal gold and silica formation, which could contribute to the development of gold deposits involving "invisible" gold, secondary supergene enrichments, or high-grade gold accumulations. The presence of gold nanoparticles in hydrocarbon-rich shale formations like the Marcellus (containing 0.6–4.1 wt % gold/opal) opens up the possibility for co-production of both gas/oil and gold. This finding not only expands our understanding of gold formation in non-traditional geological settings but also suggests potential new avenues for mineral exploration and resource extraction in shale gas formations.

Conclusion

In conclusion, this study has demonstrated the effectiveness of integrating advanced analytical techniques, including synchrotron diffraction, scattering analysis, and high-resolution electron microscopy, in unraveling the complex mechanisms of critical metals and rare earth elements enrichment in diverse geological settings (Lee et al., 2016; Lee and Xu., 2016; Lee et al., 2019; Lee et al., 2021; Lee and Guo, 2022). Through the examination of three distinct cases - trace element adsorption in ferromanganese nodules, rare earth element enrichment in hydrogenetic ferromanganese crusts, and gold nanoparticle formation in Marcellus shale gas - we have gained unprecedented insights into the atomic-level processes governing element concentration. The findings reveal the crucial role of specific mineral phases, such as proto-goethite and Fe-rich vernadite, in facilitating element adsorption and enrichment. Moreover, the discovery of gold nanoparticles associated with opal nanospheres in shale formations opens new avenues for understanding non-traditional gold deposit formation. These results not only advance our theoretical understanding of ore-forming processes but also have significant implications for mineral exploration and resource assessment strategies. By providing a more nuanced comprehension of element behavior at the nanoscale, this research paves the way for more targeted and efficient approaches to identifying and evaluating potential mineral resources, ultimately contributing to the sustainable management of critical metals and rare earth elements.

Acknowledgment

This research was supported by Chungbuk National University KNUDP program. (2023)

Reference

Lee, S., Shen, Z., & Xu, H. (2016). Study on nanophase iron oxyhydroxides in freshwater ferromanganese nodules from Green Bay, Lake Michigan, with implications for the adsorption of As and heavy metals. American Mineralogist, 101(9), 1986-1995.

Lee, S., Xu, H., Xu, W., & Sun, X. (2019). The structure and crystal chemistry of vernadite in ferromanganese crusts. *Acta Crystallographica Section B: Structural Science, Crystal Engineering and Materials*, *75*(4), 591-598.

Lee, S., Xu, H., Wempner, J., Xu, H., & Wen, J. (2021). Discovery of gold nanoparticles in Marcellus shale. *ACS Earth and Space Chemistry*, *5*(1), 129-135.

Lee, S., & Xu, H. (2020). Using complementary methods of synchrotron radiation powder diffraction and pair distribution function to refine crystal structures with high quality parameters—a review. *Minerals*, *10*(2), 124.

Lee, S., & Xu, H. (2016). XRD and TEM studies on nanophase manganese oxides in freshwater ferromanganese nodules from Green Bay, Lake Michigan. *Clays and Clay Minerals*, *64*, 523-536.

Lee, S., Xu, H., & Xu, H. (2022). Reexamination of the structure of opal-A: A combined study of synchrotron X-ray diffraction and pair distribution function analysis. *American Mineralogist*, *107*(7), 1353-1360.

Lee, S., & Guo, X. (2022). Xuite, Ca3Fe2 [(Al, Fe) O3 (OH)]3, a new mineral of the garnet group: Implications for the wide occurrence of nanominerals. *American Mineralogist: Journal of Earth and Planetary Materials*, *107*(5), 930-935.

Lee, S., & Xu, H. (2016). Size-dependent phase map and phase transformation kinetics for nanometric iron (III) oxides (γ→ ε→ α pathway). *The Journal of Physical Chemistry C*, *120*(24), 13316-13322.

CHARACTERIZATION OF A GIANT SANGDONG W–MO SKARN DEPOSIT, SOUTH KOREA

Jeonggeuk Kang[1], Jieun Seo[1], Seon-Gyu Choi[1], Young Jae Lee[1]*

[1]Department of Earth and Environmental Sciences, Korea University, Seoul 02841, South Korea
*Corresponding author: youngjlee@korea.ac.kr

The Sangdong deposit in South Korea, a significant W–Mo skarn deposit, is intricately linked with the Cretaceous Sangdong granite, a calc-alkaline S-type granite. This study examines the spatial distribution and multiple-stage mineralization within the deposit influenced by repeated hydrothermal activities. The deposit features an outer prograde skarn and a central retrograde skarn. The prograde skarn is divided into two stages: Stage I includes wollastonite–garnet–clinopyroxene zones, and Stage II displays a pyroxene–garnet assemblage. The retrograde skarn is also subdivided into two stages: Stage I with an amphibole–biotite assemblage and Stage II dominated by quartz–mica. In addition, vein mineralization is categorized into early scheelite–wolframite quartz veins and late molybdenite–quartz veins. Analysis of mineral assemblages and compositions, particularly clinopyroxene and garnet in the prograde stages, suggests an evolution from oxidized to partially reduced environments. The presence of fluorite and muscovite in the retrograde Stage II and wolframite during the vein stage, coupled with negative Eu anomalies, indicates an ore-forming fluid rich in fluorine. This condition likely enhanced the hydrothermal fluid's capacity to transport and precipitate ore metals during the skarn formation and subsequent greisenization processes at the Sangdong deposit.

Keywords: The Singsong deposit, Scheelite, W–Mo skarn, Multiple-stage mineralization, Reduced environments

THE MYEONSAN FE-TI PALEO-PLACER DEPOSIT IN SOUTH KOREA: MINERALOGICAL AND GEOCHEMICAL PROPERTIES WITH MICROSCOPIC OBSERVATION

Bongsu Chang[1], Jieun Seo[1], Young Jae Lee[1]*

[1] Department of Earth and Environmental Sciences, Korea University,
Seoul 02841, South Korea
*Corresponding author: youngjlee@korea.ac.kr

This study investigates the mineralogical and geochemical properties of the Myeonsan Fe-Ti ore deposit, a sedimentary-origin deposit in South Korea. Using X-ray diffraction coupled with quantitative phase analysis, the primary constituent minerals were identified as 30.9% of hematite, 28.4% of quartz, and 19.2% of rutile. In addition, the deposit contains less than 10% of ilmenite and phyllosilicates with minors of garnet and wollastonite. The whole-rock chemistry, determined through X-ray fluorescence, aligns with these mineralogical observations. It is worthy to note the TiO_2 content exceeds 20%, classifying this deposit as a high-grade sediment-sourced TiO_2 ore. Electron microprobe analysis provided insights into

the overall oxidation state, indicating that the Fe-Ti minerals predominantly occupy the hematite, pseudobrookite, and rutile regions on the FeO-Fe_2O_3-TiO_2 ternary diagram. This distribution highlights the highly weathered nature of the deposit. Our future research will expand to encompass the entire deposit, aiming to lay a solid foundation for successful mining development.

Keywords: The Myeonsan Fe-Ti ore deposit, Quantitative phase analysis, Ilmenite, High-grade sediment-sourced TiO_2 ore, Fe-Ti minerals

ESTIMATING SOIL HYDRAULIC PARAMETERS BASED ON GROUND PENETRATING RADAR WAVEFORM INVERSION

Minghe Zhang[1, 2], Xuan Feng[1], Maksim Bano[2], Qi Lu[1], Tseedulam Khuut[3]

[1]College of Geo-Exploration Science and Technology, Jilin University, Changchun 130026, CHINA
[2]ITES UMR-7063, EOST, University of Strasbourg, F-67000 Strasbourg, FRANCE
[3]Mongoian University of Science and Technology, Ulaanbaatar 17025, MONGOLIA

Soil hydraulic parameters are key factors for characterizing the transport of water and solute in the vadose zone. Ground penetrating radar (GPR) has recently become a powerful geophysical method to determine the soil hydraulic parameters. In this study, we developed an inversion scheme to estimate the soil hydraulic parameters from surface GPR waveform data. The inversion scheme includes a soil hydraulic model to obtain the soil water content profile from soil hydraulic parameters, a petrophysical relationship to transform the soil water content to relative dielectric permittivity, an electromagnetic wave propagation forward modeling for gaining the GPR waveform data, and a algorithm to optimize the process of inversion. The scheme allows to invert the soil hydraulic parameters from GPR waveform data, comparing with the inversion only based on traveltime data, more information in GPR data can be used. A series of numerical experiments were constructed to validate the proposed inversion scheme with initial conditions and soil hydraulic parameters. The Hydrus-1D was used to generate the synthetic soil moisture profiles which then were transformed to relative dielectric permittivity profiles by petrophysical relationship. The relative dielectric permittivity profiles further were used to generate “observed” GPR waveform data by the electromagnetic wave propagation forward modeling. Finally, based on the calculated GPR waveform data and the observed GPR waveform data, the final soil hydraulic parameters are obtained. At the same time, the proposed inversion scheme was also further applied to field experimental data. Both the results show that the proposed inversion scheme is promising and can directly determine the soil hydraulic parameters from GPR full waveform data.

AIRBORNE GEOPHYSICS IN MONGOLIA – A NEW APPROACH

Rainer Herd[1]*

[1]Brandenburg University of Technology Cottbus-Senftenberg, Cottbus,Germany German-Mongolian Institute for Resources and Technology, Nalaikh, MONGOLIA
*Corresponding author: herd@b-tu.de

D-MTUC a multi-sensor airborne investigation system based on a ultra-light aircraft and developed at Brandenburg University of Technology has been transported to Mongolia in order to perform airborne geophysical investigations for the detection of unknown mineral deposits and to verify the suitability of the system under the Mongolian climatic conditions. Three areas in different regions of Mongolia have been investigated. Several unknown anomalies could be

detected even in already geologically mapped areas showing the high potential and advantages of this new airborne investigation system.

Keywords: airborne geophysics, mineral exploration, ultra-light aircraft, Mongolia

Within the frame of the 'German-Mongolian Raw Material Partnership', the ultra-light multi-sensor airborne investigation system D-MTUC was transported 2018 to Mongolia for raw material exploration in cooperation with the German-Mongolian Institute for Resources and Technology (GMIT) and the Mineral Resource and Petroleum Authority of Mongolia. The main aims of the project were on the one hand to detect unknown raw material occurrences in Mongolia and on the other hand to test this recently developed ultra-light multi-sensor airborne system under the harsh Mongolian conditions.

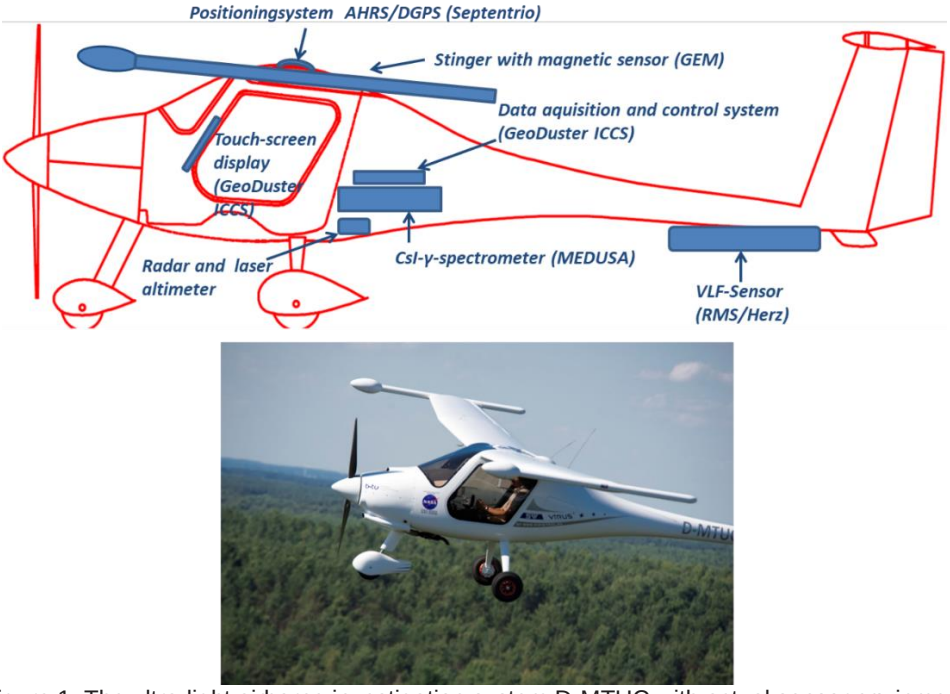

Figure 1. The ultra-light airborne investigation system D-MTUC with actual sensor equipment

The geoscientific instrumentation of the system comprehends a CsI-γ-spectrometer of MEDUSA, Netherlands, 2 K-magnetometer of GEM, Canada, a VLF-EM-receiver of RMS, Canada and a data acquisition and control system of GeoDuster, RSA with the option of further sensor installations, for details see Herd and Holst (2015). The sensor configuration enables the system to operate at low speed and low altitude for mineral exploration, geological mapping, detection of freshwater resources and brines and different environmental monitoring missions.

During the course of the project 4263 line-kilometers with a total areal extent of 662 km² have been investigated in three areas (Central Gobi, Changai mountains and greater Ulaanbaatar region). The flight altitude was always 100 m. Different sets of high resolution magnetic and radiometric maps could be produced and handed over to the Mineral Resource and Petroleum Authority of Mongolia. Up to now unknown raw material potentials could be detected even in areas which have been geologically mapped in earlier times. Results and experiences of this unusual project will be presented.

Acknowledgments

Many thanks go to the german institutions BMZ, GIZ and DAAD for their financial support of the project.

References

Herd, R. and Holst, J., 2015, D-MTUC, an airborne investigation system based on a full composite ultra-light aircraft. In: Meyer, U., Miensopust, M. (Eds.): Airborne Geophysics - New technologies in

Hardware and Interpretation, Deutsche Geophysikalische Gesellschaft Sonderband II/2015, p. 10-13, Potsdam, ISSN-Nr. 0947-1944

PROBABILISTIC SEISMIC HAZARD ASSESSMENT OF HAZARA DIVISION, PAKISTAN

Nangyal Ghani Khan[1]*, Zaighum Riaz[1], Faizan-Ur-Rehman Qaiser[1]

[1]Department of Earth Sciences, COMSATS University Islamabad, Pakistan
*Corresponding author: nangyalghani@cuiatd.edu.pk

Pakistan lies in one of the most active seismic regions in the world, as suggested by the three regional fold belts. The western part of the Himalayan syntaxis is the seismically active intercontinental domain and experiences significant seismic activity each year. The earthquakes originating from the western syntaxis have claimed thousands of lives in Pakistan and substantial infrastructural losses of billions of dollars e.g. approximately 73000 people died, more than 80,000 injured, and 3.5 million were displaced, approximately 400,000 buildings were entirely or partially destroyed as a result of the Kashmir earthquake on October 8, 2005. Valuable information can be obtained regarding the region's seismic hazard assessment and preparedness by studying the past events in the region to better understand earthquake forecasting, constructing earthquake-resistant infrastructure, and developing effective response strategies to mitigate future earthquake risks. We have computed the probabilistic seismic hazard assessment using the standard method developed by Cornell-McGuire. We have utilized, both, the instrumental, and historical earthquake catalogs to establish the recurrence relationship using a hybrid model of four attenuation equations i.e. Abrahamson et al. (2014), Chiou and Youngs (2014), Ambraseys et al. (2005), and Zhao et al. (2006) were used for active shallow crust and Abrahamson et al. (2016), Atkinson and Boore (2003), Youngs et al. (1997), and Zhao et al. (2006) for the subduction interfaces for the calculation of final hazard values. The ground motion parameters (PGA and SA at 0.2s and 1.0s) were computed at a grid increment of 0.05º × 0.05º for 10% probability of exceedance in 50yr, 100yr, 150yr, 200yr, 250yr, 475yr, 1000yr. We examined seismic hazard and ground shaking characteristics for the next 50, 100, 150, 200, 250, 475, and 1000 years, with a 10% exceedance probability in the Hazara division, revealing variations in PGA and spectral acceleration values for different sites. Seismic hazard in the Hazara division is highly variabale, with PGA values varying from 0.24g to 0.38g for the 50-year return period with a 10% probability of exceedance. The estimated Spectral acceleration values for the 0.2s and 0.1s natural period show a similar distribution in the region ranging from 0.26g to 0.49g and 0.14g to 0.22g, respectively.This study aims to construct a seismic hazard zonation based on updated seismic data to assist various agencies in developing better seismic building codes for the study area and emphasizes the importance of integrating demographic information with seismic hazard values to evaluate the potential impact of earthquakes on the region for mitigation and preparedness

The research was supported by the Department of Earth Sciences COMSATS University Islamabad, Pakistan

INVESTIGATION OF SOIL POLLUTION IN THE TERRITORY OF THE OIL FIELDS OF MONGOLIA (TAMSAG BULAG AND DZUNBAYAN) BY REMOTE SENSING METHODS

Stepanov Alexey[1]*, Gantumur Sambuu[2], Kharitonova Galina[3]

[1]Far Eastern Agriculture Research Institute, 680521 Khabarovsk, RUSSIA
[2]School of Geology and Mining Engineering, MUST, Ulaanbaatar 14191, Mongolia
[3]Khabarovsk Federal Research Center, Institute of Water and Ecology Problems FEB RAS, 680000 Khabarovsk, Russia
*Corresponding author: stepanfx@mail.ru

Abstract

The impact of oil production on soils and vegetation pollution depends on the methods of oil extraction and transportation. The study of pollution is primarily based on field sampling and subsequent analysis of soil samples. Recently, methods of remote sensing have become widespread to solve these problems. At the same time, the degree of soil pollution can be assessed both by the presence of oil spills on the soil surface and changes in the reflectivity of the surface, and indirectly by studying the degradation of vegetation cover. This article describes approaches to the study of soil pollution in the Tamsag Bulag and Dzunbayan oil fields (Mongolia). Test sites (4 km^2) were allocated in the center of the fields, as well as at a distance of 4 km and 8 km from the center of the fields (2015-2023). According to MODIS data (250 m resolution), time series of average values of the Normalized Difference Vegetation Index (NDVI) were constructed in the period from May 1 to October 31. The average NDVI values according to Sentinel-2 (10 m) and the Dual polarimetric Radar Vegetation Index (DpRVI) values according to Sentinel-1 (10 m) in August 2021 were also calculated. Degradation of vegetation cover was revealed according to multispectral and radar survey data for the Tamsag Bulag field within a radius of 4 km from the center of the field. For sandy soils with sparse vegetation of the Dzunbayan, no significant influence of pollution on vegetation degradation was revealed. According to remote sensing data, areas of soil contamination have been identified for the Tamsag Bulag and Dzunbayan oil fields.

Keywords: oil pollution, remote sensing, multispectral index, radar index, Mongolia

Introduction

The development of approaches for obtaining a comprehensive assessment of oil pollution of soils is quite relevant for many countries of the world engaged in oil production, including Mongolia. Oil pollution reduces the ecological potential of soils and increases the risks of their degradation. Physical and chemical degradation of soils, biological degradation of soils organic matter in result of oil pollution are the worldwide environment and high cost problems (Villacís et al., 2016). The consistent and phased achievement of the Sustainable Development Goals (SDGs) adopted by the United Nations (UN) back in 2015 is still of great importance for preventing further land degradation and achieving the neutralization of land degradation (LDN), which is the basis of the current and strategic global development agenda (Keesstra et al., 2016; Keesstra et al., 2018).

The reduction in reserves and production of "light" oils in Mongolia, as in most oil-producing regions of the world has recently caused increased interest in the resources of hard-to-recover oils and the production of heavy and high-viscosity oils. Such oils have a high content of paraffins and resins (Serebriakov, Kondratiev, 2012), which leads not only to technological complications during oil extraction, transportation and refining, but also to serious environmental problems. Soil pollution in oil production areas with "heavy" oils, the destruction of which is extremely slow on site, causes serious violations of their functioning and self-purification. At the first stage, one of the ways to solve environmental problems in the

case of soil contamination with heavy oils is to choose reliable and objective criteria for soil contamination.

In this regard, one of the main tasks is an objective assessment of the state of soils and vegetation of the oil fields of Mongolia – Tamsag Bulag and Dzunbayan. At the same time, the assessment of oil pollution areas directly is indeed a priority area for environmental monitoring of industrial areas of oil production, transportation or refining (Razakova, 2017). However, in the absence of spills and large oil spills on the surface, the study of hidden degradation processes leading to deviations in the development of vegetation cover comes to the fore. Remote sensing methods are often used to detect and fix oil pollution sites, although heavy pollution is most often assessed (Bin Sun et al., 2017; Dedeoglu et al., 2020). In the case of a cumulative effect with long-term use of oil wells, or for old oil spills, researchers note that due to the entry of heavy metals and other toxic substances into the soil, physicochemical and microbiological properties change, which has a depressing effect on vegetation over a long period (Razakova, 2017).

The purpose of this study was to evaluate the possibility of using multispectral and radar satellite data to identify vegetation suppression near the oil fields of Mongolia.

Materials and methods

The Tamsag Bulag field is located in the east of Mongolia, in the Dornod Aimag (47°40’ N, 117°02’ E). The Dzunbayan is located in the south-east of Mongolia, in the Dornogovi Aimag (44°27’ N, 110°05’ E).

These oil fields are located respectively in the zone of dry steppes with chestnut (kastanozems) soils and the semi-desert zone with brown semi-desert soils (Dorjgotov, 2009; Khadbaatar, 2021). Mongolian chestnut soils (loams, light loams and sands) with an annual precipitation of about 200-250 mm are characterized by the accumulation of carbonates, the duration of the growing season is 150-170 days. There is almost no continuous grass covering. The zone of brown semi-desert soils is characterized by low rainfall (100-125 mm per year or less), strong winds and dry heat and sparse vegetation (saxaul, ephedra and others). The humus content in brown semi-desert soils does not exceed 0.3-0.8% (Dorjgotov, 2009; Doljiin, Yembuu, 2021; Khadbaatar, 2021).

The soils of the studied Tamsag Bulag and Dzunbayan oil production sites are characterized by similar physical and chemical properties: high content of physical sand (up to 86-91%, particle size > 0.01 mm), alkaline pH reaction (up to 8,7-8,8). However, the total carbon content in Tamsag Bulag soils (chestnut soils of the dry steppe zone) is significantly higher than in Dzunbayan soils (brown semi–desert soils) - 1.07 and 0.24%, respectively. The content of petroleum hydrocarbons (HC) in the soils of Dzunbayan ranges from 9 to 60 mg/kg, in the soils of Tamsag Bulag – from 7 to 670 mg/kg with a maximum near operating wells. According to the level of hydrocarbon pollution, Dzunbayan soils can be classified as uncontaminated (“background”, HC concentration less than 100 mg/kg), Tamsag Bulag soils – from the “background” HC concentration to a “moderate level” of pollution (locally, near wells) (Sambuu et al., 2022).

To assess the influence of the contamination on the vegetation cover in the vicinity of the Tamsag Bulag and Dzunbayan oil fields, test sites oriented to the cardinal points with areas of 4 km^2 were considered. The centers of the studied B and A sites were located at a distance of 4 and 8 km from the center of C site, the territory of the oil field (Fig. 1a, 1b).

MODIS data were used to calculate NDVI maxima for all test sites in 2015-2023.

The state of the vegetation cover in the period 2021 on the test plots near Tamsag Bulag was assessed using NDVI and DPRI according to Sentinel-2 and Sentinel-1 satellites. The NDVI were determined as follow:

$$NDVI=\frac{NIR-RED}{NIR+RED},$$

where NIR – near-infrared reflectance; RED – red band reflectance. The values of the DpRVI were calculated according to the method (Mandal et al., 2020).

The results were processed using two-factor analysis of variance followed by pairwise comparison using the Tukey criterion.

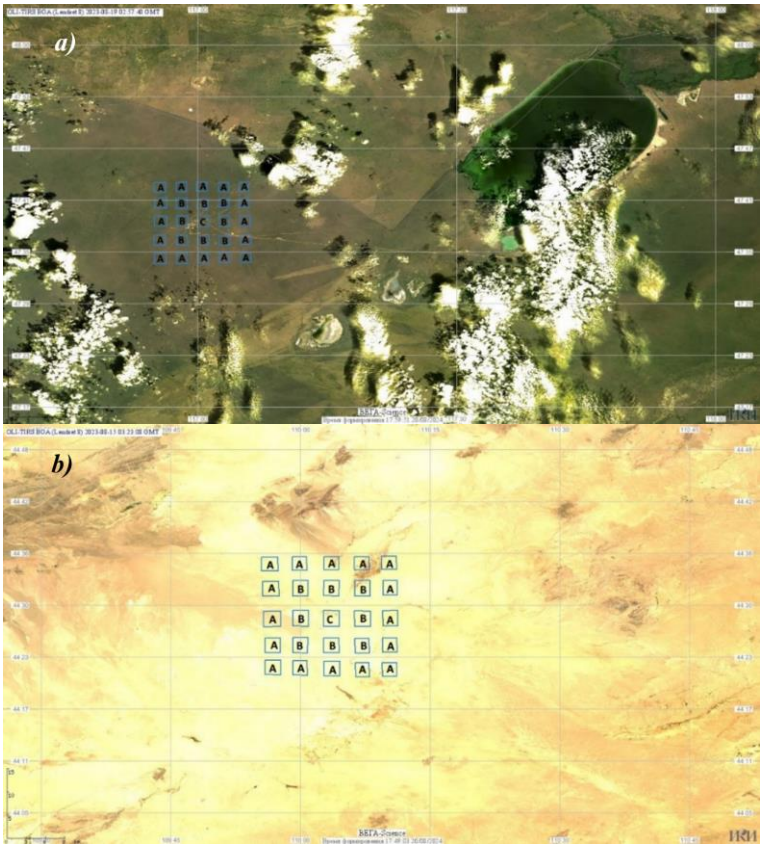

Fig. 1. The studied surface sites near the Tamsag Bulag (a) and Dzunbayan (b) oil fields: C is the center of the field, B sites - 4 km from the center, A sites - 8 km from the center.

Results

An analysis of the dynamics of NDVI maxima from 2015 to 2023 revealed the following trend – a significant increase in $NDVI_{max}$, values at a distance of more than 4 km from the center of the Tamsag Bulag oil field. Table 1 shows the average $NDVI_{max}$, values calculated for the test sites.

According to ANOVA's two-way factor analysis, $NDVI_{max}$ values depend on the year and the distance of the test sites from the field. An additional a posteriori analysis of the data using the Tukey test showed that the $NDVI_{max}$ values significantly increase at a distance of more than 4 km from the source of oil pollution. Significant differences in $NDVI_{max}$ were also found for sections A and B (Table 2). At the same time, over the years, the $NDVI_{max}$ values in the center varied from 0.33 in 2017 to 0.60 in 2020. The variability of the index values over the years of observation was 19.6%. At the same time, the coefficient of variation for sites B ranged from 3.4% in 2021 to 9.2% in 2015. The coefficient of variation for sites C ranged from 5.3% to 10.2%.

Table 1. Average $NDVI_{max}$ values for the test sites of the Tamsag Bulag field (2015–2023)

Site	2015	2016	2017	2018	2019	2020	2021	2022	2023	p-value
C	0.49	0.34	0.33	0.46	0.54	0.50	0.60	0.56	0.53	**P<0.01**
B	0.51	0.33	0.35	0.47	0.58	0.50	0.61	0.57	0.54	
A	0.51	0.34	0.38	0.49	0.58	0.51	0.62	0.58	0.55	
p-value	**P<0.001**									

Table 2. Pairwise comparison of $NDVI_{max}$ of test sites A, B and C of the Tamsag Bulag deposit according to the Tukey criterion

Site	C	B	A
C		0.027 **(P<0.05)**	0.0003 **(P<0.001)**

B	0.027 **(P<0.05)**		0.04 **(P<0.05)**
A	0.0003 **(P<0.001)**	0.04 **(P<0.05)**	

The two-factor analysis performed for the Dzunbayan field showed that the $NDVI_{max}$ values depend on the year, but do not change depending on the distance to the center of the field (Table 3). In general, as expected, the values of the NDVI maximum for Dzunbayan are 2-4 times lower than the values of the corresponding indicators for the Tamsag-Bulag field. The variability of the index values over the years of observation was 17.0%. The coefficient of variation of the NDVI maximum for sites B ranged from 4.3% in 2021 to 13.4% in 2015. The coefficient of variation of the NDVI maximum for sites C ranged from 7.4% to 18.2%. The more significant variability of the indicator for the Dzunbayan deposit is also explained by the desert nature of the area.

Table 3. Average $NDVI_{max}$ values for the test sites of the Dzunbayan field (2015–2023)

Site	2015	2016	2017	2018	2019	2020	2021	2022	2023	p-value
C	0.15	0.18	0.16	0.20	0.16	0.21	0.17	0.13	0.13	**ns***
B	0.14	0.17	0.15	0.22	0.16	0.21	0.17	0.13	0.12	
A	0.14	0.16	0.15	0.22	0.16	0.21	0.17	0.12	0.12	
p-value	**P<0.001**									

*ns - not significant at the 0.05 probability level.

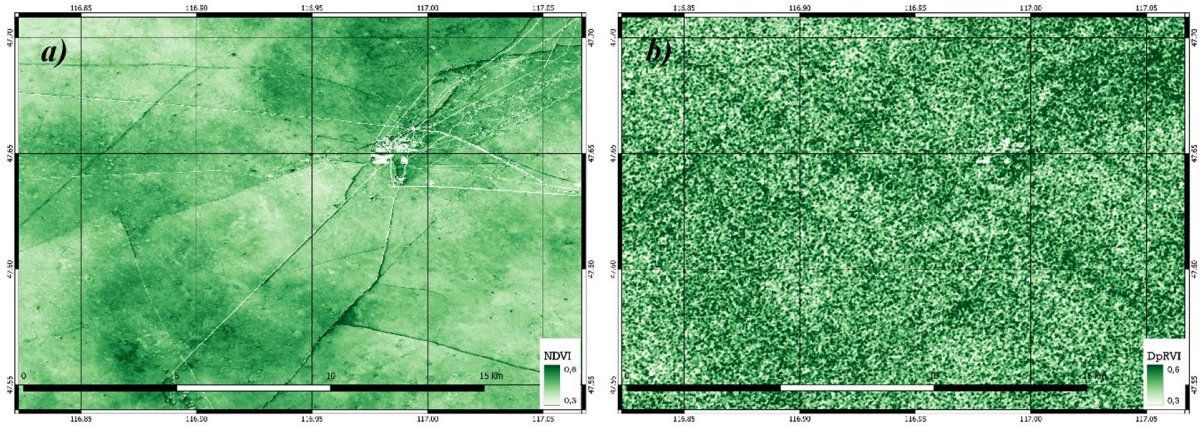

Fig. 2. NDVI (a) and DpRVI (b) values for Sentinel-2 (a) and Sentinel-1 (b) images of the Tamsag Bulag field (August 2021)

Fig. 2 shows the spatial distributions of the NDVI and DpRVI indices for the Tamsag-Bulag deposit territory. As can be seen, the area near the conditional center of the deposit is characterized by lower values of vegetation indices, as vegetation increases away from the center.

Conclusions

The degradation of vegetation cover was revealed from long-term satellite data for the Tamsagbulag field as it approached the center of the field. Significant decreases in NDVI values were found in the central part and in sections at a distance of 4 km in comparison with a zone with a radius of 8 km. For sandy soils with sparse vegetation of Dzunbayan, no significant effect of oil pollution on vegetation degradation was revealed.

References

Dedeoğlu L., Yüksel M. and Kaya F. 2020. Assessment of the vegetation indices on Sentinel-2A imagesfor predicting the soil productivity potential in Bursa, Turkey. *Turkey Environ Monit Assess* 192 16

Doljin D. and Yembuu B. 2021. Division of the Physiographic and Natural Regions in Mongolia. The Physical Geography of Mongolia, Geography of the Physical Environment, Springer Nature Switzerland AG 177-193

Dorjgotov D. 2009. National Atlas of Mongolia. Institute of Geography. Mongolian Academy of Sciences, Ulaanbaatar

Keesstra S.D., Bouma J., Wallinga J., Tittonell P., Smith P., Cerdà A., Montanarella L., Quinton J.N., Pachepsky Y., van der Putten W.H., Bardgett R.D., Moolenaar S., Mol G., Jansen B. and Fres-co L.O. 2016. The significance of soils and soil science towards realization of the United Na-tions Sustainable Development Goals. *Soi* 2 111-128

Keesstra S., Mol G., De Leeuw J., Okx J., Molenaar C., De Cleen M. and Visser S. 2018. Soil-related sustainable development goals: Four concepts to make land degradation neutrality and restoration work. *Land* 7(4) 13

Khadbaatar S. 2021. Soils of Mongolia. The Physical Geography of Mongolia, Geography of the Physical Environment, Springer Nature Switzerland AG 135-160

Mandal D., Ratha D., Bhattacharya A., Kumar V., Mcnairn H., Rao Y.S. and Frery A. 2020. A Radar Vegetation Index for Crop Monitoring Using Compact Polarimetric SAR Data. *IEEE Transactions on Geoscience and Remote Sensing* 58(9) 6321-6335

Ovsyannikova V.S., Filatov D.A., L.K. Altunina and Svarovskaya L.I. 2014. Biodestruction of Hydrocarbons of Highly Viscous Petroleum with Soil Microorganisms. *Chemistry for Sustainable Development* 5(22) 489–495

Razakova M. 2017. Identification and mapping of oil contamination of soils using remote sensing data. *Problems of Informatics* 4 1–12

Sambuu G., Kharitonova G.V., Stepanov A. S., Xionghu Zhao, Tyugai Z. and Krutikova V.O. 2022. Assessment of Pollution of the Oilfield Territories in Mongolia. *Biogeosystem Technique* 9(1) 49–59

Serebriakov A.O., Kondratiev Yu.K. 2012. Mongolian oil: physical and chemical structure, resources and ways of oil output. *Geology, geography and global energy* 45 21–26

Sun B., Li Z., Gao W., Zhang Y., Gao Z., Song Z., Qin P. and Tian X. 2017. Identification and assessment of the factors driving vegetation degradation/ regeneration in drylands using synthetic high spatiotemporal remote sensing data—A case study in Zhenglanqi, Inner Mert Mongolia, China. *Ecological Indicators* 107 105614

Villacís J., Casanoves F., Hang S., Keesstra S. and Armas C. 2016. Selection of forest species for the rehabilitation of disturbed soils in oil fields in the Ecuadorian Amazon. *Science of the Total Environment* 566–567 761–770

FROM ASEISMIC TO ACTIVE: SEISMIC PATTERNS IN EASTERN MONGOLIA'S PETROLEUM FIELDS

Khishigdelger Ulziisaikhan*, Ulziibat Munkhuu

Department of Seismology, The Institute of Astronomy and Geophysics,
MAS, Ulaanbaatar 13343, MONGOLIA
*Corresponding author: khishigdelger@iag.ac.mn

This study explores the recent increase in seismic activity in Eastern Mongolia, specifically in the Matad and Dornod regions, which have been historically considered aseismic with no known active faults. Between 2019 and 2021, the area experienced 15 earthquakes of local magnitude four (ML ≥ 4), suggesting a notable change in the region's seismic behavior. The primary objective of this research is to investigate the potential link between this heightened seismicity and petroleum production activities, such as hydraulic fracturing and wastewater injection.

To achieve this, we applied the relative double difference method to accurately locate these earthquakes' epicenters and analyze the associated fault structures. This method allows for a detailed examination of seismic data, providing precise information on the spatial distribution and characteristics of the faults. Preliminary findings indicate that the earthquakes are concentrated in specific zones within the petroleum production fields, implying a possible correlation between seismic activity and industrial operations.

The study highlights the urgent need to assess the geological stability of the region and consider the potential risks of human-induced seismicity due to petroleum extraction activities. These findings emphasize the importance of integrating seismic monitoring with industrial operations to mitigate environmental and community risks. Future research will focus on

refining fault models and evaluating the seismic risk associated with ongoing and future petroleum production activities in Eastern Mongolia. This work contributes to the broader understanding of seismic hazards and the impact of industrial activities on geological stability.

Keywords: Human-Induced Seismicity, Relative Double Difference Method, Seismic Monitoring, Eastern Mongolia

INVESTIGATING THE IMPACT OF WILDFIRES ON CLIMATE CHANGE AND PUBLIC HEALTH: FROM LABORATORY EXPERIMENTS TO FIELD CAMPAIGNS

Taekyu Joo[1, 2, 3]*, Drew Gentner[2], Nga Lee Ng[3, 4, 5], Michelle Bell[6, 7], Rodney Weber[4], Seulkee Heo[6], Jo Machesky[2], Tori Hass-Mitchell[2], Mitchell Rogers[2], Catelynn Soong[2], Linghan Zeng[4]

[1] Department of Earth and Environmental Sciences, Korea University, Seoul 02841, SOUTH KOREA
[2] Department of Chemical and Environmental Engineering, Yale University, New Haven, Connecticut 06511, USA
[3] School of Earth and Atmospheric Sciences, Georgia Institute of Technology, Atlanta, Georgia 30332, USA
[4] School of Chemical and Biomolecular Engineering, Georgia Institute of Technology, Atlanta, Georgia 30332, USA
[5] School of Civil and Environmental Engineering, Georgia Institute of Technology, Atlanta, Georgia 30332, USA
[6] School of the Environment, Yale University, New Haven, Connecticut, United States
[7] School of Health Policy and Management, College of Health Sciences, Korea University, Seoul 04129, SOUTH KOREA
*Corresponding author: taekyujoo@korea.ac.kr

Fine-mode particulate matter ($PM_{2.5}$) is a highly detrimental air pollutant, regulated without considering chemical composition, and an important component of wildfire smoke. As wildfire activity increases with climate change, its growing impact requires multidisciplinary research to examine smoke's chemical composition evolution and connect chemical composition to potential effects on health and climate change. To comprehensively understand such effects, we conducted laboratory environmental chamber experiments and an ambient field campaign. Secondary PM formation during furanoids photooxidation were investigated as the representative volatile organic compounds from wildfires at Georgia Tech Enviornmental Chamber facility. Among examined furanoids, furfural showed the greatest brown carbon (BrC) formation, which can absorb sunlight and raise global temperature. We found the amount of BrC corresponded to the formation of nitrogen-containing organic compounds, which are dominated by amines and amides formed from reactions between carbonyl and ammonia/ammonium. The field campaign was conducted at newly installed (Atmospheric Science and Chemistry mEasurement NeTwork) site in Queens, New York. Leveraging advanced real-time speciated $PM_{2.5}$ measurements in conjunction with source apportionment and health risk assessments, we evaluated the composition-dependent health effect during Canadian wildfire smoke transport to New York City during May-June 2023. The total smoke-related organic $PM_{2.5}$ showed significant associations with asthma exacerbations, and estimates of in-lung oxidative stress potentially enhanced with chemical aging, demonstrating escalating health risks owing to increasingly-frequent smoke episodes.

Keywords: Wildfire, Biomass burning, Secondary organic aerosol, brown carbon, human health

NATURAL FLOW REGIME AND WATER VARIABILITY IN THE ORKHON RIVER, MONGOLIA

Dashdorj Battsengel[1]*, Scott Kenner[2] and Gombodorj Batkhurel[3]

[1] Erdenet Institute of Technology, Mongolian University of Science and Technology
[2] South Dakota School of Mines and Technology
[3] Graduate School of Business, Mongolian University of Science and Technology
Corresponding author: orkhonwatershed@gmail.com

Streamflow patterns are recognized to be the main indicator of river ecosystems. In this study we used daily water records on the stations, chracterized the streamflow and defined the varaibility of water resources in annual, monthly and extreme conditions in the Orkhon River basin, Mongolia. Flow indicator sets have been developed for characterization of flows, which are evaluated based on the hydrological indices: magnitude, duration, time, frequency and change rate of extreme flows (minimum and maximum), low flow, and high flow.

Principal Component Analysis (PCA) was used to determine the significant flow indices to represent natural flow regimes in the Orkhon River basin using the results of the hydrological alterations. Thirteen flow indices characterized 63% of the total variations in the estimated hydrological indices. High flow decrease, November median flows, High pulse decrease rate, Annual peak flow, April median flow, seasonal and monthly maximum flows and the July low flow were the largest indicators in PC1.

The second significant flow indices are the rate of flood rise, the maximum flow date, the frequency of average and major floods, the duration of extremely low flows in PC2, which account for 24% of total variations. These main flow indices best describe the flow patterns in the Orkhon River basin.

Based on the identified flow indices, the study estimated the variability of annual and monthly flows, and water during wet and dry periods. Reliable estimates of water variability are crucial for ecosystem sustainability and socio-economic developments of human community.

Keywords: streamflow characterization, extreme flow conditions, and streamflow variability

FORMATION AND DISTRIBUTION OF GROUNDWATER IN THE DORNOGOBI BASIN: HYDROGEOLOGICAL STUDIES OF DULAAN UUL AND ZOOVCH OVOO ROLL-FRONT-TYPE URANIUM DEPOSIT IN ZUUNBAYAN AND UNEGT SUB BASIN

Bayarmaa Purevsan

Badrakh Energy LLC, Ulaanbaatar 14240, MONGOLIA
bayarmaa.purevsan@orano.group

The Zoovch Ovoo and Dulaan Uul deposits are hosted by the Upper Cretaceous Sainshand formation in the central part of the large Tsagaan Els endorheic basin. The SW-NE North-Zuunbayan Fault crosscuts the central part of the basin and defines two hydrogeologic sub-basins: Unegt with the Dulaan Uul deposit to the NW; and Zuunbayan with the Zoovch Ovoo deposit to the SE. A dense groundwater monitoring network has been established by Badrakh Energy LLC on its licenses across these two sub-basins.

Field studies of the Sainshand aquifers (K2Ss2) have revealed highly variable conductivities and salinities resulting in significant variations of density and a tendency to water stratification. The highest salinity is observed in the central deeper parts of the Zuunbayan/Zoovch Ovoo sub-basin, while lower values prevail in shallower peripheral areas.

In the Project area, hydrogeologic studies have shown that apart from the deep regional K2Ss2 aquifer, a shallower distinct low-salinity aquifer is present in the overlying Bayanshiree formation (K2Bs). This aquifer is used through a small number of herder wells. The deep, high-salinity K2Ss2 aquifer which hosts the uranium mineralization is separated by clay layers from the upper shallow aquifer and rests on the impermeable Lower Cretaceous Dzuunbayan Formation (K1Dz).

Recharge of this typically endorheic hydrogeologic system occurs through precipitation and has been estimated between 1 and 3 mm/year while discharge proceeds from evaporation in the central part of the Tsagaan Els depression, some 8 to 10 km north of the Zoovch Ovoo deposit. The hydraulic gradient is very low, on the order of 0.01%.

The hydrodynamic properties of the deep mineralized K2Ss2 aquifer have been characterized using a variety of hydrogeologic tests. The average hydraulic conductivity in the mineralized formation is 10-4 m/s, approximately. Tracer tests carried out in the area suggest effective porosity values ranging from 15% to 20%. The average ambient groundwater velocity in the Zoovch Ovoo area is estimated at 2 m/year. These overall hydrodynamic properties are considered as completely favorable for ISL mining.

A survey of all available hydrochemical data has shown that regional groundwater is slightly brackish to brackish (up to 20 g/L) and corresponds to a unique sodium/chloride (+ accessory sulfate) chemical type. Apart from sodium, several major ions are present in high concentration, and many minor elements like manganese, selenium and arsenic are also present in anomalous amounts. Excessive uranium concentration and α-activity are also observed in most of the samples. Based on these characteristics it is considered that the only potential beneficial use for groundwater in the Project area would be for mining purposes. A detailed survey of regional groundwater has been nevertheless undertaken to localize potential usable water resources, which mainly lie in the shallow to medium-depth aquifers of the Unegt sub-basin.

A regional numerical model of the whole cretaceous hydrologic basin (Unegt and Zuunbayan sub basins) has been constructed and validated. This numerical modeling has confirmed the validity of the conceptual hydrogeological system, and allowed to determine the average annual recharge, as well as the hydrodynamic parameters of the different aquifer and aquitard units at the regional scale.

Keywords: Hydrogeology, water quality, mining projects, environment, Zoovch Ovoo

COMPREHENSIVE MULTI-METAL ISOTOPIC MODEL FOR REGIONAL-SCALE ENVIRONMENTAL MANAGEMENT IN ERDENET MINE

Duk-Min Kim[1]*, Bayartungalag Batsaikhan[2, 3], Seong-Taek Yun[2]*, Dae-Gyu Im[2], Hyeon-Soo Seo[2]

[1] Department of New Energy and Mining Engineering, Sangji University, Wonju, Gangwon-do 26339, Republic of Korea
[2] Department of Earth and Environmental Sciences, Korea University, Seoul 02841, Republic of Korea
[3] Institute of Geography and Geoecology, MAS, Ulaanbaatar 15170, Mongolia
*Corresponding authors: kdukmin8@sangji.ac.kr; styun@korea.ac.kr

Major mining cities worldwide have been suffered from diverse contamination sources including tailings, mine drainages, geology enriched with toxic metals, and the other industrial and domestic sources. This study established a multi-isotopic comprehensive model for contamination sources and geochemical reactions including the city of Erdenet, Mongolia. As major metal contaminants relevant to mining have been As, Cd, Cu, Pb, Zn, and the Erdenet city was contaminated with As, Cu, Mo, Zn, and SO_4^{2-}, we principally used Cu, Mo, Pb, Zn,

and S-O isotopes in SO_4^{2-}. Contamination sources of groundwater and surface water were differentiated as tailings dump, excavated ore, heap leaching, ash pond of a power plant, and an argillic alteration zone. Also, isotopic investigation and positive matrix factorization for soil revealed the tailings dust contaminated as far as the eastern part of residential area. Furthermore, to assess oxidative dissolution of sulfides and adsorption, $\delta^{65}Cu$ and $\delta^{98}Mo+\delta^{66}Zn$ were useful, respectively.

Keywords: Metal isotopes, Erdenet mine, Water and soil contamination, Comprehensive model

LATE ORDOVICIAN MAGMATIC EVENT IN THE WESTERN GOBI ALTAI ZONE, SW MONGOLIA

Pavel Hanžl[1]*, Lucie Uhrová[1], Kristýna Hrdličková[1], Karel Schulman[1], David Buriánek[1], Orgil Gansukh[2], Jitka Míková[1]

[1] Czech Geological Survey, Prague, Czech Republic
[2] Geological Institute MAS, Ulaanbaatar, Mongolia
*Corresponding author: pavel.hanzl@geology.cz

The Mongolian Altai Domain of the Central Asian Orogenic Belt is formed by a giant Lower Palaeozoic accretionary wedge (the Mongolian Altai accretionary wedge) that was later thrust over the northerly Central Mongolian Microcontinent. It mainly consists of late Cambrian to Ordovician volcano-sedimentary rocks represented by the various formations within the Tugrug Group. These sequences were deformed, metamorphosed, and intruded by numerous plutons during the Devonian–Permian orogenic events. New U–Pb zircon ages of igneous rocks from Ar Dalangiin Range (50 km south of Biger soum) indicate the existence of so far neglected late Ordovician thermal event affecting the Mongolian Altai accretionary wedge. The felsic volcanic sheet inside the upper part of the Tugrug Group in the western part of the Gobi-Altai Zone (Mongolian Altai Domain,) yields the age of 457 ± 2 Ma and the nearby granite pluton intruding this volcano-sedimentary sequence yields the age of 445 ± 1 Ma. Both rocks are high-K calc-alkaline peraluminous, with similar geochemical patterns characterised by enrichment in mobile lithophile elements relatively to Nb, Ti, and Sr and nearly identical REE trends, which all together point to a similar magma source in volcanic arc environment. Late Ordovician magmatic event reflects the terminal stages of formation of the Mongolian Altai accretionary wedge and could represent sporadic magmatic pulses related to post-contraction event connected with the closure of the Cambrian–Ordovician fore-arc basin, following by the initial opening of the Silurian–Devonian bac-arc basin.

The research was supported by the project GAČR EXPRO 19-27682X and presented data were published in the Journal of Geosciences: http://doi.org/10.3190/jgeosci.385

PETROGENESIS OF THE KHAN BOGD RHYOLITES AND GRANITES IN THE SOUTH MONGOLIA

Ying Tong[1], PengJie Liu[1]

[1] Beijing SHRIMP Center, Institute of Geology, Chinese Academy of Geological Sciences, Beijing 100037, CHINA

Coeval and co-located rhyolites and granites often exhibit spatial, temporal, and genetic connections. Their compositions can be equivalent, complementary, or distinct from one another, making their relationship an intriguing subject for scientific study. The LA-ICP-MS U-Pb dating of rhyolite on the northeast side of the Khan Bogd alkaline granitic pluton has yielded

ages of 301 ± 3 Ma, which are comparable to those of the late intrusive Khan Bogd alkaline granites (291-300 Ma). Both these rhyolites and granites have high SiO_2 (> 72.63 wt%) contents and display A-type magmatic affinity. They are characterized by significant enrichment in alkalis (K_2O + Na_2O = 7.82-9.48 wt%), Ga, Zr, Nb, and Y, and depletion in Sr and P. Their REE patterns show strong negative Eu anomalies (0.10 - 0.20) and they have consistent Nd isotopic compositions (εNd(t) = +6.1 ~ +8.5). However, there are notable differences between the rhyolites and alkaline granites. For instance, the rhyolites lack typical alkaline dark minerals as the granites, have significantly lower Ga/Al ratios than the granites, relatively higher K_2O content, lower TiO_2 and Na_2O content, and lower Zr saturation temperatures. These distinctions suggest that while both the rhyolites and granites may originate from mantle-derived juvenile crust in a post-collisional setting, the late intrusive granites were neither formed through mush reactivation or melt extraction from mushes to create eruptible rhyolitic liquids, nor did they evolve through the crystallization of rhyolitic magma. The Khan Bogd coeval rhyolites and granites might not share a direct magmatic connection.

NEW ASSEMBLAGE OF SMALL SHELLY FOSSILS (CAMBRIAN STAGE 3) FROM THE LAKE ZONE OF WESTERN MONGOLIA

Ben Yang[1]*, Michael Steiner[2]

[1] Institute of Geology, Chinese Academy of Geological Sciences, Beijing 100037. CHINA
[2] Shandong University of Science and Technology; College of Earth Science and Engineering, No. 579 Qianwangang Road, Qingdao 166590, Shandong, P.R. CHINA.
*Corresponding author: yangben8@fomail.com

The Lake Zone in western Mongolia is an island arc terrane with a complex tectonic background. As a result, the early Cambrian strata in this area have been poorly studied, with only rare reports of small shelly fossils. This has limited our understanding of the early Cambrian stratigraphic distribution and palaeogeographic attributes of the region. In this report, we present a new assemblage of small shelly fossils from the Icheet Formation in the Khan-Khukhii region of the Lake Zone, including *Cambrocassis verrucata*, *Rhombocorniculum cancellatum*, *Lapworthella* sp., *Hyolithellus insolitus*. This assemblage effectively constrains the strata to Cambrian Stage 3, providing firm evidence for correlation with other regions in Mongolia and other continents, such as Maly Karat and Talassy Alatau in Kazakhstan, Siberia, and the Yangtze Platform.

PALAEOGEOGRAPHIC MODELS OF PRECAMBRIAN-CAMBRIAN TERRAINS: TESTED BY SMALL SHELLY FOSSIL BIOPROVINCE ASSIGNMENTS

Michael Steiner[1]*

[1] Shandong University of Science and Technology; College of Earth Science and Engineering, No. 579 Qianwangang Road, Qingdao 166590, Shandong Province, P.R. CHINA.
*Corresponding author: michael.steiner@fu-berlin.de

The Neoproterozoic-Cambrian transition marks a period of significant reorganization and innovation in Earth's geosphere, hydrosphere, and biosphere. The Cambrian explosion, a key biotic revolution in Earth's history, saw the rapid emergence of most metazoan body plans within a relatively brief span of approximately 20 million years in the fossil record. This event is primarily characterized by a substantial increase in disparity, with a more moderate rise in

metazoan diversity. While several hypotheses have been proposed to explain the Cambrian bioradiation, no consensus has been reached yet.

To better understand the causes of the Cambrian bioradiation, it is essential to further investigate the sedimentological, geochemical, palaeontological, environmental, and tectonic aspects of Earth's evolution during the Precambrian-Cambrian transition. Astronomical, geophysical, and tectonic factors likely played a critical role in this event. However, there is comparatively less detailed information available on these aspects of Earth's evolution than on other geoscientific subjects related to the Cambrian bioradiation, such as the geochemical signatures in sedimentary strata. Previous discussions have suggested that the geotectonic regime and specific palaeogeographic configurations, including the presence of large supercontinents or particular ocean configurations, may have significantly influenced biotic development during the Ediacaran-Cambrian period. Geographic speciation, driven by physical barriers such as deep oceanic basins for benthic fauna with lecithotrophic larval development, is a crucial mechanism in the evolution of metazoans, alongside competitive speciation and polyploidy. Therefore, reconstructing the palaeogeography and biogeography of the Ediacaran and early Cambrian is vital for a comprehensive understanding of the Cambrian bioradiation.

Unfortunately, the palaeogeography of the Ediacaran to early Cambrian remains poorly constrained. Recent palaeogeographic reconstructions reveal significant uncertainties regarding the positions of smaller continental blocks (e.g., North China, Mongolian microcontinents) and terrains (e.g., Kazakh terrains). While larger continents, such as Baltica and Laurentia, exhibit robust data consistency across different palaeogeographic reconstructions, smaller terrains and microcontinents within the Central Asian Orogenic Belt (CAOB) present only tentative hypotheses about their palaeogeographic positions. For instance, Mongolia consists of over 44 terrains, the geological history and pre-orogenic palaeogeographic assignments of which are still uncertain. These uncertainties largely stem from the remagnetization of cover sediments during orogenic events, such as the collisions and orogeny within the CAOB that began in the Furongian.

To test the accuracy of existing palaeogeographic reconstructions for the critical Precambrian-Cambrian transition, we compiled Small Shelly Fossil (SSF) absence/presence data across different Cambrian time intervals. We performed hierarchical cluster analyses of the SSF fauna data to assess the faunal similarities between different tectonic or geographic sub-regions. The SSF fauna was grouped into larger biogeographic provinces, enabling us to discuss palaeobiogeographic relationships and compare our findings with existing palaeogeographic models based on palaeomagnetic data. These biogeographic results allowed us to develop more precise palaeogeographic reconstructions for smaller tectonic blocks of Mongolia that underwent collisional events. Based on the palaeobiogeographic reconstruction of SSF data, we also proposed a hypothesis for early Cambrian ocean circulation patterns, drawing on modern ocean circulation constraints. This approach offers an independent toolkit to test the validity of existing palaeogeographic models from deep time, one that is less susceptible to tectonic overprinting.

AUTOMATED QUANTITATIVE MINERAL CHARACTERIZATION OF PRIMARY ORE TYPES FROM THE ERDENETIIN OVOO CU-MO PORPHYRY DEPOSIT, MONGOLIA

Batmunkh Tumen-Ayush[1], Narangerel Adiyasuren[3], Davaadulam Batbileg[3], Ganbileg Davaajav[3], Oyuntungalag Khaltar[1], Chinzorig Bavuu[2], Ganzorig Chimed[3*]

[1]Erdenet Mining Corporation SOE, Orkhon province, Erdenet 61027, Mongolia
[2]Department of Mining Technology, School of Geology and Mining Engineering, Mongolian University of Science and Technology, Ulaanbaatar 14191, Mongolia

[3]Center for Nanoscience and Nanotechnology, Department of Chemical and Biochemical Engineering, School of Engineering and Technology, National University of Mongolia, Ulaanbaatar 14201, Mongolia
*Corresponding author: ch_ganzorig@num.edu.mn

The Erdenetiin Ovoo represents the largest Cu-Mo porphyry deposit in Mongolia. This study focuses on the primary ore types of the deposit-biotite granodiorite (BGDP) and granodiorite (GDIR)-examining their mineral composition and associations. Specifically, granodiorite is analyzed for its petrographic and mineragraphic properties. Utilizing the petrographic and mineragraphic method, mineral associations, alterations, and formation types are investigated, comparing these findings with results obtained from the TESCAN Integrated Mineral Analyzer (TIMA), a sophisticated automated quantitative technique. TIMA method is employed to determine mineral composition, liberation, association, and their grain size analysis rapidly and accurately, integrating Scanning Electron Microscopy (SEM), Back-Scattering Electron Microscopy (BSE), and Electron-Dispersive X-ray Spectroscopy (EDX). Petrographic and mineragraphic analysis identifies the origin of the minerals, their content, and textural relationships. The samples used in this research are collected from six boreholes for each rock type (BGDP and GDIR), with approximately 90-meter interval into the core of the orebody. The study focuses on the relationship between these results and their respective depths. From analysis of modal mineralogy, k-feldspar and quartz are found to constitute approximately two-thirds of the content in both ore types, with k-feldspar becoming more dominant as depth increases. Chalcopyrite as the primary valuable mineral, is predominantly associated and interlocked with pyrite and magnetite, as determined by petrographic and mineragraphic analysis. Petrographic and mineragraphic characterizations are attributed to a conclusion that from the primary sulfide zones at current operation level, pyrite-chalcopyrite-magnetite and quartz-molybdenite veins are formed in inclusion structure as the elevation level decreases to 635 m. In the mineral association quantitative analysis, gangue minerals such as biotite, carbonate, clay, and silicate minerals, particularly muscovite, are associated with both ore types. In the false-color images obtained from TIMA analysis, muscovite and quartz are identified as the most common minerals in composition and are frequently associated with both ore types, compared to the petrographic method.

Keywords: chalcopyrite, granidiorite, biotite granodiorite, TIMA, petrography

CHRONOLOGY OF THE EDIACARAN-CAMBRIAN BOUNDARY: DISCUSSION WITH NEW DATA FROM AKSU AREA OF XINJIANG PROVINCE, CHINA

Ben Yang[1]

[1] Institute of Geology, Chinese Academy of Geological Sciences, Beijing 100037, CHINA

GSSP of the Ediacaran-Cambrian Boundary is currently set at the Fortune Head section in Newfoundland of Canada, indexed by the first appearance datum (FAD) of the trace fossil *Treptichnus pedum*. The Ediacaran- lower Cambrian deposits in this section are composed with siliciclastic sediments preserving no δC^{13} isotope value and missing the earliest record of body fossils (small shelly fossils or acritarchs etc.). In addition, the FAD of *Treptichnus pedum* in global sections varied in the lower Cambrian strata. These problems have been challenging the section as a GSSP. Studies are discussing on reassessing the current section or selecting other potential sections for the boundary though most of them has similar problems. Here we make a preliminary discussion on the global correlation of Ediacaran- Cambrian Boundary with new data from the Aksu region of Xinjiang Province in China. The Aksu areas, lying in the northwestern part of the Tarim Block, preserves a set of sections with the earliest small shelly fossils (*Protohertzina anabarica*, *Protohertzina unguliformis*, *Anabarites trisulcatus*, etc.), acritarchs, trace fossils, also δC^{13} isotope data around the boundary. Our data demonstrates

a consistence among different types of the data. It is with different sections globally, that not only with siliciclastic deposits containing trace fossils but also carbonatic deposits with body fossils and carbon isotope values. We would like to achieve a convincing global correlation of the Ediacaran-Cambrian Boundary with such a comprehensive data set.

SUGGESTED METHODS OF EVALUATING GROUND REINFORCEMENT TENDON INTEGRITY IN ENVIRONMENTALLY CHALLENGING GROUND IN TUNNELLING AND MILIJIE GUOING

Naj Aziz[1]*, Adel Mottahedi[1]*, Alex Remennikov[1], Kevin Marston[1], Zhenjun Shan[2]*

[1] School of Civil, Mining, and Environmental Engineering, University of Wollongong, Wollongong, AUSTRALIA
[2] University of Wollongong
*Corresponding authors: naj@uow.edu.au; am3887@uow.edu.au; r.shan@blackrockmining.net

Abstract

Ground reinforcement in tunnelling and underground structures is, in recent times, relying heavily on the use of bolting technology for effective support and structure stabilisation. Tunnels and underground constructions normally pass through geologically diverse ground formation with environmental challenging conditions. The current approach to minimise the onset of corrosion in reinforcement tendons is by covering bolts and cable bolts with protective plastic sleeves, however the integrity of the sleeve requires checking in laboratory for long term bolt endurance in the face of ground deformation and water incursion. Accordingly the following are suggested methods for evaluating the credibility of the installed bolts; a) the tensile strength characteristics of the rock bolts; b) pull-out testing of bolts out of 300-mm diameter 40 to 60 MPa strength concrete cylinders, as well as from the Short Encapsulation Double Embedment Steel Split Set (SEDESS); c) bolt integrity test fitted with CPS by shear testing using Single Shear Test (SST) and/ or Double Shear Test (DST) methods; d) the dome plate deformation tests involved pulling the supplied bolt dome grout head through the dome plate with the dome-shaped nut being used as a grouting adapter with a grouting hole and weld-on sleeve. Laboratory test results are presented on bolts used in tunnel wall reinforcements and conclusions drawn

Introduction

In underground mining and in tunnel construction, rock bolting normally involve driving through rock formation of different geological and environmental conditions. The effectiveness of the method is dependent on the rock type, rock strength, rock bed orientation and ground water condition. In surface mining rock bolting has been used for slope stability and in civil engineering it is conveniently applied in, transport road embankment, cliff and escarpment reinforcement. The Sea Cliff bridge escarpments face bolting, in North Wollongong. NSW, Australia (Figure 1) is a typical case of face stabilisation using long rock bolts. The past traditional masonry and steel arched reinforced tunnels consumed almost 15 percent of the excavated ground space. This level of reduction in space consumption formed the basis of what is now known as the New Austrian Tunnelling Method (NATM), which is also known as sprayed concrete lining method (SCL), a method of modern tunnel design and construction employing sophisticated monitoring to optimize various wall reinforcement techniques based on the type of rock encountered as tunnelling progresses. This technique first gained attention in the 1960s based on the work of Ladislaus von Rabcewicz, Leopold Müller, and Franz Pacher between 1957 and 1965 in Austria (Golser, 1976). The name NATM was intended to distinguish it from earlier methods, with its economic advantage of employing inherent geological strength available in the surrounding rock mass to stabilize the tunnel wherever possible rather than reinforcing the entire tunnel. The popularity of utilising bolting was also recognised in Australia with the application of mechanically anchored rock bolts for large diameter tunnels in highly fractured rock, typically in The Snowy Mountain Scheme (TSMS), a hydroelectricity and irrigation complex in Kosciuszko National Park, New South Wales, Australia. Now, the use of bolting system has replaced the old wooden props and steel arch

systems in mines and other underground excavations, as an efficient and economical way of tunnel construction with greater speed.

The present day tunnels are constructed in competent ground by using the modern tunnel boring machines. However, in weaker ground and in an environmentally challenging ground, the use of bolting reinforcement is recognised as an acceptable method. More recently, the application of rock bolting for long lasting purpose has necessitated a fully trusted approach in maintaining the installed bolts for longer life, thus minimising the influence of corrosive ground water to the life of the installed bolt. Effective protection of bolts is, in recent times, involves the use of specially constructed bolts to be covered with plastic sleeve and grouted in the borehole.

Figure 1: Sea bridge cliff escarpment, North Wollongong, NSW, Australia.

In mines, rock failures can occur either ground failures due to in effective support system usage or ground failures attributed to ground seismicity. In recent past, typical non-coal mines cases in Australian attributed to ground seismicity include the 1999 North Park Air Blast Mine disaster, in NSW on November 24, 1999, which killed four mine personnel. The mine was operating the block caving method of mining. The other mines rock burst occurred in Beaconsfield on 25th April 2006. Ironically, dynamic rock bolting study began initially in North America, and later dynamic testing was carried out at Kalgoorlie School of mines in WA. Initially the dynamic testing of bolts was carried out by axially tension, later on Li, et al (2019) reported on dynamic testing of small capacity bolts in shear. Recently, a number of studies have been reported from the University of Wollongong, where the methodology is currently being expanded to large capacity bolts and cables with 1.3 t capacity drop hammer with drop height exceeding 4 m.

The availability of various facilities for testing tendons, statically and dynamically at the School of Civil, Mining, Environmental and Architectural Engineering (CMEA), thus, the strength characteristics of the bolts fitted with plastic sleeves to combat corrosion and long term stability of the bolts is the subject of this paper.

Materials and Methods

In evaluating the characteristics of a tunnel tendon installed in a borehole in tunnel wall, may require the inclusion of the bolt grouting spherical head and dome plate interaction. This is different from bolts used in coal mines as well as in general civil engineering. A special type of bolting system is used, which involve the incorporation of protective sleeve over the bolt to minimise steel bolt corrosion, and the availability of spherical grouting head of the bolt as well as a special cover plate with a dome for seating the spherical grouting head as shown in Figure 2.

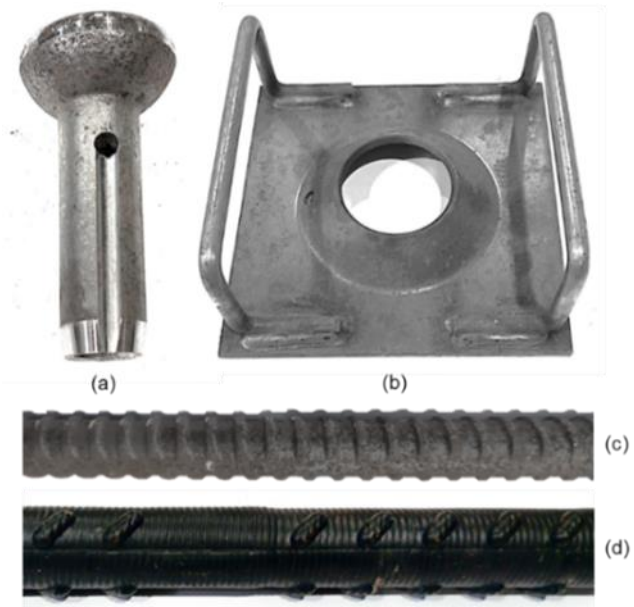

Figure 2: Tunnel reinforcement bolting system (a) spherical grout injection head, (b) dome plate, (c) rebar bolt, and (d) plastic sleeve.

The performance of the bolting system does not fall solely on the tendon/rock bolt element alone, other elements bear influence, which include:

1. Type of the host medium: The host medium can be concrete of varying strength, shape and size. The host medium should reflect on the characteristics of the ground formation the borehole diameter, and roughness: The borehole diameter should be marinated consistent with the actual diameter of the bolt used.
2. Grout type: This could be chemical resin or cementation type can generate adequate strength commensurate with the installed rock strength.
3. Bolt collar plate shape, thickness and dimension,
4. Sleeve type, wall thickness and surface roughness: 3 mm thick plastic tube

In this study, the common M24 bolt of diameter of 24 mm and core diameter of 22 mm was used. The tensile strength was designated at around 36 t failure load, and Yield load of 32 t.

Equipment

Two methods are available for evaluating bolt performance characteristics statically as well as dynamically. In general the common method of testing bolts is carried out statically, because of the past tradition of testing *in situ* as well as in laboratory. Testing for tendons dynamically has, in recent years grown, due to the interest on ground seismicity and better understanding of the rock burst ground seismicity both in coal and non-coal mine outbursts. However, dynamic testing has not been reported from field studies and is only carried out only in laboratory. Various facilities for testing rock bolts statically axially and shear, include:

- Universal tensile loading machines
- High capacity compression machine
- Single and double shear testing rigs. The double shear rigs can be carried out with and without contacts between host medium faces. A lateral truss system incorporated to the double shear rig stops adjacent host medium faces coming in contact with each other during shearing process, thus enabling true evaluation of the tendon strength.
- Host medium variety, consisting of rectangular and circular shaped types. Both circular and rectangular host medium have circular and rectangular shaped clamps.

Pull test methods

Several methods of pull testing are available. These include pull testing of bolts out of steel tubes or from composite material such as concrete cylinders. These methods are documented

by Mottahedi, et al (2024). The tensile pull testing of a bolt or a cable bolt can be carried out in several ways depending on the tested tendon. It includes;

- Single embedment pull test. A single end pull testing of tendon out of steel tube (Aziz, et al, 2006), concrete or Rock, leaving the other side bear, to be gripped to tensile testing machine gripping jaws. This method is called the Short Length Pull Test (SLPT). This method can be used both in the laboratory and in field.
- Double embedment pull test in steel tube (Aziz, et al, 2016)
- Split steel set apparatus with a fixed encapsulation hole diameter (Figure 3a)
- Split steel set with variable diameter apparatus (Figure 3b),
- Composite medium using concrete cylinders (Ur-Rahman, et al, 2015, Hagan and Chen (2010) (ACARP Project 2010) and Aziz, et al (2017)). The system is easily prepared and tested. The system can also be reinforced internally and externally (Figure 5)
- Rock medium can be prepared in the laboratory. It is a laborious task, which makes it less favourably for wider use (Clifford et al., 2001).

All the above methods are well documented by Mottahedi, et al, (2024) and in various papers in the Resource Operators Conference (formally coal Operators conference) via <https://www.resourceconference.com.au>

It should be noted that, the results of pull testing of a bolt may vary, for the same encapsulation length, depending on the medium used, the grout type, the annulus grout thickness and encapsulated hole roughness. Pulling out load of the encapsulated bolt from concrete or prepared rock host medium is likely to result in lower force value in comparison with rigid steel pipes or the split set system. The reduction in pull force from concrete and rock samples can be attributed to the occurrence lateral and axial cracking of the soft medium like concrete or rock mass, whereas the solid and stiff steel tube or steel split set will be required greater pull out force because of the steel stiffness. Accordingly the following two methods are reported in this paper.

a) Short Encapsulation Double Embedment Steel Split Set (SEDESSS) using a fixed diameter hole

Figure 4 shows the picture of the fixed diameter hole split set. The apparatus is 300 mm long split set steel block, which has a single central hole of 27 mm in diameter, machined along its 250 mm long split set section. A 400-mm long bolt section was grouted in the two sections of split set steel block in the double embedment arrangement. The encapsulation lengths in the double embedment steel set were varied, with one side being longer in length than in the other side, so that only one side of the bolt is pull out, when loaded as shown in Figure 3e. The two encapsulation lengths used in this test were 220 mm and 180 mm respectively. The grout water-to-cement (w/c) ratio was 0.35. Figure 3f shows the load-displacement graphs of two specimens subjected to the split set pull test. In test 1, the maximum load achieved was 128.4 kN, at the corresponding displacement of 1.9 mm. In test 2, the ultimate pull-out load was 136.5 kN, at the corresponding displacement of 1.7 mm. The rate of pull-out force in tests 1 and 2 were 0.713 kN/mm (128.4 kN/180mm) and 0.758 kN/mm (136.5 kN/180mm), respectively.

Since the split set system is made of steel, it is a high stiffness apparatus, with sleeve medium consisting of two steel sections, butted and firmly bolted together, they are unlikely to undergo deformation or lateral opening during the pull-out process, hence a lower level of displacement.

b) SEDESSS of the bolt covered by Corrosion Protection Sleeve (CPS)

To evaluate the pull out testing of the bolt covered with corrosion protection sleeve, a larger size SEDESSS was developed by Aziz et al., (2016) for testing tendons of various diameters ranging from 24 mm diameter rock bolts to variable diameter cable bolt of up to 31 mm diameter. As shown in Figure 4a, the device consists of two main parts, internal and external parts. When these parts are butted together and bolted tight, the 42-mm diameter grooved central holes will be formed. To assess the performance of the bolt sheathed by CPS, first, a 200-mm length protection sleeve was grouted inside the apparatus. Next, the bolt was

anchored to the depth of 200 mm using the same type of grout. The layout of this test is shown in Figure 4b. The assembled unit was then mounted into a tensile testing machine's jaw and the bolt was pulled until it was debonded along one of the interfaces.

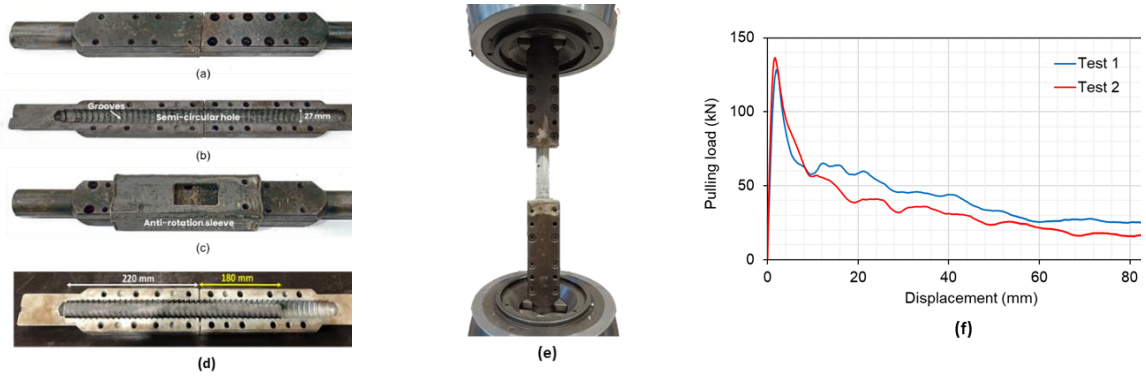

Figure 3: (a-d) Split steel set fixed diameter apparatus, (e) Pull test arrangement of a bolt with anti-rotation sleeve removed, and (f) Load-displacement of pull test results of two bolts with varied encapsulated lengths of 200 mm and 150 mm.

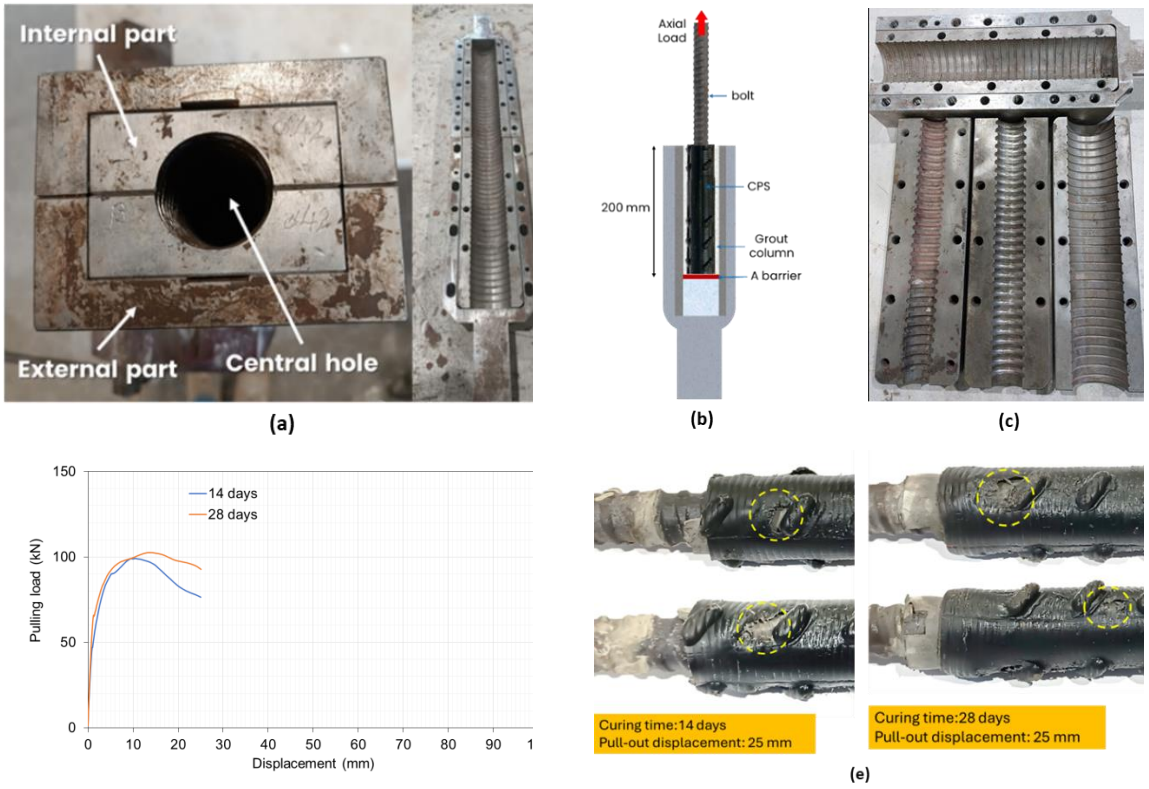

Figure 4: (a-d) Variable diameter steel split set Apparatus, (b) Pull test arrangement of the sleeved bolt, (c) multi-diameter internal section half holes, and (d) Load displacement of bolts in 14 and 28 days of sleeve installations. *c) Pull Testing of Bolts in Concrete Cylinders*

As shown in Figure 4d, the ultimate load attained was around 111.5 kN, at the corresponding displacement of 7.5 mm. In addition, the rate of pullout load was 0.558 kN/mm (111.5 kN/200mm). As can be seen, and in comparison, with tests without sleeve, in the peak point, larger displacement was resulted by less pull-out load. In addition, at displacement of 100 mm the residual load of the test specimen with plastic sleeve (around 14.7 kN) was lower than the specimen without sleeve (around 25 kN). These differences might be attributed to the softer nature of the plastic sleeve. As seen in Figure 4e, the CPS partially pulled out or stretched out by 17 mm, and the sleeve was cracked, therefore the cracked CPS may cause water leakage and bolt corrosion, thus affecting the bolt's performance and ground stability in the long term.

In this method two laboratory based methods of testing can be undertaken in 300 mm diameter concrete cylinders, varying in length between 300 mm and 450 mm respectively using: (a) the normal direct pull testing method and (b) the Reverse Pull Test Machine (RPTM) using the apparatus shown in Figure 5. The normal pull test technique involve anchoring a section of the bolt length in the first 1/3 length (from the bottom) of 450 mm long concrete cylinder (40 MPa strength) and pulling out the anchored section upwards using the facilities as reported by Chen et al. (2017), Rastegarmanesh et al. (2024). The reverse test method consists of pushing the concrete downwards from the bolt, with the top free section of the bolt being firmly anchored to the frame in Figure 5 (Anzanpour et al., 2021). The anchorage of the bolt into the steel frame ensures total stability of the concrete medium, with external steel confinement. Figure 6 shows the graph of load–displacement of the bolt being pulled out of the concrete together with pull testing.

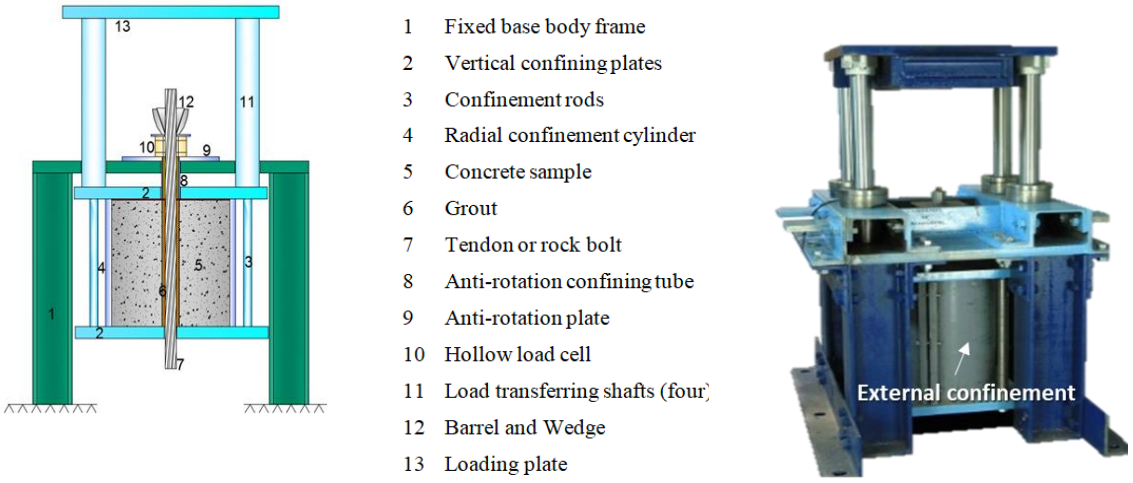

Figure 5: Reverse Pull Test Machine (Anzanpour et al., 2021).

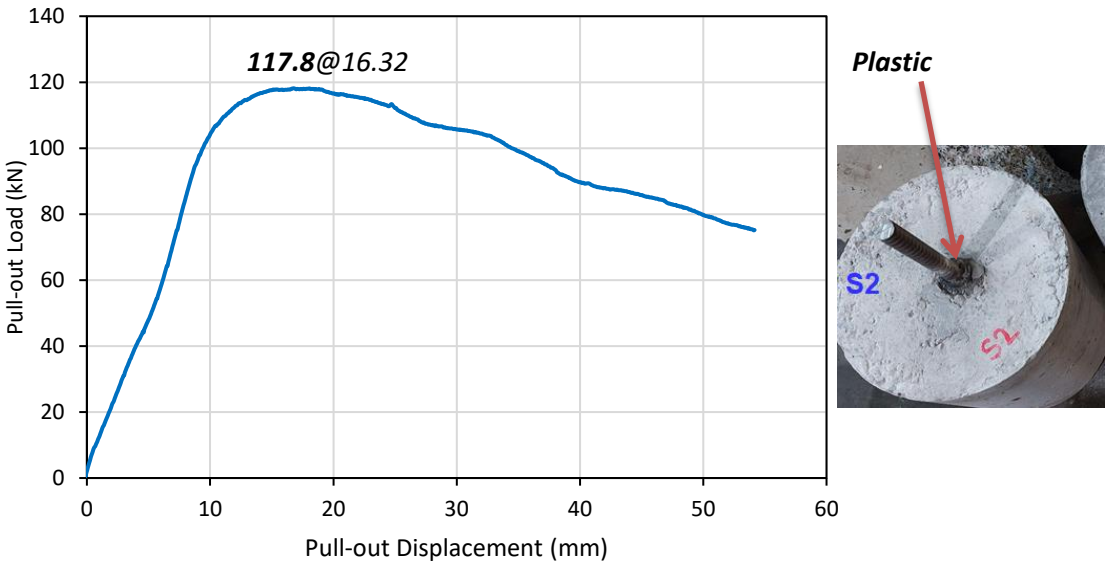

Figure 6: The load– displacement graphs with peak load of tested sample fitted with plastic sleeve.

Double Shear Tests

Different rigs has been developed for shear testing of tendons (see Figure 7). In this paper, the Double Shear (DS) Test was used to determine the integrity and the absence of damage to the corrosion protective sheath (sleeve). Each shear test was carried out using the small Size double shear apparatus (MK1), which is one of four versions of DS Systems available at

the rock mechanics laboratory at the school of Civil, Mining, Environmental and Architectural Engineering, UOW.

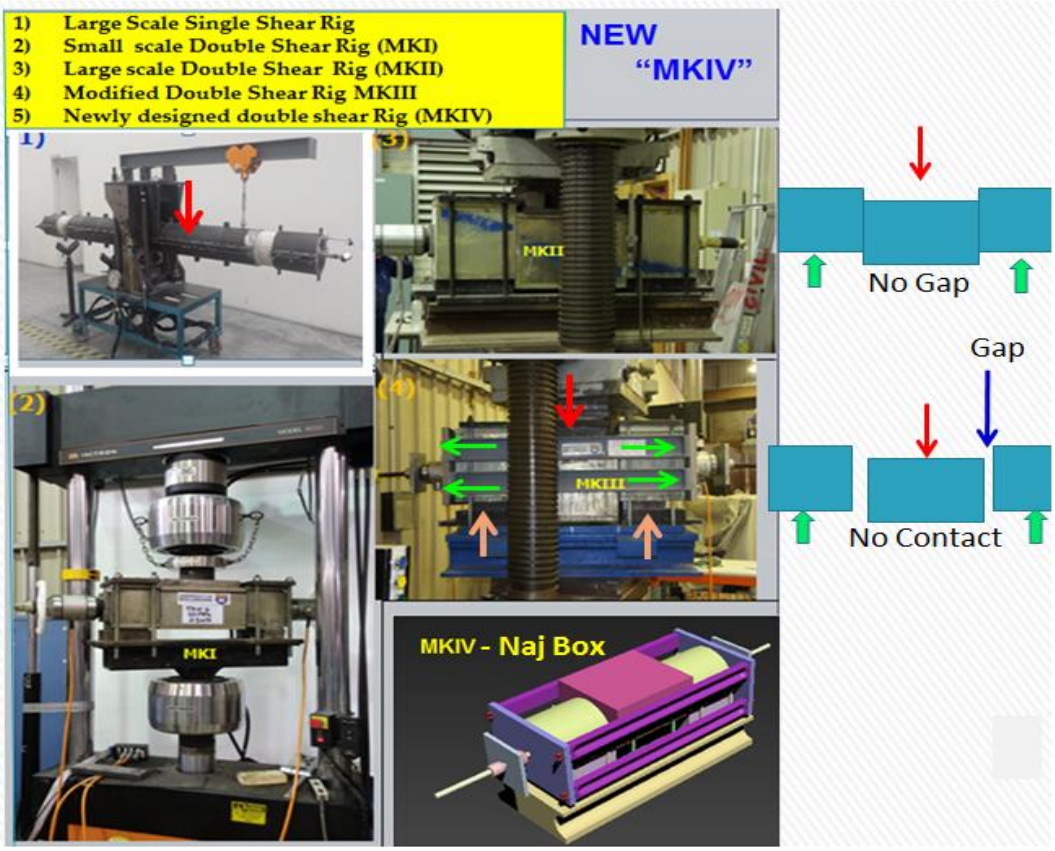

Figure 7: different versions of DS rigs for static and dynamic shear testing of tendons.

(a) (b) (c)

Figure 8: Preparation of concrete blocks for DS tests.

Shear tests were planned in concrete medium for shear displacements of 10 mm, 20 mm, 25 mm, 30 mm, and 40 mm; however, in reality shear tests were carried out in the reverse order, starting with 40 mm, 35 mm, 25 mm, 20 mm and 10 mm respectively. No further test was deemed necessary beyond the last lower shear displacement with no sign of sleeve damage. Once cast, the concrete blocks were left in a water bath to cure and reach the desired strength after 28 days. Then, bolts were installed in each DS set up, and pretensioned to 50 kN (5 t) force and monitored using 75 t capacity hollow load cells installed axially on either side of the assembled double shear set up. Each tensioned bolt was encapsulated using Crosbie cementitious grout (Type Crosbie 190). Each bolt was anchored in a 35-42 mm in diameter hole. The concrete blocks were prepared using 8-10mm gravel. The strength of the concrete was maintained at 40 MPa by testing 100 mm diameter x 200 mm long cylindrical samples prepared from poured concrete as indicated by the red arrows in Figure 8.

Each assembled bolt in the DS rig was then mounted on the 50-t capacity Instron Universal Testing Machine, and shear loaded at a rate of 1 mm/min as shown in Figure 9. Table 1 shows the results of double shear test of four bolts with vertical shear displacement between 20 and

40 mm respectively. Figure 10a shows load-displacement graphs from four tests. Figure 10b shows the individual view of sheared bolt sleeves and vertical shear displacements after the tests.

Figure 9: Double shear loading of MKI assembly by Instron testing machine

Table 1: Double Shear displacement, maximum shear load and sleeve conditions for each test

Test No.	Maximum applied load (kN)	Vertical displacement (mm)	Post-shear sleeve condition
1	192.3	20.0	Slightly bruised
2	201.6	25.0	Bruised sleeve, but un- cracked
3	196.70	30.0	Bruised sleeve, which might be cracked, but difficult to ascertain.
4	282.24	40.0	Bolt snapped, with torn sleeve

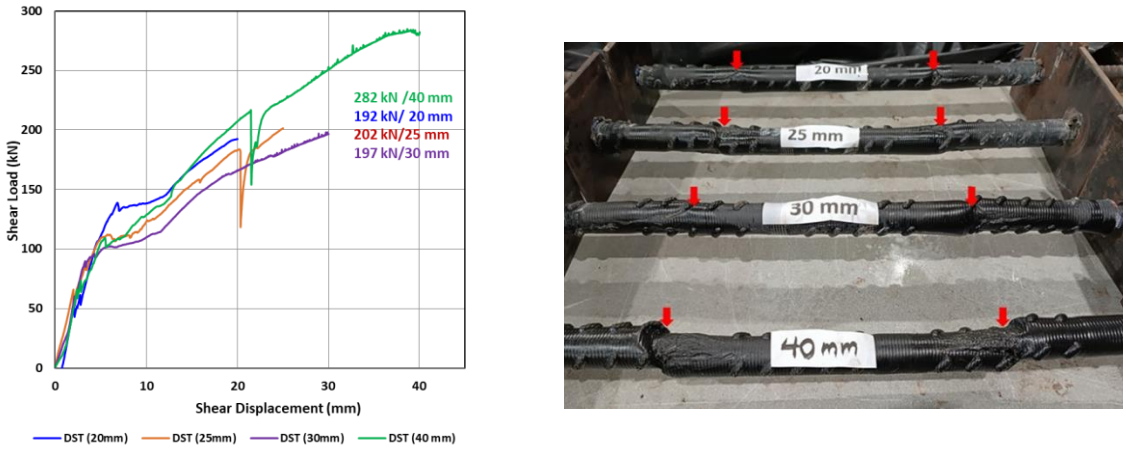

(a) **(b)**

Figure 10: (a) The load – displacement graphs of samples for shear testing and (b) post-test observation of the sheared bolt sleeves at 20, 25, 30 and 40 mm.

Single Shear Tests

In addition to double shear tests, bolts were also tested using a single shear test method as shown in Figure 11a. As a guillotine type apparatus, the encapsulated bolt was grouted in a 5 mm thick smooth wall plastic tube either cementitious or the chemical resin grout to act as

the outside protection layer. A 12 mm ring strip of the plastic cover was removed from the mid-section of the encapsulated cable section to expose the plastic tube to allow the plastic sleeve to be visually inspected when sheared. Shearing of the bolt section was carried out in four displacement steps, until cracks appeared in the plastic sleeve. Figure 11b shows test view of shearing bolts. Bolt sheared to 40 mm failed on both sides.

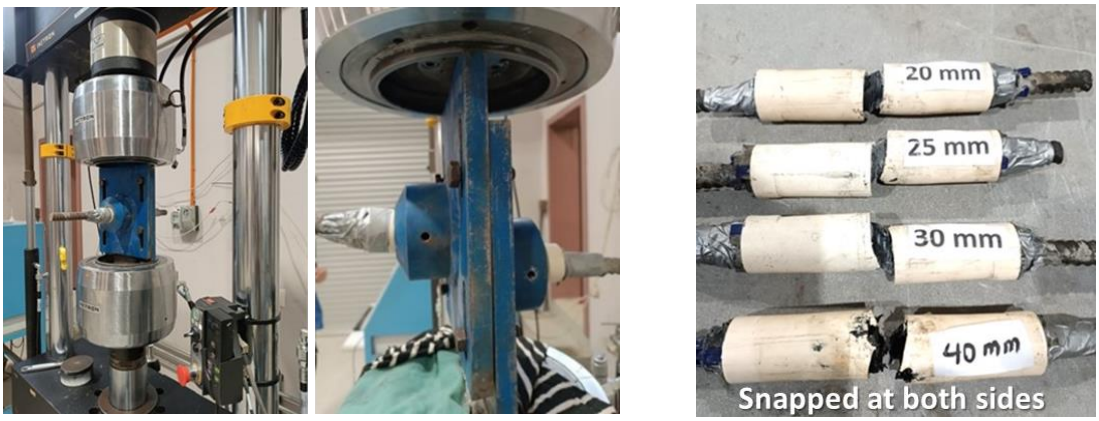

(a) **(b)**

Figure 11: (a) Pre and post-test single sheared apparatus with sheared bolt and (b) sheared bolts at different vertical shear displacement.

Table 2 shows the shear load values at vertical shear displacement by single shear method. Figure 12 shows the graphs of shearing profiles. The increase in shear displacement has contributed to the increase in sleeve bruise and the severity of such bruise increase coincides with the increase in vertical shear displacement, ultimately leading to sleeve cracking from 40 mm of vertical displacement down to 25 mm. With a closer and carful inspection of tested samples, it was found that the onset of sleeve cracking started from 25 mm of vertical shear displacement. Specifically:

a. There was no sleeve damage at 20 mm displacement,
b. The sleeve started bruising and deteriorating at a vertical shear displacement of 25 mm,
c. Clear cracks appeared at 30 mm of vertical shear displacement, and
d. The bolt snapped at a vertical shear displacement of 40 mm.

It should be noted that the single shear test was tested in a rigid environment of steel with a diameter at 50 mm. The snapped bolt was fully sheared in a stiff environment without being subjected partially to tensile load. Accordingly, the resultant shear load failures at different shear displacements will be different from that obtained with bolts being sheared using the double shear apparatus with different concrete strength medium.

Table 2: shear load and displacement by single shear technique

Test No.	Load (kN)	displacement (mm)
1	117	20
2	178	24.9
3	184	30
4	239	38

The role of medium strength characteristics

The strength of the medium and its stiffness has an influence on shear loading and shear displacement. In lower strength concrete, the applied shear load may cause the medium to crack and crush heavily, causing the bolt-hole to deform, causing the bolt to bend significantly in comparison with stiff medium (as an example: the case of shear testing of bolt in granite rock with, say UCS >130 MPa compared with shear testing in mudstone of 40 MPa strength, Higher shear load will result when testing in mudstone as against testing in granite rock. The

failure in mudstone is due to a combination of tensile and shears, as the crushed concrete causes bolt bending excessively at the crushed block end leading to tensile loading of the bolt.

The main objective of this study was, from the onset, to determine the resilience of sleeves at different shear displacements. This was achieved with crack formation due to vertical shear starting at around 25 mm and is consistent with both the single and double shear test methods.

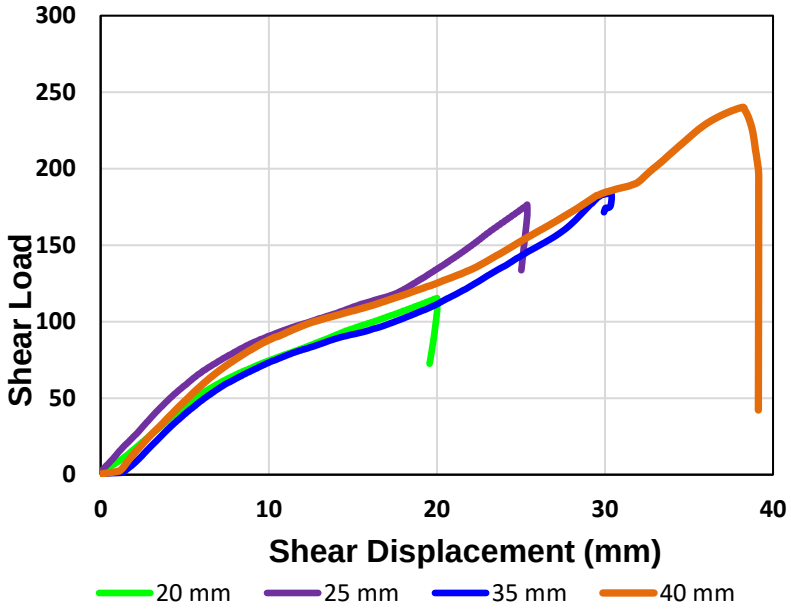

Figure 12: Shear load and shear displacement in single shear test at various vertical shear displacements.

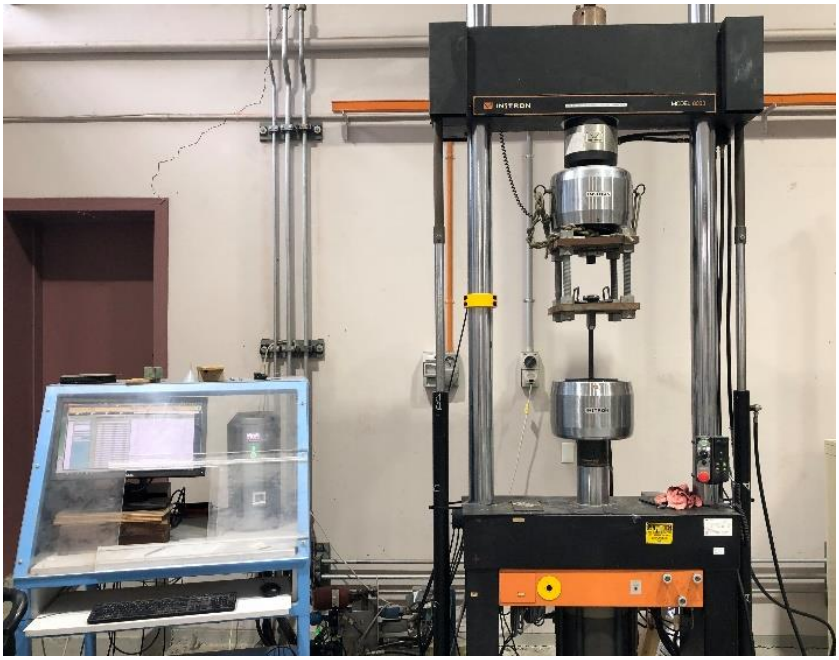

Figure 13: Test set-up for dome plate deformation test.

Dome plate deformation test

The dome plate deformation tests involved pulling out the supplied bolt with domed head, from the dome plate hole. A specially constructed frame, as shown in Figure 13, is a typical arrangement for deformation testing of the dome plate. Two tests were conducted using the 50-t capacity Instron Universal Testing Machine with the dome plate thickness of 10 mm. The test was also repeated with dome plate thickness of 5 mm. The displacement control mode was used for all tests. The loading rate for each test was maintained at 1 mm/min. Two types

for domes were tested, the 5 mm and 10 mm thick dome plates. Only one test was made with 5 mm plate thickness.

Figure 14 illustrates the load-displacement responses of the dome plates subjected to 5 mm thick plate pull test superimposed on pull testing in 10 mm thick plate It shows that the results from two tests exhibiting a significant level of consistency. Both curves shows various stages of dome plate deformation and flattening with the bolt's spherical grout injection head pulling through the loading frame hole:

1) During the first stage, the load increased as the gradual increase in displacement. The maximum peak load was achieved at around 122 kN with the corresponding displacement of approximate 12 mm for both tests.
2) The dome plate started to flatten during the second stage, and the load decreased with increase in flattening of the plate. At the end of this stage, the flattening of the plate terminated, and the load dropped to approximate 74 kN at a displacement of around 35 mm.
3) At the beginning of the third stage, the bolt grout injection spherical head started sinking through the hole of the dome plate. The dome plate hole of 76 mm began to widen further due to the spherical head pushing through the enlarged plate hole with the downward movement of the spherical head. The load increased as the dome head displaced further down the enlarged plate hole, peaking at around 97 kN with the corresponding displacement of 54 mm. A few fluctuations in load were also observed during this stage.
4) After reaching the second peak load, the spherical head fully passed the enlarged dome plate hole and the load dropped significantly within a 7 mm displacement. This plate dome washer interaction occurred when a similar test was carried out on another dome washer of 10mm plate thickness. The result was similar to the results of 5 mm thick dome washer but double in load.

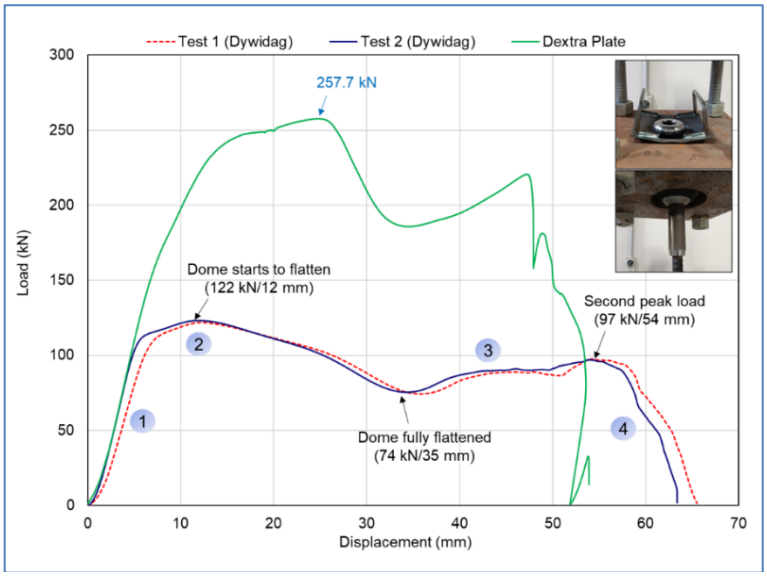

Figure 14: Load-displacement curves of the dome plate deformation tests.

Table 3: Key results of dome plate deformation test

Parameters	Test 1	Test 2
Maximum peak load (kN)	122.0	123.3
Displacement at maximum peak load (mm)	12.2	11.9
First bottom load (kN)	74.3	75.4
Displacement at first bottom load (mm)	35.8	34.3
Second peak load (kN)	97.7	97.0
Displacement at second peak load (mm)	54.3	54.0

Figure 15 shows the enlarged dome plate hole after the test. The post-test diameter of the dome plate hole increased by 34%, from 50 mm to 67 mm. The bending of the dome plate was also observed during testing as shown in Figure 15.

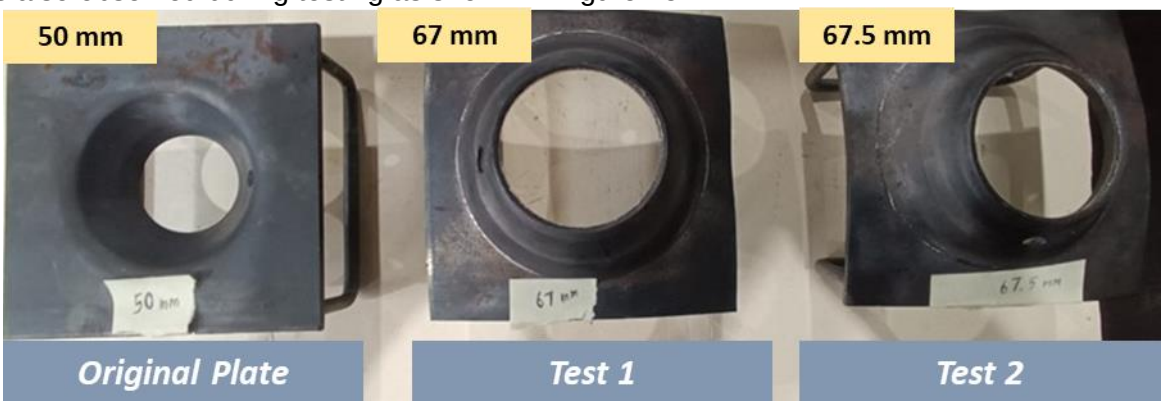

Figure 15: Enlarged dome plate hole after the test.

Conclusions

The laboratory testing of 22 mm diameter steel had a consistent strength capacity of around 36 t, which is equal to other bolts marketed in Australian of a similar type. Since the tunnel structure is likely to go along various ground formations, thus it is appropriate to ensure that the stability of the tunnel structure is maintained over a long period of time despite the exposure to various ground conditions and consequences. The use of plastic sleeve for the protection of the bolt from various adversary effect is this warranted. Accordingly, the followings can be inferred from the study,

The plastic sleeves were found stretch axially as well as in shear when tested in both ways. In both cases the sleeve was found to be damaged and cracked when stretched beyond a limited stretch in the order of between 20 to 25 mm, leading to bolt corrosion. Sleeved bolts sheared up to 20 mm of shear displacement may not lead to sleeve cracking.

The bolt pullout force using the steel split set anchorage-up was significantly higher than obtained from pull test values in concrete. This is attributed to the steel stiffness in comparison with using 300 mm diameter concrete cylinders.

Bolts sheared down to 25 mm of vertical displacement underwent bruising damage but did not suffer severe sleeve damage or cracked. However, it is likely that some minor and invisible cracks may occur on the sleeve, which could contribute to water leakage leading to bolt corrosion. Bolts sheared 25 mm and beyond, should be treated cautiously.

The strength medium the bolt is installed, and its stiffness has an influence on shear loading and shear displacement.

Fully snapped bolt with excessive sleeve cracking when sheared excessively for more than 35 mm of vertical displacement.

The dome washer plate thickness influences the nature of the dome washer and the spherical grout head.

References

ACARP Project C42012, 2017. Shear Testing of the Major Australian Cable Bolts under Different Pretension Loads (No. C42012). University of Wollongong, Wollongong, NSW, Australia, https://miningst.com/resources/pdfs/ACARP_Project_Report_C42012_Dec_2017.pdf

Alun Thomas (2019). Sprayed Concrete Lined Tunnels – 2nd ed. Abingdon, UK: Taylor & Francis. p. 288. ISBN 9780367209759.

Anzanpour, S., Aziz, N., Memcik, J., Mirzaghorbanali, A., Wallace, J., Marshall, T., Khaleghparast, S., 2021. Introduction to new methods of static and dynamic pull testing of rock bolts and cable bolts, in: Aziz, N., Mirzaghorbanali, A. (Eds.), Proceedings of the 2021 Resource Operators Conference. University of Wollongong, University of Wollongong, NSW, Australia, pp. 210–217, https://ro.uow.edu.au/coal/811

Aydan, O., Ichikawa, Y., Kawamoto, T., 1985. Load Bearing Capacity and Stress Distributions in/along Rock bolts with Inelastic Behaviour of Interfaces, in: Proceedings of the 5th International Conference on Numerical Methods in Geomechanics. A. A. Balkema, Rotterdam, Neth, pp. 1281–1292.

Aziz, N., Mirzaghorbanali, A., Holden, M., 2017a. The extent of shearing and the integrity of protective sleeve coating of cable bolts, in: Aziz, N., Kininmonth, B. (Eds.), Proceedings of the 2017 Coal Operators' Conference. University of Wollongong, University of Wollongong, NSW, Australia, pp. 240–246, https://ro.uow.edu.au/coal/661

Aziz, N., Pratt, D., Williams, R., 2003. Double Shear Testing of Bolts, in: Aziz, N., Kininmonth, B. (Eds.), Proceedings of the 2003 Coal Operators' Conference. University of Wollongong, University of Wollongong, NSW, Australia, pp. 154–161, https://ro.uow.edu.au/coal/172

Aziz, N., Rasekh, H., Mirzaghorbanali, A., Yang, G., Khaleghparast, S., Nemcik, J., 2018. An Experimental Study on the Shear Performance of Fully Encapsulated Cable Bolts in Single Shear Test. Rock Mechanics and Rock Engineering 51, 2207–2221. https://doi.org/10.1007/s00603-018-1450-0

Aziz, N., Rink, O., Rasekh, H., Hawkins, E., Mirzaghorbanali, A., Yang, G., Khaleghparast, S., Mills, K., Nemcik, J., Li, X., 2017b. Single shear testing of various cable bolts used in Australian mines, in: Aziz, N., Kininmonth, B. (Eds.), Proceedings of the 2017 Coal Operators' Conference. University of Wollongong, University of Wollongong, NSW, Australia, pp. 220–230, https://ro.uow.edu.au/coal/659

Aziz, N., Schneiderwind, A., Andanpour, S., Khaleghparast, S., Best, D., 2020. Performance of bolting systems in tension and the integrity of the protective sleeve coating in shear, in: Aziz, Naj, Kininmonth, B. (Eds.), Proceedings of the 2020 Coal Operators' Conference. University of Wollongong, University of Wollongong, NSW, Australia, pp. 155–162, https://ro.uow.edu.au/coal/769

Aziz, N., Mirzaghorbanali, A., Nemcik, J., Li, X., Rasekh, H., Wang, G. 2016. Load transfer characteristics of plain and spiral cable bolts tested in new nonrotating pull testing apparatus. Proceedings of the 2016 Coal Operators' Conference, University of Wollongong, University of Wollongong, NSW, Australia. https://ro.uow.edu.au/coal/591

Aziz, N., Yang, G., Khaleghparast, S., Marshall, T., 2019. Development of double shear testing of tendons, in: Aziz, N., Kininmonth, B. (Eds.), Proceedings of the 2019 Coal Operators' Conference. University of Wollongong, University of Wollongong, NSW, Australia, pp. 150–161, https://ro.uow.edu.au/coal/732

BS 7861-2, 2009. Strata reinforcement support systems components used in coal mines Specification for flexible systems for roof reinforcement.

Chen, J., Hagan, P.C., Saydam, S., 2017. Sample diameter effect on bonding capacity of fully grouted cable bolts. Tunnelling and Underground Space Technology 68, 238–243. https://doi.org/10.1016/j.tust.2017

Chen, J., Hagan, P.C., 2010. Optimising The Selection of Fully Grouted Cable Bolts in Varying Geotechnical Environments. ACARP Project C22010, University of New South Wales, ISBN No: 0978-0-7334-3523-2

Chen, Y., Li, C.C., 2015. Performance of fully encapsulated rebar bolts and D-Bolts under combined pull-and-shear loading. Tunnelling and Underground Space Technology 45, 99–106. https://doi.org/10.1016/j.tust.2014.09.008

Clifford, B., Lorraine, K., Altounyan, Bigby, D, (2001). Systems used in coal mine development in long tendon Reinforcement, In Proceedings, 20th International Conference on Ground Control in Mining, Morgantown, WV, USA, ISBN 0-939084-56-9, pp235-241

Craig, P., Aziz, N., 2010. Shear testing of 28 mm hollow strand "TG" cable bolt, in: Proceedings - 29th International Conference on Ground Control in Mining, ICGCM. pp. 169–174.

Golser J., 1976, The New Austrian Tunnelling methodology (NATM), Theoretical Background & sensible Experiences, 2nd Shotcrete Conference, Easton, Pennsylvania, USA, 4-8 October.

Høien, A.H., Li, C.C., Zhang, N., 2021. Pull-out and critical embedment length of grouted rebar rock bolts-mechanisms when Approaching and Reaching the Ultimate Load. Rock Mechanics and Rock Engineering 54, 1431–1447. https://doi.org/10.1007/s00603-020-02318-6

Hutchinson, D.J., Diederichs, M.S., 1996. Cablebolting in underground mines. BiTech Publishers, Richmond, B.C.

Hyett, A.J., Bawden, W.F., Reichert, R.D., 1992. The effect of rock mass confinement on the bond strength of fully grouted cable bolts. International Journal of Rock Mechanics and Mining Sciences & Geomechanics Abstracts 29, 503–524. https://doi.org/10.1016/0148-9062(92)92634-O

Khaleghparast, S., Aziz, N., Remennikov, A., Anzanpour, S., 2023. An experimental study on shear behaviour of fully grouted rock bolt under static and dynamic loading conditions. Tunnelling and Underground Space Technology 132. https://doi.org/10.1016/j.tust.2022.104915

Li, L., Hagan P.C., Saydam, S, Hebblewhite, Zhang, C. (2019). A laboratory Study of shear bahaviour of rockbolts under dynamic Loading based on the drop test using a double shear system. Jr. RMRE, March, pp3413- 3429. https://doi.org/10.1007/s00603-019-01776-x

Li, X., Aziz, N., Mirzaghorbanali, A., Nemcik, J., 2017. Comparison of the shear test results of a cable bolt on three laboratory test apparatuses. Tunnelling and Underground Space Technology 61, 82–89. https://doi.org/10.1016/j.tust.2016.10.003

Mirzaghorbanali, A., Rasekh, H., Aziz, N., Yang, G., Khaleghparast, S., Nemcik, J., 2017. Shear strength properties of cable bolts using a new double shear instrument, experimental study, and numerical simulation. Tunnelling and Underground Space Technology 70, 240–253. https://doi.org/10.1016/j.tust.2017.07.018

Moosavi, M., Bawden, W.F., 2003. Shear strength of Portland cement grout. Cement and Concrete Composites 25, 729–735. https://doi.org/10.1016/S0958-9465(02)00101

Mottahedi, A., Aziz, N., Remennikov, A., Mirzaghorbanali, A., Anzanpour, S., 2024. Aspects of testing tendon supports for strength, effective installation, and performance in different ground formation, Proceedings of the 2024 Resource Operator's Conference, University of Wollongong, University of Wollongong, NSW, Australia. pp. 146-169. https://ro.uow.edu.au/coal/914

Rastegarmanesh, A., Mirzaghorbanali A., McDougall, K., Aziz, N., Anzanpour, S., Nourizadeh, H., and Taheri, A., 2024. A look at the performance of barrel and wedge assembly in cable bolts applications. Journal of Scientific Reports, February. https://doi.org/10.1038/s41598-024-54999-6

Ur-Rahman, I., Hagan, P., Chen, J., 2015. The Influence of Concrete Sample Testing Dimensions on Assessing Cable Bolt Load Carrying Capacity. Resource Operator Conference, Wollongong, Australia. https://ro.uow.edu.au/coal/558

Windsor, C.R., 1992. Invited lecture: Cable bolting for underground and surface excavations. Rock support in mining and underground construction, in: Proceedings of the International Symposium on Rock Support. Sudbury, Ontario, Canada, pp. 349–366.

Zhao, D., Wen, S., Wang, L., Zhang, B., Yang, L., 2021. Structural parameters and critical anchorage length of tunnel system bolts made of basalt fibre. Construction and Building Materials 310. https://doi.org/10.1016/j.conbuildmat.2021.125081

CROWN PILLAR OPTIMIZATION FOR FLUORITE MINE IN MOGOLIA -TANSFER FROM OPEN PIT TO UNDERGROUND-

Takashi Sasaoka[1]*, Bat-Erdene Bugnei[1], Koki Kawano[1], Amarsaikhan Tsedendorj[2], Tumelo Kgetse M. Dintwe[3], Akihiro Hamanaka[1], Hideki Shimada[1]

[1] Department of Earth Resources Engineering, Kyushu University, Fukuoka, 819-0395, JAPAN
[2] ORGILOKHBURD LLC, Ulaanbaatar, 14241, MONGOLIA
[3] Department of Mining and Geological Engineering, Botswana International University of Science and Technology, Palapye, 10071, BOTSWANA
*Corresponding author: sasaoka@mine.kyushu-u.ac.jp

Abstract

In the Zuun Tsagaan fluorite mine in eastern Mongolia, open-cut mining was used in the past, but due to increasing demand, a transition to underground mining using the sublevel stoping method is being considered. A safety pillar called a crown pillar is left between the bottom of the pit formed by open-cut mining and the mining cavity to maintain the stability of the pit slope and the pit bottom, but its design guidelines have not yet been fully studied. In this study, we used the three-dimensional finite difference analysis software RS2 software to variously examine the optimal design and mining method of the crown pillar in the Zuun Tsagaan fluorite underground mine using the sublevel mining method, which allows large-scale mechanized mining.

Keywords: Transfer from open pit to underground mine, crown pillar, slope stability

Introduction

In case that the deposits are exposed or close to the surface, surface mining is carried out. If this deposit is deep underground, the ratio of waste rock to ore, which is the ratio of waste rock to ore, will increase, so it is essential to shift to underground mining at some stage in consideration of the economics and safety associated with mining. In the case of open-pit mining of deposits that are endowed with steep slopes, the depth and stripping ratio of the open-pit pit increase rapidly as mining progresses, so a feasibility study and the transition to underground mining needs to be considered. There have been many examples of

development of steep-slope, high-grade deposit and/or high price ores (Brummer et al. 2006; Carter 1992, 2000; Carter and Miller 1995; Szwedzicki 1999, 2001), but there have been few examples of development from open-pit mining to underground mining for large-scale steep-slope, low-grade deposits and/or not high price ores. In addition, when developing low-grade steeply sloping deposits, mining cannot be continued unless a large-scale unfilled mining method such as sub-level mining or VCR (Vertical Crater Retreat) mining is used from an economic point of view. Furthermore, when applying a large-scale unfilled mining method, it is desirable to establish a method that can safely mine deeper deposits by accurately designing a security ore column called a crown pillar between the bottom of the pit and the mining panel. This study presents the optimal design and mining method of crown pillars in underground mines using a sub-level mining method that enables large-scale mechanized mining, the Zuun Tsagaan fluorite mine in Mongolia, as a case study.

Overview of Reserch Area

The Zuun Tsagaan Del mine is one of the mines that produces the most fluorite ore in Mongolia. It is located in central Mongolia, about 280 km southeast of the capital Ulaanbaatar, and about 150 km north of the provincial capital Sainshant. This mine produced fluorite by open-cut mining from 1978 to 2007, but as the limit of open-cut mining has been reached, future underground mining is being considered. This mine produces fluorite (CaF_2), with an average annual production of 109.3 ktons and an average grade of CaF_2 of about 32.4% (The Bureau, 1992).

The sublevel open stoping method is planned to be adopted as the underground mining method.

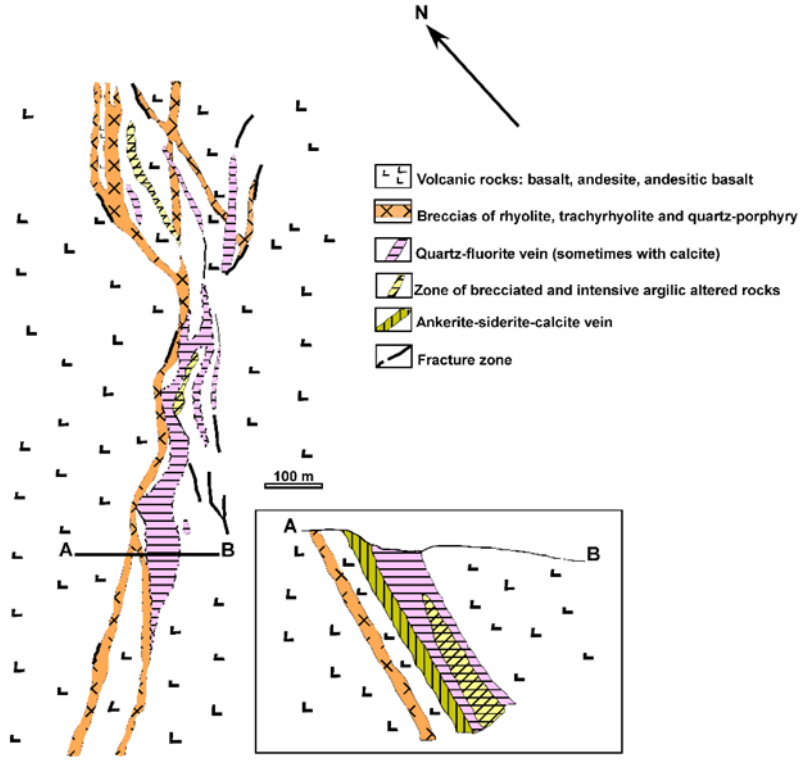

Figure 1. Geological cross section of the Zuun Tsagaan Del Flourite deposit (modified from (Khashbat and Jargalan 2016))

The fluorite deposit in this mine is of the calcite-quartz-fluorite type, which has been metasomatically altered. The ore body is irregular, with a lenticular shape in the shallow part and a wedge shape in the deep part (Khashbat and Jargalan 2016). The characteristic of this type of deposit is that it has an irregular shape due to the replacement of marble and limestone with quartz and fluorite. The deposit is mainly composed of quartz, fluorite, carbonate minerals, etc., and is vein-like. The host rock is mainly composed of andesite and basalt from the late Mesozoic era, which are irregularly distributed around the deposit (see Fig.1). A vertical cross section of the geological model is shown in Fig.2. There are mainly seven independent

deposits in this mine, with the maximum length of the deposit being 530 m. The width and dip angle vary depending on the location and depth, with the width ranging from 0.5 m to 20 m and the average being 14 m, and the dip angle being 60 to 75°. Fig.3 shows the photos of the targeted are in this research.

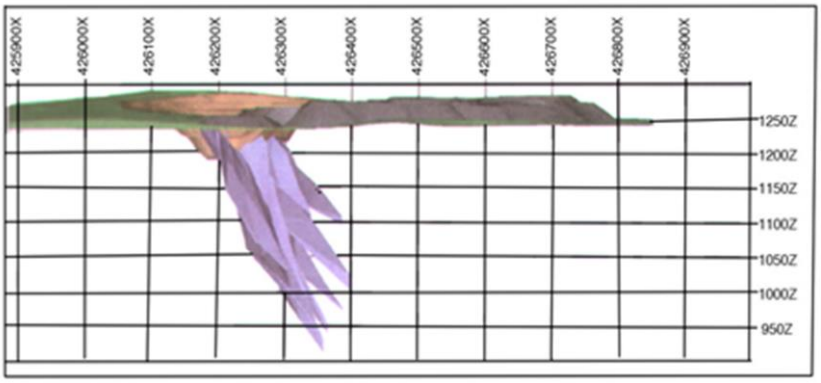

Figure 2. Cross section of fluorite orebody.

Figure 3. An overview of the open pit
(note the fault zone on the hangingwall side)

Figure 4 shows a cross-section of the area where underground mining is planned to take place. The pit formed by open-cut mining is about 150 m deep, and underground mining will be completed about 100 m below the surface. Characteristics of this mine are that the ore vein is steeply inclined, the volume of the ore body is large, and the value per volume is relatively low. For these reasons, the sublevel open stope method is used to mine the deposit, taking into consideration economics and safety. In order to apply this mining method, it is necessary to have a non-mined area called a crown pillar between the bottom of the pit and the top of the underground stope (see Fig. 5). The application of the crown pillar reduces the influence of the top and bottom of the pillar, improving the stability of the roof of the mining cavity and the slope of the pit. This reduces the use of supports, which leads to cost reduction.

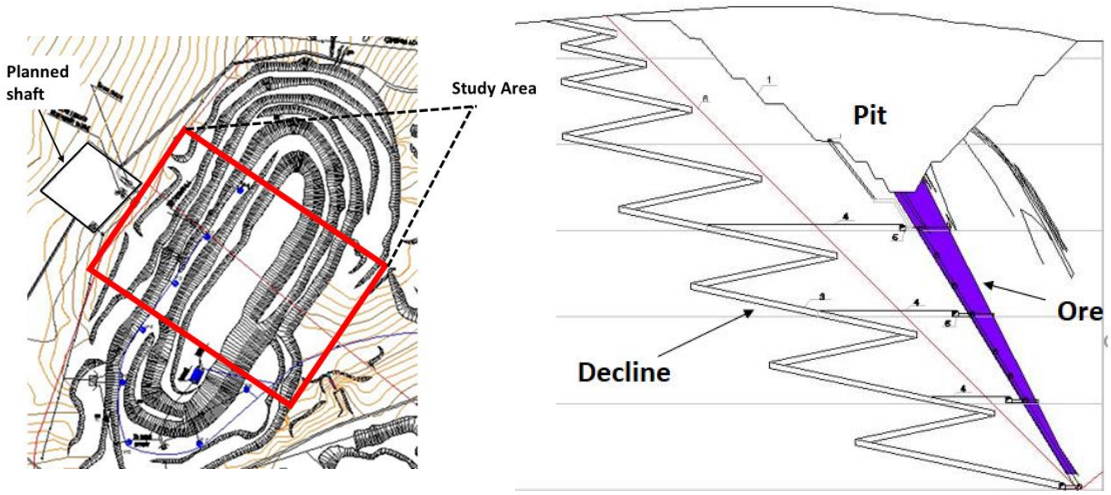

(a) (b)

Figure 4. Cross section of study area (a) Plan view of the study area (b) Cross section

Numerical Analysis

Numerical Modeling

Figure 6 shows an example of a finite element model used in this analysis. RS2 software (Rocscience, 2021) was applied in a series of numerical analysis. As an analytical procedure, a pit was formed by open-cut mining after performing an initial stress analysis. Then, a stope with 10 m wide and 30 m high was formed along the deposit with the dip of 70 degree by using sublevel open stoping method with leaving ore between the bottom of the pit and stope as a crown pillar. The stabilities of crown pillar, stope, and pit slope under different thickness of crown pillars were discussed. Since the rock mass condition can be determined about 62.5 in terms of the Geological Strength Index (GSI) based on the analysis of boring data around the target site, the mechanical properties were determined and used in this analysis as shown in Table 1. In addition, an elastic-plastic analysis was performed and the Mohr-Coulomb failure criterion was used as the failure criterion.

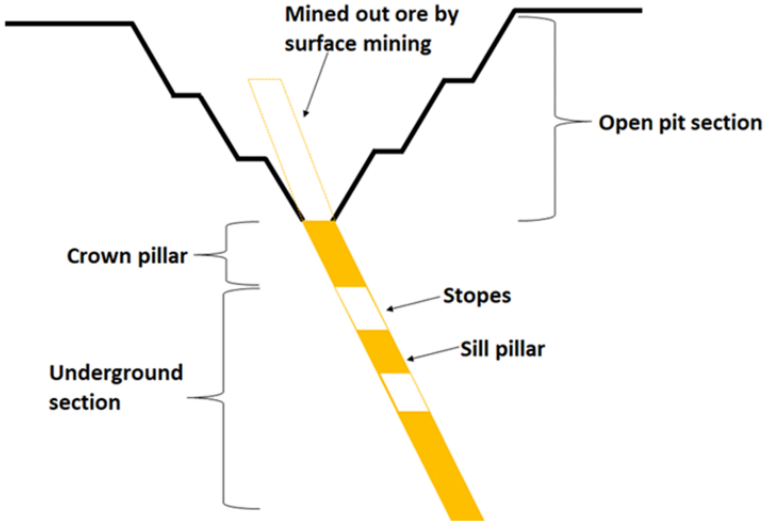

Figure 5. Schematic view of the crown pillar

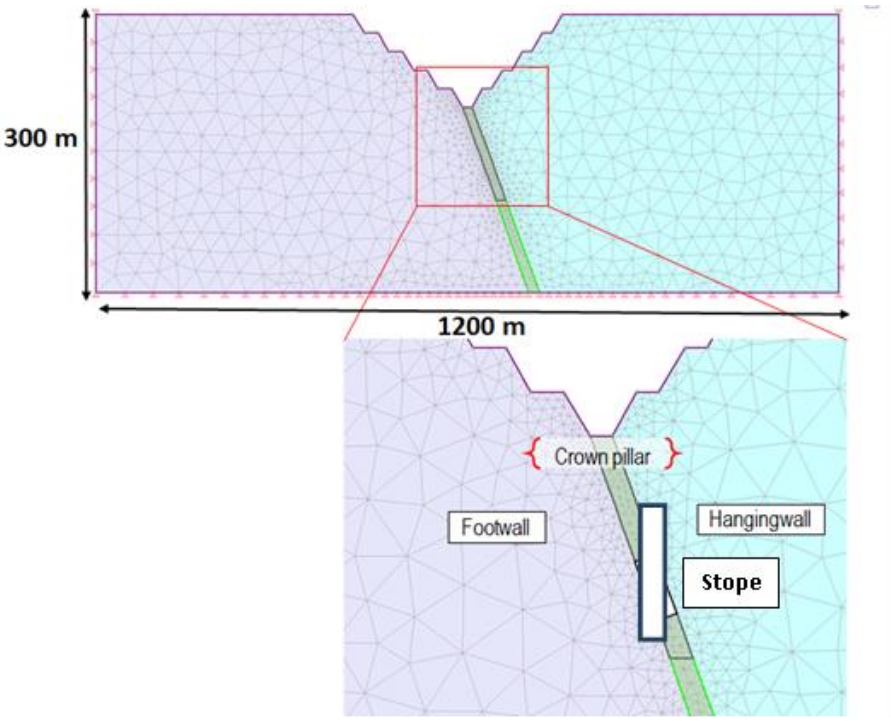

Figure 6. Finite element model in RS2

Table 1. Mechanical properties of rock mass

Merial	Elastic modulus (GPa)	Poisson ratio	Cohesion (MPa)	Friction Angle (°)	Tensile strength (MPa)
Footwall	13.4	0.26	2.1	58.6	0.28
Hangingwall	12.3	0.25	1.8	54.4	0.21
Vein	13.4	0.24	1.72	56.2	0.19

Results and Discussions

Appropriate thickness of crown pillar: Fig. 7 shows the distribution of yield element under the different thickness of crown pillar. From this result, it was clarified that when a deposit with a 70-degree incline is excavated with a stope with 10 m in width and 30 m in height, by leaving a crown pillar with 15 m or more thickness, the impact of stress concentration at the toe of the pit slope on the crown pillar and stope will be mitigated and then the underground mine can be developed from the bottom of the open pit by using sublevel open stoping method.

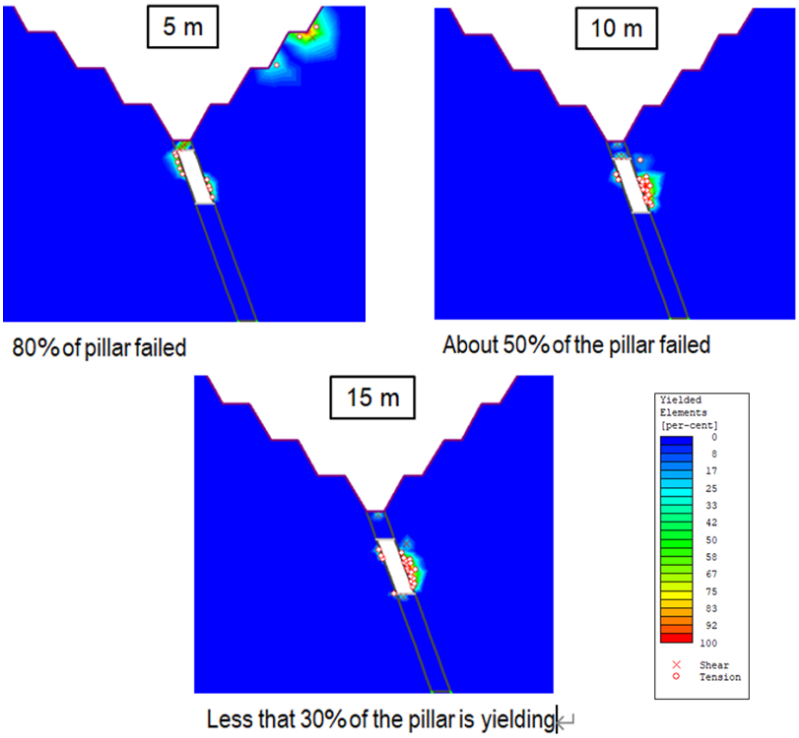

Figure 7. Distribution of yield element under the different thickness of crown pillar

Crown pillar optimization: base on this result, it is observed and that 15 m crown pillar is suitable for maintaining stability. However, a considerable amount of ore has to be left as a crown pillar. Especially, in case that the grade of ore is high, it may be considered to recover the crown pillar as much as possible. From this point, a specific recovery method is proposed in which an 8m-long cable bolt is driven into a 5m-thick crown pillar, the ore directly below the crown pillar is excavated to a thickness of 5m, and the stope is filled with cement mixture to form an artificial roof. Then, the stope with 10 m in width and 30 m in height is excavated by underhand stoping method. Fig. 8 shows the procedures the specific recovery method of crown pillar. Table 2 and 3 shows the input parameters for cable bolt and backfilling material.

Table 2. Parameters for cable bolt

Cable Bolt Properties	
Type	Fully Bonded
Length (m)	5-10
Diameter (mm)	19
Bolt Modulus (MPa)	200,000
Tensile Capacity (MN)	0.1

Residual Tensile Capacity (MN)	0.01

Table 3. Parameters for backfilling materials

Backfill type	E (MPa)	*V*	*σ* (MPa)	(ϕ) (deg.)	C (MPa)
Consolidated (cemented rockfill)	2,850	0.34	0.7	25.4	1.4

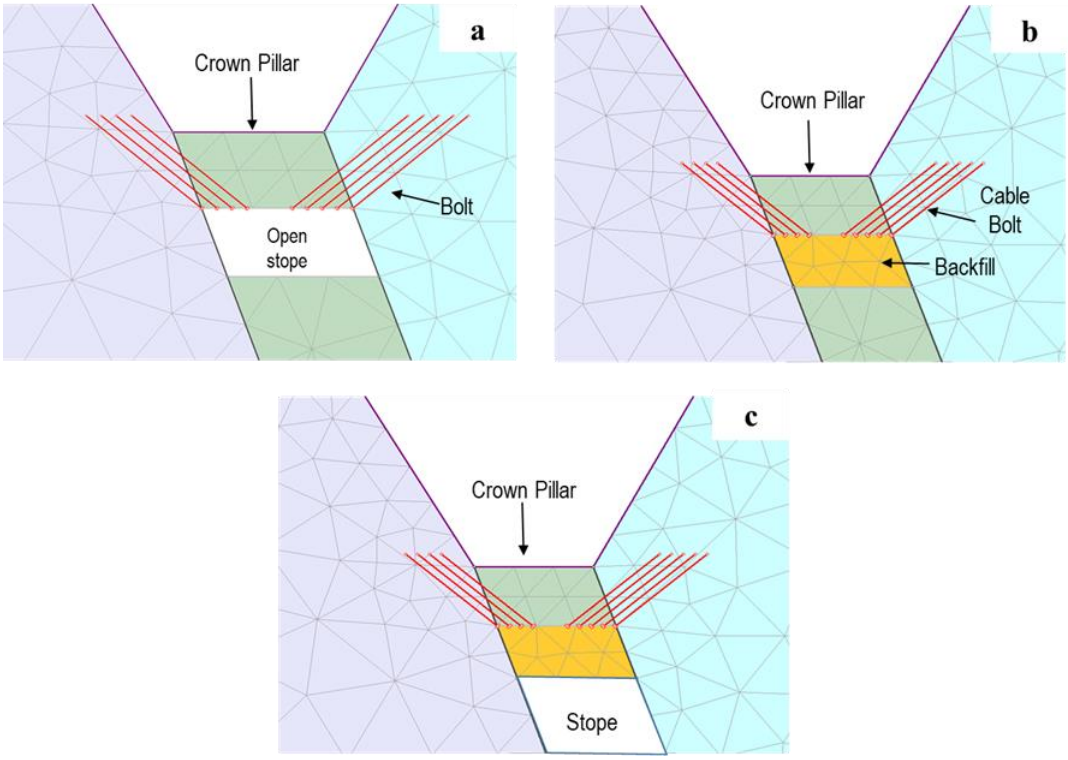

Figure 8. Recovery method for crown pillar

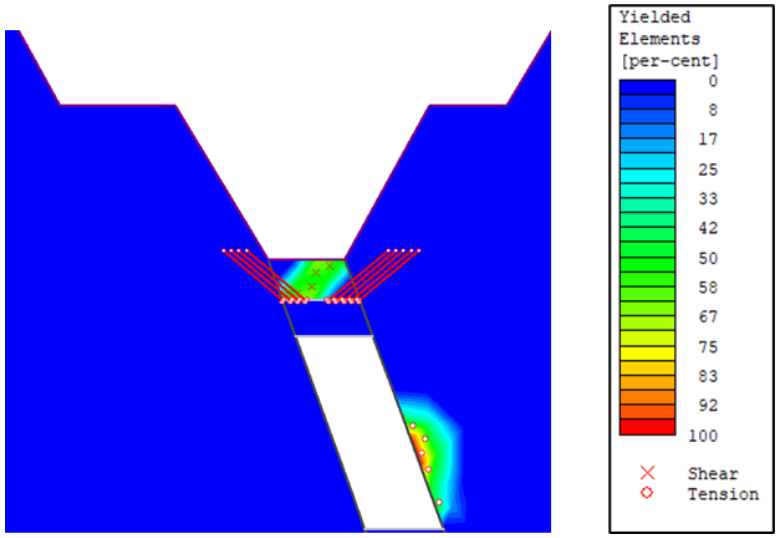

Figure 9. Distribution of yield elements by applying the recovery method

Fig. 9 shows the result by applying the proposed recovery method for crown pillar. It can be found that this recovery method significantly improves the stability of the ground pillar and the rock around the toe of the pit slope, and it is made clear that a stope with 10m in width and

30 m in height can be set up under the artificial roof using the underhand mining method, while 10 m of the crown pillar can be recovered compared to the above-mentioned mining plan.

Conclusions

Based on the results of a series of numerical analyses, the following results can be obtained.

The condition of the ore deposit and the rock mass above and below it is good, which has demonstrated that underground development using the sublevel mining method is possible. Furthermore, as a result of examining the design of the crown pillar for underground development, it has been clarified that when a deposit with a 70-degree incline is mined in a mining section with a mining width of 10 m and a mining height of 30m, by leaving a crown pillar 15 m thick, the impact of stress concentration at the toe of the pit slope on the crown pillar and mining section can be mitigated, making underground development using the sublevel mining method possible.

Moreover, the recovery method of the crown pillar assuming that high-grade ore is present around the bottom of the pit is proposed and discussed. An 8-m-long cable bolt is driven into a 5 m thick crown pillar, and then the ore directly below the crown pillar is mined to a thickness of 5 m, and an artificial roof is formed by filling the stope with cement mixture. It can be clear that this recovery method significantly improves the stability of the crown pillar and the rock mass around the toe of the pit slope, making it possible to excavate a stope with 10 m in width and 30 m in height by using the sublevel underhand mining method under the artificial roof, and clarifying that it is possible to recover 10 m of crown pillar compared to the above-mentioned mining plan.

Acknowledgments

The authors would like to thank Zuun Tsagaan Del fluorite mine for their support of this study.

References

Brummer RK, Li H, Moss & A, et al (2006) The transition from open pit to underground mining: an unsual slope failure mechanism at Palabora. In: The South African Institute of Mining and Metallurgy International Symposium on Stability of Rock Slopes in Open Pit Mining and Civil Engineering. pp 411–420

Carter TG (1992) A New Approach to Surface Crown Pillar Design. In: Proc. 16th Canadian rock mechanics symposium. Sudbury, pp 75–83

Carter TG, Miller RI (1995) Crown-pillar risk assessment - planning aid for cost-effective mine closure remediation. Trans - Inst Min Metall Sect A 104:41–57. https://doi.org/10.1016/0148-9062(95)99786-w

Carter TG (2000) An update on the scaled span concept for dimensioning surface crown pillars for new or abandoned mine workings. In: 4th North American Rock Mechanics Syposium. Seattle, pp 465–472

Khashbat DK, Jargalan SJ (2016) Fluorite resources of Mongolia. J-stage 66:95–102

Szwedzicki T (1999) Pre- and post-failure ground behaviour : case studies of surface crown pillar collapse. Int J Rock Mech Min Sci 36:351–359

Szwedzicki T (2001) Geotechnical precursors to large-scale ground collapse in mines. Int J Rock Mech Min Sci 38:957–965

The Bureau (1992) Mineral Yearbook, pp 258 (https://books.google.co.jp/books?id=Ls-OZvS-cisC&pg=PA258&lpg=PA258&dq=zuun+tsagaan+del&source=bl&ots=Sj65XEnz2O&sig=ACfU3U0nb4PpEj5lEZv6KUSCSojXf3YmPQ&hl=ja&sa=X&ved=2ahUKEwiA_7Gjn7fnAhWLHKYKHU9MCrkQ6AEwAnoECAkQAQ#v=onepage&q=zuun%20tsagaan%20del&f=false)

Rocscience (2021) RS2 finite element analysis software manual.

EXPRESS - METHOD FOR DETERMINING PARAMETERS OF HEAVING OF WATER-SATURATED ROCKS TAKEN INTO ACCOUNT OF PRESSURE IN THE PORE FLUID

Shapoval V.H[1], Shashenko O.M[1], Skobenko O.V[2], Chukharyev S.M[3], Holovko Yu.M[4], Olishevska S.O[5]

[1] Doctor of Technical Sciences, Professor of the Department of Construction, Geotechnics and Geomechanics, Dnipro University of Technology, Dnipro, Ukraine
[2] Candidate of Technical Sciences, Associate Professor of the Department of Construction, Geotechnics and Geomechanics, Dnipro University of Technology, Dnipro, Ukraine
[3] Candidate of Technical Sciences, Associate Professor of the Department of Mineral Deposits Development and Mining Engineering, National University of Water and Environmental Engineering, Rivne, Ukraine
[4] Candidate of Physical and Mathematical Sciences, Associate Professor of the Department of Applied Mathematics, Dnipro University of Technology, Dnipro, Ukraine
[5] PhD student of the Department of Construction, Geotechnics and Geomechanics, Dnipro University of Technology, Dnipro, Ukraine

The problem of determining the contours of the area in which rock heaving occurs is important when designing underground workings.

In writing this article, an attempt was made to find answers to the following questions:

- is heaving possible in water-saturated rock;
- if yes, what outlines does the heaving area have;
- how does the pressure in the pore fluid affect the stability of the rock during its heaving.

Simple analytical relationships have been obtained that make it possible to calculate the boundary of the base area in which heaving of water-saturated rock occurs and the stability coefficient of this area.

As a stability coefficient, it is proposed to use the ratio of the projection onto the vertical axis of the forces holding the rock mass subjected to heaving to the projection of the forces shifting this massif.

Scientific novelty

1. It was established for the first time that with increasing pressure in the rock pore fluid, all other things being equal, the maximum depth of the base heave region decreases.
2. It is shown that with increasing pressure in the rock pore fluid, other things being equal, the stability coefficient of the maximum depth of the base heave region decreases.

Practical significance.

The results we obtained allow us to perform the following using mathematical methods:

1. Prediction of the stability of horizontal workings in the area of rock heaving, taking into account the depth of the working, its geometric dimensions, specific gravity, strength properties of the rock and pressure in the pore fluid.
2. Boundaries of the rock heaving region, taking into account the depth of the working, its geometric dimensions, specific gravity, strength properties of the rock and pressure in the pore fluid.

Also, the theoretical results we obtained have a natural generalization to the solution of such technological problems as silicatization, cementation and high-pressure cementation of soil foundations. In this case, using the results we obtained, we can find:

- the maximum permissible value of pressure in the water-silicate solution injected into the rock at which the destruction of the base does not occur during the process of its strengthening by the silicization method;
- the maximum permissible value of pressure in the water-cement solution injected into the rock at which the destruction of the base does not occur during the process of its strengthening by the cementation method;

- the range of pressures in the water-cement solution injected into the rock at which local destruction of the base occurs in the process of its strengthening by high-pressure cementation.

Keywords: mining working, Mohr-Coulomb strength criterion for water-saturated rock, O. M.Shashenko strength criterion for water-saturated rock, rock heaving, arch effect, rock pressure, pointed arch with straight semi-arches, arch lifting boom, rock strength at compression, tensile strength of rock, pressure in the pore fluid, stability coefficient, holding forces, destructive forces, functional, minimum of functional, parameter, silicization of the base, cementation of the base, high-pressure cementation of the base.

NUMERICAL RESEARCH ON THE IMPACT OF RAINFALL ON THE SLOPE STABILITY OF OPEN-PIT MINES

Gang Huang[1, 2, 3]*, Jianhua Zhang[1, 2, 3], Tingting Jiang[2]

[1] Key Laboratory of Green Utilization of Critical Non-metallic Mineral Resources, Ministry of Education, Wuhan University of Technology, Wuhan 430070, CHINA
[2] School of Resources and Environmental Engineering, Wuhan University of Technology, Wuhan 430070, PR CHINA
[3] Hubei Key Laboratory of Mineral Resources Processing and Environment, Wuhan 430070, PR CHINA
*Corresponding Author: huanggang2016@whut.edu.cn

Abstract

The stability of open-pit mine slope is related to the safety of stope production and the life safety of mining workers, and rainfall leads to poor slope stability. Taking an open-pit slope as the research background, based on the limit equilibrium method and using GeoStudio software, the slope stability of the overall slope under rainfall was analyzed based on the current field conditions of the mine. The results show that the minimum value of the final slope stability coefficient under the action of rainfall is 1.78, which is greater than the allowable safety factor of 1.20, and the safety factor of the slope profile can meet the minimum safety factor required by the specification.

Keywords: slope stability; Limit equilibrium method; Numerical simulation; Rainfall

NON-CONVENTIONAL SOURCES AND METHODS OF MINERAL EXTRACTION – CHALLENGES AND OPPORTUNITIES

Carsten Drebenstedt

TU Bergakademie Freiberg, Professorchip Surface Mining, GERMANY

The availability of mineral resources is essential for the functioning of the economy, the services in the society, security, health, welfare and others. The last years shows, that mineral resources becomes more and more a geo-political instrument, even if there is a concentration on few producers, and in no political stable regions. Protectionism and single country interests lead to a shortage of mineral exports and higher prices, which sets economic regions as Europe with low resource potential under pressure. In result the European Union published the “Critical Raw Material Act” to find answers for a certain self-supply of strategic for the economy minerals by new exploration and mining projects, by increase of processing, metallurgical and recycling capacities, and by R&D to realize. An important role plays the use of the own mineral resource potential in European Union. Near surface primary deposits mostly discovered and exploited in the last 1.000 years. A new resource for mineral resources

can be the residuals of the mining, processing and metallurgical processes, e.g. waste dumps, tailings, ashes, slags, and uneconomic for conventional technologies, e.g. small size and complex mineralized deposits. To extract the minerals from these non-conventional deposit's new technologies as phytomining, leaching, high selective mining, robotics can be used. The article gives an insight in the latest developments at TU Bergakademie Freiberg.

USE OF AI/ MACHINE LEARNING AND GIS – CASE STUDY EVALUATION OF DUMP STABILITY

Carsten Drebenstedt

TU Bergakademie Freiberg, Professorchip Surface Mining, GERMANY

Slope and dump stability is an important element of occupational and public safety of a mining operation. If dump deformations are happening, different tools are used to investigate the reasons. Learning from mistakes in the past is the basic to improve acting for the safety in future. Because the reasons for dump deformations can be multicriterial, a result of a chain reaction analytical tools may be not able to give adequate answers and solutions. Was the mistake found, especially in case of dump deformations in closed mines it's a need to proof the long-term stability of the whole dump area, sometimes with thousands of hectares and billions of m^3. In such situations, e.g. data collection by exploration and test of material samples are not efficient or not led to the right result to predict dangerous areas. Such a difficult case in German lignite mines is the sudden liquefaction of dump material after decades by dynamic stimulation. To find dangerous dump areas the combination of Geoinformation systems and Neural Networks was applied. The article presents the use of this tool, the possible prediction results, limitations, and further development's needs.

INVESTIGATION OF REUSED PREPARATORY WORKINGS DEFORMATIONS OF AS A RESULT OF CLEANING OPERATIONS

Nazarenko V[1], Brui.H[1], Kuchin O[2], Balafin I[2]

[1] Technical University "Metinvest Polytechnic", UKRAINE
[2] National Technical University "Dnipro Polytechnic", UKRAINE

Modern requirements of economically efficient and safe underground mining of coal seams are best met by the technology of preserving workings for reuse.

Failure to reuse mine preparation workings leads to an increase in the length and cost of workings required to prepare the mine pillar. Due to the intensification of mining operations, there is a shortage of preparatory workings. Therefore, the main attention is paid to the aimless technology of seam mining. This technology provides for maintenance of excavation workings behind the face in order to reuse them.

The parameters of excavation faces supported after the longwall face are determined on the basis of calculated roof displacements.

The displacements are calculated on the basis of the identified dependencies of the excavation contour displacements on its mining and geological and mining engineering parameters. Due to the influence of moistening and rheological processes, deformation characteristics of rocks decrease. This causes an increase in the actual displacements in the workings compared to the calculated ones, which is not taken into account in the calculations, but is relevant for the mines of Western Donbass.

Therefore, the purpose of this work is to conduct field measurements to determine the main regularities of deformation of the roof and soil of the workings in the zone of influence of cleaning works. The method of calculation of displacements for the conditions of mines of Western Donbass assumes constant and uniform in time (except for the initial period of 20...40

days after the excavation) growth of displacements of the rock contour of the excavation even outside the zone of influence of cleaning works. The monitoring data presented in this paper indicate the unsatisfactory condition of the workings that are reused. This indicates the imperfection of the calculation methodology. The study presents the results of surveying instrumental measurements and monitoring of the condition of preparatory workings during their reuse. The regularities of deformation of excavations under the influence of cleaning works in the conditions of Western Donbass are established.

Further use of the results of the performed researches will give an opportunity to improve the condition of preparatory excavations. One of the conditions for this is the timely application of measures to strengthen the problem areas of reused excavations in the conditions of weak rocks prone to soaking.

Key words: mine workings, reuse, support, deformations, convergence, mine surveyor's measurement.

MODELING THE PROCESS OF DYNAMIC DEVELOPMENT OF CRACKS IN THE EXPLOSION OF ADJACENT CYLINDRICAL CHARGES FOR DIRECTED DESTRUCTION

Anakhin V.D, Dambaev Zh.G, Mantatov V.V, Mizhidon A.D

Federal State Budgetary Educational Institution of Higher Education, “Buryat State University, ULAN-UDE

Abstract

The objectives of the work are to consider the theoretical calculations of a model explosion and the development of gas-dynamic processes in the charging cavity and the start of radial cracks along the line of the charge location.

As a hypothesis of the study, an explosion in quartz glass is accepted, the development of the movement of gaseous explosion products and the simultaneous development of radial cracks are visible. In this case, the simultaneous development of gas movement and crack development are considered, which is impossible to see in rock. Comparison of velocities is of great interest for the mechanics of fracture of solids.

Keywords: explosion, model explosion, outflow of gas-dynamic processes in the charging cavity, quasi-static pressure, propagation of stress waves between adjacent charges, tensile stresses, initiation of a directed radial crack, rate of development of a main crack.

In this work, two different problems are considered: - consideration of the gas-dynamic process in a well and the development process in a solid medium and comparison of the rates of different processes.

The result of the work is that the proposed approaches create simultaneous processes in different environments and phase barriers to the digital transformation of two interrelated problems of mechanics.

The process of development of the main crack between adjacent elongated charges and the process of development of crack formation are modeled, taking into account the outflow of gaseous explosion products. In this case, model experiments determine the rate of development of the outflow of gaseous explosion products and the dynamic development of a crack in a solid medium. The simultaneous process and justification of the resource capabilities of quasi-static pressure on the process of destruction of main cracks are considered.

To consider the complete picture of the crack development process between adjacent charging cavities, model experiments were carried out on optically transparent materials. The

interaction of stress waves between adjacent charges, which form maximum tensile stresses along the line of charge location due to wave interference, is considered [1]. In this case, a very important role is played by the primary initiation of a radial crack along the line of charge location due to the optimal dynamic load, i.e. ensuring directional start of radial cracks along the line of charge location.

Figure 1 (a, b) shows the qualitative processes of development of main cracks between adjacent charging cavities.

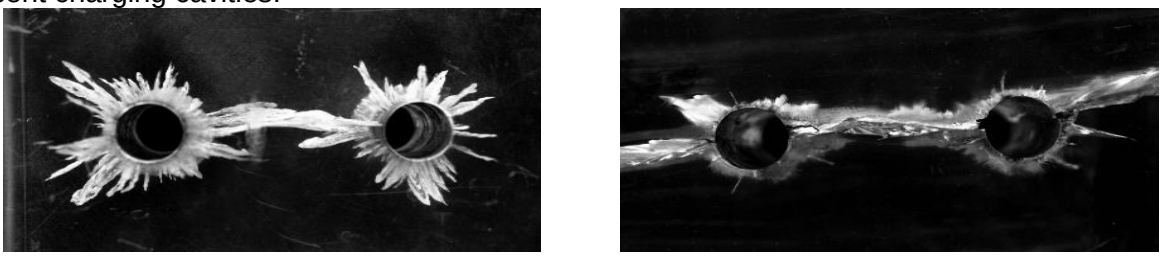

a) b)

Fig. 1 Comparative and qualitative indicators of directed destruction.

A cylindrical explosion in a solid medium forms equiprobability processes of the nucleation of initial radial cracks around the charging chambers. It is known that the physical basis for the directed destruction of solids between adjacent charges is based on the interference of waves, which create a voltage asymmetry around the charging chambers. The process of development of the main crack along the line of arrangement of charges forms crack formation between adjacent charges due to the superposition of stress waves.

The initial start of a radial crack along the line of charge location occurs due to the asymmetry of the stress field around the charging cavities, which are formed due to optimal dynamic load [2].

During an explosion, the cylindrical cavity expands under the influence of the pressure of the explosion products and the initiation of radial cracks around the chamber is an equally probabilistic process. The initiation of a radial crack along the line of charge placement is a very difficult task and is achieved through optimal dynamic load, distances between charges and the gas-dynamic process of explosion of an elongated charge. The expansion of the charging cavity ends when the maximum pressure of the explosion products is reached, and this will be followed by the start of radial cracks. The main goal of contour blasting is the initiation of a radial crack along the line of charge location.In this case, it is necessary to consider two different problems of continuum mechanics (gas dynamics and mechanics of a deformable solid) together, and the determination of the parameters is a necessary condition for solving the process of crack formation between adjacent elongated charges. The determining parameter of the initiation of a directed radial crack is the interference of stress waves depending on the kinetics of the explosive transformation that form the gaseous products of the explosion. To determine the loading mode of a solid, it is necessary to consider the boundary conditions on the inner surface of the charging chamber.

To achieve this goal, it is necessary to develop a method for controlling gas-dynamic processes in the cavity of the charging chamber depending on the length of the cylindrical charge and the distance between adjacent boreholes.

To solve this problem, it is necessary to use sufficiently flexible approaches associated with stress asymmetries around the charging cavities for the development of directed cracks along the line of symmetrical charges.

The gaseous products resulting from the explosion are preserved for some time, but a portion of the energy is spent on the work of the compressed solid and on its destruction, and the other part is carried away from the charging cavity by radiation. Immediately after the explosion, the volume of the explosion products changes little. The temperature and pressure of the products significantly exceed the initial values. Thus, uneven movement of the solid medium occurs and a stressed state of the solid medium appears, and tensile stresses appear on the generating surface. The uneven distribution of pressure parameters, expressed by

narrow transition zones along the length of the charging cavity, is an essential property of this problem. Sharp changes in parameters at the front of the detonation wave, shock waves arise and the front of which are narrow zones of parameter change.

The kinetics of the explosive transformation of the explosive charge, which turns into gaseous explosion products at different angles of pressure increase in the charging chamber, is mathematically modeled.Achieving complete interference of stress waves between charges and establishing a critical stress on the generatrix of the charging chamber ensures the initiation of a radial crack along the charge location line.

For optimal loading of the charging chamber, a combined composition of the explosive charge is used, which ensures the initiation of a radial crack along the charge location line. In the mathematical modeling of the process, there is an interaction of stress waves between the charging cavities, which require an optimal dynamic load to create an optimal asymmetry around the charging cavities. In this case, it is necessary to take into account the interaction of stress waves that ensure the initiation of radial cracks in the direction of the charge location. As a result, approximate expressions for the laws of dynamic loading are used, obtained on the basis of approximate data on the kinetic transformation of the explosive.

The process of considering the interaction of stress waves from the explosion of adjacent elongated charges was carried out by high-speed photography using the Tepler IAB-451 installation. In this case, the shooting speed is one million frames per second and a cinematogram of the crack formation process is shown in Fig. 2 (a, b, c, d) with a time interval of 18 μs.

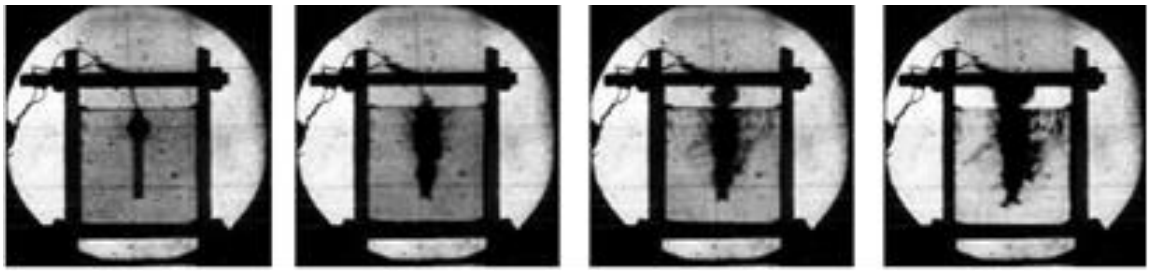

Fig. 2. Cinematogram of the explosion of an elongated cylindrical charge

The figure of the model experiment shows how the detonation products radially expand and transform in the material in the form of a stress wave with a conical front along the length of the charging chamber. The propagation of the stress wave causes local displacements of the material particles, which create a stressed state of the medium, and dark lines (isochromes) appear in optically active materials, propagating at the speed of propagation of longitudinal waves.

When stress waves interact in the region between adjacent charges, a main crack appears, the size of which is (0.3–0.4) cp , where cp is the speed of the longitudinal wave in optical glass. Further development of crack formation leads to merging into a single plane of cleavage. Based on the visual picture of the propagation of stress waves in the process of crack formation, one can imagine the destruction of a solid medium as follows. In the vicinity of the charge, the tensile stresses exceed the tensile strength limit and therefore the starts of a system of radial cracks are formed, and the crushing of the forming part of the explosion cavity does not occur, since the pressure of the explosion products is less than the compressive strength limit. The stepped surface of the split plane of the optical glass model shows that the crack development process is of a jump-like nature. The pulsating nature of the crack movement due to intermediate relaxation processes of stresses at its crack tips.Jumps in the development of cracks are due to the required magnitude of stress concentration and crack formation due to the replenishment of the required stress level.

To confirm the theoretical calculations, we considered a model that consisted of cubes measuring 100 x 100 x 100, in the center of which there were cylindrical cavities with a diameter of 7 mm and a depth of 75 mm, in which a cylindrical charge with a diameter of 2 mm, a height of 50 mm and a mass of PETN was 1.4 g.

To consider modeling the process of interaction of stress waves from adjacent charges, smooth rigid plates were applied to the two side faces of the model. The process of explosion of an elongated cylindrical charge was recorded by high-speed filming. The filmogram (see Fig. 1) shows the speed of detonation development - 6000 m/s, and the speed of outflow of gaseous explosion products is 700–800 m/s. Stress waves propagate at the speed of a longitudinal wave of a solid medium. As a result of the interference of stress waves from rigid boundaries (axes of symmetry), directed radial cracks are formed, which determined the split of the sample under study. In this case, the speed of development of the main crack is about 2000 m/s, and the splitting process occurs within 25□10-6s. Consequently, the determining role in the development of the main crack is played by the interaction of stress waves, which are formed due to the quasi-static pressure of the explosion products.

Conclusions

1. The preservation of gaseous explosion products in the cavity of the charging chamber depends on the depth of the charging chambers, which indicates a quasi-static process of destruction of solids.

2. The process of starting a radial crack along the line of the charge location depends on the loading dynamics, on the duration of pressure in the charging cavity, which indicates their interconnection of the processes of gas dynamics and the mechanics of dynamic destruction of solids.

References

Baranov E.G., Kovalenko V.A. Formation of shock wave energy during the explosion of adjacent charges. Collection. Explosion energy management, - Frunze, "Ilim" 1970. - 246 p.

Dambaev Z.G. Estimation of Quasi-Static Action of Explosion Products in the Directed Destruction of Rock (Scopus). Proceedings of the 8th International Conference on Physical Problems of Rock Destruction. Metallurgical Industry Press. China, 2014, Pp.64-67.

RESEARCH PROGRESS, TRENDS, AND INNOVATIONS OF DEVELOPMENT ON MINING BACKFILL TECHNOLOGY OF UNDERGROUND METALLIFEROUS MINE

Lijie Guo[1,2*], Xiaopeng Peng[1,2], Yue Zhao[1,2], Guoxing Tang[1,2]

[1] Beijing General Research Institute of Mining and Metallurgy, Beijing, CHINA
[2] National Centre for International Research on Green Metal Mining, Beijing, CHINA

Abstract

Backfill mining technology used extensively in underground metal mines is critical for conducting green and low-carbon mining operations. Also, backfill mining can achieve the maximum recovery of underground mineral resources and environmentally friendly disposal of mining wastes. This paper systematically reviews the development of backfill mining methods. The latest technology application progresses from three aspects: high-efficiency and large-scale backfill mining, continuous backfill mining, and how to reduce backfill mining costs. Then the backfill mining technology used in metal mines evolved and developed. The application and development trend of the whole process of backfill technology covering the preparation and transportation of tailings backfill slurry, barricades design, and the drainage of backfill slurry in the stope are analyzed. The mechanism of heterogeneous characteristics and self-weight consolidation behavior of tailings backfill slurry are analyzed, and the comparison of the traditional method used for strength requirement analysis of the backfill structure with the improved strength calculation-design method is made. Also, the field monitoring method of the backfill slurry is introduced. Based on the above research, it is proposed that innovation of backfill mining technology is the core element to achieve low-cost backfill mining, the development of a whole-process backfill mining system is the key to the

stable preparation of high-quality underground tailings backfill slurry, and the stability of the underground backfill structure is the base to ensure the safe, efficient, and economical application of backfill mining technology. Also, the improvement of the standard system is the guarantee for accelerating the promotion of the application of backfill mining technology. At the same time, the research direction that should be focused on in the future is clarified. Accelerating the development of new technologies, materials, and equipment for green and low-carbon filling is the driving force to promote the transformation and development of backfill mining.

Keywords: Metal Mine, Backfill Mining, Green Mining, Mine Backfill, Backfill Mechanics

Introduction

For a long time, the world will still be in the middle and late stages of industrialization and rapid urbanization, and the rigid demand for metal mineral resources and the contradiction between supply and demand will still exist for a long time. With the depletion of the mining of shallow mineral resources in the world, the development of mineral resources in the future will fully enter the deep deposits within the second depth space (1000-2000m), and deep mining of metal mines will become the norm. Deep mining faces a complex environment of 'three highs and one disturbance'. Filling mining can effectively control ground pressure and movement of overlying strata and will be widely used in deep metal deposit mining. The recovery rate of filling mining resources is high, and the solid waste accumulated on the surface can be backfilled into the goaf underground, which can not only improve the safety of mining operations but also prevent the occurrence of surface disasters and can fully absorb the surface solid waste. The application of cemented filling technology can enable the filling mining method to control the movement of rock strata and surface subsidence effectively, making it possible to mine under water bodies and structures and to preferentially mine high-grade ore bodies in deep parts or footwalls, providing an excellent opportunity for the effective use of resources and the improvement of enterprise competitiveness.

In recent years, with the integration of advanced cross-technology, advanced experimental methods, and filling mining technology, metal ore filling mining technology and technology has also developed rapidly, and many new theories, new methods, and new technologies have emerged in the basic theory and application technology of mine filling technology. Therefore, the author systematically sorts out and summarizes the research progress of metal ore filling mining technology to inspire future technological innovation work.

Application progress of backfill mining in underground metal mine

The evolution of backfill mining

Backfill mining is an ancient mining method. Backfill technology was first used in mining in the 16th century, mainly by Spanish colonists at some mines in Mexico, using wood and waste rock as supports to create a safe mining. Tailings and other types of solid wastes were introduced into underground metal mining in the 19th century, but a dedicated backfill mining method was not yet been formed.

The hydraulic backfill mining method appeared in the 1950s and was popularized in metal mines in Canada and South Africa. The overhand cut-and-fill mining and open stoping with subsequent backfill mining using the high-density cemented tailings backfill appeared in Canada in the 1960s.

In the early 1970s, large-diameter long-hole backfill mining was first applied in the Copper Cliff North Mine. In 1975, the vertical crater retreat (VCR) mining method with a hole depth of 40 m and large diameter (165 mm) was applied in the Levack Mine successfully. In 1982, the VCR mining method was first used in China at underground mines, and Professor Sun Zhongming [0] at the Beijing General Research Institute of Mining and Metallurgy (BGRIMM) led a team to start the field test and application at Fankou Lead-Zinc Mine. After its successful application, it was gradually used in Jinchangyu Gold Mine, Shizishan Copper Mine, and Fenghuangshan Copper Mine in China. At the beginning of the 21st century, the team led by Professor Sun Zhongming further developed the massive ore-dropping technology based on

the spherical charge funnel blasting, which allowed the establishment of an underground super-mining ore factory. After 2000, with the development of advanced mining equipment, the panel mechanized cut-and-fill method has been successively applied in Jinchuan No. 2 mining area and the Fankou lead-zinc mine in China.

At present, most of the large-scale metal mines are developed on thick-inclined or steeply inclined deposits. The methods adopted for such deposits are mainly the pillarless caving method and the open stopping with subsequent backfill mining. The latter, with large-diameter deep holes, has been paid more attention due to its high production efficiency, high recovery intensity, and the ability to prevent surface subsidence.

The vertical staggered continuous mining with high stopes for thick and large ore bodies was proposed by Professor Yang Xiaocong at BGRIMM. As shown in Figure 1, this mining method allows a safe and efficient recovery under the backfill roof without leaving a horizontal ore pillar using the high stopes.

High-efficiency and large-scale backfill mining

High-efficiency and large-scale mining is the eternal pursuit of mines because efficiently recovering ore from the ore body means more significant economic benefits. The caving method using large-scale blasting and high-efficiency mining equipment is widely applied in underground metal mines in China, especially iron mines. In recent years, with the country's emphasis on environmental protection and solving the problem of underground voids and tailings disposal, more and more mines adopt open stoping with subsequent backfill mining.

As shown in Figure 2, the ore body is generally divided into a series of primary and secondary stops using the open stoping with subsequent backfill mining. The typical mining sequence is mining the primary stope first and filled with cemented backfill, and then the secondary stope is mined with the support of the adjacent cured backfill.

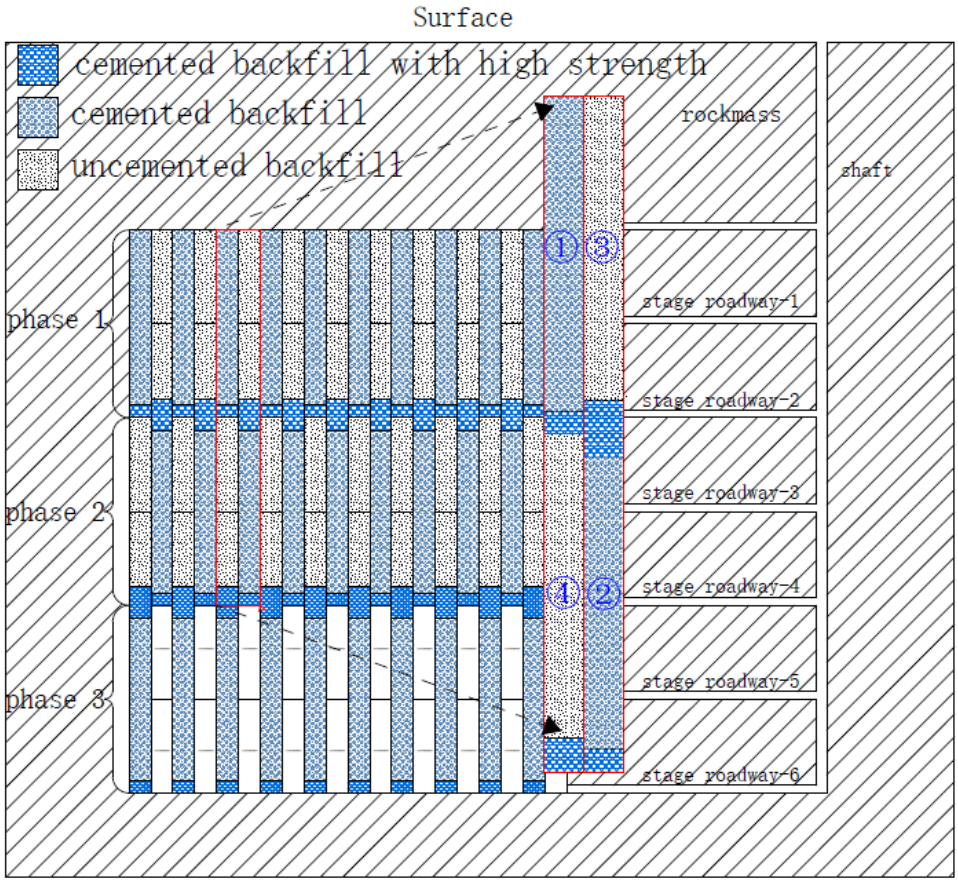

Figure 1 The vertical staggered continuous mining with high stopes

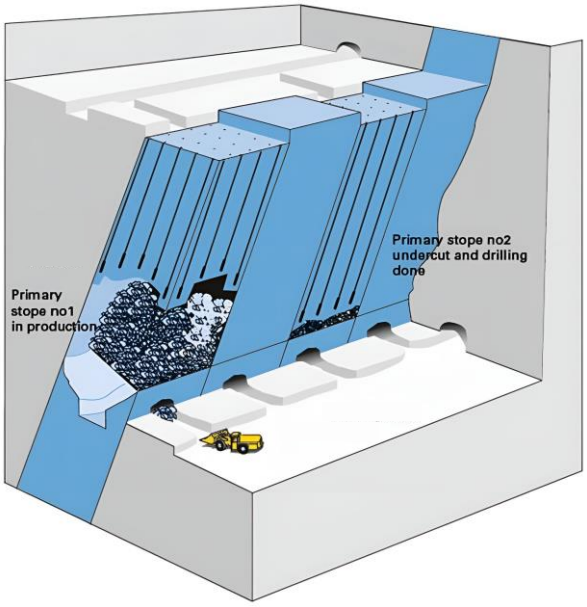

Figure 2 Open stoping with subsequent backfill mining

The length of the primary or secondary stope is generally controlled below 60 m, the width is usually 6~30 m, and the height is generally 40~60 m in mines using the open stoping with subsequent backfill mining in China. The large-diameter and deep-hole rock drilling equipment is often used to match the large-size stope. The commonly used Simba364 drilling jumbo at Anqing Copper Mine in China can achieve a drilling depth of 51 m a day with a drilling diameter of 90~178 mm [0]. The Dongguashan Copper Mine in China, which adopts the open stoping with subsequent backfill mining, has a comprehensive panel production capacity of 2400 t/d.

Continuous backfill mining

The underground void with an exposed area that reaches a critical value is prone to collapse, so different mining methods take various measures to limit the exposed area. For example, the open stoping with subsequent backfill mining methods limits the exposed area by dividing the ore body into primary and secondary stopes. The overhand/underhand cut-and-fill mining methods limit the exposed area by dividing the ore body into a series of aligned drifts. The common feature of these two mining methods is that in each mining cycle, the filling process is delayed after the mining process. Therefore, the waiting time between mining and backfill processes increases the difficulty of production management and reduces mining efficiency. For this reason, some scholars have proposed the continuous mining and backfill method. The basic concept is to use some mined areas within the partially mined stope as temporary working spaces and backfill the mined voids before the completion of mining [0].

The continuous dry filling long room method (Avoca, Figure 3) addresses the efficient continuous mining of steeply inclined and medium thick orebody [0]. The mining is carried out from one end to the other end of the stope, and the LHD is used for continuous ore extraction, followed by continuous dry filling of the formed voids. Because the void is filled in time and the exposed area is small, the stope length is not limited, which has significant safety management advantages compared with the large exposed area and long exposure time of the void in the open stoping with subsequent mining. For medium-thick ore bodies, this continuous method can achieve considerable production capacity. The modified Avoca mining method used in the Qinglonggou gold mine in China, as shown in Figure 4, allows ultimately continuous mining and filling, and its production capacity can reach 307 t/d with a 9.6% ore loss rate and 7.5% ore dilution rate.

Underhand cut-and-fill mining is suitable for broken ore bodies surrounded by cracked rock mass, which has low mining efficiency, high backfill costs, and complex safety management. By changing the existing mining process, the underhand sublevel continuous backfill mining with the medium-deep hole was proposed by BGRIMM. This method can reduce the preparatory work, improve the individual stope's production efficiency and reduce the mining

operations' cost. Figure 5 shows the underhand high-sublevel continuous mining method of the Karatunk copper-nickel mine. After successful application, the production capacity of the panel increased from 164.27t/d to 423.21t/d, and the production cost was reduced from RMB 108/t to RMB 50/t, with significant economic benefits.

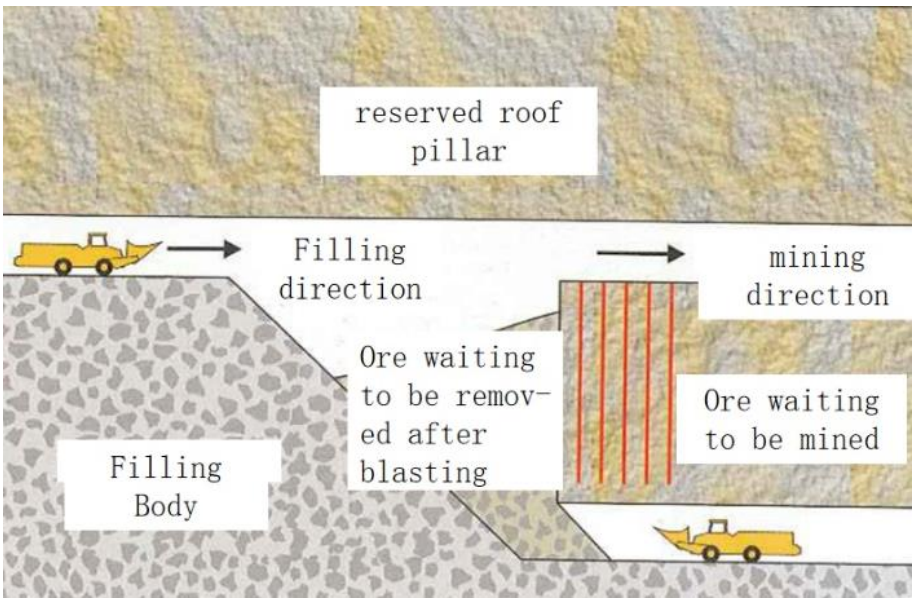

Figure 3 Diagram of Avoca mining method

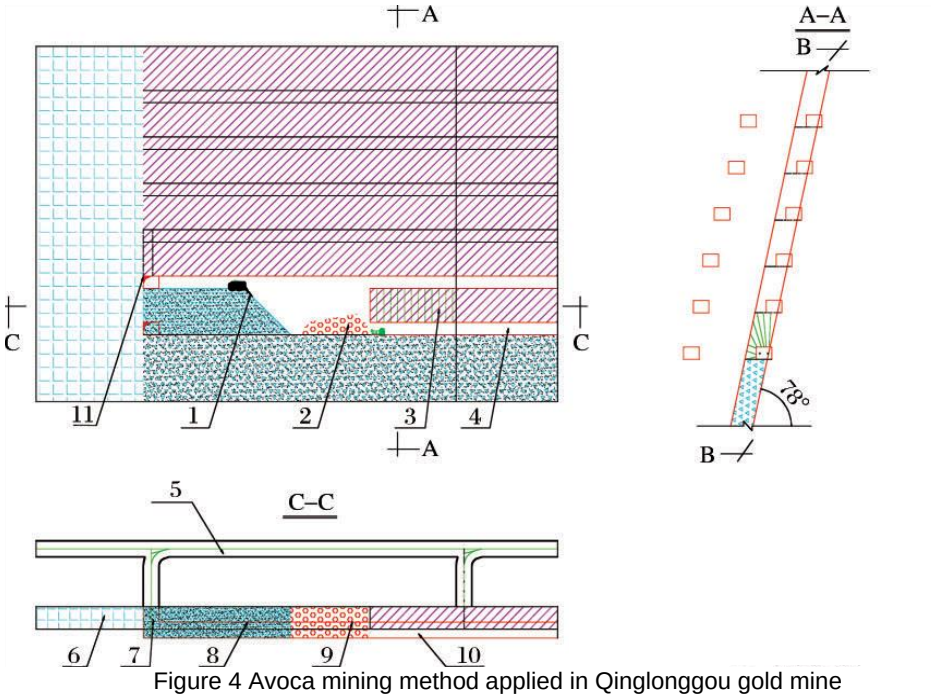

Figure 4 Avoca mining method applied in Qinglonggou gold mine

1- cemented rock fill, 2- ore, 3- fan-shaped drilling pattern, 4- drilling roadway, 5-sublevel roadway, 6-surrounding rock, 7- cutting roadway, 8- cemented rock fill, 9- ore, 10- drilling roadway, 11- cutting shaft

Reduce the backfill costs

Backfill mining mainly relies on the support provided by the backfill structure to perform safe and efficient mining processes, which requires a specific strength of the backfill to play the functions of man and machine walking, self-standing, and high-strength roof protection.In order to meet the strength requirements of the backfill, cement and other cementitious materials are commonly added to the backfill slurry, resulting in a considerable consumption of cementitious materials and making the cost of cementitious materials account for 70-80% of the total cost of backfill operations. On the one hand, this is due to the unreasonable design

of the required backfill strength, leading to a conservative backfill design. In addition, the high price of cement and other cementitious materials and the inappropriate mining methods used by mines also lead to a large proportion of the cost of cementitious materials. Therefore, the scientific optimization of the backfill design, the development and application of low-cost cementitious materials, and the reasonable use of efficient mining methods are the main ways to reduce the cost of backfill mining.

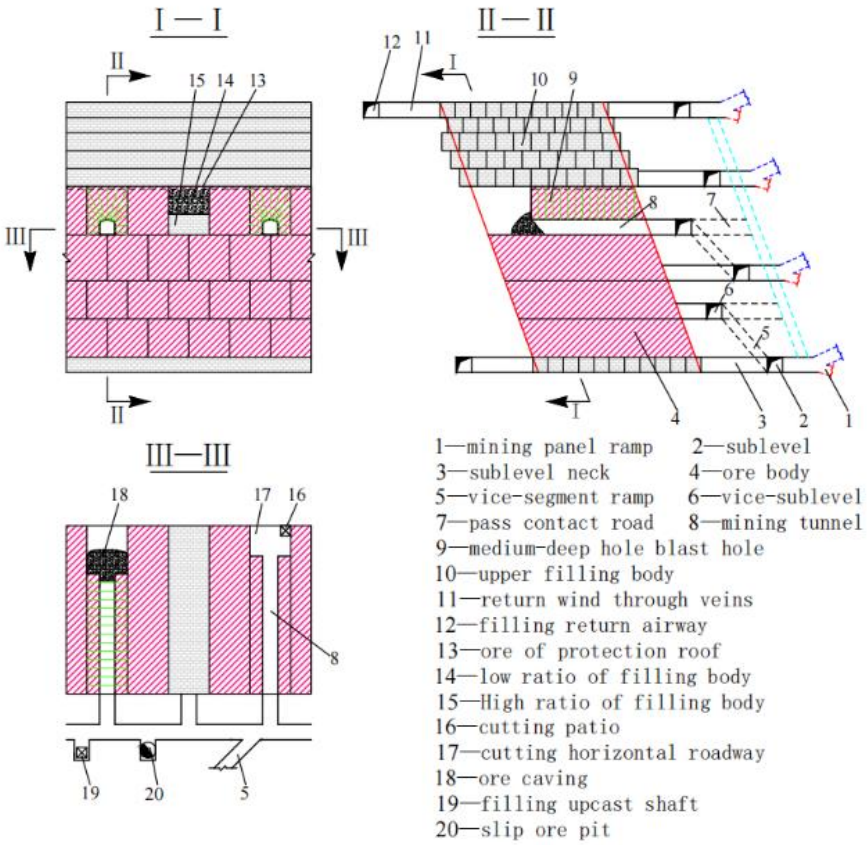

Figure 5 Downward high-segmented continuous mining method

Scientifically optimize the required strength of the backfill to reduce the cement consumption reasonably. Canada, Australia, and other foreign-developed mining countries attach great importance to the fundamental theories and methods of backfill mechanics. Starting from the stress analysis within the backfilled stope, they have established the backfill mechanics analysis and backfill strength requirements calculation methods represented by the classical Mitchell method using model tests, analytical analysis, or numerical calculations, forming the theoretical basis for the backfill mechanics. Liu Guangsheng of BGRIMM proposed a three-dimensional analytical model and calculation method for the required backfill strength with front wall exposure and back wall pressure. In addition, rationally optimizing the design of the spatial distribution of the strength of the cemented backfill is also the key to reducing cement consumption. For example, the required strength of the plug pour and the final pour should be optimized to reduce backfill costs.

Develop new cementitious materials to replace cement. It reduces cemented backfill costs by developing and applying cheaper cementitious materials to replace cement partially. Fly ash and non-ferrous metallurgical slag (copper slag, nickel slag, lead-zinc slag) contain mineral components such as silicate, aluminate, and iron-aluminate shown in Figure 6. Under the excitation of activation excitation and phase reconstruction, it can be activated to form C-S-H gel, so it has the potential and feasibility of making cheap cementitious materials used for backfill. Existing studies have shown that [0] adding fly ash and non-ferrous metallurgical slag

to ordinary Portland cement can increase the long-term strength of the backfill containing sulfide.

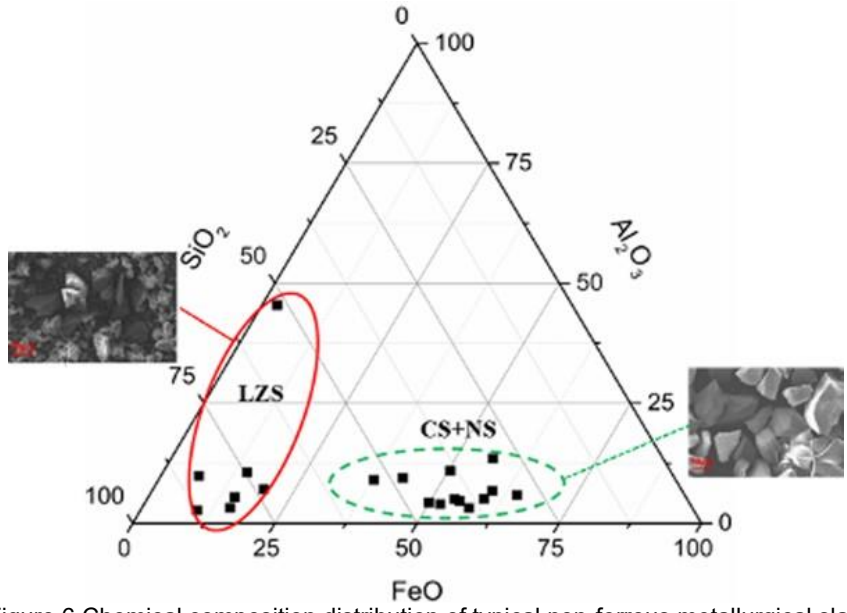

Figure 6 Chemical composition distribution of typical non-ferrous metallurgical slag

Research progress of metal ore solid waste backfill technology

Evolution and development of mine backfill technology

Mine backfilling technology is the core element of metal ore-filling mining technology. It has always troubled or restricted early backfill mining methods' development, application, and promotion. Until 1957, the cemented filling of graded tailings and Portland cement was established in the Canadian Eagle Bridge Company. Hardy Nickel Mine was successfully applied, and the cemented filling process was applied to the production stage for the first time. This prompted the rapid development of the filling mining method during this period.

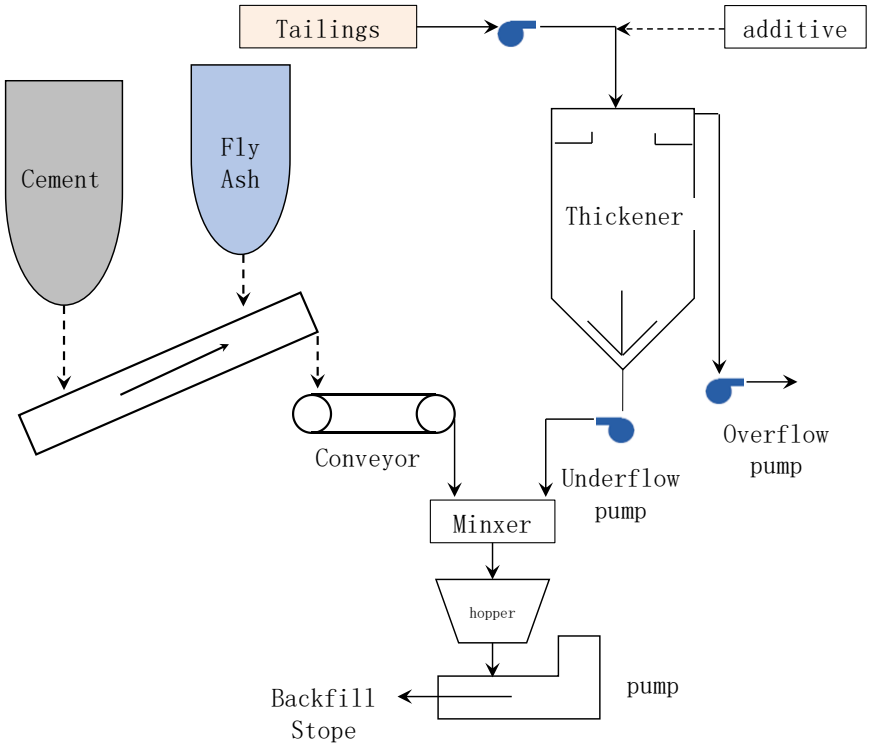

Figure 7 Backfill technology applied in metal mine

In 1977, Australia's Mount Isa Mine and the University of New South Wales jointly developed a low-cost cemented filling process using slag as an auxiliary gelling agent; since the 1980s, China began to develop high-concentration mortar filling and block stone cement slurry cemented filling At the same time, Canada is developing high-concentration tailings cemented filling based on vertical sand bins, and Australia is developing low-cost waste rock tailings cemented filling technology. In the late 1980s, Germany built the world's first paste backfill mine in the Bad Grund lead-zinc mine; in 1994, China built the first paste-filling process system in Jinchuan No. The Tonglushan Copper Mine and the Huize Lead-Zinc Mine built an unclassified tailings paste filling system, as shown in Figure 7; after 2000, two technological modes of tailings high-concentration cemented filling and paste cemented filling dominated The filling of metal mines has also evolved a new filling technology on this basis.

Backfill slurry preparation technology

The metal mine backfill process is still dominated by tailings filling, mainly divided into tailings high-concentration backfill, tailings paste backfill, and waste rock tailings paste backfill.

Classified tailings filling is still one of the most widely used filling technologies at present, and it is mainly gravity conveying. The graded tailings filling adopts the technology of swirl classification and vertical sand bin hydraulic joint slurry making, and the mass concentration of the filling slurry prepared by it is generally 65% to 72%. The vertical sand bin preparation system is generally used for the high-concentration slurry of graded tailings. The traditional process has the problems of tailings compacting in the bin, significant fluctuations in sand concentration, and reduced tailings mortar. In 2012, Professor Guo Lijie of the Beijing General Research Institute of Mining and Metallurgy proposed a vertical sand silo tailings wind and water two-stage time-sharing slurry-making technology around the wall (Figure 8), which realized the stable preparation of graded tailings high-concentration filling slurry. In 2014, the Beijing General Research Institute of Mining and Metallurgy developed a high-concentration filling technology for an optimized combination of tailings based on the beneficiation process (Figure 9), using classified coarse tailings and overflowed fine sand to concentrate separately and then optimize the combination in proportion, transformed into a high-concentration filling with good gradation and stable filling quality. This technology effectively improves the filling quality and solves the problem of insufficient classified tailings for backfill purposes.

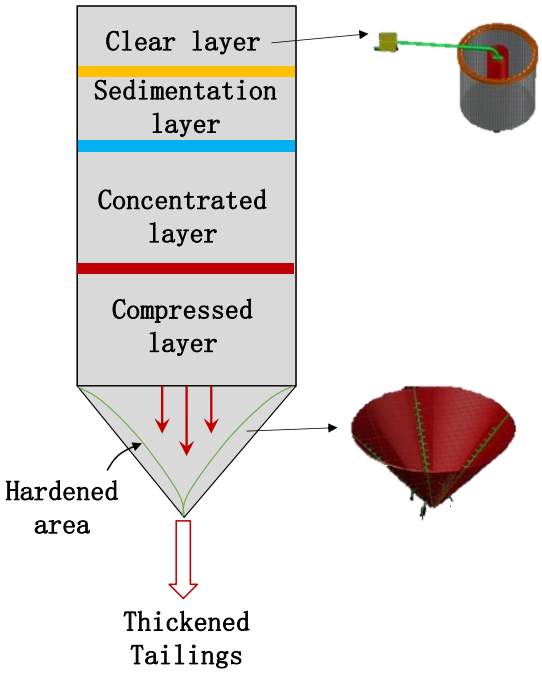

Figure 8 A new slurry preparation technology used in the vertical sand tank

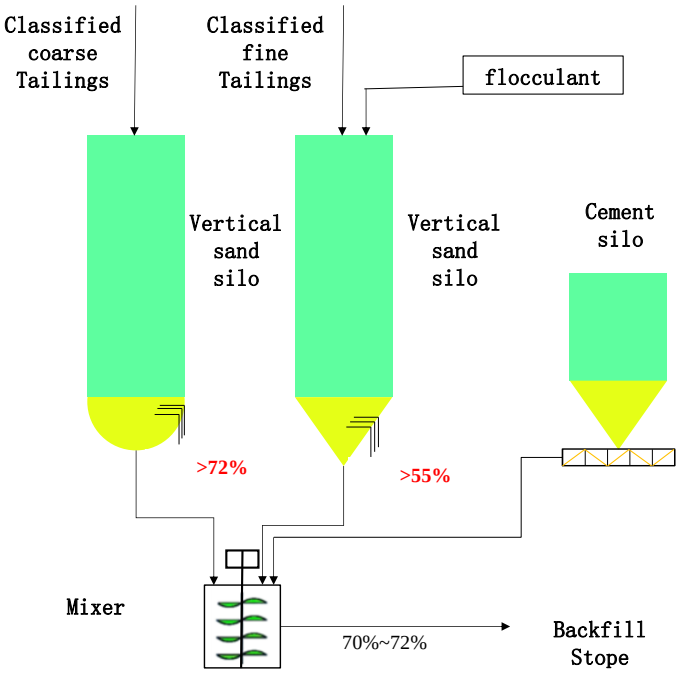

Figure 9 High concentration backfill technology based on mineral process

Paste slurry is a backfill slurry that does not segregate and has excellent and stable plasticity and fluidity. Due to the wide range of filling aggregate sources, the material properties vary greatly. Quantifying the paste with a single index, such as mass concentration, is difficult. The yield stress is mainly used to evaluate the paste in the world quantitatively. It is believed that when the yield stress of the slurry is greater than 200±25Pa, it can be regarded as a paste Paste tailings slurry is generally prepared by dehydration equipment such as a deep cone thickener (Figure 10) and filter press/filter. Tailings gradation is the decisive factor affecting filling quality. With the advancement of mineral processing technology, the particle size of metal ore dressing tailings is getting finer and finer, resulting in poor tailings settlement concentration. It is not easy to prepare a stable paste. Chris Lee from Canada's Gundam Consulting Co., Ltd. proposed a combination of different gradation tailings, first cyclone classification, and then using different high-efficiency concentration and dehydration methods to prepare the paste (Figure 11). This method realizes the stable and efficient preparation of fine tailings paste.

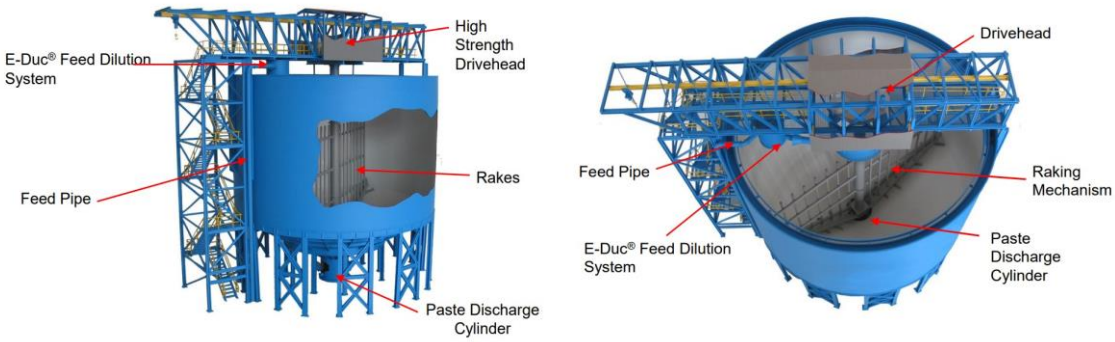

Figure 10 Deep cone thickener for tailings paste

Backfill retaining wall technologies

The filling retaining wall appeared as an essential safety support structure for the closure of the filling stop. At first, it was mainly supported by simple wooden structures. With the development and perfection of mining technology and scale, the structure and form of the filling retaining wall in underground metal mines have experienced various forms, such as

wooden structures, reinforced concrete structures, brick structures, and steel structures. Currently, the filling retaining walls of underground metal mines domestically and overseas can be divided into reinforced concrete retaining walls, concrete block retaining walls, and flexible retaining walls supported by steel and wood structures. The structure and form of the retaining wall are closely related to the filling mining process.

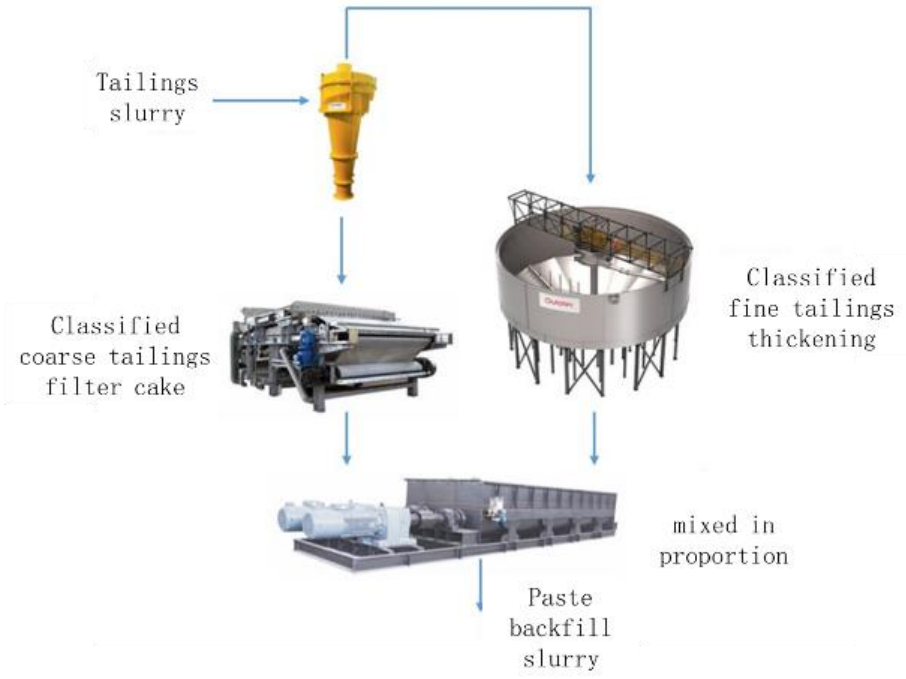

Figure 11 Combined-process preparation for cemented paste backfill

The reinforced concrete retaining wall has a large bearing capacity and strong universality. It is used in various filling process conditions, but its engineering cost is relatively high, as shown in Figure 12a shown; Concrete blocks (such as concrete prefabricated bricks, Figure 12b) and flexible closed retaining walls are suitable for drift backfill mining method with low load-bearing requirements; In addition to the traditional concrete retaining wall, brick retaining wall and flexible retaining wall, in recent years, with the gradual deepening of people's understanding of the mechanical characteristics of filling stopes, some green and low-cost filling stope sealing technologies have emerged, such as adopting detachable and recyclable assembled retaining wall with metal components. The primary force-bearing member of this retaining wall is a curved steel beam, which adopts assembled parts and can be disassembled and recycled, which significantly reduces the cost of filling stope closure. In China, Anqing Copper Mine, Axi Gold Mine, and other mining are applicating this retaining wall, as shown in Figure 12c.

(a) Concrete rigid retaining wall

(b) Brick retaining wall

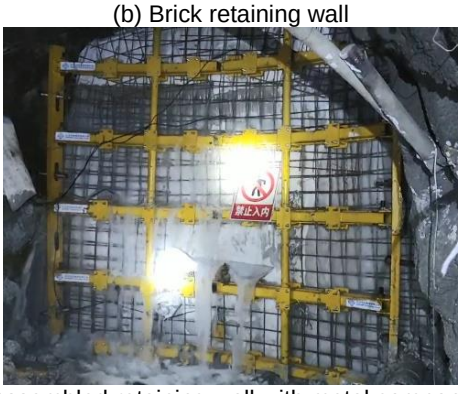

(c) Assembled retaining wall with metal components

Figure 12 Types of retaining wall

The selection of the closed structure form of the filling stope needs to consider various factors such as filling quality, filling mechanics, manufacturing process, and cost, among which the stress characteristics of the retaining wall and stope dehydration are the key points. Hughes' research shows that the load characteristics on the filling retaining wall have a great relationship with the shape of the slurry, and the wall pressure calculated using the limit equilibrium theory has a great relationship with the selection of the limit slip surface. If the load on the wall achieves rapid consolidation and hardening under good drainage conditions or a better technological level, the measured stress on the wall is much smaller than the theoretical value. The mechanical model is proposed to deepen people's understanding of the bakcfill body. If considering the arch effect, the force on the retaining wall will no longer be a linear relationship of height. Yang thought that the mechanical effect of the traditional arching effect was not apparent at the initial stage of filling and only appeared in the later stage of filling slurry curing and forming, so a mechanical model of shear yielding-induced arching effect was proposed to describe short-term loads on retaining walls. From the traditional simplified model to the progressive mechanical thinking proposed according to the characteristics of working conditions, the research results have enriched people's understanding of filling retaining walls. For example, Lu introduced a new type of lightweight retaining wall, which has significant advantages in terms of bearing capacity and engineering slurry; Berndt introduced a retaining wall of permeable brick walls, which play an essential role in achieving stope dehydration and ensuring the bearing capacity of the filling stope.

With the continuous expansion of the filling mining scale of underground mines, new and higher requirements have been put forward for safe, efficient, green, and low-cost stope closure technology, which is mainly reflected in the precise matching between the structural design of the filling retaining wall and the filling process, high efficiency, low-cost new construction methods, accurate measurement and safety monitoring about retaining wall loads. In the future, safer, low-cost, and monitorable methods will inevitably become the main development method for the technology of filling stope closure in the underground mine.

Advances in mine backfill mechanics research

The traditional analytical method to determine the strength of backfill in stopes

The open stoping with subsequent backfill mining method represents the development direction of large-scale, high efficiency, green and clean mining. However, the cemented backfilling cost of the backfill in primary stopes accounts for more than 70% of the total backfilling cost. How to ensure the stability of the cemented backfill when it is laterally exposed during the mining process while optimally controlling the cemented backfilling cost is a bottleneck for safe, economical, and efficient backfill mining.

In Canada, Australia, and other foreign countries with the developed mining industry, starting from the stress analysis of the backfill in stopes, the theory and method of mechanical analysis and strength design of the backfill in open stoping with subsequent backfill mining represented by Mitchell's method have been established and widely adopted in foreign mines, which has extensively promoted the development of backfill mechanics and backfill mining technology abroad.

In the 1980s, foreign backfill mining researchers mainly drew on the self-weight stress of the overburden ($\sigma c \geq \gamma H$) or the laterally exposed slope model ($\sigma c \geq \gamma H/2$) in soil mechanics for the design of the stress and strength requirement of the backfill in stopes (where σc is the strength requirement of the backfill, γ is the bulk unit weight of the backfill and H is the height of the laterally exposed face of the backfill). However, both of these methods do not consider factors such as the confinement of the backfill by the surrounding rock and its three-dimensional stress state, resulting in an overly conservative backfill design strength and high backfilling costs. On this basis, Mitchell et al. carried out a series of indoor physical model tests of the backfill with unilateral exposure, researched and proposed a three-dimensional wedge sliding analytical model and method for calculating the strength requirement of the lateral exposure backfill, which took into account the three-dimensional failure mode and mechanical behavior of the backfill in stopes, reasonably reduced the backfill strength design index, and was successfully applied in many Canadian mines using backfill mining methods, which is of historical importance.

Figure 13 shows the analytical model of three-dimensional limit equilibrium constructed by Mitchell et al. based on the sliding failure of unilaterally exposed cemented backfill with different sizes and strengths in indoor physical model tests, Figure 13 shows the analytical model of three-dimensional limit equilibrium constructed by Mitchell et al. based on the sliding failure of unilaterally exposed cemented backfill with different sizes and strengths in indoor physical model tests, in which the sliding failure of the backfill is assumed to occur along the potential plane through to the back wall of the backfill, and only the cohesion of the contact surfaces between the backfill and the surrounding rock of both sidewalls is considered, ignoring the angle of internal friction on the contact surfaces of the sidewalls, and both the cohesion and angle of internal friction on the contact surface between the backfill and the surrounding rock of the back wall of the stope are assumed to be zero, resulting in an analytical equation for the strength requirement of the cemented backfill with lateral exposure and its safety factor (as in equation (1)).

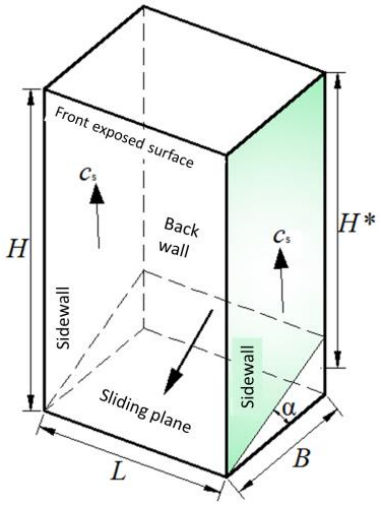

Figure 13 Illustrations of required strength model of cemented backfill with lateral exposure (Mitchell's

method)

$$\sigma_c = \frac{1}{2M} \cdot \frac{\gamma L\left(FS\tan\alpha - \tan\phi\right)\left[H - \frac{B\tan\alpha}{2}\right]\sin\alpha}{L\tan\alpha + r_s\left(FS\tan\alpha - \tan\phi\right)\left[H - \frac{B\tan\alpha}{2}\right]\sin\alpha} \quad (1)$$

Where: σc is the uniaxial compressive strength (kPa) required for a laterally exposed cemented backfill to be self-supporting; FS is the safety factor for a laterally exposed backfill; L is the length of the exposed face of the backfill (m); B is the width of the backfill (m); H is the overall height of the exposed face of the backfill (m); H* is the equivalent height of the potential sliding wedge of the backfill (m), H*=H-(Btanα)/2; γ is the bulk unit weight of the cemented backfill (kN/m³); M is the ratio of the cohesion c of the backfill to the uniaxial compressive strength σc of the backfill (M=c/σc); ϕ is the angle of internal friction of the backfill (°); α is the angle between the potential sliding plane and the horizontal plane (°), α=45+ϕ/2; rs is the ratio of the cohesion cs on the contact surface between the surrounding rock and the backfill to the cohesion c of the backfill (rs=cs/c), Mitchell's method assumes rs=1.

Mitchell et al. further assumed that the angle of internal friction of the backfill ϕ=0, M = 0.5 (i.e., σc=2c), rs=1 (i.e., cs=c), and that H>>B makes H*≈H, based on the analysis of the backfill in the physical model. A simplified classical Mitchell's method was obtained for the limit equilibrium state with the safety factor FS = 1, as in equation (2).

$$\sigma_c = \frac{\gamma H}{1 + \frac{H}{L}} \quad (2)$$

This simplified classical Mitchell's method has been widely used in industry and academia worldwide in backfill mining and provides the basis for calculating the strength requirement of laterally exposed backfill. However, Mitchell's method has many assumptions, and although the method agrees well with the physical model test results, some of the assumptions do not match the actual situation, e.g., Mitchell's method assumes that the angle of internal friction of the backfill is 0. Although Mitchell's method has certain limitations, the model provides a solid basis for later developing lateral exposure backfill strength calculation methods.

An improved method for calculating and designing the strength requirement of backfill in stopes

The stress distribution of the backfill is the mechanical basis for calculating the strength requirement of the backfill and its stability analysis under lateral exposure conditions in the open stoping with subsequent backfill mining methods. International and domestic scholars have conducted exploratory studies on the arching stress effect of the backfill in stopes. Due to the ease of analysis of backfill stress and strength requirement, researchers have continued to improve and develop analytical models of backfill stress and strength requirement in stopes, allowing them to be quickly applied to guide the design of backfill strength in mines.

Based on Mitchell's original model, Zou, and Nadarajah considered the top load of the backfill in stopes, and Dirige et al. considered the effect of the angle of inclination of the backfill and improved the analytical calculation method of the backfill strength requirement respectively. However, they still followed all the assumptions of Mitchell's original model. In Canada, Li and Aubertin et al. systematically combined the research basis of the stress distribution characteristics and anisotropic mechanical boundaries of the backfill, gradually overcame the limitations of the assumed conditions in Mitchell's original model, and extended the theory and method of calculating the strength requirement of the backfill by considering the delamination phenomenon of the actual backfill in stopes, the frictional effect between the backfill and the surrounding rock of the stope sidewalls.

However, the previous analytical model for the correction of the strength of the backfill mainly focuses on the lateral exposure of the cemented backfill in a single isolated stope and does not take into account the influence of the backfill in adjacent stope and its mechanical contact with the surrounding rock of the stope during the actual mining and backfilling process (e.g., Figure 14a), and the theoretical approach for the design of the strength requirement of

the backfill is still not mature and perfect. In this regard, Liu Guangsheng et al. proposed a three-dimensional analytical model and calculation method for the strength requirement of the cemented backfill with the front wall exposed and the back wall compressed, based on the actual excavating-backfilling sequences of the two-step open stoping with subsequent backfill mining method, focusing on the lateral pressure effect of the non-cemented backfill in the secondary stopes on the adjacent cemented backfill in the primary stopes. By comparing the numerical simulation solution of the strength requirement of the backfill in the limit equilibrium state with its analytical results, it was determined that the numerical simulation and analytical calculation results of the strength requirement of cemented backfill in primary stopes agree best when the potential sliding plane angle of the backfill $\alpha=45°+\phi/2$ and the angle of internal friction between the backfill and the sidewall surrounding rock $\beta=45°-\phi/2$. This backfill strength calculation method has been successfully applied to the backfill strength design of mines such as Sanshandao Gold Mine, CaoLou Iron Mine, and Karatunk Copper-Nickel Mine.

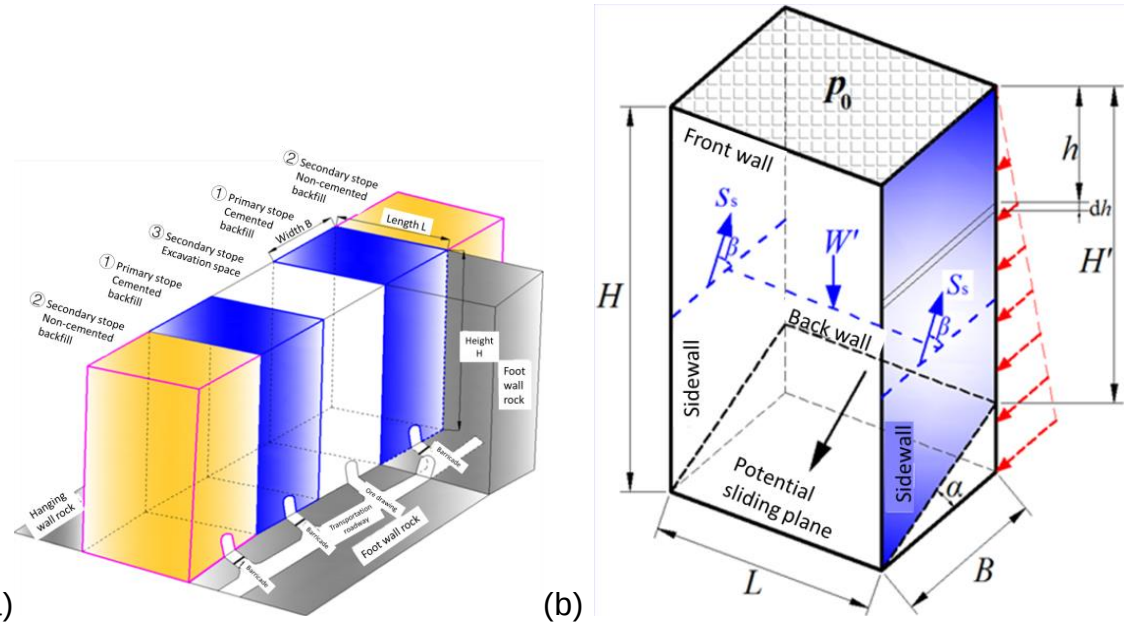

Figure 14 Spatial relationships between the backfill and rock mass and illustrations of required strength model of the backfill of two-stage open stoping with the subsequent backfill mining method

On this basis, how to reasonably transform the theoretical value of strength requirement into the actual strength requirement and ration parameters matching the technical level of the mine backfilling according to the quality control effect of the stopes backfilling in different periods of different mines is a crucial link to improve the design of the backfill strength of underground metal mines. For this, a statistical calculation method for the floating safety factor FS was proposed by combining the statistical analysis of backfill specimens' strength and in-situ core specimens' strength, as in equation (3).

$$FS = \frac{UCS_{\mathrm{p}}}{\overline{x} - 2\varpi} \tag{3}$$

Where: UCSp is the standard reference value of uniaxial compressive strength of a backfill specimen measured by indoor proportioning tests under a particular backfill ratio parameter, MPa; $\overline{x}$ is the average of the specimen set of uniaxial compressive strength data from core specimens drilled in the in-situ backfill after the slurry prepared by the mine backfill station has cured in the stope for at least 28 days using the same backfill proportioning parameters, MPa; $\overline{\omega}$ is the standard deviation of the strength of the same in-situ backfill core specimens. This equation recommends a range of 2 times the standard deviation of the sample mean of the core sample strength, which can cover 95.45% of the sample data area and is an empirical equation in line with the engineering application significance of mine backfill mining.

By combining the theoretical, analytical solution for the strength requirement of the backfill in different stopes with the floating safety factor for different periods in different mines, the actual strength requirement of the backfill in the current period of the mine can be derived, thus determining the values of the proportioning parameters of the mine backfill system.

By incorporating in-situ backfill coring and core specimen strength testing into the daily production tasks of the mine, the sample database of mine backfill quality control effects can be continuously supplemented with feedback to derive floating safety factors for different periods of the mine and achieve floating optimization of mine backfill strength requirement. When the stability of the mine backfill system and the quality control of the backfill are significantly improved, it will increase the average strength and decrease the dispersion of the core samples of the mine backfill. The floating safety factor calculated by core testing and mathematical statistics will be reduced accordingly. The actual strength requirement of the mine backfill will then be reduced. Conversely, if the stability of the backfill system is reduced, this will eventually feed through to an increase in the design index of the actual strength requirement.

Conclusion

This paper systematically reviews the development of backfill mining methods. The latest technology application progresses are introduced from three aspects: backfill mining methods used in metal mines, backfill technology, and backfill mechanics. The research progress and development trend of backfill mining are analyzed.

(1) Backfill mining is an important carrier to realize the green mining of metal mines. Advanced backfill mining theory and technological innovation is the key to the efficient recovery of mineral resources, minimizing environmental impact and reducing mining and backfill costs.

(2) Large-scale and high-efficiency continuous backfill mining is a significant development direction of underground mining technology for metal mines in the future. The open stopping with subsequent backfill mining is critical to realize large-scale and efficient mining of thick ore bodies. Continuous backfill mining is a revolutionary development of achieving highly efficient mining of broken ore bodies.

(3) Backfill technology is the core element of backfill mining. The stable density of the backfill slurry in the pipeline is more important than the level of the slurry concentration itself. A stable, reliable, and simple transport process of the backfill slurry is more effective than the complex automatic control.

(4) The innovation in the low-cost backfill material is critical to promoting the development of backfill technology. The green and low-carbon backfill technologies, new materials, and new equipment should be paid more attention, such as developing the cemented paste backfill systems with a capacity of more than 250 m3/h, promoting the application of slag cementitious materials instead of ordinary Portland cement, and using the dismountable barricades instead of a traditional concrete retaining wall.

(5) The test methods and standards for cemented backfill's basic physical and mechanical parameters are not uniform, and the correlation model between laboratory and in-situ backfill strength has not yet been established. Emphasis should be placed on developing scientific and unified backfill mechanics testing methods and constructing the required backfill strength model that matches the in-situ stress state within the stope.

Acknowledgement

Financial support from the National Key Research and Development Program of China (Grant No. 2022YFE0135100), National Nature Fund Project (No.: 52104131), and the Exploration fund of BGRIMM（02-2229）is gratefully acknowledged.

References

Landriault, D. (2001). Backfill in underground mining. Underground mining methods: engineering fundamentals and international case studies, 601-614.

Lang, L. C., SUN, Z. (1980). Funnel blasting methods devel-oped into new underground mining techniques. Mining Engineering, 6(7): 43-50.

Sun, Z. M., Chen, H., & Wang, H. X. (2006). Huge ore caving technology with spherical explosive cartridges and cluster drilling holes. In A collection of papers of forum on new advances in mining science and technology of metal mines (pp. 4-6).

Xiao-Cong, Y. A. N. G., Zhi-Qiang, Y. A. N. G., Lian-Ku, J. I. E., & Ming, W. E. I. (2013). Experimental Research on the New Non-pillar Continuous Mining Method for Underground Metal Mines. Metal Mine, 42(07), 35.

Liu, G. S. (2017). Required Strength Model of Cemented Backfill with Research on Arching Mechanism Considering Backfill-Rock Interaction (Doctoral dissertation, Dissertation]. Beijing: University of Science and Technology Beijing, 2017

Tommila, E. (2014). Mining method evaluation and dilution control in Kittilä mine (Master's thesis).

Wang, X., Xu, Z., Xu. H. (2017). Discussion on mining technologies for open stoping with subsequent filling. China Mining Magazine, 26(8): 99-103.

Chen, Q., Zhou, K., Gu, D. (2012). Cavity synergetic utilization mechanism. Journal of Central South University (Science and Technology), 43(3): 1080-1086.

Zhang, T., Zhao, X., Li, H. (2019) Continuous dry filling of long room method for steeply inclined and medium thick orebody. Gold Science and Technology, 27(5): 704-711.

Potvin, Y., Thomas, E., & Fourie, A. (2005). Handbook on mine fill. In Not available (p. 179). Australian Centre for Geomechanics.

Hai-yong, C. H. E. N. G., Ai-xiang, W. U., Shun-chuan, W. U., Jia-qi, Z. H. U., Hong, L. I., Jin, L. I. U., & Yong-hui, N. I. U. (2022). Research status and development trend of solid waste backfill in metal mines. Chinese Journal of Engineering, 44(1), 11-25.

Grabinsky, M., Bawden, W., & Thompson, B. (2021). Required Plug Strength for Continuously Poured Cemented Paste Backfill in Longhole Stopes. Mining, 1(1), 80-99.

Guo, L., Zhang, L., Li, W. (2020) Progress and pro-spects of the preparation of cementitious materials based on nonferrous metallurgical slags. Gold Science and Tech-nology, 28(5): 321-636.

Ai-Xiang, W. U., Ying, Y. A. N. G., Hai-yong, C. H. E. N. G., Shun-man, C. H. E. N., & Yue, H. A. N. (2018). Status and prospects of paste technology in China. Chinese Journal of Engineering, 40(5), 517-525.

Ai-Xiang, W. U., Yong, W. A. N. G., & Hong-Jiang, W. A. N. G. (2016). Status and prospects of the paste backfill technology. Metal Mine, 45(07), 1.

Guo, L., Peng, X., Yang, X., Shi, C., Yu, B., Xu, W., ... & Jia, Q. (2017). Industrial practice on optimizing tailings composition combined with ore concentration processes. In 12th International Conference on Mining with Backfill 2017, Minefill 2017, Denver, United States 19-22 February 2017 (pp. 69-79). Society for Mining, Metallurgy and Exploration.

Jewell, R. J., & Fourie, A. B. (Eds.). (2006). Paste and thickened tailings: a guide. Australian Centre for Geomechanics, The University of Western Australia.

Mitchell, R. J., & Roettger, J. J. (1984). Bulkhead pressure measurements in model fill pours. CIM Bull.;(Canada), 77(868).

Zheng, J., & Li, L. (2020). Experimental study of the “short-term” pressures of uncemented paste backfill with different solid contents for barricade design. Journal of Cleaner Production, 275, 123068.

Cui, L., & Fall, M. (2017). Modeling of pressure on retaining structures for underground fill mass. Tunnelling and Underground Space Technology, 69, 94-107.

Lu, H., Qi, C., Li, C., Gan, D., Du, Y., & Li, S. (2020). A light barricade for tailings recycling as cemented paste backfill. Journal of Cleaner Production, 247, 119388.

Berndt, C. C., Rankine, K. J., & Sivakugan, N. (2007). Materials properties of barricade bricks for mining applications. Geotechnical and Geological Engineering, 25, 449-471.

Li, L., & Aubertin, M. (2009). Horizontal pressure on barricades for backfilled stopes. Part II: Submerged conditions. Canadian Geotechnical Journal, 46(1), 47-56.

Hughes, P. B., Pakalnis, R., Hitch, M., & Corey, G. (2010). Composite paste barricade performance at Goldcorp Inc. Red Lake Mine, Ontario, Canada. International Journal of Mining, Reclamation and Environment, 24(2), 138-150.

Pengyu, Y., & Li, L. (2015). Investigation of the short-term stress distribution in stopes and drifts backfilled with cemented paste backfill. International Journal of Mining Science and Technology, 25(5), 721-728.

Duncan, J. M., Wright, S. G., & Brandon, T. L. (2014). Soil strength and slope stability. John Wiley & Sons.

Mitchell, R. J., Olsen, R. S., & Smith, J. D. (1982). Model studies on cemented tailings used in mine backfill. Canadian Geotechnical Journal, 19(1), 14-28.

Liu, G., Li, L., Yang, X., & Guo, L. (2016). Stability analyses of vertically exposed cemented backfill: A revisit to Mitchell's physical model tests. International Journal of Mining Science and Technology, 26(6), 1135-1144.

Li, L., Aubertin, M., & Belem, T. (2005). Formulation of a three dimensional analytical solution to evaluate stresses in backfilled vertical narrow openings. Canadian Geotechnical Journal, 42(6), 1705-1717.

Pirapakaran, K., & Sivakugan, N. (2007). Arching within hydraulic fill stopes. Geotechnical and Geological Engineering, 25(1), 25-35.

Ting, C. H., Shukla, S. K., & Sivakugan, N. (2011). Arching in soils applied to inclined mine stopes. International Journal of Geomechanics, 11(1), 29-35.

Liu, G., Li, L., Yang, X., & Guo, L. (2016). A numerical analysis of the stress distribution in backfilled stopes considering nonplanar interfaces between the backfill and rock walls. International Journal of Geotechnical Engineering, 10(3), 271-282.

Hassani, F. P., Mortazavi, A., & Shabani, M. (2008). An investigation of mechanisms involved in backfill-rock mass behaviour in narrow vein mining. Journal of the Southern African Institute of Mining and Metallurgy, 108(8), 463-472.

Zou, S., & Nadarajah, N. (2006, June). Optimizing backfill design for ground support and cost saving. In Golden Rocks 2006, The 41st US Symposium on Rock Mechanics (USRMS). OnePetro.

Dirige, A. P. E., McNearny, R. L., & Thompson, D. S. (2009, May). The effect of stope inclination and wall rock roughness on back-fill free face stability. In Rock Engineering in Difficult Conditions: Proceedings of the 3rd Canada–US Rock Mechanics Symposium (pp. 9-15).

Li, L. (2014). Analytical solution for determining the required strength of a side-exposed mine backfill containing a plug. Canadian Geotechnical Journal, 51(5), 508-519.

Liu, G., Li, L., Yang, X., & Guo, L. (2018). Required strength estimation of a cemented backfill with the front wall exposed and back wall pressured. International Journal of Mining and Mineral Engineering, 9(1), 1-20.

Liu, G. S., Yang, X. C., & Guo, L. J. (2019). Models of three-dimensional arching stress and strength requirement for the backfill in open stoping with subsequent backfill mining. Journal of China Coal Society, 44(5), 1391-1403.

OPTIMIZING UNDERGROUND DEVELOPMENT CYCLES AND GROUT QUALITY WITH PERFORMANCE MINE GROUTS

Precious Jere[1], Dorjpalma Enkhbayar[2]

[1] Sika Australia Pty LTD, AUSTRALIA
[2] MSM Group LLC, MONGOLIA

Cementitious grouts are integral to underground mine cable bolting and anchoring systems. The mining industry employs a range of cements, batching methods, and placement equipment, yet achieving consistent and reliable performance remains a challenge. Ground support grouts must meet performance criteria such as ease of use, workability, chemical resistance, and strength development. Cement selection is influenced by factors ranging from availability and tradition to specific working conditions, including workability, temperature, water quality, and strength requirements. Typically, choices are limited to general-purpose cements, with most operations relying on ordinary Portland cement or low-heat cement. Emerging performance mine grouts, specifically designed for underground rock bolting, are gaining traction. These grouts offer significant improvements across multiple performance metrics. This paper will explore the benefits of performance mine grouts compared to standard cement, highlighting their potential to enhance underground development processes.

Keywords: Cable bolts, cementitious anchors, performance mine grout, cycle time, early re-entry, Quality control

OYU TOLGOI GEOTECHNICAL MONITORING SYSTEM: LEVERAGING TECHNOLOGY FOR ENABLING INFORMED DECISION MAKING

Manlai Purevdorj, Munkh-Erdene Ulziijargal, Erkhembayar Enkhtaivan, Herry Purwanto, Karta Simanjuntak, Thomas Moorcroft

The underground mass mining method, block caving has gained prominence in the mining industry, presenting unique challenges in ensuring safe and productive operations. The scale of these operations necessitates a comprehensive monitoring system to effectively oversee ongoing plans and inform decision-making processes, thereby mitigating potential risks to personnel and the overall business.

This study focuses on implementing a large-scale geotechnical monitoring system within the Oyu Tolgoi Panel 0 Block Cave. The monitoring system's robustness is emphasized, covering all stages from initial footprint development to sustained cave propagation and the breakthrough phase. The results obtained from this monitoring system have evolved to become a primary drive of daily operational decisions at the Oyu Tolgoi mine.

This substantial investment in geotechnical monitoring has made an invaluable contribution to the successful completion of Panel 0 Undercut and the establishment of the cave system. This paper aims to share insights into the practical application of the monitoring system at Oyu Tolgoi and its substantial value addition to the mining business.

THE METHODS AND PRACTICES OF DEMOLISHING BUILDINGS AND STRUCTURES WITH USE OF BLASTING TECHNIQUES IN VARIOUS COUNTRIES

Batjargal Dashbal1*, Tsedenbat Ariunjargal2 , Gaapil Tulga3, Yagaanbuyant Duinkherjav4

[1] Doctoral Candidate, School of Geology and Mining Engineering, Mongolian University of Science and Technology, Ulaanbaatar 14191, MONGOLIA
[2] Ph.D., Associate Professor, School of Geology and Mining Engineering, Mongolian University of Science and Technology, Ulaanbaatar 14191, MONGOLIA
[3] Ph.D., Consulting Engineer, Ulaanbaatar 14191, MONGOLIA
[4] Sc.D., Professor, School of Civil Engineering and Architecture, Mongolian University of Science and Technology, Ulaanbaatar 14191, MONGOLIA
*Corresponding author: dashbal_b@yahoo.com

Abstract

The selection of demolition methods for buildings and structures involves consideration of various factors such as environmental conditions, the type and structure of the building, its age, and the specific advantages of the chosen method. Historically, traditional mechanical methods have been widely used across the world for building demolition and remain prevalent today. These methods employ a variety of excavators with changeable working unit, concrete crushers, cutting tools, hydraulic and pneu-matic hammers, and electric, hydraulic, and vibrating equipment. However, mechanical methods are labor-intensive, costly, time-consuming, and generate significant noise and dust, prompting the development and use of alternative demolition methods. Among these, blasting techniques hold a significant position. Further research on the use of blasting energy for the demolition of buildings and structures has become an essential and pressing issue.

Keywords: demolition of buildings and structures, blasting energy, explosives, blasting operations, blast design parameters

Introduction

Although the use of blasting techniques for demolishing buildings and structures dates back to the late 1700s, it was after World War II that these methods, along with various other demolition techniques, saw significant development. This growth was driven by the need to dismantle war-damaged buildings and construct new ones. Today, blasting methods are widely employed in the United States, Germany, and various European countries for demolishing damaged or outdated buildings, as well as structures such as chimneys of power plants, towers, and tunnels [1].

Blasting techniques are widely used in the mining industry for breaking up rock masses [3, 4, 5, 6, 7], but their application extends across various other sectors, including dismantling metal structures, metal processing, welding, destroying military equipment, and constructing channels and dams. The scope of their use continues to expand [3, 5, 6, 8]. The selection of appropriate blasting methods and explosives types is critical for any blasting operation. Additionally, the blast design parameters play a significant role in determining its effectiveness.

According to Russian experience [6], when the thickness of concrete structures does not exceed 5 meters, the use of short hole charge (d<75 mm) is preferred, while for structures thicker than 5 meters, the borehole charge method (d>75 mm) is predomi-nantly used. In such cases, highly effective industrial explosives, such as Ammonite 6ZhV, Granulite, and Detonite, are utilized for their superior fragmentation capabilities. Cartridge-type Ammonite 6ZhV, in particular, has been the most widely used for demolishing concrete structures, with a powder factor of 0.45–0.55 kg/m³. The total quantity of explosives required can be determined based on the volume of the material to be blasted (V), using the following formula.

$$Q_{com} = V * q \quad (1)$$

The required number of holes can be determined using the formula:

$$N = \frac{Q}{P * l_{ch}} \quad (2)$$

P - amount of explosives per meter of hole (in kilograms)

l_{ch}- charge length (in meters)

l_{ch} - 0,52; l_h - hole depth (in meters)

When using 32 mm diameter cartridge-type Ammonite 6ZhV explosives, the spacing between boreholes and the spacing between rows can be determined as follows.

$$a = b = 0.6\sqrt{\frac{1}{q}} \quad (3)$$

The maximum permissible charge for blasting near industrial buildings and structures can be determined as follows.

$$Q = 0.3 * Rc^{1.5} \quad (4)$$

R_c - minimum distance from the explosive charge to the foundation of the building, measured in meters.

In the United States, dynamite and nitroglycerin-based explosives are commonly used for the demolition of buildings and structures [8, 10]. Depending on the specific conditions, the powder factor varies between 0.3 and 0.9 kg/m³.

While the blasting method allows for the demolition of buildings and structures in a very short time and at a relatively low cost, it is essential to ensure that the air shock waves, seismic vibrations, and fly rock or debris from the blast do not cause damage to neighboring buildings or pose risks to residents. Moreover, it is necessary to verify that the levels of gas and dust emissions, as well as noise (which should not exceed 80 dB), comply with the relevant standards during the blasting operation.

In open-pit mining conditions, research in this area has been conducted on a broader scale. According to the recommendations provided by the Russian "Soyuzvzryvprom Trust" [4], the safe distance from the surface affected by blasting can be determined using the following empirical formula.

$$r_{on} = 120\sqrt[3]{Q_{exp}} \quad \text{when} \quad (Q_{exp.} \geq 1000) \quad (5)$$

$$r_{on} = 35\sqrt[3]{Q_{exp}} \quad \text{when} \quad (Q_{exp.} \leq 1000) \quad (6)$$

$Q_{exp.}$ - equivalent amount of explosive charge, measured in kilograms

According to research conducted by the Institute of Physics of the Earth (now IPKON) under the Russian Academy of Sciences [4], the safe distance from buildings and structures to avoid the impact of seismic vibrations generated by a single detonation of a concentrated explosive charge can be determined using the following formula.

$$r_c = k_r * k_c * a * \sqrt[3]{Q} \quad (7)$$

r_c - distance from the blasting site to the protected building or structure, measured in meters.

k_r –coefficient that depends on the characteristics of the foundation soil of the building or structure.

k_c - coefficient that depends on the type of building or structure.

α is a coefficient that depends on the blasting conditions.

Q- is the amount of explosive charge, measured in kilograms.

Additionally, to determine the safe distance for protection from fly rock or debris during the detonation of a borehole charge, the following formula has been recommended.

$$r_h = 1000 * \eta_f * \sqrt{\frac{f}{1+\eta_{f.s}}} * (d/a) \quad (8)$$

η_f - coefficient of filling explosive charge in the blast hole.

$\eta_{f.s}$ - coefficient of filling stemming (inert material) in the blast hole.

f - rock strength factor.

d - blast hole diameter, measured in meters.

a - distance between boreholes, measured in meters.

According to research conducted by the Institute for Comprehensive Exploitation of Mineral Resources (IPKON) of the Russian Academy of Sciences and the Moscow State Mining University [11], the following relationship has been established to determine the maximum distance that blasted rock particles may be thrown.

$$r = 378 * (f * q)^{0.33} * d^{0.5} * (\Delta * l)^{0.17}, m \quad (9)$$

f - rock strength factor.

q - powder factor, measured in kg/m³.

d - explosive charge diameter, measured in meters.

Δ - charge density, measured in kg/m³.

l - explosive charge length, measured in meters.

Researchers at the Siberian Branch of the Russian Academy of Sciences, Institute of Mining, developed the following formula to calculate the amount of explosive charge needed to ensure vibration safety in the conditions of the Novo-Baykal's open-pit mine in the Urals [12].

$$g_{ad.} = \left(\frac{V_{ad.}}{773 * a * k_\beta}\right)^{1.68} * r^{exp.}, \text{ kg} \quad (10)$$

$V_{ad.}$ - permissible velocity of ground vibration for residential buildings:

$V_{ad.}$=5cm/s when the distance r≤200 m; $V_{ad.}$=3cm/s when the distance r ≥200 m

r –distance from the blast site to the nearest residential building, measured in meters.

a -coefficient related to the diameter of the blast hole.

k_β-coefficient depending on required level of reliability of the prediction calculations.

In 1975, Swedish researcher Lundborg developed an equation to determine the maximum throw range of rock particles based on explosive charge diameter. This equation relates the blast effects on rock displacement to the size of the explosive charge, providing an important tool for predicting debris throw distances in blasting operations.

$$d = 30 * d_e^{0.667}, m \quad (11)$$

d_e – is the explosive charge diameter, measured in millimeters.

In Norway, the NS8141: 2001 [13] standard is followed to protect buildings and structures from vibrations. The key indicator in this standard is the Peak Particle Velocity (PPV) of the

blast-induced vibrations. For fragile buildings located on loose soil, the maximum allowable PPV is 3 mm/s, whereas for reinforced concrete structures built on solid rock, it can reach up to 80 mm/s. Similarly, the United Kingdom adheres to BS7585 – 2, Germany follows DIN4150-3:2016, and in the United States, federal regulations by the Surface Mining Control and Reclamation Office take into account both vibration direction and frequency.

In Japan, high-rise buildings are often constructed with robust metal frameworks, making their demolition particularly challenging when necessary. To address this, some cases employ a method of sectional blasting using elongated charges [14].

In Russia [15] and other countries [13, 14], various protective structures such as shelters and barriers are widely used in confined spaces to mitigate or eliminate the effects of flying debris, air shock waves, and seismic vibrations from blasting. Additionally, methods such as creating sand or water covers, vacuum sealing, and covering the site with old tires are employed. Protective shelters and barriers are typically constructed from materials like wood logs, metal, and reinforced concrete. These structures are designed to be sturdy, affordable, lightweight, and portable. Metal shelters, in particular, have proven to withstand up to 100 blasts.

In confined spaces, it is recommended that blast holes diameters not exceed 100 mm. Based on these experiences, before performing demolition blasting of buildings and structures, a thorough inspection and assessment of the site must be conducted. A blasting plan and technical documentation should be prepared, and necessary precautions must be taken, including obtaining the appropriate permits, temporarily shutting off water, electricity, and heating systems, and ensuring safety measures are in place. All necessary preparations must be completed prior to the blast.

In the United States, blasting techniques are widely used to demolish large structures such as tall chimneys, towers, bridges, stackers, and multi-story buildings. According to information from Protec Documentation Services (www.science.howstuffworks /engineering/structural/building-implosion), a 10-story building in Newark, New Jersey, was demolished in three stages. Prior to the blast, a 3D computer model of the building was created and utilized for planning. Similarly, in 1990, the grain facility in Philadelphia was demolished by first blasting the central foundation columns to bring it down on its existing foundation. Based on the experience of Grant MacKay Company (www.grant-mackey.com), when demolishing buildings using explosives, dynamite charges are placed at key structural points that bear the building's load. The demolition process uses electronic detonators, wireless systems, and highly accurate timing devices. To prevent fly rock and minimize other negative effects, durable protective equipment—such as blast mats—are extensively used.

In the United Kingdom, when demolishing chemical plant structures, coal-fired power stations, and cooling towers (www.cross-safety.org), significant attention is given to structural analysis and safety measures. For safety purposes, it is recommended to select and use various protective barriers according to the specific conditions. These include mesh fences, geotextile nets, rubber barriers, covers, metal plates, and water covers, all of which are tailored to the demolition environment to minimize risks and ensure safety.

In China, due to the rapid development of urban areas, there is a shortage of land for new construction, which necessitates the demolition of old, unusable buildings to repurpose the land. To achieve this, blasting techniques are being widely used. According to common methodologies, used in China (www.hillpublisher.com/journals /engineeringadvances/, 2023, No. 3(1)), demolition methods involve careful planning and the use of explosives to efficiently demolish buildings while minimizing the impact on the surrounding area. In these cases:

Spacing between blast holes (charges) is determined by the following formula:

$$A = (1.5 - 1.8) * W \quad \textbf{(12)}$$

Distance between blast hole rows is given by:

$$B = (0.85 - 0.9) * A \quad (13)$$

Blast hole depth is calculated as:

$$L = (0.67 - 0.7) * H \quad (14)$$

The amount of explosive charge per blast hole is determined as:

$$q = K * V \quad (15)$$

Where:

W - minimal burden distance

H - thickness of the support columns.

K - powder factor (for reinforced concrete structures, $K = 0.7 - 0.9$ kg/m)

The maximum charge of the main explosive (Q_{max}) can be determined using the following equation:

$$V_v = K * \left(\frac{\sqrt[3]{Q_{max}}}{R}\right)^a \quad (16)$$

Where:

K –coefficient, ranging from 250 to 350

a - coefficient, ranging from 1.8 to 2.0.

V_v - vibration velocity, measured in, cm·s^{-1}

R- distance from the blast site, measured in meters.

Studies and monitoring vibrations during the demolition of 180-meter-high chimney in China (Xiawu Huang, Hiangi Xie, Jinshan Sun, and others) showed that blast-induced vibrations vary differently depending on damping coefficient of the buildings and structures.

Approximately 250 kg of explosives were used during the demolition of an 18-story, 60-meter-high building complex In Bonn, Germany in 2017, (www.inshorts.com/en/news). Similarly, in Frankfurt, to demolish the 116-meter-high, 50,000-ton AfE Tower, 1,500 boreholes were drilled, and about 1 ton of explosives were used. To prevent damage to surrounding buildings, protective barriers up to 6 meters high were erected, and 1,000-liter water tanks were placed around the site to suppress dust (www.dw.com /en/demolition experts).

Additionally, in 2022, in North Rhine-Westphalia, a 72-meter-high, 55-year-old bridge was demolished using 120 kg of explosives. New bridge constructed adjacent to old one sustained no damage during the demolition (www.createddigital.org.au).

In Romania, during the demolition of a 72-meter-high cooling tower at an oil refinery, 43 kg of dynamite, 500 meters of detonating cord, 45 electric detonators, and 25 non-electric connectors with a 25 ms delay were used (www.doi.org-/10.1051matecconf /202030500072).

Researchers from Jeonbuk National University and Korea Kako Co., including Hoon Park, Hyeong-Ki Park, Jin-Hee Ko, and Chul-Gi Suk, conducted studies on the demolition and crushing of large building foundations using blasting techniques. Based on their findings, they established correlations between several key parameters, such as the Peak Particle Velocity (PPV) of ground vibrations, the average fragmentation size (D_{av}), the specific explosive consumption (S_c), the volume of blasted concrete (V_c), the charge per borehole (W), and the coefficient K.

$$PPV = K * \left(\frac{D_{av}}{\sqrt{W}}\right) \quad (17)$$

$$PPV = K * \left(\frac{D_{av}}{\sqrt{S_c + V_c}} * V_c\right) \quad (18)$$

Researchers from Korea Kako Company, including Chul-Gi Suk, Woo-Jing Jung, and Hyoung-Ki Park, along with K. Katsuyama from Ehime University in Japan, studied methods for demolishing wall-slab buildings. They noted the importance of pre-weakening the building structure before demolition. In their experimental blasts, they used non-electric detonators from Hanwha Inc. and Megamite 22 gelatin dynamite explosives. When the wall thickness exceeded 300 mm, they employed Haikord Plus 100 explosives. To suppress the dust generated during the demolition, vinyl bags were placed on the 1st and 3rd floors, as well as on the roof, and a total of 80 tons of water was pumped into the bags, which proved effective (Science and Technology of Energetic Materials, Vol. 69, No. 2, Seoul, 2008).

Conclusion

1) Traditional mechanical methods for demolishing buildings and structures have been widely used across the world for centuries and continue to be prevalent. However, these methods are labor-intensive, costly, time-consuming, and generate significant noise and dust, leading to the development and adoption of alternative demolition methods. Among these, blasting techniques have gained prominence.
2) Blasting methods offer the advantage of demolishing buildings and structures in a very short time and at a relatively lower cost. However, the negative impacts of air shock waves, seismic vibrations, and flying debris from the blasts pose risks of damage to adjacent buildings and danger to residents.
3) Various countries have developed numerous calculation methodologies and tools to ensure the safe execution of demolition blasting projects. These methods are often tailored to specific conditions, relying primarily on empirical relationships derived from experimental results to calculate the parameters of blasting operations and ensure safety.

References

П.С.Миронов “Взрывы и сейсмобезопасность сооружений” Москва, Недра, 1973.

“Тэсэлгээний ажлын аюулгүй ажиллагааны нэгдсэн дүрэм” Улаанбаатар. 2019. ("Unified Regulations for Safe Blasting Operations," Ulaanbaatar, 2019.)

Г.И.Покровский “Взрыв” Москва, Недра, 1980.

Б.Н.Кутузов, В.Н. Мосинец, Л.В. Дубнов “Справочник взрывника” Москва , Недра, 1988.

Б.Н.Кутузов “Разрушение горных пород взрывом”.-Взрывные технологии в промышленности. Москва, Изд-во МГГУ, 1994.

Б.Н.Кутузов “Методы ведения взрывных работ”, Часть 1. Разрушение горных пород взрывом. Часть 2. Взрывные работы в горном деле и промышленности. Москва , Горная книга, 2018.

Б.Н.Кутузов, В.А.Белин “Проектирование и организация взрывных работ” Москва, Горная книга.

“Blaster’s Handbook “ International Society of Explosive Engineers, USA, 2014

K.J.Konya, E.J.Walter “ Rock Blasting and Overbreaking Control”, USA, 1991

“Building Implosion “Wikipedia, the free Encyclopedia, 2024.

Викторов С.Д (ИПКОН РАН), Кузнецов В.А (МГГУ) “К расчёту зон, опасных по разлету кусков взорванной породы” Сборник №92/49, Взрывное дело–Развитие теории разрушения горных пород взрывом, Москва, Межведомственная комиссия по взрывному делу, 1999.

Воробьева Л.С., Яковлев М.В., Мухаметшин А.М., Федоров В.А (ИГД УрО РАН) “Закономерности обеспечения сейсмической безопасности жилых зданий и сооружений от взрывных работ горных предприятий в условиях городской застройки” Сборник № 92/49, “Взрывное дело – Развитие теории разрушения горных пород взрывом” Москва , Межведомственная комиссия по взрывному делу, 1999.

K.M.Nore’n Cosgriff., N.Ramstad., A.Neby., C. Madshuss. “ Building damage due to vibration from rock blasting” Norwegian Geotechnical Institute and Public Roads Administration, Oslowww.elsevier.com.Science Direct, Soil Dynamics and Earthquake Engineering 138 (2020) 106331

ttps://www.jstage.jst.go.jp/article/jscej1984/1989/403/1989_403_173/_article/char/japan.

Н.Н.Мельников, К.Н.Трубецкой, К.Е.Виницкий, Р.Ю.Подерни, П.И.Томаков, С.Е.Чирков и другие. Справочник – Открытые горные работы. Москва, Горное бюро, 1994.

INSIGHT INTO IN-SITU MODIFICATION OF WHITE CARBON BLACK WITH SURFACTANT/SILANE COUPLING AGENT VIA SURFACE GRAFTING AND ITS PERFORMANCE

Shenxu Bao[1, 2, 3*], Bo Chen[1, 2, 3*], Shun Wang[2]

[1] Key Laboratory of Green Utilization of Critical Non-metallic Mineral Resources, Ministry of Education, Wuhan University of Technology, Wuhan 430070, CHINA
[2] School of Resources and Environmental Engineering, Wuhan University of Technology, Wuhan 430070, PR CHINA
[3] Hubei Key Laboratory of Mineral Resources Processing and Environment, Wuhan 430070, PR CHINA
*Corresponding Author: sxbao@whut.edu.cn; bochen2012@whut.edu.cn

Abstract

Hydrophobic and highly dispersed modified white carbon black (WCB) particles were prepared using surfactant sodium dodecyl sulfate (SDS) as a modifier and the vanadium-extraction residue (VER) as raw material. This study investigated the effects of modification temperature, pH value, aging time and dosage of modifier. In order to reflect the advantages of surfactant SDS modification, the silane coupling agent γ-methacryloxypropyl trimethoxysilane (KH570) is used to compare with it. The modified WCB prepared by in-situ grafting method with SDS and KH570 was compared. XRD and FTIR results indicate that the modified product has an amorphous structure and the modifier exists on the surface of WCB in the form of chemical grafting. The modified product is added as fillers to rubber and the mechanical properties of rubber show that the WCB modified by SDS has a lower modulus of elasticity, a higher maximum tensile stress and the strain at yield. The results of SEM images of rubber and particle size of modified WCB demonstrate that the fine-grained modified WCB particles are more likely to form a network structure with the rubber to enhance the mechanical properties of the rubber.

Keywords: White carbon black; Surface modification; Surfactant, Rubber; Vanadium-extraction residue; Silane coupling agent

ALTERNATIVE METHODS FOR RECOVERY OF VALUABLE METALS FROM WASTE PRINTED CIRCUIT BOARDS

Altansukh Batnasan[1]*, Kazutoshi Haga[2] and Atsushi Shibayama[2]

[1] Institute of Chemitsry and Chemical Technology, Mongolian Academy of Sciences, Ulaanbaatar, 13330, Mongolia.
[2] Graduate School of International Resource Sciences, Akita University, 1-1 Tegata-Gakuen machi, Akita, 010-8502, Japan,
*Corresponding author: altansukh.b2008@gmail.com

This study proposes an alternative approach for recycling waste printed circuit boards (WPCBs) to recover valuable metals. The proposed approach consists of five stages -1). incineration of WPCBs; 2) removal of impurity elements from WPCBs by oxidative high-pressure leaching; 3). precious metals dissolution from the residue of WPCBs with alternative leaching agents; 4). Recover precious metals from a pregnant leach solution by selective precipitation; 5) reuse the spent solution in the WPCBs recycling.

Results showed that under optimized conditions, over 97% of Au and less than 1% of Ag and Pd were dissolved with iodine-iodide and iodide solution from the solid residue of WPCBs obtained from a combined method of incineration at 800 °C and high-pressure oxidative

leaching with a diluted sulfuric acid at 120 °C. The leaching efficiency of main metal impurities (Cu, Ni, Co, and Zn) did not exceed 10%.

The precious metals and metal impurities as base metals in the pregnant leach solution were recovered distinctly by the precipitation method using aqueous solutions of L-AA and NaOH as precipitation agents.

About 99.8% Au was recovered from the pregnant solution by adding 0.1 M L-AA at pH 2, while the recovery of Ag and Pd was 81.'% and 72.8%, respectively. The minor amounts of precious and base metals that remained in the solution were recovered at pH 13 using 1 M NaOH solution.

The spent lixiviant from sequential processing was regenerated using hydrogen peroxide and hydrochloric acid. As a result, over 90% of gold was recovered from the WPCBs using the regenerated lixiviant solution.

Keywords: thiourea, iodine, iodide, waste printed circui boards, alternative method

CORRELATION BETWEEN ROCK FORMING MINERALOGICAL COMPOSITION AT DIFFERENT DEPTHS AND BOND WORK INDEX FOR THE ERDENETIIN OVOO CU-MO PORPHYRY DEPOSIT, MONGOLIA

Batmunkh Tumen-Ayush[1], Chinzorig Bavuu[2], Davaajargal Darambazar[3], Ganbileg Davaajav[3], Khaliun Amartuvshin[3], Narangerel Adiyasuren[3], Tsend-Ayush Tserendagva[1], Undrakhtamir Alexander[1], and Ganzorig Chimed[3]*

[1]Erdenet Mining Corporation SOE, Orkhon Province, Erdenet 61027, Mongolia
[2]Department of Mining Technology, School of Geology and Mining Engineering, Mongolian University of Science and Technology, Ulaanbaatar 14191, Mongolia
[3]Center for Nanoscience and Nanotechnology, Department of Chemical and Biochemical Engineering, School of Engineering and Technology, National University of Mongolia, Ulaanbaatar 14201, Mongolia
***Corresponding author: ch_ganzorig@num.edu.mn

The Erdenetiin Ovoo Copper-Molybdenum (Cu-Mo) porphyry deposit in Mongolia is the largest copper mine corporation in the nation. In this study, we investigate the grinding properties of biotite granodiorite (BGDP) and granodiorite (GDIR) rock alteration relative to variations in mine depth, with a specific focus on their correlation with mineral composition. The Bond Work Index (BWI) experimental tests are applied to the Cu-Mo porphyry ore from the Erdenet Mining Corporation in Mongolia. The samples used in this study were collected representing 10 composites of 5 different depth levels with an interval of ~90 m within the 1175-725 m sampling elevation. The chemical, surface analytical, and mineralogical characterizations of the two types of BGDP and GDIR ores are performed using Inductively Coupled Plasma (ICP), X-ray fluorescence (XRF), and X-ray diffractometer (XRD) methods. Results of the chemical analysis indicate that the Cu and Mo percentages of both BGDP and GDIR consistently decreased with depth profiling. The XRD data of mineral composition are used in setting up the prediction of the BWI estimation model. An equation-based approach to the BWI estimation model demonstrates a strong linear correlation (R^2 = 0.895) with the measured BWI from experimental tests, with the highest BWI measured at 19.06 kWh/t. Our experimental results indicate that strong correlations were identified between the major mineral phases and the BWI values through the integration of ore hardness and mineralogical data. The key findings of this study, including hardness values and their predictions relative to the mining operation levels, may have significant implications for the future design of milling circuits.

Keywords: Copper porphyry, bond work index, estimation model, biotite granodiorite, granodiorite, mineralogy

PREPARATION AND PERFORMANCE RESEARCH OF THERMAL INSULATION MATERIALS FROM IRON AND COPPER COMPOSITE TAILINGS

Li Ye[1]*, Zhang Zhanpeng[1], Zhou Feng[1], Zhang Hongquan[2], Wang Jianyu[1]

[1] School of Resources and Environmental Engineering, Wuhan University of Technology, Wuhan 430070, Hubei, CHINA
[2] School of Materials Science and Engineering, Wuhan University of Technology, Wuhan 430070, Hubei, CHINA
*Corresponding author: whly1218@126.com

Abstract

In order to enhance the total tailings blending in thermal insulation materials, in this study, Erdenet copper tailings were substituted for potassium feldspar, and Bayangol iron tailings and Erdenet copper tailings were utilized in the composite preparation of thermal insulation materials (foamed ceramics), and the optimal formulation was determined by comparing the physical properties of foamed ceramics prepared with different iron tailings/copper tailings ratios and firing regimes. The results showed that the optimum mass percentages of Bayangol iron tailings, Erdenet copper tailings, waste glass, sodium carbonate, and SiC were 40%, 30%, 25%, 5%, and 0.35%, respectively, and the apparent density of the thermal insulation materials prepared under the firing system with a firing temperature of 1070°C, a holding time of 25 min, and a temperature increase rate of 4°C/min at the end was as low as 0.645 g/cm^3, compressive strength of 10.48 MPa, apparent porosity, total porosity of 3.71%, 75.46%, respectively, the thermal conductivity of 0.125/W (m·K), the total tailings mixing up to 70%, the total solid waste utilization rate of up to 95%, to achieve the synergistic use of different tailings of high mixing. This study provides a method for the preparation of thermal insulation materials (foamed ceramics) from composite tailings, which advances the application of composite tailings in thermal insulation materials.

Keywords: Iron tailings, Copper tailings, Thermal insulation materials, Physical properties, GeoMine

Acknowledgements

This work was supported by the National Key Research and Development Plan of China(Grant No. 2022YFE0197200).

OPTIMIZATION AND CONTINUOUS IMPROVEMENT OF THE OYU TOLGOI CONCENTRATOR

G.Malkhuuz[1]*, A.Zarantonello[1], A.Supryadi[2], O.Jaldin[1], B.Erdenebaatar[1], M.-U.Ganbold[1]

[1] Oyu Tolgoi LLC. Monnis Tower, Chinggis Avenue 15 Sukhbaatar District—14240, Ulaanbaatar, MONGOLIA
[2] Rio Tinto Canada Management Inc. 400-1190 Av Des-Canadiens-De-Montreal, Montreal H3B 0E3, CANADA
*Corresponding author: ganbold.malkhuuz@riotinto.com

The Oyu Tolgoi (OT) copper operation in southern Mongolia has provided an excellent setting for incremental optimization and continuous improvement.

The concentrator was commissioned in 2013 and ramped up quickly to its daily nominal nameplate production within 6 months. It became evident that many factors would prevent this daily throughput from being sustained day in, and day out across a full production year. To address the shortfall, OT embarked on a program designed to target a 25% increase in copper

metal, through productivity enhancements to milling rates and operating time. The program focused on improving the fundamentals and establishing sustainable practices.

Throughput improvements involved a holistic mine-to-mill effort, including high-intensity blasting for finer ore fragmentation, primary crusher gap control, SAG discharge grate slot redesign, and screen media aperture optimization to balance (SABC circuit) loads. Other projects focused on increasing pebble crusher utilization through improved grinding media and upgrading magnets for tramp metal recovery. A series of wear-life improvement and defect elimination projects have lengthened component life and thus reduced unscheduled breakdowns. These advances have extended the planned shutdown intervals and have facilitated the alignment of major equipment to a common scheduled maintenance cycle, driven by SAG mill liner life.

A suite of Advanced Process Controls (APCs) was applied across each unit operation to optimize the respective circuit efficiency. An expert system then leverages these APCs to undertake the crucial role of linking all unit operations together and establishing “End to End” control of the “total system”. The ultimate objective is to increase feed passing through the total system, until a circuit constraint limit is reached, all whilst maintaining volumetric stability throughout the connected unit operations.

The sequential improvements swiftly exceeded the nominal plant capacity and have sustainably delivered throughputs of ~40 million tonnes per annum (Mt/a), for the past seven years representing a 43% increase in production over 2014.

This paper summarizes the optimization and continuous improvement journey undertaken at Oyu Tolgoi Concentrator to bring about its current state.

THE VALUE-ADDED UTILIZATION OF COPPER SMELTER AND REFINERY WASTES

Chinbat Enkhchimee

[1] Erdenet Institute of Technology, Mongolian University of Science and Technology, Erdenet, MONGOLIA
*Corresponding author: enkhchimee@erdenetis.edu.mn

Abstract

The efficient and sustainable utilization of waste generated from copper smelting and refinery operations has become a significant area of research and practical interest as the global demand for copper continues to rise, accompanied by a concomitant increase in the generation of various waste streams. Modern matte smelting processes produce three main products: copper matte (sulfides, metals), slag (oxides, gauges), and gas (volatilizable elements, dust). Copper slag is a byproduct of the smelting processing of metals from concentrates. The high concentration of flue gas is an important raw material to produce sulfuric acid and the element sulfur. Recognizing the potential to transform these waste streams into valuable resources, researchers and industry leaders have explored various innovative approaches to the value-added utilization of copper smelter and refinery wastes. Recently, relevant studies have indicated that the contact process, the smelter off-gas is used for the generating of sulfuric acid. Sulfuric acid is a significant chemical raw material for producing mineral fertilizer and leaching in hydrometallurgy. Besides, sulfur in the form of elemental sulfur plays an important position in the dye, rubber, paper, military, and others. Traditionally, elemental sulfur production technology is the direct reduction of SO_2 to sulfur, but it has many different reducing agents. This paper is associated with two significant objectives. The first of them is to illustrate a critical review of the utilization of copper slag. The second is to mention the reduction of SO_2 in the smelter off-gas generated from copper smelters.

Keywords: Copper slag, flotation, refined copper, smelting process

Introduction

The production of copper is an important industry that plays an imperative part in an advanced society, providing important materials for a wide range of applications, from electrical wiring and alloys to renewable vitality advances and electronic gadgets. All copper applications are derived from two main sources: recycled and mined copper (cons & SX-EW). According to the United States Geological Survey data, the total production of copper reached 22 million metric tons in 2023 (Scientific Investigations Report, 2023). Currently, copper concentrate is generated via beneficiation from copper sulfide ores by mineral processing, which includes ore dressing, classification, and flotation. The concentrate is the primary raw material used to produce metallic copper (copper matte) through pyrometallurgical processes. Modern matte smelting processes produce three main products: copper matte (sulfides, metals), copper slag (oxides, gauges), and off-gas (volatilizable elements, dust).

Copper slag consists of silica-based oxides, gauges depending on minerals in copper concentrate as well as metals such as copper (Cu), silver (Ag), zinc (Zn), nickel (Ni), lead (Pb), cadmium (Cd) and Iron (Fe) in oxide, sulfide, and metallic forms. The valuable parts in copper slag have long posed financial challenges, as they regularly contain determined concentrations of critical metals that are accumulated in dumps or stockpiles, representing a missed opportunity to recover these assets back into the products (Daehn et al., 2019), (Krishnan et al., 2021). Recognizing the potential to transform these waste streams into the production cycle, researchers and scientists have explored various innovative approaches to the value-added utilization of copper smelter and refinery wastes. Therefore, several research studies have investigated the potential of various recovery methods, including pyrometallurgical, hydrometallurgical, and biohydrometallurgical approaches, to extract metals from the copper smelter and refinery wastes (Krishnan et al., 2021), (Xolo et al., 2021).

As a typical nonferrous metallurgy, high concentrations of sulfur dioxide (SO_2) in off-gas are generated via processes such as smelting, converting, and fire-refining. The environmental aspect of sulfur dioxide emission is a serious concern, affecting to local ecosystem and public health (Tao et al., 2022). However, the high concentration of off-gas is an important raw material to produce sulfuric acid and the element sulfur. Recently, relevant studies (Streets & Waldhoff, 2000), (Bakker et al., 2003), (Zeng et al., 1999) have indicated that the contact process, the smelter off-gas with Ψ (SO_2) is higher than 3% is used for the generating of sulfuric acid. Sulfuric acid is a significant chemical raw material for producing mineral fertilizer and leaching in hydrometallurgy. In Mongolia, hydrometallurgy plants use sulfuric acid for HL-SX-EW technology. Besides, sulfur in the form of elemental sulfur plays an important position in the dye, rubber, paper, military, and other industries. Traditionally, elemental sulfur production technology is the direct reduction of SO_2 to sulfur, but it has many different reducing agents (Ge et al., 2018).

This paper is associated with two significant objectives. The first of them is to illustrate a critical review of the utilization of copper slag. The second is to mention the reduction of SO_2 in the smelter off-gas generated from copper smelters.

Utilization of copper slag

Copper slag, a by-product of copper smelting, has become a growing concern due to the significant quantities generated worldwide and the potential environmental risks associated with refinery waste. The International Copper Study Group (ICSG) estimated that the world's total refined copper production amounted to 21.49 million tonnes in 2022 (Scientific Investigations Report, 2023). Refined copper production has increased over the last decades when copper slag has exceeded 50 million tonnes (Wu et al., 2023). It is calculated that 2.2-3.0 tons of copper slag are produced and regularly dumped near the refinery. However, refinery solid wastes are accumulated in tailing locations by copper smelters due to the lack of effective utilization methods (Tian et al., 2023). The slag phase consists of silica-based oxides, gauges depending on minerals in copper concentrate as well as metals such as copper (Cu), silver (Ag), zinc (Zn), nickel (Ni), lead (Pb), cadmium (Cd) and Iron (Fe) in oxide, sulfide, and metallic forms. Their properties and chemical components are important aspects of

determining the number of valuable metals and what technique routes can be taken to use them. The different applications are made of various characteristics of copper slag. Many research papers discussed five applications last decades. There are limited studies on some applications. Table 1 presents applications of copper slag.

Table 1. The applications of copper slag

Application of copper slag	Description	References
Cement and concrete	The raw material for clinker contains CaO, SiO_2, Fe_2O, Al_2O_3, grain size 4mm Copper slag has a positive impact on the compressive strength of concrete	(2008) Zement-Taschenbuch. Verlag Bau+Technik GmbH (Shi et al., 2008)
Blasting abrasives	Granulated copper slag has a high hardness of 6-7 on the Mohs scale and an angular grain shape The particle density is 3.3-3.9kg/dm^3	(Murari et al., 2015) (Beck et al., 1975) (Xolo et al., 2021)
Construction of roads and pavements	A higher content of copper slag decreases the stability of the mixture but increases the interlocking effect Fayalite slag originating from copper-zinc production in Sweden used for road construction	(*Sustainable Construction Materials*, 2017) (Lidelöw et al., 2017)
Geotechnical applications	Copper slag decreases the permeability of soil. The particle size and shape can affect the parameters of compression.	(*Sustainable Construction Materials*, 2017) (Beck et al., 1975)
Other applications	Copper slag has low density and high hardness material for the ceramics industry Fe metal in slag can catalyst for the hydrogenation of CO to CH_4	(Sarfo et al., 2017) (Fuentes et al., 2020)

Utilization of smelter off-gas

As aspects of environmental and economic, gas must be treated with a high concentration of SO_2 in gas from copper smelters by transforming these waste streams into the production cycle. A high concentration of SO_2 (10-30vol%) in smelter off-gas is discharged when the smelting process of the sulfide ores in oxygen-enriched oxidation conditions, such as pyrite, chalcopyrite, and covellite ores (Tian et al., 2019). According to the traditional method, sulfuric acid manufacture has a few steps: cooling and cleaning gas, drying the gas with 93% H_2SO_4-7%H_2O sulfuric acid, catalytically oxidizing the gas's SO_2 to SO_3, absorbing this SO_3 into 98% H_2SO_4-2%H_2O sulfuric acid (Schlesinger et al., 2022). Modern smelting processes collect most of their SO_2 at sufficient strength for economic other SO_2-capture products such as liquid SO_2, gypsum, and elemental sulfur.

Conclusion

Copper slag treatment and utilization is still one of the most discussed topics in the field of copper smelting and refinery. The copper smelting process was mentioned as a resource of the most hazardous environment and life health. However, products of pyrometallurgical processes will contribute significantly to the possibilities for more manufacturing, chemical industries, and construction. After the copper smelter is established, value-added products and their utilization will expand the economy and industrialization in Mongolia.

References

Beck, M. L., Freihaut, B., Henry, R., Pierce, S., & Bayer, W. L. (1975). A serum haemagglutinating property dependent upon polycarboxyl groups. British Journal of Haematology, 29(1), 149–156. https://doi.org/10.1111/j.1365-2141.1975.tb01808.x

Fuentes, I., Ulloa, C., Jiménez, R., & García, X. (2020). The reduction of Fe-bearing copper slag for its use as a catalyst in carbon oxide hydrogenation to methane. A contribution to sustainable catalysis. Journal of Hazardous Materials, 387, 121693. https://doi.org/10.1016/j.jhazmat.2019.121693

Lidelöw, S., Mácsik, J., Carabante, I., & Kumpiene, J. (2017). Leaching behaviour of copper slag, construction and demolition waste and crushed rock used in a full-scale road construction. Journal of Environmental Management, 204, 695–703. https://doi.org/10.1016/j.jenvman.2017.09.032

Murari, K., Siddique, R., & Jain, K. K. (2015). Use of waste copper slag, a sustainable material. Journal of Material Cycles and Waste Management, 17(1), 13–26. https://doi.org/10.1007/s10163-014-0254-x

Sarfo, P., Das, A., Wyss, G., & Young, C. (2017). Recovery of metal values from copper slag and reuse of residual secondary slag. Waste Management, 70, 272–281. https://doi.org/10.1016/j.wasman.2017.09.024

Schlesinger, M. E., Sole, K. C., Davenport, W. G., & Flores, G. R. F. A. (2022). Extractive metallurgy of copper (Sixth edition). Elsevier.

Scientific Investigations Report (Scientific Investigations Report). (2023). [Scientific Investigations Report].

Shi, C., Meyer, C., & Behnood, A. (2008). Utilization of copper slag in cement and concrete. Resources, Conservation and Recycling, 52(10), 1115–1120. https://doi.org/10.1016/j.resconrec.2008.06.008

Sustainable construction materials: Copper slag. (2017). Woodhead publishing.

Tian, H., Liu, J., Sun, J., Zhang, Y., & Li, T. (2023). Cross-media migration behavior of antibiotic resistance genes (ARGs) from municipal wastewater treatment systems (MWTSs): Fugitive characteristics, sharing mechanisms, and aerosolization behavior. Science of The Total Environment, 893, 164710. https://doi.org/10.1016/j.scitotenv.2023.164710

Wu, L., Li, H., Liu, K., Mei, H., Xia, Y., & Dong, Y. (2023). An efficient approach to utilize copper smelting slag: Separating nonferrous metals and reducing iron oxide at high temperature. Waste Management, 172, 182–191. https://doi.org/10.1016/j.wasman.2023.10.017

Xolo, L., Moleko-Boyce, P., Makelane, H., Faleni, N., & Tshentu, Z. R. (2021). Status of Recovery of Strategic Metals from Spent Secondary Products. Minerals, 11(7), 673. https://doi.org/10.3390/min11070673

CONCEPT OF ECONOMIC POLICY OF A MINING COMPANY IN MODERN CONDITIONS

Dambaeva Irina

[1] Faculty of Economics, Buryat State Agricultural Academy named after V.R. Filippova, Ulan-Ude 670013, RUSSIA

*Corresponding author: www.dig92@mail.ru

Abstract

"The semantic content of the concept category is initially, by origin, associated with planned public administration, ensuring the functioning of the state and society as a whole. The concept covers almost all management functions, areas of activity and areas of development of a mining company.

Initially formed at the level of state power, the policy has expanded its application to public organizations and business entities."

"The economic policy of an enterprise is a system of basic provisions (elements) determined by the interests of certain categories of individuals or their groups and determining the characteristics of the activity and behavior of an entrepreneurial structure; influencing the composition and characteristics of elements of the internal environment of an entrepreneurial structure and its interaction with economic agents of the internal and external environment."

Shapiro D.V. believes that "economic policy is a set of measures or measures taken by a firm to solve its problems.

Keywords: economic policy, mining company, liquidation fund

An important result of the formation of economic policy is a set of documents, instructions, etc., formalizing rules, techniques, management technologies, etc. the components of economic policy.

There are polar opinions about the company's strategy and policy. So I.A. Blank believes that policy is being formed to implement the strategy, and I.N. Gerchikov determines that policy development affects the formation of the company's goals and strategy.

Thus, economic policy is determined and determined by the goals and objectives developed in the company's development strategy. The goal may be competitiveness, profit based on cost reduction and ensuring the required level of quality, etc.

Stroiteleva I.V. suggests taking into account the economic and non–economic interests of the internal stakeholders of the enterprise and believes that "the economic policy of the enterprise is a system of basic provisions (elements) determined by the interests of certain categories of individuals or their groups

By the nature of intra-company management and relations with external stakeholders, politics can be aggressive, conservative, moderate, and compromise.

The author believes that economic policy determines the conditions of activity (goals, objectives, priorities, principles, mechanisms and tools) in the field of economic responsibility, economic relations and economic development in the internal and external environment of the corporation

Let's consider the main provisions of the economic policy of a mining company using the example of Ozerny GO Ka.

"The strategic priorities of the company are:

Maximizing the resource potential of the asset portfolio through integrated field development and the use of modern technologies

Ensuring sustainable results and creating value for all stakeholders.

The company is focused on achieving operational and financial targets, but also pays special attention to non-financial indicators and the quality of corporate governance.

INNOVATION CHALLENGES IN THE MONGOLIAN MINING INDUSTRY

Oktyaber Buriglaa[1], Tsolmongerel Enkhtuya[2*],Erdenebulgan Tsogtsaikhan[3*]

[1] Erdenet Institute of Technology, Turyakov St., Bayan-Undur Soum, Orkhon province, MONGOLIA

[2] Erdenet Institute of Technology, Turyakov St., Bayan-Undur Soum, Orkhon province, MONGOLIA

*Corresponding authors: tsolmongerel@erdenetmc.mn, erdenebulgan.ts@erdenetmc.mn

Nowadays the global mining industry faces various challenges, such as improving safety standards, addressing environmental concerns, implementing sustainable practices, adopting advanced technologies, optimizing resource extraction processes, remaining competitive, and most of all it is crucial to be responsive to changing market dynamics and societal expectations. By embracing innovations in new technologies and practices, mining companies attempt to overcome difficulties like upgrading outdated equipment and technologies at reasonable cost, mining companies can drive growth, improve operational efficiency, and contribute to a more sustainable future for the industry.

The Mongolian mining industry has been experiencing significant growth and has faced several innovation challenges within the last decade. Most challenging areas of innovation in the Mongolian mining industry are technological advancements, sustainable performance, safety improvements, resource exploration, human resource knowledge, community engagement, regulatory framework. As the industry becomes more knowledge-driven, there is a need for a highly skilled workforce capable of performing complex tasks through automated systems. By leveraging these innovative trends, companies can expect to achieve greater efficiency, safety, and sustainability in their operations. In this article, we will compare the innovation experience of Mongolian and international mining companies.

WATER GOVERNANCE IN THE CONTEXT OF MINING

Bolormaa Purevjav[1*], Bern Klein[2] Julian Dierkes[3], André Xavier[4]

[1] Industrial Engineering, GMIT, Mongolia, Nalaikh, Ulaanbaatar School N.B.K Institute of Mining Engineering, University of British Columbia 2329 West Mall, Vancouver, V6T 1Z4, BC, CANADA
[2] Bern Klein, Professor,
[3] Julian Dierkes, Associate Professor,
[4] André Xavier, Honorary Professor
*Corresponding author: bolormaa.p@gmit.edu.mn

Water governance is a critical global concern exacerbated by climate change and rapid industrial development. Effective water governance in mining regions is critical due to the intricate dynamics among water use, environmental sustainability, and socio-economic impacts. This abstract explores current practices and challenges in water governance specific to mining operations, emphasizing regulatory frameworks, and stakeholder engagement.

Governments play a pivotal role in allocating water rights and defining discharge limits tailored to mining activities, underlining the need for robust regulatory frameworks. Equally essential is community engagement, which ensures sustainable development and equitable resource management. In the mining context, inclusive decision-making processes that integrate local communities are vital for fostering trust, enhancing transparency, and securing the social license to operate.

This abstract focuses on the significance of aligning mining practices with effective water governance principles, highlighting the critical role of community involvement in achieving environmental stewardship and socio-economic sustainability. It examines current water use practices in Mongolian mining regions such as Gobi Desert and Forest Steppe and proposes potential solutions to enhance water governance. By addressing these issues, stakeholders can mitigate environmental impacts and promote sustainable development in mining areas.

Keywords: Water governance, mining, sustainable water management, community engagement

APPLICATION OF ROLLING ROCK-CUTTING ELEMENTS IN PDC DRILL BITS

Khomenko V.L[1], Pashchenko O.A[2], Ratov B.T[3], Nurshakhanova L.K[4], Kenzhegaliyeva Zh.M[5]

The drilling of oil and gas wells is a critical operation in the energy industry, necessitating the use of advanced technologies to enhance efficiency, reduce costs, and improve safety. Among the various tools employed in this process, polycrystalline diamond compact (PDC) bits have emerged as a pivotal innovation. PDC bits, known for their exceptional hardness and wear resistance, offer significant advantages over traditional roller cone bits and other conventional drilling technologies. Their relevance in contemporary drilling operations can be attributed to several key factors.

The economic and operational efficiency provided by PDC bits is unparalleled. Their superior cutting action and durability lead to faster penetration rates and longer bit life, which in turn reduces the frequency of bit replacements and the associated non-productive time (NPT). This is particularly crucial in deep and ultra-deep drilling scenarios where rig time is exceedingly expensive.

The unique design of PDC bits enables them to maintain consistent performance in a wide range of geological formations, from soft to hard rock. The ability to drill through various lithologies without the need for frequent bit changes translates to smoother and more continuous drilling operations. This adaptability is essential in complex drilling environments, such as those encountered in shale formations and other unconventional reservoirs.

Additionally, advancements in PDC bit technology, including the development of innovative cutter geometries and enhanced materials, have further solidified their position in the drilling industry.

The environmental impact of drilling operations is another aspect where PDC bits offer significant benefits. Their efficiency in cutting through rock reduces the overall energy consumption of the drilling process, thereby lowering the carbon footprint. Moreover, the extended life of PDC bits means fewer bits are discarded, contributing to reduced waste.

PDC bits, despite their many advantages, have several disadvantages that can impact drilling operations. One of the primary issues is their susceptibility to abnormal wear. This wear can occur due to several factors, including thermal degradation, where high temperatures encountered during deep drilling can damage the diamond structure, leading to reduced efficiency. Impact damage is another concern, as PDC bits can suffer from fractures when they encounter hard or abrasive formations like chert or pyrite. These micro-fractures cause rapid and uneven wear, compromising the bit's performance. Additionally, poor hydraulic design can exacerbate wear by failing to provide adequate cooling and cuttings removal, resulting in localized heating and increased friction. Improper bit selection, where a bit is used in a formation it is not suited for, can also lead to accelerated wear.

The consequences of abnormal wear are significant, leading to increased non-productive time (NPT) as bits need to be replaced more frequently, disrupting the drilling schedule and escalating costs. The frequent need for replacements and the associated downtime increase overall operational expenses. Reduced penetration rates are another result, as worn bits lose their cutting efficiency, slowing down the drilling process and extending project timelines. The variability in drilling performance due to abnormal wear complicates operations and can lead to inconsistent results, affecting wellbore quality and increasing the risk of deviations. Safety risks also arise from abnormal wear, as sudden bit failures can lead to stuck pipe situations or other downhole complications, jeopardizing both personnel and equipment.

Beyond abnormal wear, other disadvantages of PDC bits include their high initial cost compared to traditional roller cone bits. This higher cost can be a barrier, particularly for smaller operators with limited budgets. PDC bits also have formation limitations; while they are versatile, they can be less effective in very hard or abrasive formations, leading to rapid wear and reduced lifespan. Lastly, PDC bits are less repairable than roller cone bits. When damaged, PDC cutters often necessitate complete bit replacement rather than repair, further adding to operational costs and waste. Despite these disadvantages, ongoing research and technological advancements aim to mitigate these issues and maximize the benefits of PDC bits in drilling operations.

An innovative and radical solution to most of these problems is the use of rock-cutting elements rolling around their axis. PDC drill bits with rolling rock-cutting elements are particularly useful in abrasive environments that tend to cause and accelerate wear on PDC cutters. The benefits of these bits include extended durability, increased run footage, and higher average rates of penetration (ROP). Additionally, they improve thermal dissipation, which helps extend the life of the cutters. These bits have features such as cutters that revolve 360 degrees, ensuring they stay sharper for longer periods. The number and placement of cutters can be customized to maximize durability in areas of the bit that experience high wear. Furthermore, these cutters can be integrated into any PDC bit cutting structure without needing to change the cutter size.

The purpose of the work, the results of which are reflected in this article, was to analyze the most modern designs of PDC bits with polycrystalline diamond cutters. For this, literary and patent sources on this topic, prospectuses of leading manufacturers of drill bits were analyzed. It is shown that the modern development of ONYX 360 and Enduro 360 cutters by Smith Bits confirmed the prospects and efficiency of the earlier development of specialists from Dnipro University of Technology and the V. N. Bakul Institute for Superhard Materials of National Academy of Sciences of Ukraine.

In this work, modern designs of PDC bits with rolling rock-cutting elements were analyzed. It is shown that the modern development of the Smith Bits company, ONYX 360 and Enduro 360 cutters, confirmed the promise and performance of the earlier development of specialists

from the Dnipro University of Technology and the Bakul Institute of Superhard Materials of the National Academy of Sciences of Ukraine.

It has been established that the main factor in eliminating the abnormality of such bits is the uniform distribution of operating conditions of various cutters.

ENHANCING POWER GRID RELIABILITY FOR MINING INDUSTRY

Ariunbolor Purvee*, Erdenetsetseg Saijaa, Binderiya Taivan

School of Geology and Mining Engineering, Mongolian University of Science and Technology, Ulaanbaatar 14191, MONGOLIA
*Corresponding author: ariunbolorp@must.edu.mn

Abstract

This paper investigates the reliability of the power grid system in a strip coal mine, which combines overhead transmission lines and flexible cables. The study analyses the causes of failures within the power grid, focusing on data collected from 2020 to 2022. The primary causes of system failures were identified as issues in transmission lines and flexible cables, accounting for 74.9% of the total 824 recorded failures. The reliability of different subsystems, including substations, transmission lines, distribution boxes, and flexible cables, was evaluated using key metrics such as Mean Time to Failure (MTTF), Mean Time to Repair (MTTR), and Mean Time Between Failures (MTBF). The analysis revealed that the reliability of the system decreases over time, particularly during winter months.

Additionally, the study conducted a techno-economic evaluation to estimate the financial impact of power interruptions, revealing significant losses in coal production and revenue. The findings of this paper highlight the reliability statistics regarding power grid failures, including the calculations of mean time to failure (MTTF), mean time to repair (MTTR), expected failure rate (λ), expected repair rate (μ), mean time between failures (MTBF), cycle time (T), cycle frequency (f), unavailability (U), and availability (A). The paper concludes that the current reliability of the power supply in the Baganuur strip coal mine is insufficient, leading to substantial economic losses due to frequent power interruptions.

Keywords: coal strip mine, power overhead transmission lines, substations, coal strip mine, industrial power supply systems.

Introduction

Baganuur strip coal mine has been in operation for 38 years since its establishment in 1978, supplying coal to thermal power plants within the Central Power SystemThe coal extracted from this mine is primarily consumed by power plants in Ulaanbaatar. Currently, the Baganuur coal mine produces around 4 million tons per year.

The annual production capacity is 4.0 million tons. Depending on domestic consumers' coal needs, 3.6 to 3.8 million tons of coal are mined, along with the removal of 16 to 18 million cubic meters of overburden. Mining is conducted using a combined system that operates both with and without transportation. The mine supplies 60% of Mongolia's coal needs and more than 70% of the central region's coal requirements. Coal sized 0-200 mm is delivered to consumers via railway.

The objective of this study is to assess the dependability of power grid systems in coal mining operations.

Introduction to power grid systems and causes of failure

A. Power grid system of the strip coal

The power grid system of the strip coal mine is a hybrid setup utilizing both overhead transmission lines and power flexible cables. The power grid system is illustrated in Figure 1.

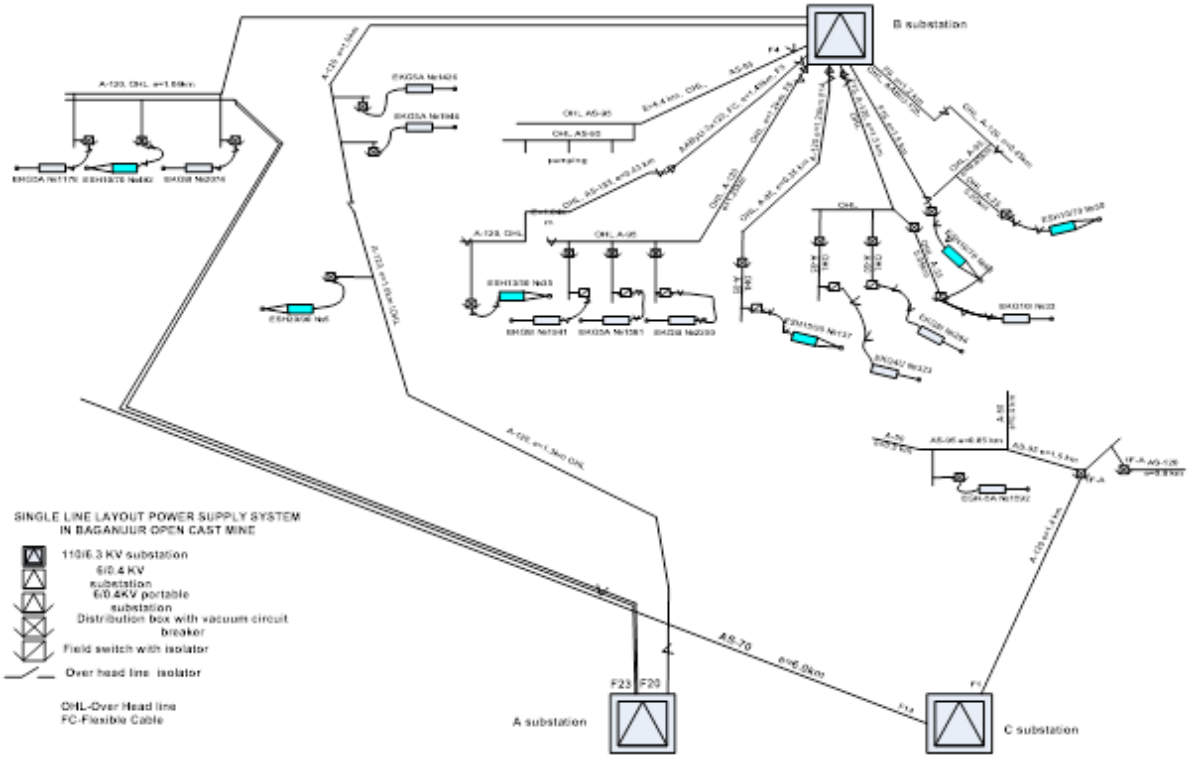

Figure 1. Layout of power grid system

The primary substation "S" is connected to the regional central power station, receiving a supply of 110kV on its primary side. From substation "S," a 6kV power line distributes electricity throughout the mine. In addition to substation "S_B," the mine includes two more distribution substations, denoted as "S_A" and "S_C."

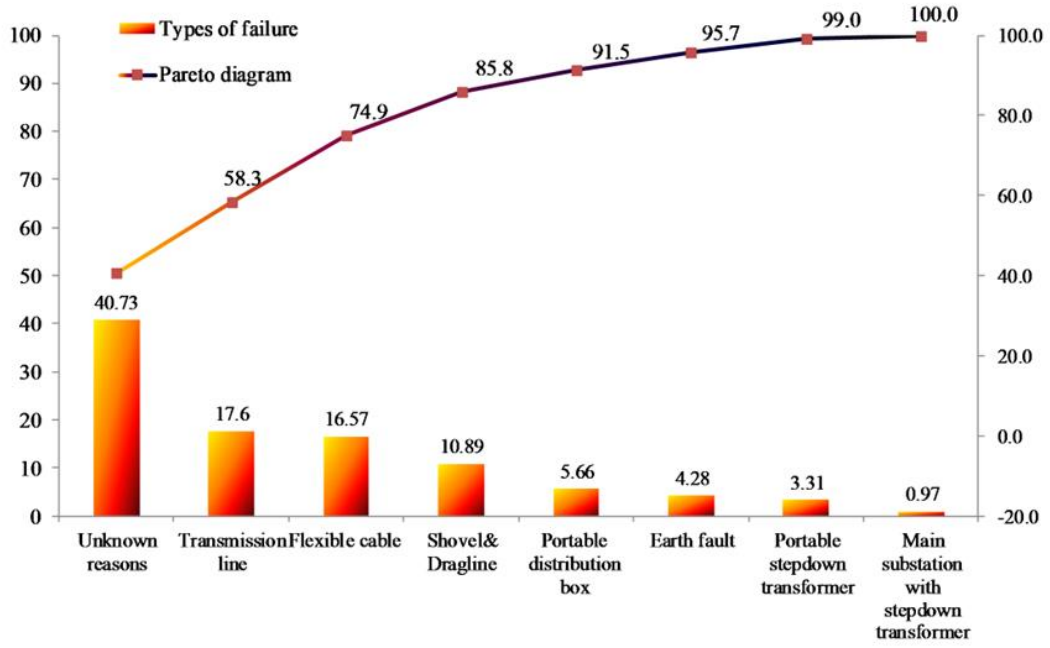

Figure 2. Causes of failures by Pareto diagram

B. Failure of power grid system

The analysis of power grid system failures at the strip coal mine, depicted in Figure 2, was conducted between 2020 and 2022. Data was gathered from handwritten breakdown logbooks of substations "SA," "SB," and "SC." The power supply system for each excavator was segmented into five subsystems: substation, transmission line, distribution box, flexible cable,

and machine (as illustrated in Figure 1). Alongside failures within these subsystems, several electrical faults were linked to unknown causes within each power supply system. Earth faults within the system were classified separately. Throughout the investigation period, a total of 983 failures were documented

Many failures in transmission lines and flexible cables are attributed to unknown causes, accounting for 74.9% of total failures. The highest number of failures typically occurs during winter, with the lowest number in the summer. Failures of unknown causes make up 40.73% of all failures.

Reliability analysis of power grid system

A. Unavailability of Different Subsystems

For each subsystem, the uptime (t_{ui}) and downtime (t_{di}) were observed, as shown in Figure 3. Mean Time to Failure (MTTF) is the ratio of Total Repair Time (uptime) to the number of failures (downtime).

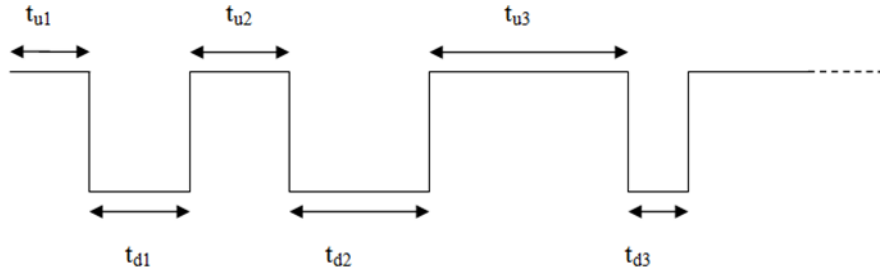

Figure 3. Uptime and downtime of subsystem

Mean Time to Repair (MTTR) is the average time required to fix a power grid system. The repair rate (μ) is the inverse of MTTR. For example, if the MTTR is 10 hours, the repair rate is 0.1 repairs per hour. The repair rate is calculated as follows:

$$Repair\ Rate(\mu) = \frac{1}{MTTR} = \frac{1}{10} hours \quad 0.1\ repairs\ per\ hour$$

Mean Time Between Failures (MTBF) is the sum of Mean Time to Failure (MTTF) and Mean Time to Repair (MTTR), including diagnosis and testing time, as shown in Figure 4.

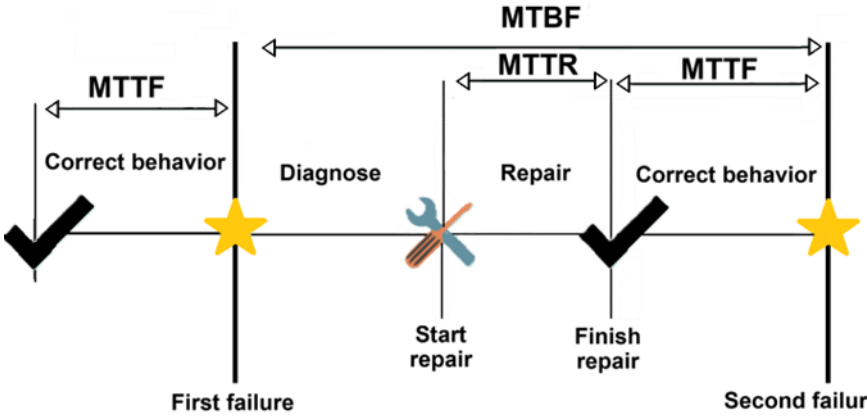

Figure 4. Mean time between failures (MTBF) [12]

Meantime To Repair (MTTR) is the amount of time needed to repair and restore functionality after a failure occurs. On the other hand, Mean Time Between Failures (MTBF) measures the reliability of a system by calculating the time between failures during operation. By analysing both MTTR and MTBF, valuable insights can be gained regarding system performance, maintenance efficiency, and overall reliability.

Unavailability (U) is the proportion of time that a system is not operational or unable to perform its required functions. It can be expressed mathematically as:

$$U = \frac{Downtime}{Total\ Time}$$

Unavailability accounts for all types of downtime, including maintenance, repairs, and unforeseen failures.

Availability is the proportion of time that a system is operational and able to perform its intended function. It is often calculated as:

$$A = \frac{Uptime}{Total\ Time} = 1 - U$$

Availability can also be expressed in terms of Mean Time Between Failures (MTBF) and Mean Time to Repair (MTTR):

$$A = \frac{MTBF}{MTBF + MTTR}$$

While unavailability measures the time a system is down, availability measures the time it is operational, and both are crucial for understanding system reliability as shown in Table 1.

Table 1. Unavailability of different subsystem

Names	Abb	Types of failures							
		F201	F202	F203	F204	F205	F206	F207	F208
No of failures		13	15.25	4.8	10.35	4.25	7.1	29.556	3.8333
Total repair hrs		15.933	34.106	7.675	13.558	5.5625	5.0625	43.669	7.5444
MTTR	r	1.2256	2.1433	1.599	1.31	1.1843	3.0763	1.4775	1.9681
Repair rate	m	0.8159	0.4666	0.6254	0.7634	0.8444	0.3251	0.6768	0.5081
MTTF	m (hrs)	1346.5	1146.6	3648.4	1691.4	4121	2466.1	591.3	4568.5
failure rate	l	0.0007	0.0009	0.0002	0.0006	0.0002	0.0004	0.0017	0.0002
MTBF	T	1347.7	1148.8	4221.6	1692.8	4122.2	2469.2	592.78	4570.4
Cycle frequency	f	0.0007	0.0009	0.0002	0.0006	0.0002	0.0004	0.0017	0.0002
Unavailability	U (FOR)	0.0009	0.0019	0.0004	0.0008	0.0003	0.0012	0.0025	0.0004
Availability	A	0.9991	0.9981	0.9996	0.9992	0.9997	0.9988	0.9975	0.9996

Here: F201 – substation; F202 – power transmission line; F203 – portable distribution box; F204 – power flexible cable; F205 – electrical components in a dragline; F206 – electrical components in a shovel; F207 – unknown reason; F208 – earth fault; Abb – Abbreviations and symbols; MTTF- mean time to failure; MTTR- mean time to repair; λ- expected failure rate; μ- expected repair rate; MTBF- mean time between failures; f-cycle frequency; U-unavailability; A- availability.

B. Reliability Analysis of Subsystem

Figure 5 depicts a standard power supply system for excavators. In Model A, power is supplied to the power shovels and excavators from either SA & F20 or SB & F3. In Model B, the power shovels and excavators are only connected to SB & F8. Similar configurations were used for each power shovel and dragline in the strip mine, utilizing parallel and series power lines to calculate the system's reliability.

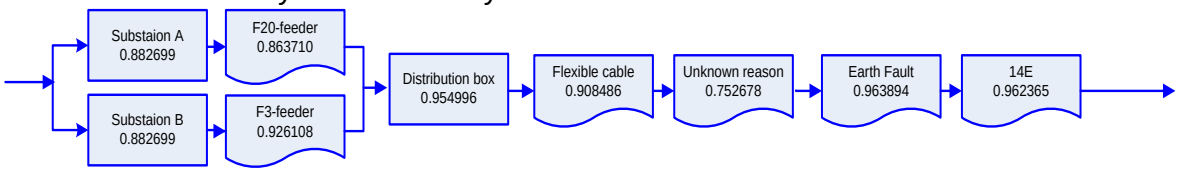

a. Model A

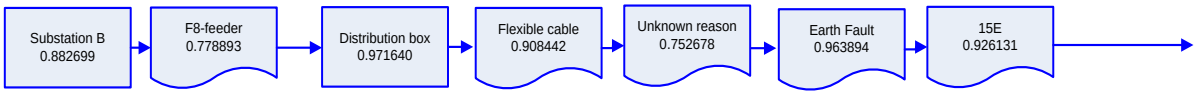

b. Model B

Figure 5. Power grid systems for the power shovel and excavators

In conducting the reliability analysis, we focused on failure time for the power grid series system and switching time for the power grid parallel system. We calculated the reliability of the power grid for each individual shovel and dragline over 7-day, 30-day, and 90-day periods. The reliability results for each shovel and dragline can be found in Figure 6.

a)

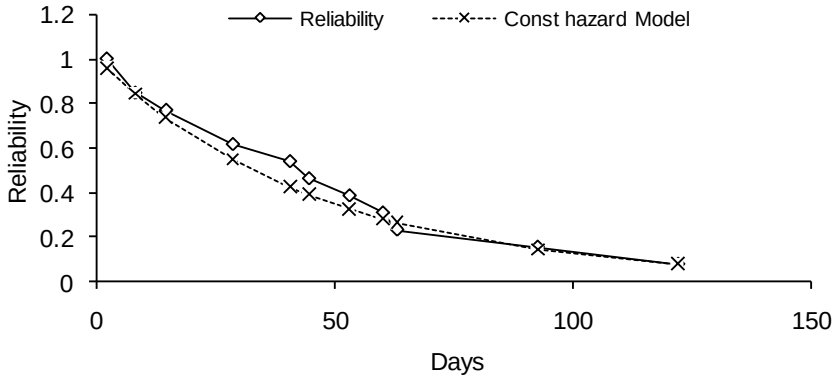

b)

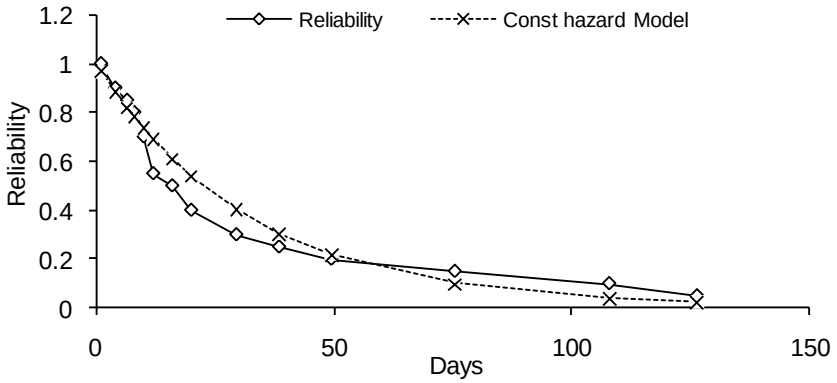

c)

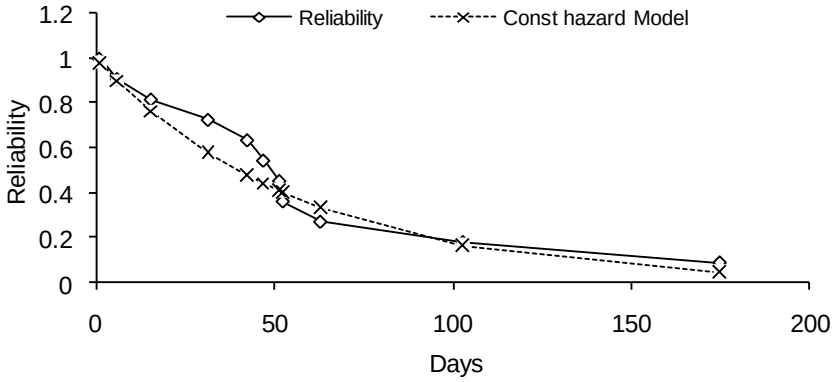

Figure 6. Reliabilities of failure of power shovels and excavators such as a) EKG-8I, b) ESH-15/90, c) EKG-5A

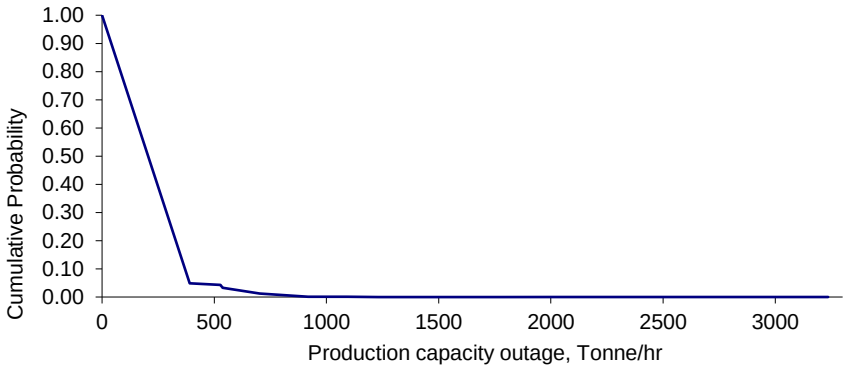

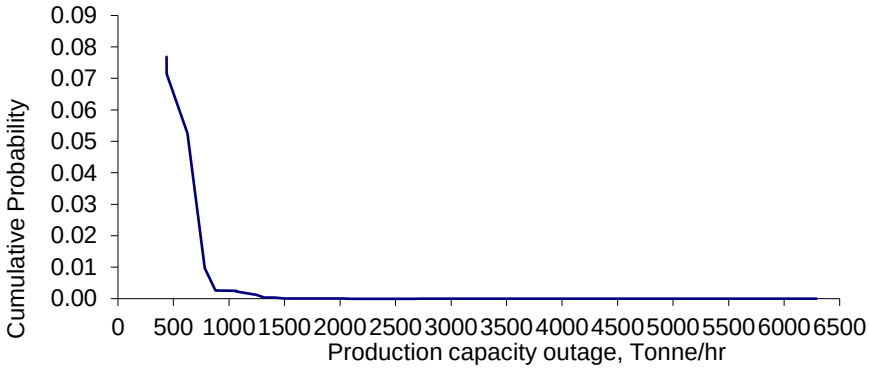

Figure 8. Cumulative probability with total mine capacity of 6290 Tonne/hr

Based on the results, it is evident that reliability is decreasing over time.

C. Outage of Probability

The cumulative probability with a total mine capacity of 3,235.09 tons per hour and 6,290 tons per hour, considering power failures, is shown in Figures 7 and 8, respectively.

Conclusions

The findings of this investigation underscore the crucial significance of equipment design in ensuring the reliability of a power supply system. Components such as junction boxes, cable separation boxes, and similar units are pivotal in this regard.

It is evident that a significant number of failures occur subsequent to the failure of the earth-fault protection system. This indicates that the issues primarily stem from the inadequate reliability of equipment such as cable lines, distribution boxes, junction boxes, switching points, and portable switching points.

The absence of information on indeterminate failures presents a notable challenge for data analysis in the power supply system of a strip coal mine. This highlights the need for further research and development in this area to enhance the overall reliability and efficiency of the system.

References

U. -O. Damba, O. Zagdaa, E. Adyasuren, A. Purvee and G. Banerjee, "Analysis of power supply system in Mongolia," 2012 7th International Forum on Strategic Technology (IFOST), Tomsk, Russia, 2012, pp. 1-4, doi: 10.1109/IFOST.2012.6357691.

Bekeron, P. G. (1975). Methods of the data analysis of statistical information for reliability of the mining power supply system. I.M.M, Russia.

Billinton, R., & Allan, R. N. (1996). Reliability evaluation of power systems (2nd ed.). Plenum Press.

Trutt, F. C., Rivell, R. A., & King, R. L. (1979). Balanced fault analyses of coal mine electrical power supply systems. Mining Industry Technical Conference, 1st Conference Record, Pittsburgh, PA, June 7-8. IEEE, New York, NY, 42-56.

Acker, F. E., & Henderson, S. T. (1980). Modeling harmonic generation on a coal-mine power-distribution system. Conference Record of the IAS Annual Meeting, 15th, Cincinnati, Ohio, September 28-October 3. IEEE, Piscataway, NJ, 114-121.

Walker, A. J. (1982). Engineering reliability into AFCs. Mining Technology, 64(736), 88-91.

Lambert, G. F. P. (1981). Mining electrical distribution systems: Observations on some pertinent present-day problems. Mining Technology, 63(734), 467-475.

Hassan, M. M. (1980). Evaluations of alternate network layouts for mine electrical distribution systems. In E. K. Stanek (Ed.), Proceedings of the WVU Conference on Coal Mine Electrotechnology, 5th, Morgantown, WV, USA, July 30-August 1. West Virginia University, Morgantown, USA, 3.1-3.17.

Nilsson, D., & Reddy, N. P. (1983). Energy consumption in open pit mining. World Mining, 36(7), 36-39.

Understanding failure metrics. (n.d.). Toucan Toco. https://www.toucantoco.com/en/blog/understanding-failure-metrics.

RESEARCH ON DETERMINING THE SPEED OF HAUL TRUCKS DEPENDING ON MINING TECHNICAL FACTORS

Orkhontuul Borya[1]*, Byambadagva Bayaraa[2], Purevtogtokh Baldan[1]

[1] School of Geology and Mining Engineering, Mongolian University of Science and Technology, Ulaanbaatar 14191, MONGOLIA
[2] Ministry of Industry and Mineral Resources, Ulaanbaatar, MONGOLIA
*Corresponding author: orkhontuulbo@gmail.com

One of the main ways to improve the efficiency of mining auto transport is to establish and maintain an optimal operating mode that is suitable for certain mining technical factors. One of the main factors that determine the basic productivity and safety of the operating mode is the speed of movement. Having accurately determined the truck speed, it will be possible to accurately plan, organize and manage the operation of mining auto transport.

There are several ways to determine the speed of a haul truck where the analytical method is usually used to determine the speed under safe operating conditions at curved section and high grade section. The graph-analytical method determines the truck speed on each section of the road according to the graphs of dynamic factors, speed and load of the haul truck.

Analytical and graph-analytical methods for determining the truck speeds are calculated with an error of 10-15% which does not meet modern requirements. Mining trucks operate in stable and variable motion modes with different characteristics during one cycle where the speed in these multiple motion modes cannot be determined by simple analytical methods. But it is worth noting that in big data processing , it is possible to carry out high-precision measurements and production tests to obtain mathematical equations and models in the motion mode, and also make it possible to program the entire movement of the haul truck.

In this research work, using a big database of haul truck operation in the open-pit mining of Erdenet ore, the patterns of influence of the quarry depth, transportation distance, grade of road as well as various mining and technical factors of the road surface were determined on the speed of movement. Using this method, it is possible to carry out various analytical tests and develop models as well as quickly determine the truck speed in certain production conditions.

Keywords: haul truck, mining haul road, transport route, truck speed, big data

ABILITY TO CALCULATE THE OPTIMAL OPERATING TIME OF THE OPEN-PIT DRILLING MACHINE BASED ON THE SDM

Bazarvaani Altansanaa*, Khavalbolot Kyelgyenbai

School of Geology and Mining Engineering, Mongolian University of Science and Technology, Ulaanbaatar 14191, MONGOLIA
*Corresponding author: altansanaa@erdenetis.edu.mn

The Erdenet Ovo copper-molybdenum deposit has been in use for 45 years, but the mineral content has decreased, making mining more challenging. Our goal for the plant employing the deposit is to lower expenses and keep the equipment used as reliable as possible. In this article, based on the operational data of Erdenet Industry State-Owned Industry Department (SOE) and the operational data of 2010-2020 of the SBS type drilling machines used in it, the operational reliability indicators are calculated, and the purpose of calculating the optimal period of use of the drilling machine fleet and unit drilling machine. Put In doing so, mine operation and drilling machine operating parameters were modeled using system modeling software Vensim, and the operation was considered dynamic based on methods such as probability theory, Markov model, and system dynamics modeling based on previous statistical data. In doing so, mine operation and drilling machine operating

parameters were modeled using system modeling software Vensim, and the operation was considered dynamic based on methods such as probability theory, Markov model, and system dynamics modeling based on previous statistical data. Within the framework of the study, 8 sub-models were developed, from the basic operation of the mine to the reliable operation of the unit and rig fleet, and the fixed costs during the life cycle, which are closely related models. Our main goal is to calculate the service life of the drilling machine used in the above field based on statistical data, and in doing so, the main criterion is the comprehensive reliability indicator of the machine park, and it is estimated that 5 years is the optimal time for the park's reliability level to be at the highest possible level. When optimizing the life of a mining machine, based on the theory of system modeling, reliability performance is the main criterion, which can be achieved by reflecting the actual condition of the machine rather than the cost-based calculations that we commonly use.

Keywords: reliability, maintenance mining machine, lifetime, system dynamic

STUDY OF OPTIMAL BLASTING PARAMETERS FOR IN-PIT CRUSHING AND CONVEYING SYSTEMS

Ganzorig Dugarsuren*, Khavalbolot Kyelgyenbai

[1]School of Geology and Mining Engineering, Mongolian University of Science and Technology, Ulaanbaatar 14191, MONGOLIA
*Corresponding author: ganzorig.d@must.edu.mn

Abstract

Production processes in open-cast coal mining typically encompass drilling, blasting, extractoin, hauling, and stockpiling. Effective coordination of these processes, along with enhancing production and cost efficiency, necessitates a comprehensive analysis of the primary production processes. This study developed an operational cost modeling framework for mining production activities. Post-blast rock fragmentation parameters and blast hole diameters are integral to all mining processes, exerting a significant influence on costs. The associated costs were analyzed using algorithms that account for these variables. Furthermore, the impact of fluctuations in explosive prices and equipment operating costs on the overall production cost was evaluated through sensitivity analysis. This research was conducted at the Tavantolgoi coal deposit.

Keywords: rock fragmentation, mining processes, cost modeling

Introduction

The mining industry is often reliant on mineral sale prices and profitability. However, predicting mineral prices and assessing price volatility are challenging tasks, as future market fluctuations can significantly impact mining operations. Consequently, mining companies prioritize the reduction and control of production costs to maintain profitability. The core processes in open-cast mining include preparation for excavation and loading, excavation and loading, transportation, and stockpiling. By minimizing the costs associated with these essential processes, mining companies can enhance their profitability.

Focusing solely on reducing the cost of one process can be misleading; instead, cost reductions can be achieved by optimizing the coordination and efficiency of all production processes. Although each open-cast mining process incurs distinct costs, rock fragmentation parameters influence the costs across all processes. After blasting, the fragmentation and granulation of the rock directly affect the excavation, transportation, and crushing processes. Higher rock fragmentation generally increases drilling and blasting costs. However, greater fragmentation can also lower the costs associated with excavation, transportation, and crushing operations.

Drilling and blasting

In drilling and blasting, as the diameter of the borehole increases, both the quantity and the parameters of the explosives increase (Fisonga M, Garcıa YD, Besa B, 2017). When the spacing between rows and holes, or the blast pattern ratio, increases, the quantity of explosives decreases while the fragmentation parameters increase (Nielsen K, 1983). Additionally, the ratio of charge length to blast pattern increases (Chugh YP, Behum PT, 2014). Conversely, when the charge length to blast pattern ratio decreases (Singh P, Roy M, Paswan R, Sarim M, Kumar S, Jha RR, 2016), a reduction in bench height leads to an increase in the blast pattern ratio (Kecojevic V, Komljenovic D, 2007). The dependency of rock fragmentation parameters on drilling and blasting operations can be calculated through mathematical modeling.

Loading and hauling

Excavation performance is influenced by factors such as collision conditions, rock properties and fragmentation parameters. The presence of large particles in blasted rock reduces the productivity of excavation equipment. The thinning of the blast block and the degree of rock fragmentation serve as indicators of crushing quality.

The profitability and cost efficiency of open-cast mining are heavily dependent on rock mechanical properties such as Rock Quality Designation (RQD), compressive strength, and the presence of cracks. The characteristics of blasted rock fragmentation, thinning, and geometric parameters significantly affect the performance of excavation, loading, and transportation processes.

Among the processes in open-cast mining, transportation is particularly costly. Reducing transportation costs is a primary objective. The utilization of transportation capacity has a substantial impact on the rate of mine development, deepening, and associated costs. This is because the vehicle's load capacity is highly dependent on the grain size of the blasted rock. In the case of smaller rock fragments, it is possible to optimize the vehicle's load efficiency and accelerate mining operations. While over-crushing can improve vehicle productivity, it also increases the costs of drilling and blasting.

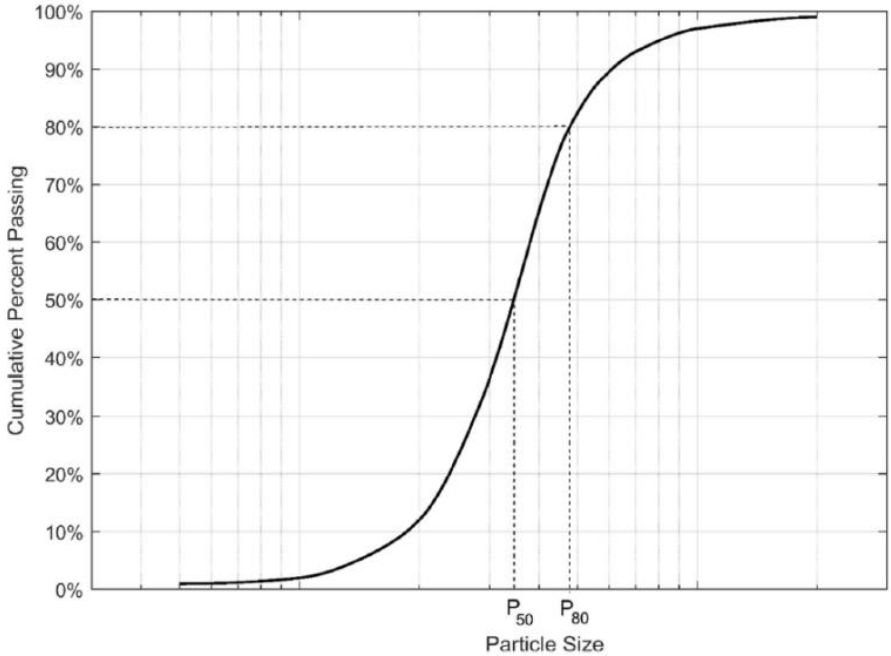

Fig 1. Typical cumulative particle size distribution curve

Crushing

The size of the fragmented rock produced by drilling and blasting is controlled by the mesh size of the crusher hopper. Crushing large-grained rock requires more electricity (Pothina R, Kecojevic V, Klima MS, Komljenovic D, 2007), whereas crushing smaller-grained rock consumes less electricity, significantly reducing the crusher's operational costs.

Given that post-blast rock fragmentation has a substantial impact on the cost and productivity of the open cast mining processes, accurately determining the average rock fragmentation rate is a critical issue. Drilling and blasting parameters are adjusted, tests are conducted, and the resulting fragmentation parameters are evaluated. Additionally, the cost of drilling and blasting influences the determination of these fragmentation parameters. The parameters of the distribution are obtained by sieving analysis or image analysis. Typically, it shows a cumulative distribution as given in Fig. 1. Mean fragmentation size (P50) is the sieve interval in which 50% of the material passes. Similarly, P80 is the sieve interval in which 80% of the material passes and derived by the Rosin–Rammler particle size distribution function which is given below (Vesilind 1980).

Optimal blasting parameters

The fundamental processes in open-cast mining include drilling, blasting, excavation, hauling, stockpiling, and crushing. The average rock fragmentation rate after blasting is closely related to the costs of all subsequent mining processes. To reduce overall mining costs, it is essential to study the average rock fragmentation parameters in relation to the cost variations of each individual process.

The total cost of mining comprises the expenses associated with core mining activities such as drilling, blasting, excavation, hauling, stockpiling, and crushing.

By adjusting the diameter of the blast hole and the average fragmentation parameters, it is possible to reduce the overall operational costs. However, calculating these variables with precise methodology is challenging. To address this, a variational algorithm was employed to solve the simulation (Pothina R, Kecojevic V, Klima MS, Komljenovic D, 2007). Variational algorithms, though effective, have two main disadvantages: 1) Optimization is not always guaranteed, and 2) The specific parameters for the algorithm are often chosen arbitrarily. Nevertheless, defining an optimal solution interval can aid in accurately identifying the best solution. Utilizing different variable parameters helps mitigate the uncertainty associated with the algorithm.

The cost of each open-pit mining process was calculated based on the fragmentation parameters. The parameters for blast fragmentation were determined from ongoing blasting operations at the Tavantolgoi open-cast mine, and experimental work was conducted within the research area.

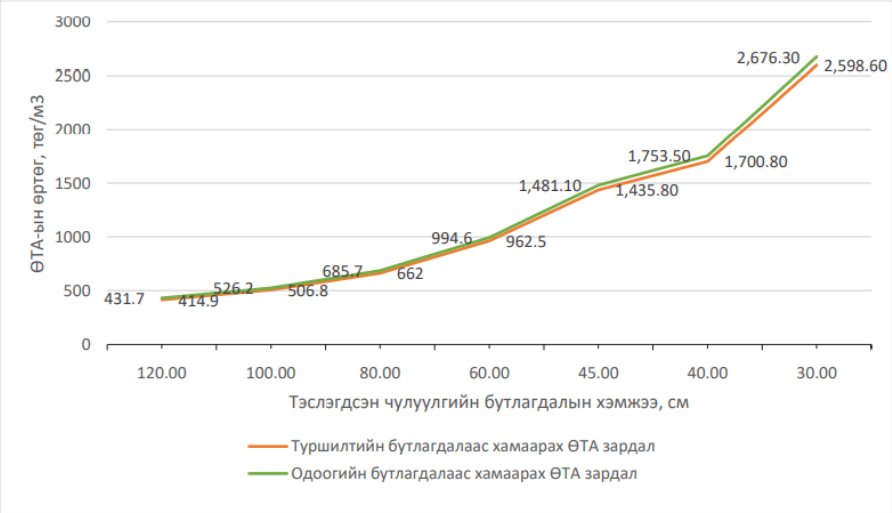

Fig 2. Comparison of the costs associated with S/B:1.15 and S/B:1.67 grids

When the crushing parameters for experimental drilling and blasting range from 10 to 120 cm, the cost of drilling and blasting is calculated 1 m^3 of blasted rock. The costs are as follows: 2598.6 MNT for rock crushed to a size of up to 30 cm, 962.5 MNT for rock crushed to a size of up to 60 cm, 662.0 MNT for rock crushed to a size of up to 80 cm, and 414.9 MNT for rock crushed to a size of up to 120 cm.

At the Tavantolgoi open-cast mine, a roller crusher will be used. This crusher will not handle rocks smaller than 30 cm and will operate on rocks ranging from 30 to 120 cm. Rocks with sizes greater than 120 cm will be processed using a hydraulic crushing device. The following graph presents the calculated electricity costs for crushing 1 m^3 of rock.

Fig 3. The cost of electricity for operating the crusher is dependent on the size of the rock being fed into the crusher

According to the calculations, the cost of electricity for crushing rock sizes ranging from 0 to 30 cm is considered a normal load. The parameters for the rock entering the crusher are as follows: 33.9 MNT for crushing 1 m^3 of rock up to 35 cm, 62.3 MNT for rocks up to 40 cm, 86.8 MNT for rocks up to 45 cm, 144.2 MNT for rocks up to 60 cm, 198.86 MNT for rocks up to 80 cm, 239.7 MNT for rocks up to 100 cm, and 279.4 MNT for rocks up to 120 cm.

The cost comparison of drilling, blasting, and crushing is illustrated in the following figure. The graph demonstrates that the electricity cost for crushing 1 m^3 of rock is less variable compared to the costs associated with drilling and blasting.

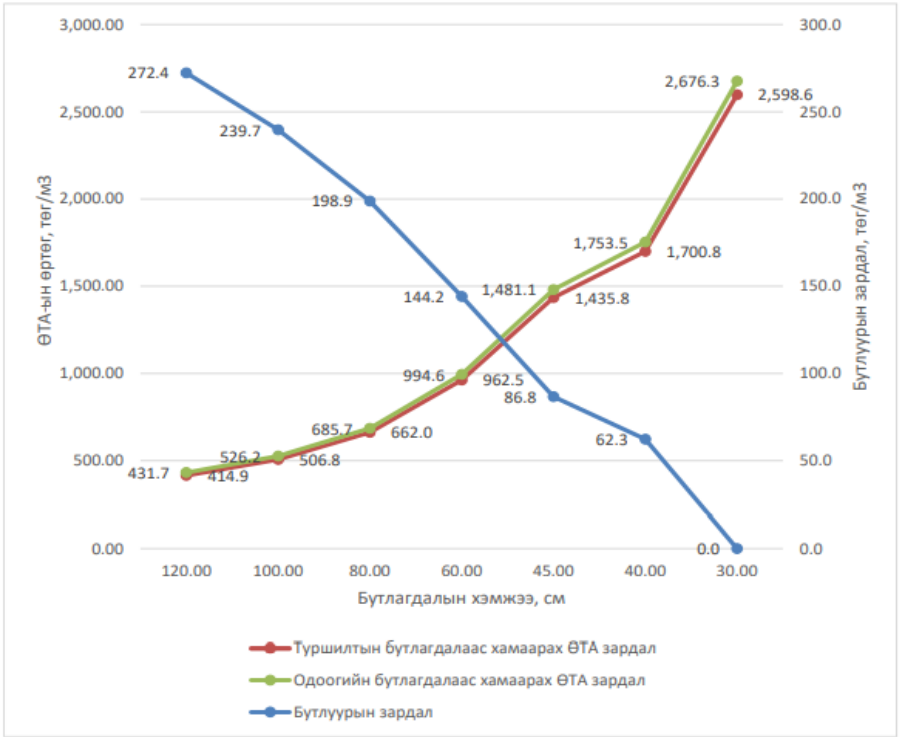

Fig 4. The cost comparison of blasted rock and crushing operations

Table 1. Bench geometry and rock characteristics

Rock density	2.3
Emulsion density	1.2
ANFO density	0.85
Blasting parameter	
Blast geometry constant	1.1
Hole diameter	229 мм
Hole length	11.1 м
Burden	8.4 м
Spacing	7.3 м
Stemming	0.1 м
Bench height	18.6 м
Required amount	468.61 кг

Based on the above calculations, the minimum cost of blasting and crushing will be achieved with a rock size of 50 cm.

Conclusions

Open-cast production processes are highly dependent on the average rock fragmentation parameters. The cost of the blasting process is inversely related to the average rock fragmentation rate, while the costs of transportation and crushing are directly related. Mining production processes are interrelated, and to minimize overall costs, it is necessary to optimize these processes as a cohesive system.

In the Tavantolgoi coal mine, the average costs of crushing 1 m^3 of rock are as follows: 14473 MNT for rock fragmented to 10 cm, 1753 MNT for 40 cm, 685.7 MNT for 80 cm, and 431.7 MNT for 120 cm.

The cost of drilling and blasting varies between 17 to 400 MNT to 1 m^3, depending on the current crushing parameters and experimental results. By optimizing blasting parameters according to those tested in the research, it is possible to save between 17 and 400 MNT to 1 m^3.

According to the research, the cost of electricity for crushing rocks in the crusher is as follows: 33.9 MNT for 1 m^3 of rock up to 35 cm, 62.3 MNT for 40 cm, 86.8 MNT for 45 cm, 144.2 MNT for 60 cm, 198.86 MNT for 80 cm, 239.7 MNT for 100 cm, and 279.4 MNT for rocks up to 120 cm.

References

Fisonga M, Garcıa YD, Besa B, “Burden estimation using relative bulk strength of explosive substances”. Appl Earth Sci 126(1):31–37. https://doi.org/10.1080/03717453.2017.1296673, 2017.

Nielsen K, “Optimisation of open pit bench blasting”. Paper presented at the 1st international symposium on rock fragmentation by blasting, Lulea, Sweden, 1983.

Chugh YP, Behum PT “Coal waste management practices in the USA: an overview”. Int J Coal Sci Technol 1(2):163–176. 2014. https://doi.org/10.1007/s40789-014-0023-4

Singh P, Roy M, Paswan R, Sarim M, Kumar S, Jha RR “Rock fragmentation control in opencast blasting”. J Rock Mech Geotech Eng 8(2):225–237, 2016.

Kecojevic V, Komljenovic D “Impact of burden and spacing on fragment size distribution and total cost in quarry mining”. Trans Soc Min Metall Explor 320:133, 2007.

Singh S, Narendrula R “Factors affecting the productivity of loaders in surface mines”. Int J Min Reclam Environ 20(01):20–32, 2006.

Osanloo M, Hekmat A “Prediction of shovel productivity in the Gol-e-Gohar iron mine”. J Min Sci 41(2):177–184, 2005.

Bogunovic D, Kecojevic V “Impact of bucket fill factor”. Min Eng 63(8):48–53, 2011.

Taherkhani H, Doostmohammadi R “Transportation costs: a tool for evaluating the effect of rock mass mechanical parameters on blasting results in open pit mining”. J Min Sci 51(4):730–742, 2015.

Dickerson AW, Alexander RB, Hollis AJ “Measurement of payloads carried by mine haul trucks and the influence of payloads on production rates and material movement costs”. Paper presented at the Symposia Series—Australasian Institute of Mining and Metallurgy, 1986.

Workman L, Eloranta J “The effects of blasting on crushing and grinding efficiency and energy consumption”. In: Proc 29th Con Explosives and Blasting Techniques, Int Society of Explosive Engineers, Cleveland OH, pp 1–5, 2003.

Pothina R, Kecojevic V, Klima MS, Komljenovic D “Gyratory crusher model and impact parameters related to energy consumption”. Miner Metall Process 24(3):170–180, 2007.

Monjezi M, Khoshalan HA, Varjani AY “Optimization of open pit blast parameters using genetic algorithm”. Int J Rock Mech Min Sci 48(5):864–869, 2011.

Neale AM “Blast optimization at Kriel Colliery”. J South Afr Inst Min Metall 110(4):161–168, 2010.

AminShokravi A, Eskandar H, Derakhsh AM, Rad HN, Ghanadi A “The potential application of particle swarm optimization algorithm for forecasting the air-overpressure induced by mine blasting”. Eng Comput 1:1–9. https://doi.org/10.1007/s00366- 017-0539-5, 2017.

Kahriman A, Ceylanoalu A “Blast design and optimization studies for a celestite open-pit mine in Turkey”. Mineral Resour Eng 5(2):93–106. https://doi.org/10.1142/S095060989600008X, 1996.

Martin PL “Drill and blast optimization at the Sparkhule Limestone Quarry”. J Explos Eng 23(4):6–12, 2006.

Intl Sociaty of Explosives, “ISEE Blaster’s Handbook 18th Edition”, ISBN-10-189239619X, 2011.

Konya CJ “Blast design. In: Sendlein LVA, Yazicigil H, Carlson CL (eds) Surface mining environmental monitoring and reclamation handbook”. Elsevier, New York, 1983.

EFFECT OF MINERAL PHYSICAL PROPERTIES ON BENEFICIATION OF COPPER MOLYBDENUM SULFIDE ORES

Bolormaa Chuluun[1]*, Shinebaatar Davaajantsan[2], Battogtokh Otgoi[3]

[1] School of Geology and Mining Engineering, Mongolian University of Science and Technology, Ulaanbaatar 14191, MONGOLIA
[2] Erdenet Industrial Quality Control Department quality specialist,
[3] Consultant engineer of Mongolia,
*Corresponding author: chbolor@must.edu.mn

Abstract

Due to the different conditions of the origin of the ore, the characteristics of the ore in different parts of the deposit are not the same. In this study, there was no significant difference in minerals when conducting mineralogical analysis of two different ores, but the mineralogical analysis determined that copper minerals were seen with bullets. This indicates that the collector reagent was insufficient. In the flotation tailings, copper minerals were disposed in open and closed intergrowths with quartz, albite, pyrite, amphibolite, and biotite. The copper ore grains formed open and closed grains with other non-ore minerals and were thrown into waste because they were not sufficiently separated by ore grinding.

Mineral type, grain size, and free surface area of minerals were determined by mineralogical analysis. The amount of free surface of minerals by ore grinding and the form of minerals in the waste were analyzed by mineralogical analysis. It shows how the copper grains in the waste combine with other minerals. The purpose of the study is to investigate the mineral dilution and composition in ore processing and flotation tailings.

Keywords: Deposit, ore, aggregate, granule, concentrator waste

Introduction

The Erdenet porphyry copper-molybdenum deposit is related to the Late Triassic and Early Jurassic volcanic units and shaped stockwork ore body. In stockwork, mineralisation occurs in the brittle deformation zone in the crust where there is a fracturing of the rocks and formation of closely spaced veinlets. Most of the world’s copper and molybdenum deposits extracted from stockwork deposits.

The chalcopyrite and molybdenite mineralization is associated with granodiorite porphyry and dacite; and granite porphyry and leucogranite. The concentration of sericite and feldspar-

quartz metasomatites will decrease and the mineralized strength porphyry rocks will increase in the ore as the mine depth increases, which could have an impact on the grinding and metal recovery rate. Both the ore forming and host rock minerals are crucial in the ore processing. Copper porphyry mineralization is often characterized by medium, fine, and very fine-grained textures. The ore's texture has a specific influence on the release of minerals from the host rock while crushing and grinding it.

The total amount of crushed ore in the concentrator is determined by granular analyses of ore crushing samples No.0406 and 0409, as shown in Table 1.

Table 1. Results of particle analysis of mill grinding

Sample №	0.212мм, %	+ 0,075мм , %	-0,075мм, %
0406	9.72	30,09	60.19
0409	9.9	29,99	60.11

The contents of the entire section measuring -0.075 mm are 60.11-60.19, which is in accordance with the / >60 / requirement stipulated in the ground ore standard. The mineralogy analysis results for mineral types, grain size, and free surface area in that ore (No. 0406, 0409) are shown in Table 2.

Table 2. Analyses of minerals

ERDENET_Mineral_Group / Sample	**Ore-0406**	**Ore-0409**
Albite	30.5796	31.0831
Alumosilicate - mixture	2.8065	3.2041
Amphibole/ Pyroxene	0.0054	0.0073
Anorthite	0.0327	0.046
Apatite	0.0985	0.1662
Biotite	0.0073	0.068
Bornite	0.0328	0.0167
Calcite / Dolomite	0.3524	0.7315
Chalcocite	0.0457	0.0187
Chalcopyrite	0.8513	0.8147
Chlorite	0.8978	1.2513
Covellite	0.0173	0.0072
Cu Oxide	0.0021	0.0002
Enargite - Tennantite	0.0776	0.0493
Galena	0.0014	0.0003
Gypsum	0.0528	0.2061
Iron_Carbonate	0.0024	0.0014
Iron_Oxide	0.438	0.1805
K_Feldspar	4.1519	3.737
Kaolinite	2.1539	1.883
Molybdenite	0.0256	0.0248
Muscovite	12.4191	13.3354
Other Cu	0.0038	0.0028
Other minerals	0.7085	0.8074
Pyrite	4.4979	3.5625
Quartz	39.3403	38.3155
Sphalerite	0.0105	0.005
Ti Oxide	0.3867	0.4741

Table 3. Grain size distribution of ore minerals

Grain size	**Midpoint [µm] / Sample**	**Ore-0406**	**Ore-0409**	**Ore-0406**	**Ore-0409**	**Ore-0406**	**Ore-0409**	**Ore-0406**	**Ore-0409**
	Ore			**Secondary ore**		**Molybdenite**		**Pyrite**	
≥1.00<10.00	3.16	16.451	18.23	29.811	42.437	11.961	16.041	6.809	6.982
≥10.00<20.00	14.14	16.954	18.911	40.921	41.654	14.511	22.506	6.915	7.14
≥20.00<45.00	30	33.286	30.52	21.896	9.506	34.435	37.562	27.776	22.438

≥45.00<75.00	58.09	21.563	22.875	7.373	6.402	39.093	23.892	39.368	34.518
≥75.00<106.00	89.16	10.242	5.879	0	0	0	0	16.496	19.381
≥106.00<150.00	126.1	1.503	3.585	0	0	0	0	2.637	4.652
≥150.00<212.00	178.33	0	0	0	0	0	0	0	4.888
≥212.00<600.00	356.65	0	0	0	0	0	0	0	0
All grains		**100**	**100**	**100**	**100**	**100**	**100**	**100**	**100**

Table 3 shows that ore minerals in the range of / ≥106.00<150.00 in sample number 0409 are 4,888%, but they are not present in 0406 ore.

Therefore, the amount of free surface of minerals after grinding ore and the form of minerals in the waste were analyzed by mineralogical analysis in Table 4.

Table 4. Free surface area of ore minerals, %

	Ore-0406	**ore-0409**	**Ore-0406**	**ore-0409**	**Ore-0406**	**ore-0409**	**Ore-0406**	**ore-0409**
	Primary ore		**Secondary ore**		**Molybdenite**		**Pyrite**	
<20	18.57	27.59	39.5	47.44	17.97	20.69	5.03	5.43
≥20<80	34.43	28.34	44.22	41.3	1.1	28.29	13.01	12.05
≥80	47	44.07	16.27	11.26	80.93	51.02	81.96	82.52
All particles	**100**	**100**	**100**	**100**	**100**	**100**	**100**	**100**

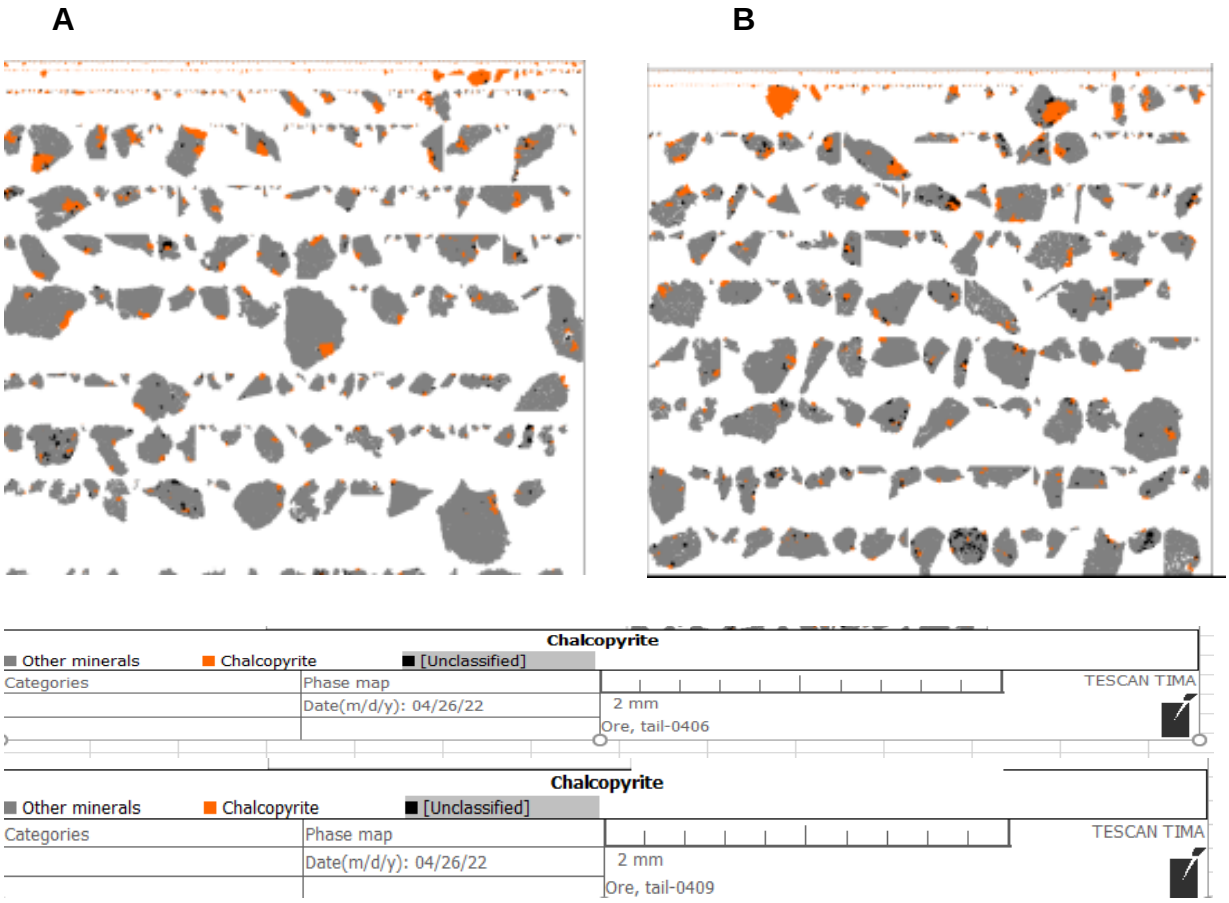

Figure 1. Chalcopyrite grains in ore flotation tailings /A-0406, B-0409/

The association between chalcopyrite and other minerals in the ore flotation tailings can be seen in Fig 2-3.

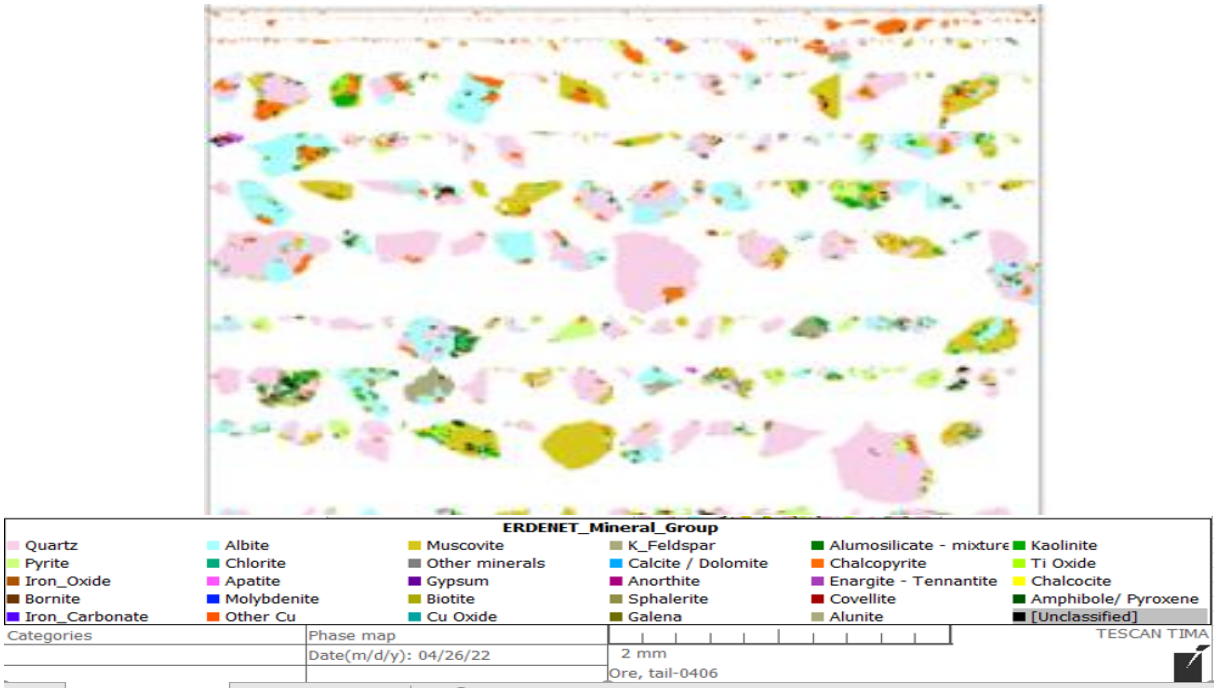

Figure 2. Minerals in ore flotation tailing. /Sample 0406/

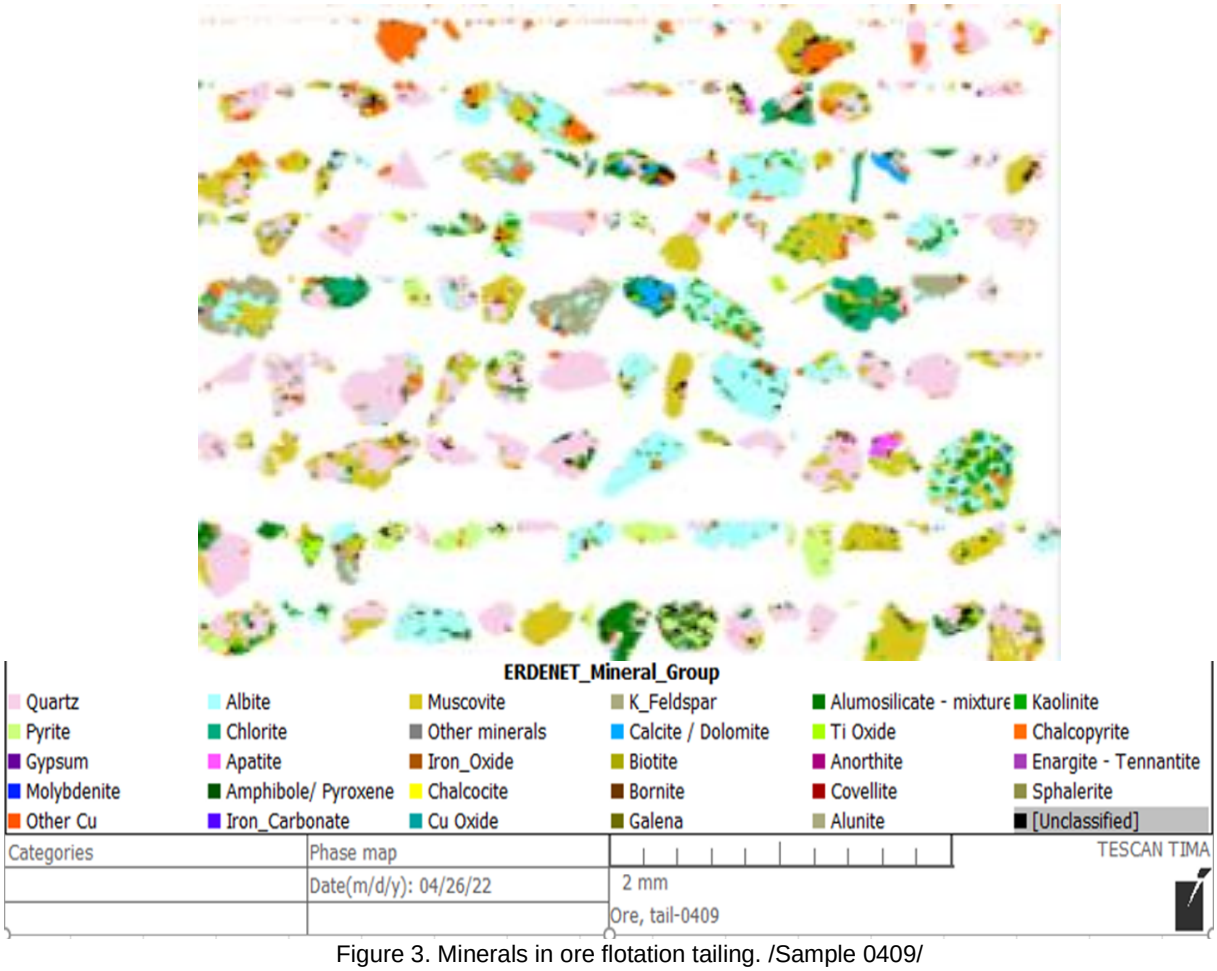

Figure 3. Minerals in ore flotation tailing. /Sample 0409/

Figure 1 depicts chalcopyrite being combined with other non-ores as well as on its own.

In particular, chalcopyrite was weakly discarded in samples 0406. In the 0409 sample, the amount of free surface of ore minerals is 44.07 for primary ore, 11.26 for secondary ore, and

51.02 for molybdenite, which indicates that the weakening of mineral has not been done enough.

The copper minerals in the flotation tailings are found in intergrowths with Quartz, Albite, Pyrite, Amphibolite, and Biotite, as shown in Figures 2-3.

To summarize, ore grains that contained other rock-forming minerals were not adequately separated from the host rock during ore grinding, thus they were discarded.

Conclusion

1. Using technological mineralogical methods, experiments were conducted on two types of ore to determine the mineral composition and grain size.

2. Samples were taken from the ore grinding of the mill, tests were conducted according to laboratory methods, and the distribution of mineral grains was analyzed by mineralogical analysis. It was determined that potassium feldspar 4.15%, quartz 39.34%, pyrite 4.49%, and copper minerals with these minerals were discarded in the form of chalcopyrite plants.

3. The copper mineral chalcopyrite is weakly discarded, indicating an insufficient amount of collecting reagent.

References

D. Davaasambuu, J. Lhamsuren, J. Damdinjav 2000. Extraction, production and use of mineral elements. Erdenet-Ulaanbaatar city. 268 p.

S. Davaanyam 2000. Technology of beneficiation of copper molybdenum using collectors with selective service. manual, Erdenet City.

A.R. Smolyakov 2007. Discovery of minerals during ore crushing.UDC 541.1

STRATEGIC STUDY OF TECHNOLOGY FOR THE DEVELOPMENT OF MINING-METALLURGY COMPLEX (AS AN EXAMPLE OF THE POLICY OF COMPREHENSIVE EXPLOITATION OF IRON ORE DEPOSIT)

Bolor-Erdene Otgonkhuu

School of Geology and Mining Engineering, MUST, Ulaanbaatar 14191, MONGOLIA
*Corresponding author: o.boggie33@gmail.com

Abstract

The rapid development of mining, infrastructure, and construction industries in Mongolia has led to an increasing demand for ferrous metals and their derivative products. Currently, the majority of ferrous products are imported from abroad. Within Mongolia, the ferrous metallurgy sector is represented by entities such as the Darkhan Metallurgical Plant, the Erdenet Plant Repair and Mechanical Factory, and several smaller plants and workshops. These facilities produce steel and cast iron products using scrap metal as the primary raw material in electric arc and induction furnaces. However, the availability of scrap metal, both domestically and internationally, has been steadily decreasing. Consequently, there is a growing necessity to shift towards using Mongolia's abundant iron ore reserves as the primary feedstock for steel production. Despite having approximately 1.8 billion tons of iron ore reserves, Mongolia has yet to establish a fully integrated iron and steel industry capable of processing these ores into finished steel products. Iron ore extracted by local companies is predominantly exported as raw ore or concentrates, bypassing the opportunity for further domestic processing.

Keywords: Iron ore, concentrate pellets, cast iron, steel products

Introduction

Mongolia, characterized by its vast geographical expanse and underdeveloped infrastructure, is witnessing a consistent rise in steel consumption driven by the growth of its

construction, mining, and infrastructure sectors. Despite possessing abundant reserves of key raw materials necessary for steel production—such as iron ore, coking coal, limestone, and water—Mongolia remains reliant on imported steel to meet domestic demand. This scenario presents a significant opportunity for establishing a domestic steel industry aimed at reducing imports and fulfilling internal needs.

As of January 1, 2024, Mongolia's national registry reported approximately 1.8 billion tons of iron ore reserves, with nearly half of these reserves located in the Darkhan-Selenge region. Since 2006, iron ore mining operations have been concentrated around deposits near the central railway infrastructure. These operations have focused on exporting iron ore and concentrates to China, thus promoting the development of an export-oriented iron ore mining sector. As a result, exploration activities have increased, contributing to the growth of reserves recorded in the national resource registry.

The establishment of a mining and metallurgical complex in Darkhan offers several strategic advantages. The region is situated only 220 kilometres from Ulaanbaatar, Mongolia's primary market, and can benefit from proximity to domestic sources of high-quality coking coal. Additionally, the availability of ample water resources and a relatively inexpensive labour force compared to international markets further enhance the region’s suitability for developing a competitive steel production industry that could serve both domestic and international markets.

According to a study by the World Steel Association, each job created in the steel industry generates an additional 6-7 jobs in related sectors. Furthermore, every dollar of value added in steel production results in an additional $2.50 of value creation in both the supply chain and downstream industries. Based on these estimates, the establishment of a steel production industry in Mongolia could potentially generate up to 11,000 indirect jobs and contribute up to MNT 1.6 trillion in indirect economic value. The steel production sector encompasses four key stages: exploration, extraction, beneficiation, and metallurgical production. Taking into account the infrastructure and associated factors, the establishment of a “Mining and Metallurgical Complex” in Darkhan could increase import substitution, foster export-oriented production, and yield significant socio-economic benefits. Therefore, this study aims to evaluate the technological strategies necessary for developing a “Mining and Metallurgical Complex” based on Mongolia’s iron ore reserves.

Research Section

1) Mongolia’s Steel Demand

As of 2020, Mongolia imported 695.7 thousand tons of steel products. Over the following four years, the country’s steel imports grew at an average annual rate of 25%, with imports reaching approximately 700 thousand tons in 2023. Domestic production, led by the Darkhan Metallurgical Plant and 16 smaller steel-producing entities, meets only about 20% of Mongolia’s demand for construction-grade rebar, while the remaining 80% is supplied through imports.

According to global trends, countries with a per capita Gross Domestic Product (GDP) exceeding approximately USD 6,000 typically experience a sharp increase in steel consumption, reaching 200-500 kg per capita. This elevated level of steel consumption tends to be sustained for about 20 years, after which it gradually declines, stabilizing at around 100-200 kg per capita, depending on the country’s economic structure. Based on these trends, Mongolia's long-term domestic steel demand is projected to range between 0.7 and1.0 million tons annually.

2) Iron Ore Reserves in Mongolia

As of April 30, 2024, Mongolia had a total of 2,760 active mineral licenses, of which 1,732 were for mining operations and 1,028 for exploration. Among these, 82 licenses are dedicated to the extraction of iron ore. The total iron ore reserves registered in the national inventory amount to approximately 1.8 billion tons.

3) Distribution of Iron Ore Deposits in Mongolia

When grouped by size, 11 deposits with reserves exceeding 50 million tons account for 1.28 billion tons of iron ore, representing 73% of Mongolia's total reserves. The remaining 471.88 million tons, or 27%, are distributed among 58 smaller deposits.

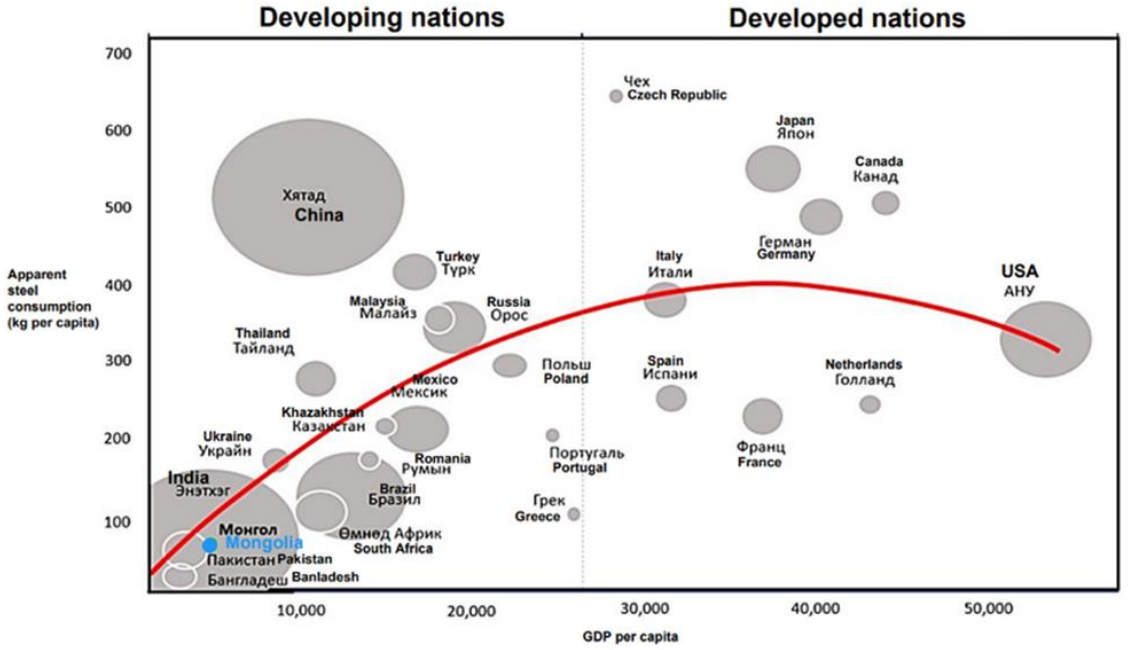

Chart 1. GDP and Steel consumption per capita

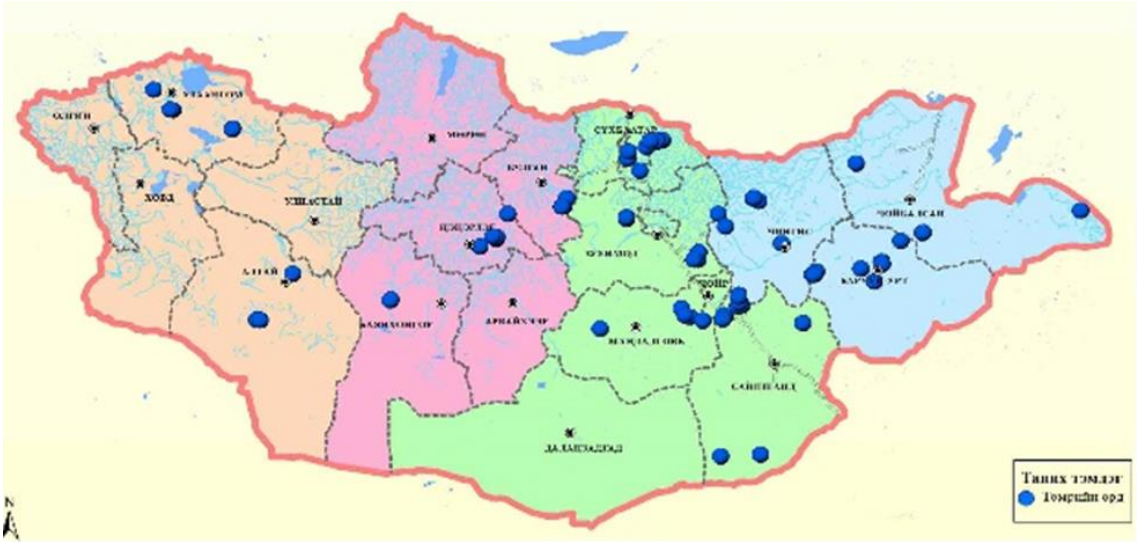

Figure 1. Geographical location of the iron ore deposits in Mongolia

4) Distribution of Iron Ore Reserves in the Darkhan-Selenge Region

As shown in Table 2.2, the Darkhan-Selenge region contains 40.5% of Mongolia's total identified iron ore reserves, all of which are currently fully operational. This concentration of reserves provides a fundamental basis for the development of a mining and metallurgical complex in the Darkhan-Selenge region.

5) Regional Overview

The Darkhan-Selenge region is situated in the northern part of Mongolia, encompassing an area of 327,500 hectares within the eastern-northeastern basin of the Kharaa River, nestled among the foothills of the Khangai Mountains. Of the total land area, 70.7%, or 231,700 hectares, is utilized for agricultural purposes. The regional center, Darkhan city, is a major industrial hub in Mongolia.

Table 1. Distribution of Iron Ore Deposits

#	Province	Iron ore reserves, mln ton	Percentage
1	Selenge	690.5	39.4%
2	Dundgobi	188.6	10.8%
3	Khentii	137.8	7.9%
4	Uvs	130.7	7.5%
5	Sukhbaatar	111.6	6.4%
6	Bulgan	111.2	6.3%
7	Dornogobi	108.6	6.2%
8	Gobi-Altai	83.7	4.8%
9	Arkhangai	63.2	3.6%
10	Tuv	52.9	3.0%
11	Dornod	42.2	2.4%
12	Darkhan-Uul	19.8	1.1%
13	Bayankhaongor	11.9	0.7%
Total		1,752.7	100.0%

Table 2. Large deposits of iron ore

#	Deposit name	Reserves, mln ton
1	Tumurtei	229.3
2	Bayangol	147.49
3	Bayantsogt	249.4
4	Ereen	126.59
5	Bayanmunkhtolgoi	84.5
6	Turgen	70.3
7	Tsakhiurt ovoo	89.97
8	Ulziit ovoo	87.6
9	Dartsagt	52.7
10	Tayannuur	78.65
11	Tamiriin gol	52.8
12	Others	471.88

Administratively, the region is divided into four soums: Darkhan, Orkhon, Khongor, and Sharyn Gol, which are further subdivided into 26 bags. The climate is characterized by an average annual temperature of 0.3°C, with the hottest month being July at 33.3°C and the coldest month being January at -37.7°C. Annual precipitation averages 326.1 mm, with relative humidity ranging from 57% to 78%. The average wind speed is 3.0 m/s during April and May.

The region benefits from well-developed infrastructure, including its location at a key junction on the Ulaanbaatar-Sukhbaatar railway line, connection to the central power grid, high- speed fiber optic cables, digital radio relay systems, and comprehensive mobile communication services. The total population is 91,093, with 74,526 residing in Darkhan city. Approximately 64.5% of the population is under the age of 35.

The city of Darkhan is intersected by the Beijing- Ulaanbaatar-Moscow railway corridor, part of the Asian international railway transport network. Darkhan is connected to Ulaanbaatar by a railway line 246 km in length and to Erdenet by a 180 km railway. All soums in Darkhan-

Uul aimag are connected to the international railway network. The main rail routes have a combined length of 329.9 km, with 266.6 km on the Sukhbaatar- Ulaanbaatar route and 63.3 km on the Darkhan- 1-Sharyn Gol route.

The Asian Highway Network's AH-3 corridor, connecting Asia and Europe, also passes through Darkhan and Khongor. Additionally, construction is underway to upgrade the Darkhan-Ulaanbaatar road to a four-lane, dual-carriageway.

6) Product Market

The development of the steel industry in Mongolia is aimed at satisfying a significant portion of the domestic market. Since 2016, Mongolia's economy has been steadily growing, with the exception of a 5.3% contraction in 2020 due to the impact of the COVID-19 pandemic. This economic growth has been accompanied by increased consumption of steel and rolled products in the mining, processing, and construction sectors.

In 2019, the import volume of construction steel rebar and sections for building projects was 261,300 tons, which decreased to 238,880 tons in 2020. This decline was primarily due to the COVID-19 pandemic, economic downturns in Mongolia, and shortages of cement in the domestic market. However, following government policies to support the economy, large-scale construction projects for housing and infrastructure have commenced since 2021.

Currently, the demand for long-rolled steel products is predominant, with imports from China and Russia. These products are mainly used in the construction and mining industries. Other steel products include steel pipes and a limited quantity of steel sheets. The use of railway rails saw a significant increase in 2020, driven by the Tavantolgoi-Züünbayan railway project. Additionally, steel balls are identified as a critical product with growing demand.

Table 3. Large deposits of iron ore

	Steel products, thousand ton	Year				
		2018	2019	2020	2021	**2022**
1	Rebar	71.64	104.16	191.80	261.30	238.88
2	Steel pipes	39.73	58.96	63.87	72.90	64.62
3	Flat steel	0.04	0.47	0.28	8.50	0.58
4	Angle steel, H steel, other sections	15.12	15.40	19.71	22.50	21.06
5	Rail steel	7.47	19.25	21.95	28.20	204.87
6	Wire rod	3.35	4.07	6.77	8.40	13.23
7	Steel balls	28.45	4.94	0.43	0.64	0.43
8	Others	45.38	76.24	160.12	163.06	152.07
	Total	211.18	283.47	464.97	565.5	695.74

Source: Mongolian Customs database

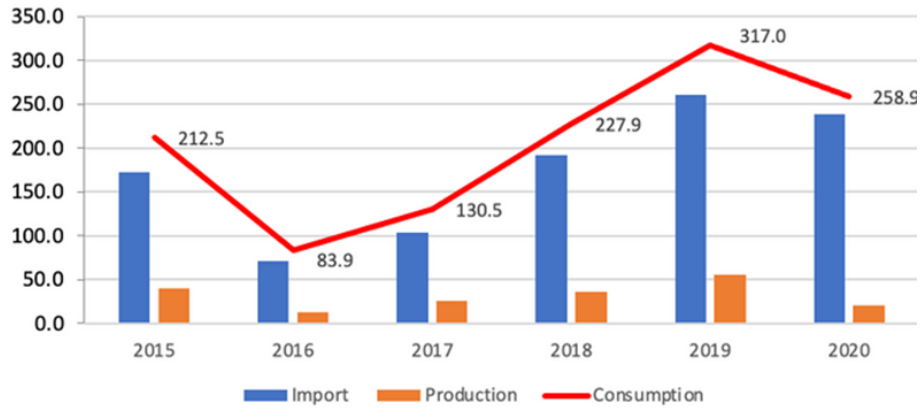

Chart 2. Steel rebars usage indicators in Mongolia
Source: Mongolian statistics office database

7) Domestic Steel Production

Including the Darkhan Metallurgical Plant, 16 small steel mills in Mongolia produce construction steel rebars. In 2019, the total production of these mills was only 55,700 tons.

Some of these facilities have struggled to maintain consistent production levels. Specifically, the Darkhan Metallurgical Plant utilized only 28.5% of its total production capacity in 2019, resulting in the production of 15,900 tons of steel. The remaining steel production, amounting to 71.5% or 39,000 tons, was contributed by other steel mills.

Table 4. Steel products widely used in industrial sector

#	Industrial sector	Steel product types in demand
1	Construction	Rebars Round bars Angle steel H steel Flat steel Wire rod
2	Mining	Steel ball Steel for support Rock bolt Wire rod

#	Hot rolled long products	2025 year forecast (thous. ton)	2030 year forecast (thous. ton)
1	Rebars	400	600
2	Round bars	90	120
3	Sections	70	90
4	Wire rod	60	80
5	Others	15	25
	Total consumption	**635**	**915**

Source: Hatch FS

8) Growth of the Steel Market

Mongolia's steel market has expanded significantly from 35,000 tons in 2005 to 695,740 tons in 2020. In recent years, economic growth and substantial investments in the mining sector have driven an increase in demand for associated infrastructure and social projects, contributing to this rise in steel consumption.

9) Future Trends in Steel Product Usage

The use of steel balls in the steel product mix is expected to increase in the future. As the mining sector, particularly copper concentrate and copper production, expands, it is anticipated that the current usage of 75,000 tons of steel balls will rise to 140,000 tons by 2030, representing a two-fold increase.

Processing Methods and Technologies for Iron Ore

The production of steel products from iron ore involves several stages, including mining and preparing the iron ore, producing pig iron, manufacturing steel, casting, and rolling. Additional processes such as cold rolling, stamping, machining, and thermal treatments may also be applied to impart specific properties.

Three primary processes are used to extract steel from iron ore, utilizing coke, coal, natural gas, and blast furnace gas. These processes are:

The traditional blast furnace process is combined with the oxygen converter process, which uses iron ore and coke.

The direct reduction process employs coal and natural gas. The smelting reduction process is based on coal.

The latter two methods are referred to as non-blast furnace processes as they do not use coke. In any chosen method, the initial stage involves the mining and beneficiation of iron ore to meet the requirements for subsequent processing stages. Figure 2 illustrates these three processes schematically.

Iron Ore Beneficiation Technology

The beneficiation of iron ore depends on the ore's chemical composition, mineral content, and structure. The most commonly used method is magnetic separation. This technique relies on the magnetic properties of the minerals and is carried out in a magnetic field. Magnetic separation can be conducted in either wet or dry forms, depending on the size and distribution of iron particles, as well as changes in ore texture and structure.

Iron ore deposits in the central region typically include skarn magnetite ores with strong magnetic properties. The primary mineral is magnetite, with martite as an accompanying mineral, and pyrrhotite, which contains sulphur, is a harmful impurity. Pyrrhotite, which contains sulphur, is present in lower concentrations in the oxidized zone. For these ores, the primary mineral is easily beneficiated using magnetic methods. Therefore, magnetic separation is the most suitable method.

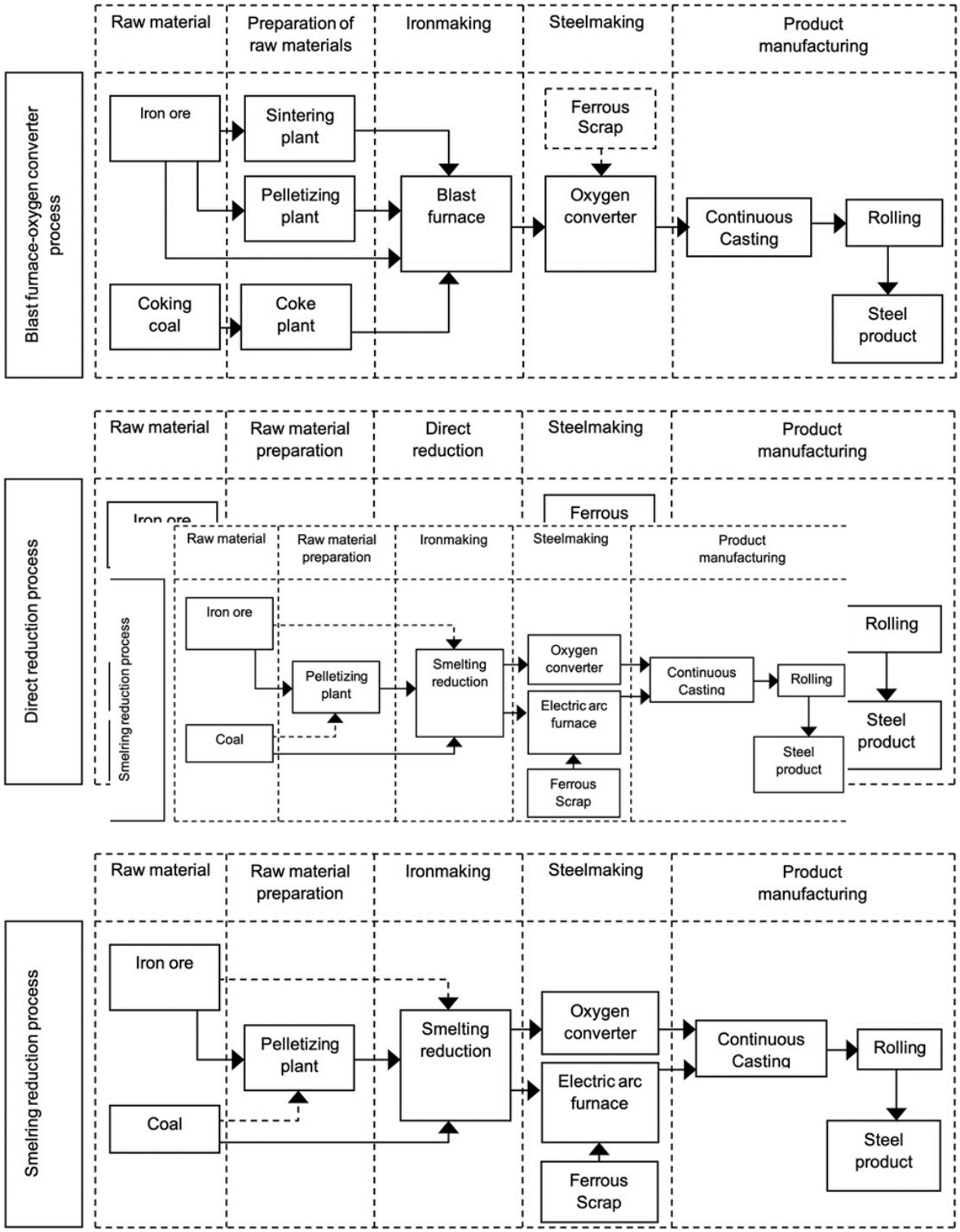

Figure 2. Steel products widely used in the industrial sector

For oxidized ores with low sulphur content, the iron content averages 51-53%, while sulphur content ranges from 0.1% to 0.16%. The iron content averages 50-52% for sulphurous ores, and sulphur content ranges from 2.0% to 3.0%. To meet metallurgical production requirements and improve economic efficiency, it is essential to process ores with high iron content (above 53%) and low sulphur content (below 0.3%). These ores can be directly used in blast furnaces and smelting reduction furnaces after crushing and adjusting the particle size. Sulphurous ores, however, require beneficiation through dry and wet magnetic separation to

increase iron content, followed by size adjustment and further treatment to reduce sulphur content through roasting and sintering processes.

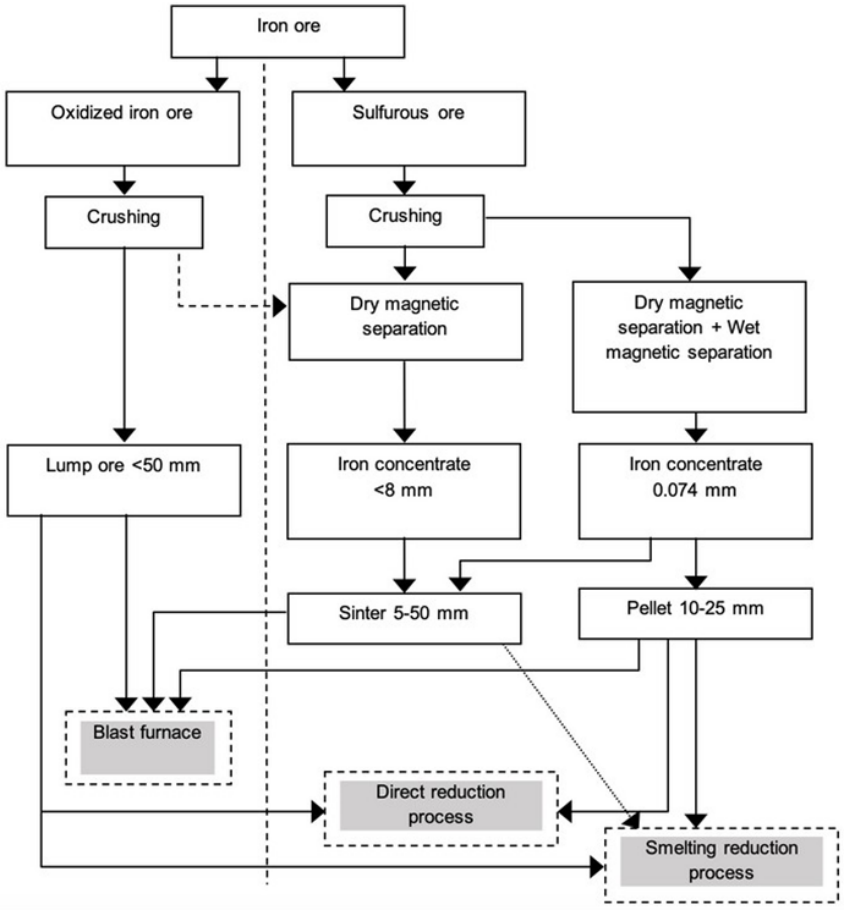

Figure 3. Iron ore beneficiation flow diagram

Table 5. Iron ore beneficiation flow diagram

Process indicators		Blast furnace ironmaking process	Direct reduction process		Smelting reduction process - COREX
			ITmk3	SL/RN	
Raw material		Lump ore, Sinter, Pellet	Pellet	Lump ore, Pellet	Lump ore, Sinter, Pellet
Iron ore requirements:	Fe, %	>50 (62)	>48	>64	50-55
	S,%	0.1-0.3	None	0.1-0.3	0.1-0.3
Energy source		Coke, oxygen blowing, pulverized coal	Coal, Coal gas	Coal, Coal gas	Coal, oxygen blowing
Material consumption:					
Iron ore, ton/ton		1.7	-	1.46	-
Sinter, ton/ton		-	-	-	-
Pellet, ton/ton		-	1.5	-	1.45
Coke, kg/ton		400	-	-	-
Coal, kg/ton		150	500	450	900
Oxygen, Nm3/ton		52	-	-	540
Electrical power, kWh/ton		27	200	60-80	60
Process output product		Iron	DRI	DRI	Iron

Conclusion

The issue of industrialization policy is often considered a key factor for national development, as evidenced by the experiences of industrialized countries. Therefore, at this pivotal moment in Mongolia's development, establishing a mining and metallurgical complex and producing value-added products is essential for addressing fundamental social, economic, and environmental issues. This approach will create significant economic opportunities.

Process indicators	Blast furnace ironmaking process	Direct reduction process		Smelting reduction process - COREX
		ITmk3	SL/RN	
Iron ore (oxidized)	Direct use in the blast furnace.	Beneficiation of iron ore through wet magnetic separation, flotation then pelletizing	Direct use	Direct use of iron ore. Beneficiation of iron ore through wet magnetic separation, flotation then pelletizing
Iron ore (sulfurous)	Beneficiation of iron ore through wet magnetic separation, flotation then pelletizing or sintering		Beneficiation of iron ore through wet magnetic separation, flotation then pelletizing.	Beneficiation of iron ore through wet magnetic separation, flotation then pelletizing or sintering
Fuel, reductant	Use of coke. Coke-chemical plant is required	Use of non-coking coal	Use of non-coking coal	Use of non-coking coal and low volume of coke
Energy	Low use of electricity and oxygen	High use of electricity.	Low use of electricity and high use of oxygen	Low use of electricity and high use of oxygen
Environmental impact	High CO_2 emissions (from coke plant, pellet plant and sinter plant)	Relatively low CO_2 emissions	Low CO_2 emissions	Relatively low CO_2 emissions
Recycling of process wastes	Process waste gas can be recycled	Process waste gas can be recycled	Process waste gas can be recycled	Process waste gas can be recycled
Quality of input materials	-	-	-	Sensitive to the quality of the input materials
Product quality	Liquid iron	Raw material for steelmaking to be used with scrap in electric arc furnace	Raw material for steelmaking to be used with scrap in electric arc furnace	Liquid iron

Lowest capacity	300-500 m^3 300-500 thousand ton annualy	500 thousand ton annualy	150 thousand ton annualy	C-1000 600 thousand ton annualy
Technological Process stages	Blast furnace-Oxygen converter-Casting-Rolling	Direct reduction-Electric arc furnace-Casting-Rolling	Direct reduction-Electric arc furnace-Casting-Rolling	Corex- Oxygen converter or Electrical arc furnace-Casting-Rolling
Total investment	>700 mln US$	~250 mln US$ (DRI plant)		
Investment cost, US$ per 1 ton a year	$211(BF)+$100(BOF)= ~$311	(DRI)+(EAF)= ~$220		(SRI)= ~$320
Raw material (scrap), and electricity cost US$ per 1 ton a year	~$92	~$214		~$198
Implications for the expansion of Darkhan metallurgical plant	Construction of new manufacturing plants and infrastructure (sintering/pelletizing plant, coke plant, blast furnace, new steelmaking plant etc)	Inclusion of DRI plant into existing facilities and infrastructure (DRI can be used in electrical arc furnace along with scrap)	Inclusion of DRI plant into existing facilities and infrastructure (DRI can be used in electrical arc furnace along with scrap)	Construction of new manufacturing plants and infrastructure (sintering/pelletizing plant, Corex plant, new steelmaking plant etc)
Technology choice:				
-short term palnning of DMP expansion (by low capacity)	Suitable	**Very suitable**	**Very suitable**	Suitable
-long term planning –Mining and metallurgical complex	**Very suitable**			**Very suitable**

In developing a long-term ferrous metallurgy complex project, it is necessary to consider the following criteria: first, the characteristics of raw materials (iron ore and coal); second, the domestic and international markets for increasing steel products; third, investment and economic efficiency; and fourth, the environmental impact.

Implementing this plan will involve several key actions: integrating iron ore deposits into economic circulation, making substantial investments, creating a new mining and metallurgical production complex, introducing new technologies in metallurgy, producing substitute products to reduce imports, ensuring a full supply of raw materials domestically, gradually increasing production capacity, creating new jobs, training skilled personnel, establishing new sales markets, enhancing Mongolia's export capabilities, and significantly increasing revenue for national and local budgets.

For processing iron ore from the Darhan- Selenge region and producing steel products, it is advisable to consider two main technological directions: processing oxidized and low-sulfur ores, and processing sulfurous ores.

Oxidized and low-sulfur iron ores can be crushed and used in blast furnaces with iron content greater than 50%, but using ores with more than 62% iron content is more economically advantageous. Therefore, processes such as dry and wet magnetic separation, roasting, and sintering are required to increase iron content.

For sulphurous ores, sulphur can be removed through dry magnetic separation and roasting or through a combination of dry and wet magnetic separation, flotation, and sintering processes.

The potential to build the main and auxiliary facilities and infrastructure at the Darhan Metallurgical Plant site presents a favourable condition for project implementation and is a significant advantage. The well-developed infrastructure in Darhan-Uul Province will be a crucial asset for the project's infrastructure development.

References

Expansion of Darkhan metallurgical plant SOSC and establishment of Mining and metallurgical complex project based on Tumurtolgoi iron ore mine. Darkhan metallurgical plant SOSC, 2010.

Feasibility Study of Darkhan metallurgical plant expansion and rewamping based on Tumurtei iron ore mine. Darkhan metallurgical plant SOSC, 2008.

Voskoboinikov V.G., Kudrin V. A., Yakushev A.M. General metallurgy 6th edition,«Akademkniga», 2005 - 768 p: 253. ISBN 5-94628-062-7.

Vegman E.F., Jerebin B.N., Pohvisnev A.N., Yusfin Yu.S., Kurunov I.F., Parenkov A.E., Chernousov P.I., Metallurgy of Iron, 3rd edition, «Akademkniga», 2004.-774 p.

Bondarenko B.I., Shapovalov V.A., Garmash N.I., Theory and technology of non-coke metallurgy, Kiev, Naukova Dumka, 2003.

Yusfin Yu.S., Pashkov N.F., Metallurgy of Iron, «Akademkniga», 2007.

Changes in paradigm, development of iron and steel industry by applying coal based DR processes: Fastmelt and ITmk3, Kosuke Seki, Hideotoshi Tanaka, 2008

Corex process in ironmaking, Report Submitted by : Aditya Kumar Singh (5207), Bachelor in Technology, Metallurgy & Materials Engineering, National Institue of Foundry & Forge Technology, Ranchi, Jharkhand

"Convention on clean, green and sustainable technologies in iron and steel making", W.Grill, 15-17 July, 2009

Amit Chatterjee, Ramesh Singh, Banshidhar Pandey, "Metallics for Steelmaking – Production and Use" , Allied Publishers Ltd. ,2001.

ETSAP Energy Technology Systems Analysis programme, IEA – ETSAP – Technolgy brief may 2010.

Emerging Technologies for Iron and Steelmaking, Article by C.P. Manning and R.J. Fruehan, 2001,

Mining Infrastructure support project – Feasibility Study Report of Darkhan metallurgical plant expansion, 2016, HATCH.Mongol Gan Project – 1, Feasibility Study, , QMC LLC, "Darkhan metallurgical plant" SC, 2

THE CURRENT STATE OF E-LEARNING, FUTURE TREND, WAYS TO MAKE IT SOPHISTICATED AND PERFECT, ITS SIGNIFICANCE AND RECOMMENDATIONS

Nanzad Tseveen*

Department of Mineral Processing and Engineering, School of Geology and Mining, Mongolian University of Science and Technology, Ulaanbaatar, Mongolia
nanzad_57@yahoo.com

Keywords: e-learning, education, quality, performance, methods, evaluation, object

Each country has its own educational system that depends on many factors such as language, culture, stage of development, demographics, and geographic location. These education systems have evolved and developed in accordance with the country's features and, thus, each country has its own unique educational system, though most countries share commonalities directly copied or slightly modified from each other. In the current globalized world, countries exchange experiences and collaborate on research to find better and more sophisticated education systems and implement the most effective ones. Today, people can travel anywhere around the world and, therefore, it is important to follow international teaching norms, creating the opportunity for people to participate in any training regardless of place, time, or distance. With the demands of the current developmental stage of society wherein artificial intelligence, electronic environment, and the fourth and even fifth industrial revolution prevail, it is essential to reconsider even long-held teaching strategies to match the demands of a rapidly changing present and swiftly approaching future.

In recent years, much has been made about various learning methods such as distance learning, online learning, and e-learning. In some cases, we began the initial stages of testing and introducing these new strategies but could only go so far without clear rules and regulations. But the world did not wait. It has been almost two years since the outbreak of the global pandemic, when all countries were forced to stop or reduce traditional classroom teaching and made to implement different forms of teaching such as electronic, distance, and telelearning, not only for elementary and high school students, but even for college and university students! However, it is evident that there are differences in the methods and quality of education, in learning, in grading, in attendance and participation of students, in the ability to learn independently, and in attitudes and evaluations of parents and the public. There are both good and bad aspects to e-learning. Therefore, this article aims to analyze the state of e-learning implemented at Mongolian University of Science and Technology (MUST) and make recommendations.

CAPITAL AND OPERATIONAL COST ESTIMATION ON ISR PROCESS ON THE EXAMPLE OF ZUUVCH OVOO DEPOSIT

Ermal KOPLIKU[1]*, Altantsooj Bayarmaa[1]* Shagdar Khaltar[2]

[1] Badrakh-Energy LLC
[2] School of Geology and Mining Engineering, MUST, Ulaanbaatar 14191, Mongolia
*Corresponding author: ermal.kopliku@orano.group, bayarmaa.altantsooj@orano.group

In situ recovery -ISR technology is mainly used and developed for sedimentary type of uranium deposits in the world wide since 1960. But this technology implementation is new and 1st time for Mongolia. ISR technology has significant advantages than using conversional mining (underground, open pit) such as profitable on lower grade deposits, low to moderate costs for mine development, low environmental impacts, lower CAPEX, OPEX, no waste rock, no tailings.

One of the main differences of ISR than conventual mining method is hydrometallurgical process is going through underground mineralized body, the metal in solution come out directly to the ground. So, there is ore bearing sediment should be permeable, isolated by impermeable layers from upper and lower layers. For successful ISR, commodities need to be readily amenable to dissolution by leaching solutions over a reasonable period, with an acceptable consumption of leaching reagents. Typical ISR mines comprise wellfield(s) and processing plant. Leaching solutions are pumped into the mineralised zone(s) through a network of injection wells and extracted by production wells. In the process, the leaching solution dissolves uranium, which are brought to the surface in a pregnant solution. The pregnant solutions are treated at an extraction plant to produce a chemical concentrate of uranium.

Zuuvch Ovoo project is covered for Zuuvch Ovoo and Dulaan Uul 2 uranium deposits. Zuuvch Ovoo project comprise 2 major parts such leaching wellfield and processing plant.

Estimation of Operating Expenditure (OPEX) and Capital Expenditure (CAPEX) for Processing plant and construction is quite common and carried out in the same manner as conventional mining projects.

OPEX requirements for ISR should be estimated based on the Liquid to Solid (L/S) ratio which reflects how much solution (m3) is required to reach the target extraction of a specific commodity for one ton of ore. Liquid to Solid Ratio (L:S) is a key parameter for ISR. L:S ratio is used for estimation of geometallurgical and economic parameters of the project. For ZO project has 2 different ore morphologies. So that L:S is 3 for basal mineralization zone is 55% of ore body (Recovery is simulated as 91%), and 4.4 for perched mineralization zone is 45% of ore body (Recovery is 82%). Average leaching recovery of ISR is 83%, Processing recovery is 99%.

For Zuuvch Ovoo project maximum NPV is matched to 15 mg/l optimized the breakeven cutoff grade for pregnant solutions to processing plant capacity is for 6000 m3/h, 2500t U per year simulated for minng plan and production plan. For ZO project ISR operation cell pattern is selected hexagons systems, the distance between wells depends on the permeability and dynamics of leaching, as well as the cost of drilling and well construction. Wells distance is planned 42 m, and 1 block consists 18 cells, will be average operate for 3 years for ZO project.

OPEX for ISR projects usually consists of reagents for leaching and processing (sulfuric acid hydrogen oxide, resin, ammonium nitrates, ammonium hydroxide), electrical power, manpower, water, management, maintenance.

CAPEX for ISR projects usually consists of lixiviant preparation plant or storage, processing Plants including initial loading of reagents, mine infrastructure, barren and pregnant solutions ponds, central pump station, administration office, and laboratory.

Wellfield construction is also CAPEX but is distributed over almost the full period of the mining. Mining/leaching operational CAPEX is consisted of (injection, extraction and monitoring) wells including pumps, facilities for operational cells: wellhouses, local pipes for connection wellhouses with operational cells, air lift (if required) for injection solutions, facilities for connection of wellfields with the mine site including pipes, roads, powerlines.

For ZO project mining /leaching Capex is 70 % of total CAPEX, it is consisted of drilling, piping, wellhouse, acid preparation unit costs, but processing plant CAPEX is 14% of total CAPEX.

Mining/leaching OPEX is 3.08% of OPEX of ZO project, processing plant OPEX is 25.5% of total OPEX of ZO project.

56.8% of Mining OPEX cost is electrical usage cost, 85.8% of processing plant OPEX is for reagent costs. Lixiviant sulphuric acid for uranium leaching will be produced on ZO site, Lixiviant production on site leads to increased CAPEX but decreasing OPEX. Electrical power production is usually a by-product in a lixiviant preparation plant.

Keywords: in-situ recovery, OPEX, CAPEX, uranium, Zuuvch Ovoo

METHODOLOGICAL RESEARCH OF RISK ASSESSMENT OF MINING PROJECTS

Nandintsetseg S.[1*], Khaltar Sh.[2], Purevdash S.[2], Ariunzaya Kh.[2], Enkhbayasgalan B.[3]

[1] School of Geology and Mining Engineering, MUST, Ulaanbaatar 14191, Mongolia
[2] Gazar Mend NGO
[3] National University of Mongolia
*Corresponding author: nandintsetsegs@must.edu.mn

Abstract

Although technological development is accelerating and new methods of risk management are being developed, social evolution and environmental degradation continue to increase the risks faced by the mining industry. Due to repeated crises in the global financial market, the high-investment mining industry is closely examining the theoretical foundations and applications of risk management. New methods developed by scientists are being swiftly implemented. Each mining project has a unique risk profile. Therefore, it is essential to select and evaluate the appropriate risk assessment methodology based on the project's stage. This work aims to conduct a systematic study of risk assessment within the “Feasibility study for the Utilization of Mineral Deposits”. As a result of the research work, seven main factors of both external and internal environment of the project and 28 sub-risk factors were determined. Qualitative and quantitative methods were used to analyze the factors and determine the level of risk. Additionally, a methodology for summarizing the risks using a RADAR chart was proposed. Conducting a risk assessment for the "Feasibility Study on the Utilization of Mineral Deposits" is considered feasible.

Keywords: Risk identification, risk analysis, feasibility study for the mining, project risk assessment

Introduction

Mongolia's mining sector is the main source of financing, accounting for one-third of the country's budget revenue. By the end of 2024, the mining sector will make up 24 percent of the GDP of Mongolia, 29 percent of the general budget revenue, and 91 percent of the total export revenue, while creating more than 62,000 jobs.. Investment serves as the primary driving force of the economy, with over 60% of the total investment in our country coming from foreign sources. By the end of 2024, Mongolia received a total of 3.1 billion US dollars in foreign direct investment (FDI), of which 2.4 billion US dollars, or 79.2 percent, was directed towards the mining sector [1]. For the efficient implementation of these investments, it is important to make technical and economic justifications and calculations for the use of deposit using a risk-based methodology.

Risk assessment is crucial for identifying potential organizational risks, disasters, and crises before they arise. It ensures business operations and critical functions remain uninterrupted, helps prevent and resolve issues, enables swift and effective disaster and crisis response, and supports efficient recovery and compensation efforts. In the mining industry, risk assessment was once a key part of business planning, but it has now evolved into a legal requirement for all organizations. [2].

The feasibility study for the utilization of mineral deposits is an extensive document grounded in resources listed in the State Register. It encompasses mining, beneficiation, and processing projects, addressing technology selection, engineering solutions, environmental impact, labor safety, hygiene, legal aspects, human resources, management, organization, infrastructure, supplies, and social services. The study also includes detailed calculations of economic efficiency, supported by relevant drawings, explanations, and other related considerations. [3].

A noticeable trend has emerged where administrative bodies, courts, and arbitration panels reject certain terms of contracts between mineral license holders, mining company shareholders, and investors, even when those terms were voluntarily agreed upon. However, these contracts are not recognized as invalid, which undermines the principle of freedom of contract [4]. Additionally, there are disputes related to the cancellation of special licenses, including conflicts over the designation of water reservoirs in protected zones, bans on mineral activities, and license revocations due to non-compliance. Other disputes involve the use of special protection areas, local protection zones, and cases where provincial assemblies deny water usage. Conflicts also extend to the legal recognition of decisions not to approve Environmental Protection Plans, disputes over the Sumy land management plan, and orders from the Professional Inspection Organization to halt pipeline operations. Furthermore, disagreements arise over the distribution of sales revenue by provincial assemblies and administrative acts from the National Assembly prohibiting mineral activities. [5].

Anticipating and preparing for events that may impact project objectives is a fundamental aspect of risk management. By identifying potential business threats and their effects on operations, organizations enhance their ability to respond effectively, protecting stakeholder interests, reputation, brand, and value creation activities. In our country's mining sector, a standardized method for risk assessment is not in use, and there is a lack of experience in identifying and evaluating risk factors at each stage of a project. This hinders the development of effective risk protection practices, the sharing of risk mitigation methods, and collaborative risk management efforts. Internationally, risk assessment in business disaster management plans is regarded as the fastest, most flexible, and accurate risk evaluation technique within the mining industry. [6].

The goal of pre-project risk assessment is to identify potential risks that may occur during project execution, evaluate socio-economic, ecosystem, and production resources along with their management capabilities, and provide informed conclusions.

Risk assessment methods

Risk assessment follows these steps according to ISO 31000:2018: 1. Risk identification, 2. Risk analysis, and 3. Risk evaluation (figure 1). If the risk is accurately and logically defined, the analysis and evaluation will be conducted in a realistic manner. Therefore, identifying project risk factors is a critical and highly responsible task

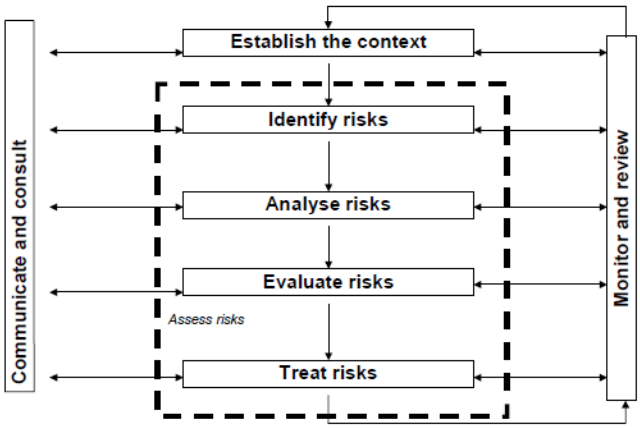

Figure 15. Risk management process model[1]

Business threat and risk assessments should not only focus on the external environment and major incident reviews but also take into account key indicators of the organization's vulnerability and resilience. [7].

As per the ISO 31010:2011 international standard, selecting a risk assessment method requires ensuring its suitability and relevance to the particular context. The chosen approach

[1] National Minerals Industry Safety and Health Risk Assessment Guideline, Version 6, June 2007

must effectively represent the risk scenario and highlight the interconnections between influencing factors.

Risk identification

The risk assessment process should not depend exclusively on known, unknown, or unreported hazards, as it can be time-intensive. Consequently, the process must involve adaptable, step-by-step stages. Identifying all possible hazards is essential when addressing risks in mining operations [8].

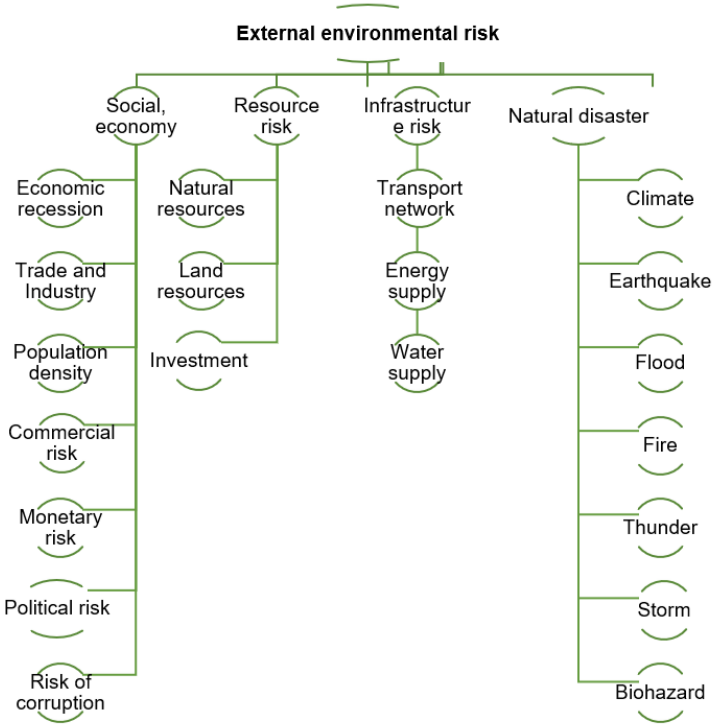

Figure 2. External environmental risk

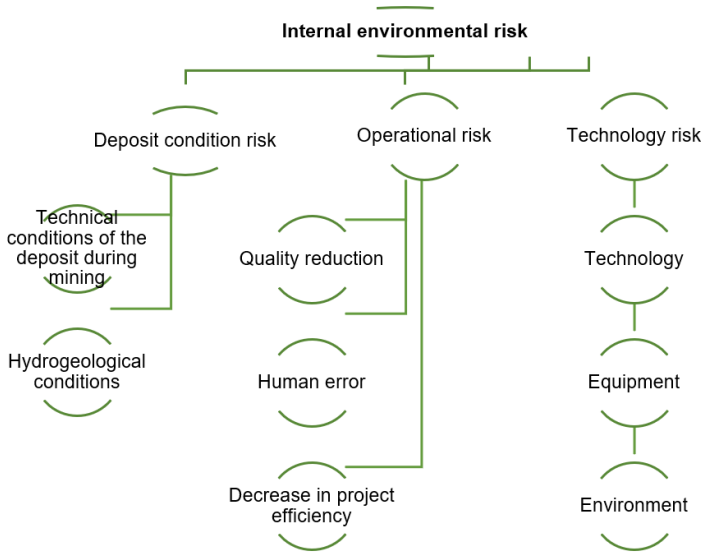

Figure 3. Internal environmental risk

Researchers have identified that the risks associated with a mining project stem from a variety of complex factors. These include macroeconomics, consent rights, public relations, social license to operate, recession, investment, liquidity, resource access and substitutability, political instability, regulatory changes, compliance, operating costs, environmental risks, new regulations, and the loss of skilled professionals (Trevor Hart, 2019). Other risks encompass natural disasters, disease outbreaks, economic and political instability, changes in

government regulations, disease severity, financial risks, credit and liquidity issues, interest and currency rate fluctuations, shareholder risk, reputational risk or goodwill loss, corporate project delays, operational risks, strategic risks, business compliance risks, and human error (Pairote Pathranarakul, 2018). These risks are defined based on the specific hazards and threats identified by the researchers within their country's mining projects.

The risk of external factors is often very difficult to manage, and it can lead to capital loss due to high pressure and harm. The internal risk factor usually depends on the strategies and tactics adopted by the business entity in the course of business operations [9].

Risk Analysis model

When conducting risk analysis:

Using the qualitative method, experts assign 1-5 points based on the feasibility study and research data for each factor. This includes:

5 points for a threat that could immediately halt business operations,
4 points for a vulnerability threat,
3 points for a high-risk threat,
2 points for low risk,
1 point for a safe condition.

Additionally, 5 points are given for the ability to mitigate danger, and 1 point for the inability to do so.

Apply the following formula to calculate the risk level using the scores for hazard and capability.

$$R = \frac{H}{C} \quad (1)$$

where R- risk level; H- threat point, C- ability point. The corresponding calculated values of the risk level are shown in Table 1.

Table 1. Risk level

	Low risk	Medium risk	High risk	Very High risk
Evaluative dimension	0-1	1.1-2.5	2.6-3.5	3.6-5

Risk evaluate

Calculate the risk for each risk factor and display the results on the RADAR chart. Risk assessment is based on the following points.

Table 2. Basic rule of evaluate risk

	Prioritize implementation of risk mitigation measures and stop operations
	Plan and finance measures to control and reduce risk
	Plan risk mitigation measures and plan to implement them without disrupting day-to-day operations
	There is no need to take any action, but monitor and improve

Data and results

The feasibility study for a 5-year exploitation of the "Zeeg" limestone deposit in Bayanjargalan sum, Tuv Province, was utilized. The project requires an initial investment of 12.8 billion MNT. Over the project period, sales revenue is expected to reach 74.4 billion MNT, while production and operational costs are projected at 51.8 billion MNT. The net profit is estimated at 20.3 billion MNT, with the investment anticipated to be recovered within 2.7 years. It was concluded that the project could bring significant social and economic benefits to the company, the country, and the local community [10].

The risk analysis for the "Zeeg" limestone deposit project was conducted using 4 main and 20 sub-external environmental risk factors, as well as 3 main and 8 sub-internal environmental risk factors. According to the analysis, the risk level for natural disasters is 1.3, which falls under the medium-risk category. In contrast, the risk factors related to social and economic

conditions, resources, infrastructure, geological features, operations, and technology are all categorized as low risk (Fig 4., Table 3).

Table 3. External and Internal environmental risk level

№	Risk factors	Threat point	Ability point	Risk level
Deposit condition risk				
1	Technical conditions of the deposit during mining	2	3	**0.7**
2	Hydrogeological conditions	2	5	**0.4**
	Level			**0.7**
Operational risk				
1	Quality reduction	2	5	**0.4**
2	Human error	4	4	**1.0**
3	Decrease in project efficiency	3	4	**0.8**
	Level			**1**
Technology risk				
1	Technology	2	5	**0.4**
2	Equipment	3	5	**0.6**
3	Environment	2	4	**0.5**
	Level			**0.6**
Social and economic risk level				
1	Economic recession	1	5	**0.2**
2	Trade and industry	1	5	**0.2**
3	Population density	1	5	**0.2**
4	Commercial risk	1	4	**0.3**
5	Monetary risk	3	3	**1**
6	Political risk	4	4	**1**
7	Risk of corruption	3	3	**1**
	Level			**1**
Resource risk				
1	Natural resources	2	4	**0.5**
2	Land resources	2	3	**0.7**
3	Investment	3	4	**0.8**
	Level			**0.8**
Infrastructure risk				
1	Transport network	1	5	**0.2**
2	Energy supply	4	4	**1**
3	Water supply	1	5	**0.2**
	Level			**1**
Natural disaster				
1	Climate	3	4	**0.8**
2	Earthquake	4	3	**1.3**
3	Flood	3	3	**1.0**
4	Fire	2	3	**0.7**
5	Thunder	3	3	**1.0**
6	Storm	2	4	**0.5**
7	Biohazard	2	5	**0.4**
	Level			**1.3**

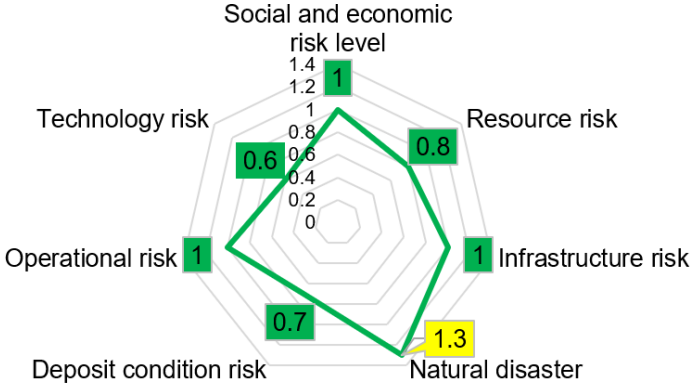

Figure 4. Project risk assessment results

Conclusion

There are no significant risks associated with social, economic, natural resource, or infrastructure factors in the execution of the Zeeg white limestone deposit project. However, the risk of natural disasters, particularly earthquakes, has been rated as "LOW." Based on the risk analysis of mountain geology, operations, and technology within the internal environment, operational risks are not expected during project execution.

A development plan for the deposit can be established using the low-risk earthquake assessment from the external environment, ensuring it reflects current conditions. Since the low-risk rating is within acceptable limits, the project does not require additional funding, capital, human resources, or special management. It can proceed fully as outlined in the feasibility study.

References

University of Finance and Economics, "The impact of foreign direct investment in the mining sector on the society and economy of Mongolia", Research report, 2024.

Debi Prasad Tripathy, Charan Kumar Ala, “Identification of safety hazards in Indian underground coal mines”, Journal of Sustainable Mining, Vol 17, Issue 4, 2018, Pages 175-183.

“Preliminary assessment of mineral resources, preliminary assessment of the feasibility of using mineral deposits, basic requirements for the technical and economic basis of the mining project and the procedure for receiving the technical and economic basis", Order No. 074 of the Ministry of Education and Culture dated 04.17.2012, https://mrpam.gov.mn/

Mendsaikhan T, “Personal royalty terms of the contract between the mineral license holder and the investor", 2024-03-30 https://legaldata.mn/b/2084.

A Study of Disputes Related to the Mineral Sector, https://legaldata.mn/b/1122.

Linlin Wang, Qinggui Cao, “Research on the influencing factors in coal mine production safety based on the combination of DEMATEL and ISM”, Safety Science,Vol103, March 2018, Pages 51-61.

Nandintsetseg Sosorbaram, Seungbum Ryoo, Chongsoo Cheung, “Risk analysis in mongolian centralregion coal mines”, International Journal of Police and Policing, 2020 5(2) 47-55.

Debi Prasad Tripathy, Charan Kumar Ala, “Identification of safety hazards in Indian underground coal mines”, Journal of Sustainable Mining, Vol 17, Issue 4, 2018, Pages 175-183.].

Ganzorig A, Bayansan P, Tsolmon S, Uuganbayar T, “Risk management”, ISBN 978-99978-2-547-6].

Graphite Pit Mining LLC, “Feasibility study of the open-pit exploitation of the white limestone deposit” 2023.

Mendsaikhan T, "Private royalty terms of the contract between the mineral license holder and the investor", 2024-03-30 https://legaldata.mn/b/2084

Borgil S, Munkhtogtokh B, "Evaluation of the regulation of corruption risk in the decision-making process of the Mongolian mining project" Natural Resource Governance Institute, 2023.06.

Badri A, Nadeau S, Gbodossou A, “A mining project is a field of risks: a systematic and preliminary portrait of mining risks” Int. J. of Safety and Security Eng., Vol. 2, No. 2 (2012) 145–166

Pengyuan LiQunyi LiuPing ZhouYing Li “Mapping global platinum supply chain and assessing potential supply risks, DOI: 10.3389/fenrg.2023.1033220.

ISO 31000:2018

STUDY ON THE TECHNOLOGY FOR SEPARATING COPPER-MOLYBDENUM-PYRITE CONCENTRATES

Namuungerel Baljinnyam*

Head of the Planning and Monitoring Department of the Production and Technical Department, Erdenet mining SOE, MONGOLIA

Abstract

Copper-porphyry ore is the primary source of raw materials for the global copper industry, with a significant portion of molybdenum often found alongside it. The main minerals in copper-molybdenum ores from copper-porphyry deposits include chalcocite (Cu_2S), covellite (CuS), chalcopyrite ($CuFeS_2$), bornite (Cu_5FeS_4), molybdenite (MoS_2), and pyrite (FeS_2).

Most copper-porphyry ore beneficiation plants use co-flotation to concentrate the valuable minerals, followed by a separation process based on standard technological layouts. The efficiency of this separation process significantly influences the technical and economic outcomes of copper-porphyry ore processing, particularly when separating copper-molybdenum-pyrite co-concentrate.

The separation method depends on the mineral composition of the co-concentrate, the reagent regime used during co-flotation, reagent costs, electricity consumption, environmental considerations, and the quality standards required for the final concentrate. Copper and molybdenum sulfides are separated by depressing pyrite with lime, followed by the sequential separation of copper and molybdenum concentrates to meet industry quality standards.

Keywords: Copper-porphyry, co-flotation, separation, depressants

Reagent regime for the separation process in copper-molybdenum concentrate technology.

Sulfide group reagents, such as sodium sulfide (Na_2S), sodium hydrosulfide (NaHS), ammonium sulfide ($(NH_4)_2S$), as well as Noakes-P_2S_5+NaOH and Noakes-arsenic (As_2O_3+Na_2S), are widely used in the separation of copper-molybdenum concentrates.

The consumption of sodium sulfide depends on the mineral composition of the concentrate and the co-flotation reagent regime, typically ranging from 9 to 20 kg per ton. To reduce sodium sulfide consumption, various techniques are employed, including concentrate thickening, heating or thermal treatment ("cooking") of the slurry, and the addition of cyanide during the cleaning process.

Over 30% of Mineral processing plants use Nox as a depressant, which is considered highly effective due to its ability to enhance wettability through phosphate and arsenate ions. Nox-arsenic is especially effective for separating concentrates with high grade secondary copper sulfide.

An efficient method to reduce the consumption of depressant reagents in co-concentrate separation is the use of nitrogen. When first implemented at the Caujon plant, this approach reduced the consumption of 'Anamol D' by 50%. 'Nitrogen' technology is particularly beneficial for separating concentrates rich in chalcopyrite, reducing depressant consumption by 30-80%.

The ferrocyanide method was first introduced at the Morenci plant, yielding high profits in separating concentrates containing secondary copper sulfides. For concentrates with a high chalcopyrite grade, ferrocyanide is added to enhance separation efficiency.

Erdenet Plant's Copper-Molybdenum Separation Technology

Phase 1 (1978-2000): This period used a "cooking" technology to process ores dominated by secondary copper minerals.

Phase 2 (Since 2000): A "non-cooking" technology has been employed to process ores dominated by primary copper minerals.

During Phase 1, ores from the secondary enrichment zone were processed using a technology developed by the Soviet Union's 'Mechanobr' Research and Design Institute in the mid-1970s. The process involved co-flotation to produce a copper-molybdenum-pyrite concentrate, which was then thickened and washed to remove excess reagents and slimes. The concentrate was 'cooked' in a lime environment with steam at 80-90°C for 1 to 1.5 hours to remove the collectors adsorbed on the sulfide minerals' surface. This allowed the material to proceed to the next stage.

In the molybdenum flotation process, large amounts of sodium sulfide were added to depress copper and pyrite. The foam product underwent 6-8 stages of cleaning to produce a concentrate containing 50% molybdenum. The depressed fraction was then subjected to copper flotation, where pyrite was suppressed with lime milk, and copper minerals were concentrated using 'butyl xanthogenate' collector reagents. This 'cooking' technology was used to process secondary sulfide ores (Fig. 2)."

Researchers at the Erdenet plant developed a new method to improve the copper-molybdenum concentration technology. According to studies implemented at the plant, when using the 'cooking' technology, issues arise when the content of primary copper sulfides exceeds 35%. In such cases, copper and molybdenum concentrate production becomes inefficient, the quality of the concentrate decreases, and separating copper from molybdenum becomes increasingly difficult. As a result, the molybdenum content in copper concentrates increased significantly beyond standard requirements, and molybdenum concentrate production nearly ceased (Fig. 1).

In collaboration with experts from the Russian Federation's 'Gintsvetmet' Institute, a new technology was developed in 2000. This technology replaced the hot steam cooking process with the use of high-efficiency selective collector reagents such as S-703G, BK-901B, and Beraflot-3026, which effectively target pyrite ores containing up to 50% primary copper (Fig. 3). This innovation allowed the plant to process ores with up to 50% primary copper sulfide, stabilizing production and enabling the production of concentrates containing up to 26% copper with a recovery rate of 84%.

While the use of these reagents is technologically effective, their consumption is high (15-30 kg/ton), accounting for 60% of the total reagent costs in ore processing.

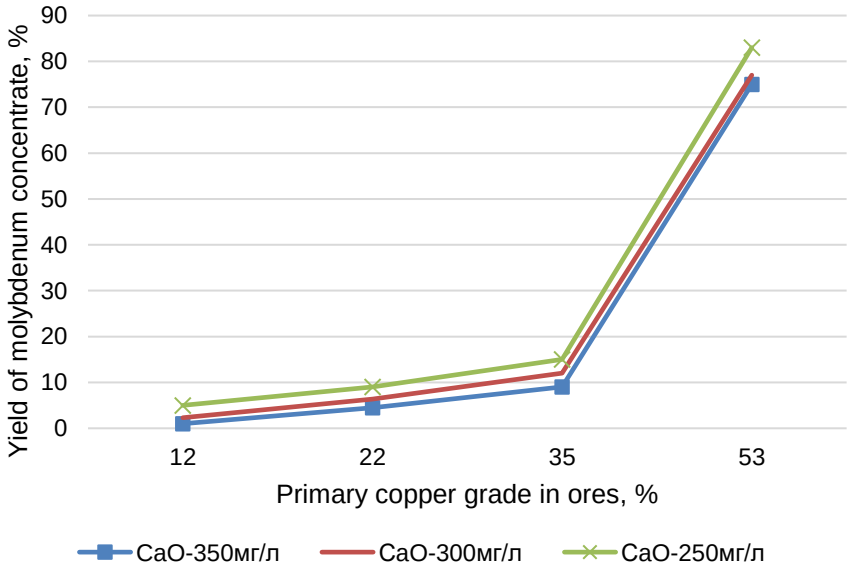

Figure 1. The effect of primary copper content in ore on molybdenum concentrate yield during the separation of concentrates using lime-based cooking technology

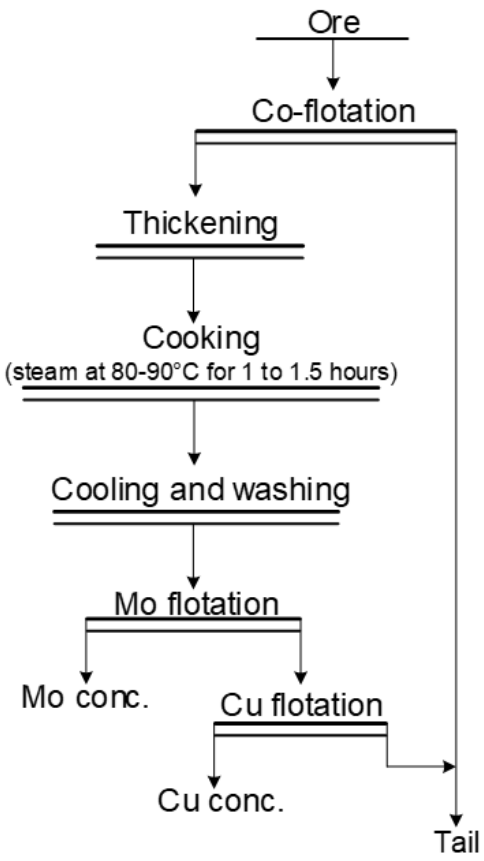

Figure 2. Diagram of the 'cooking' technology for secondary copper ore at the Erdenetin-Ovoo deposit

Efforts to reduce sodium sulfide and hydrosulfide consumption often lead to complications such as a more complex technological scheme, increased electricity usage, the need for specialized equipment, and worsened working conditions. Methods like ozone and electrochemical treatment are not used in production due to their high cost and low efficiency. Therefore, improving the efficiency of the copper-molybdenum concentrate separation process, stabilizing flotation operations, reducing reagent consumption and costs, and enhancing working conditions are critical concerns.

Additionally, stricter global regulations, particularly in countries like China, regarding the production, transportation, and export of toxic substances have raised the risk of supply interruptions and technological failures. Consequently, there is an urgent need to replace high-consumption, low-selectivity reagents with environmentally friendly alternatives.

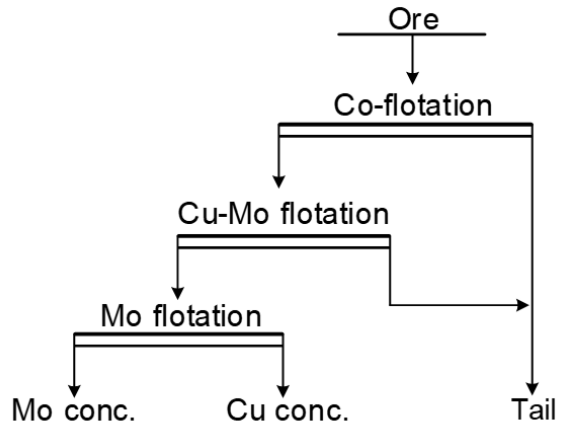

Figure 3. 'No-cooking' technology for primary copper ore at the Erdenetin-Ovoo deposit

Copper-molybdenum sulfide from copper-porphyry deposits
Recent trends in depressant technology for flotation applications

A promising approach in copper-molybdenum concentrate separation technology is the use of low molecular weight and organic polymeric depressants for copper sulfides and pyrite. Recently, there has been a significant increase in the use of organic depressant reagents in flotation to remove sulfides. This technology is being actively researched and developed in the United States, which processes over 60% of the world's copper-molybdenum ores. Despite extensive studies, the exact mechanisms of how these reagents interact remain unclear.

Organic depressants offer several advantages over inorganic ones. They are used in much smaller quantities—5 to 10 times less—are free from nitrogen, and do not require heating of the slurry. Additionally, they do not need prior desorption before application, are

biodegradable, and have minimal environmental impact. These benefits also contribute to improved occupational health.

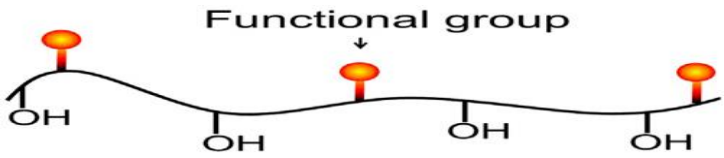

Figure 4. General Structure of an Organic Polymer Depressant

Current Status of Organic Depressants Research

1. Chitosan Polymer Depressant: Experiments on the selective depressant of copper sulfide minerals using Chitosan polymer (Figure 5) in the copper-molybdenum ore from the Jiama deposit have demonstrated its potential as a substitute for sodium sulfide, a traditional depressant. Chitosan is advantageous due to its low consumption rate and non-toxic properties (Figure 6).

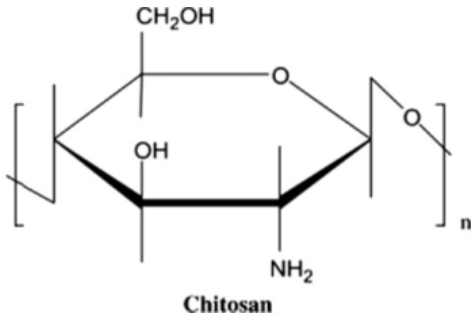

Figure 5. Structure of Shitosan

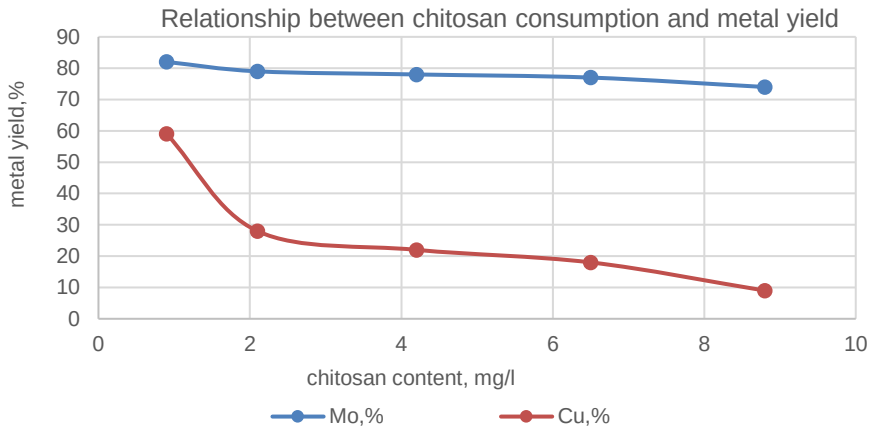

Figure 6. Relationship between chitosan consumption and metal yield

2. Tannins (Polyphenols): Extracted from the quebracho tree, tannins are used to depress pyrite with organic reagents, enhancing the quality of copper concentrate. Experiments on copper porphyry ore samples from Argentina, Chile, and Peru revealed that at pH levels between 9.5 and 10.5, pyrite recovery decreased and copper quality in the concentrate improved (Figure 7). These findings suggest that tannins could serve as an effective, non-toxic alternative to traditional pyrite suppressors in sulfide flotation.

3. MFTC: The implementation of MFTC technology for separating copper-molybdenum-pyrite concentrates at PO 'Balkhashmed' led to a 2-3% increase in copper production, a 5-8% reduction in molybdenum loss, and a 30-50% decrease in sodium sulfide consumption. Additionally, the elimination of steam heating improved sanitation and hygiene conditions.

4. Aero 8371 PRN Polymer Depressant: When introduced at the Wunugetu copper and molybdenum ore concentration plant of Inner Mongolia, Aero 8371 PRN reduced sodium

hydrosulfide consumption by 45%, enhanced the efficiency of the copper-molybdenum separation process, and improved environmental and workplace hygiene.

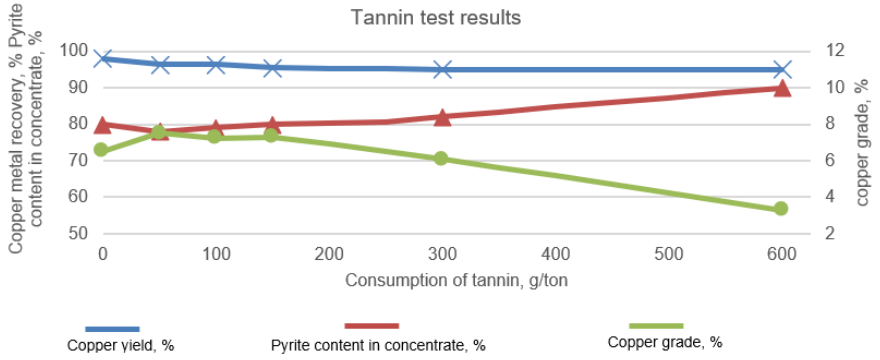

Figure 7. Tannin test results

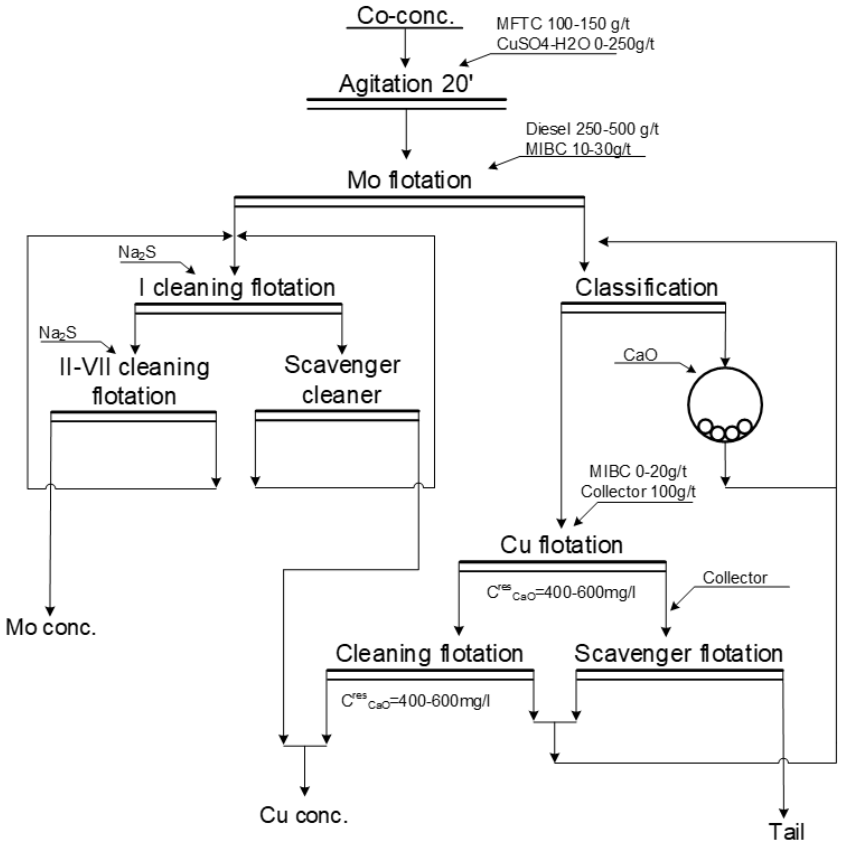

Figure 8. Developed technology scheme and reagent mode

5. Aero 7260HFP Polymer Depressant: At Codelco Chuquicamata, the use of Aero 7260HFP in copper-molybdenum separation flotation reduced sodium hydrosulfide consumption by 35% and decreased H_2S gas emissions. This reagent was subsequently tested and implemented at the Teghout and Kadjaran plants in 2017-2018.

Research on Organic Depressants for Copper-Molybdenum Ore at the Erdenet Ovo Deposit

Separation Technology Using MFTC Reagent: A reagent scheme and technological process for using MFTC depressant in co-concentrate separation were developed (Fig. 8). Experiments demonstrated that this technology could reduce annual sodium sulfide consumption by 5,000 tons and increase molybdenum metal recovery by 4-5%. However, it was found that while MFTC adsorption on chalcopyrite increased with higher usage, it was

less effective compared to adsorption on chalcocite and covellite (Fig. 9). Consequently, this technology may be less effective under conditions of increased primary copper content.

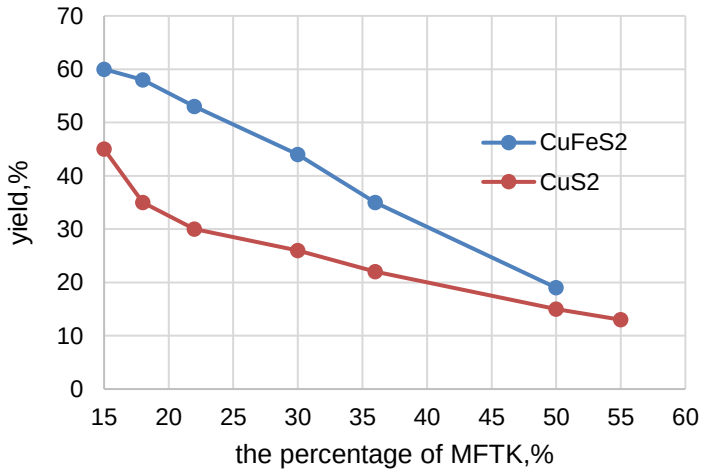

Figure 9. Effect of MFTC Consumption on the Flotation performance of Copper Sulfide Minerals

Technological Study of Cytec's Sulfide Depressant Reagent AERO-7260 in the Copper-Molybdenum Separation Process: In collaboration with Cytec specialists, experimental research on the AERO-7260 reagent was conducted at both laboratory and industrial scales. It was found that the use of AERO-7260 can reduce sodium sulfide consumption by up to 26%, leading to its adoption in production starting in 2016. However, recent declines in the reagent's performance may be attributed to changes in ore characteristics and an increase in primary copper content (from an average of 60% in 2015 to 76% now).

Conclusion

Inorganic reagents (such as NaSH, Na2S, and Nokes) used to depress copper minerals in Cu-Mo co-concentrates are costly, have unpleasant odors, and negatively impact occupational health and the environment by emitting toxic H_2S gas. Additionally, the high transportation requirements contribute to supply disruptions. Therefore, there is a need to replace these with alternatives that are more cost-effective, environmentally friendly, and healthier for occupational safety.

The use of organic depressant reagents for copper sulfide and pyrite shows promise as a more effective separation method.

Further research is needed to find organic depressants with selective action on pyrite and primary copper sulfide minerals, with the goal of introducing these alternatives into production.

References

Technological Instruction of Mineral processing plant, Volume I, 1998.

Plaksa, N.E. "Combined Reagent and Selective Flotation of Copper-Molybdenum Concentrates" // Non-ferrous metals, 1972, No. 1.

Tuya, S. "Research on Improvement of Copper Porphyry Ore Flotation Technology Considering Changes in Mineral Composition and Increasing Molybdenum Extraction" / Doctoral Thesis /.

Gezegt, Sh. "Research on the Use of Gaseous Nitrogen in Molybdenum Flotation" // Mountain Journal of Mongolia, 2003, No. 3.

"A Review of Recent Advances in Depression Techniques for Flotation Separation of Cu-Mo Sulfides in Porphyry Copper Deposits." Metals - Open Access Metallurgy Journal, October 2020.

A Literature survey on synthetic polymeric reagents used in sulfide mineral flotation https://www.researchgate.net/publication

Sarquís, P.E., Menendez-Aguado, J.M., Mahamud, M.M., Dzioba, R. "Tannins: Organic Depressants as Alternatives in Selective Flotation of Sulfides." Journal of Cleaner Production, 84 (2014).

Khersonsky, M.I. "Main Directions in the Development and Use of Flotation Reagents for Sulfide Ores of Ferrous Metals." In New Frontiers in Ferrous Metallurgy, Moscow.

Heroic, J. "Scientific Basis and Development of Effective Technology for Flotation of Copper-Porphyry Ores Based on the Study of Genetic and Morphological Features." Dissertation, Ph.D.

Karnaukhov, S.N. "Research and Development of Technologies for Processing Copper-Molybdenum Ores at 'Erdenet' Using Selective Collectors and Organic Depressants to Increase Molybdenum Extraction." Autoreferat k.t.n., Moscow, 2007.

Desyatov, A.M., Shcherbakov, V.A., Khersonskyi, N.I., Gorodetskaya, L.A. "Separation of Copper-Molybdenum-Pyrite Concentrates with MFTK-E Depressant." Non-ferrous metals, 1988, No. 4

RESULTS OF TERRESTRIAL LASER SCANNING FOR CROSS PENETRATION LENGTHS AND VOLUMES IN UNDERGROUND MINING

Erdenechimeg Purevjav[1]*, Khosbayar Orosoo[2]

[1] School of Geology and Mining Engineering, MUST, Ulaanbaatar 14191, MONGOLIA
[2] Geosurvey Co Ltd, Ulaanbaatar 14191, MONGOLIA
*Corresponding author: Erdenechimeg.geo@must.edu.mn

In this paper, the traditional measurement methods and GPS/GNSS technologies used for large-scale infrastructure projects and continuous linear objects in tunnels often present challenges in terms of manpower, time consumption, and do not meet the required precision in imagery. Terrestrial laser scanning technology, with its speed, accuracy, and convenience, has become a modern and suitable method for tasks such as underground construction in mining, including tunnels.

The purpose of the measurements was to verify whether the excavation work and tunneling at the Oyu Tolgoi project were progressing according to the planned alignment, total length, and volume.

Additionally, the accuracy of the selected underground geodetic network points was checked, and the durability of these points was evaluated during blasting and operational activities.

During the control measurements at these points, the angle guidance method was used with a Trimble level 1 accuracy electronic total station tachometer, and the data was processed using the Compass/Bowditch method which achieving a 94% accuracy rate in the required points.

Based on these points, the length and volume of the excavation were determined using terrestrial laser scanners (TLS), namely the Trimble X7 and Trimble SX12.

The discrepancy between the fieldwork measurements and the actual values measured using a laser scanner was calculated by means of a comparison method.

In recent years, laser scanning technology has rapidly gained applications in numerous engineering fields, such as cross-sectional and volumetric calculations, deformation monitoring of structures and infrastructures, mining, road and bridge monitoring, as well as archaeological and historical artifact studies. Its high precision, speed, and capability to generate highly detailed 3D spatial representations of various objects make it an effective tool for these purposes.

Keywords: laser scanning; comparison area; mining tunnel monitoring; overbreak volume

VOLTAGE FLUCTUATIONS IN THE MINING POWER SUPPLY SYSTEM

Binderiya Taivan*, Ariunbolor Purvee

Department of Mineral Processing And Engineering, School of Geology and Mining Engineering, Mongolian University of Science and Technology, Ulaanbaatar 14191, MONGOLIA
*Corresponding author: binderya@must.edu.mn,

Abstract

The power consumption of a unit of mining industry, the reliability of power supply, the continuous operation of industrial technological processes, and the normal operation of the power supply system are highly dependent on the quality of power. Correlation and interaction between the normal reliable operation of electrical equipment and the parameters of the power supply system is evaluated by power quality parameters called electromagnetic compatibility.

Due to the increasingly complex nature of modern industrial technological processes, the widespread introduction of adjustable valve devices, high-power arc and induction furnaces, laser devices, welding devices, and the increased content of higher harmonics, the requirements for power quality are becoming higher. The problem of electromagnetic compatibility can be solved by establishing power quality indicators and maintaining them at standard levels.

This article describes how changes in the main parameters of the electrical circuit, such as current, voltage, power, and frequency, affect the operation of consumers working in the power supply system, creating distortions, and the possibility of correcting the resulting distortions. In the power supply system, the consumption of electricity continuously changes by hours, minutes, days, and seasons, and the prevailing load characteristics and the amount of current at that moment are random processes. Following this state of the load, the voltage on the node of the power supply changes and fluctuates in a certain way, and the dependence of this voltage fluctuation on the time was studied. Internal and external factors affect the voltage fluctuations. Industrial power quality issues are part of the infrastructure of the power supply system. Having quality control equipment in the shop helps to reduce economic losses while increasing the quality of work, maintenance and equipment life.

Keywords: power quality, electromagnetic compatibility, voltage fluctuation, flicker

Power quality indicators in power supply system

The power consumption of a unit of mining industry, the reliability of power supply, the continuous operation of industrial technological processes, and the normal operation of the power supply system are highly dependent on the quality of power.

According to domestic and foreign standards, the quality of electricity includes the following indicators. It includes following indicators. Harmonics, Voltage swells, sags, Frequency, Flicker, Transient voltages, Implement voltage regulation, Unbalanced voltage, Voltage interruption, Power factor, Reactive power analysis

Determination of voltage fluctuations in the mining power supply system

The results of 24-hour measurement (summer time measurement) of the voltage variation on the generator of the power supply system of the open pit mine, divided by meter scale into 3 tariffs, and at which time of the day the voltage fluctuation occurs the most. Several parameters were measured in the power supply system of Erdenet ore open pit mine.

Voltage fluctuation is a continuous change in the voltage when devices or appliances that require a higher load are extensively used. Therefore, it can be seen from the above pictures that all machinery with high-power electric motors work in mining operations, and voltage changes and fluctuations are inevitable in the mining power supply system. As can be seen

from the figures the change in voltage does not reach 10%, but it tends to decrease between 6-17, 17-22, and increases between 22-06.

Reference

Iglesias et al, “Power Quality in European electricity supply networks”, 1st Edition, Euroelectric, Brussels, 2002.

Binderya.T Investigating power quality assessment of mining power supply systems. Proceedings of the 49th conference of professors and teachers of GUUS. 191p. 2021.

Ariunbolor P, Purevdash D, "Dynamic Modeling for Power Quality Determination". Proceedings of Science and Technology University 2/232, 2019, Ulaanbaatar, Mongolia, Pages: 185-1941. ISSN 1560-8794

RESEARCH ON INCREASING THE LEVEL OF COAL PROCESSING AND REDUCING THE COST OF PRODUCTS

Batzorig Avarzed

Mongolian consulting engineer, PhD student
batzorigzor@gmail.com

Abstract

Currently, more than 90% of Mongolia’s electricity and heat production is produced using coal.

Domestic consumption of coal is increasing every year and will reach 13.2 million tons in 2023, and the main consumers are Thermal Power Stations, Enterprises and Households in the central region. Although the economy cannot exist without coal, on the other hand, the use and consumption of coal is not only a source of environmental pollution but also a flammable mineral that causes many negative effects on human health.

The negative effects of coal are divided into four categories: mining, coal enrichment, transportation and burning process. When coal is burned ash, slag, smoke, sulfur and nitrogen oxides, carbon monoxide and dioxide, greenhouse effect, particles and harmful rare elements Cr, As, Pb, Cd, Hg are produced and polluted.

In Mongolia, it is important to increase the processing level of mining products by producing briquettes from coal and supplying users.

In our country “ Tavan Tolgoi Tulsh” LLC has started operating in this field, but the financial capabilities and benefits are not enough for the economy. It is research to improve the benefits of briquettes production and reduce costs based on technological optimization.

Through this research work, the advantages and disadvantages of the use of new types of binders and the reduction of sulfur dioxide released into the air during the burning of improved briquettes determined by analysis.

Keywords: Coal Sulfur Dioxide, Binders, Drying, Productivity, Cost Reduction

Introduction

Coal accounts for 24 percent of the world’s Energy consumption, which is the same as oil about 38 percent of the total electricity production is based on Coal. Coal is a cheap and abundant raw materials compared to oil and natural gas, so its demand is increasing year by year.

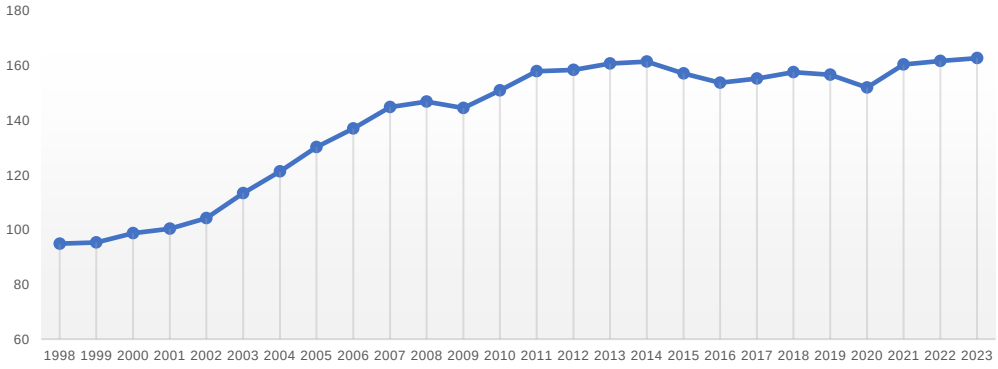

Graph 1. Growth of Coal consumption countries around the world /exajoules/

The global economy cannot exist without coal, but on the other hand, coal consumption is still one of the main sources of environmental pollution.

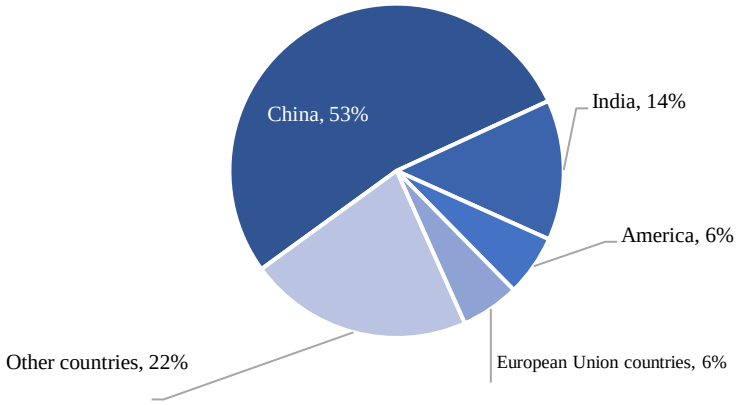

Graph 2. Share of Coal consumption

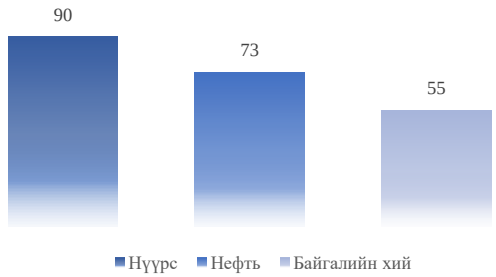

Graph 3. The amount of Carbon emitted to produce 1gj of heat (кg)

From an ecological point of view, coal is the most polluting burning mineral. In recent years, the population of Ulaanbaatar has increased due to the increase in concentration and the consumption of raw coal, air pollution has increased, which affects not only the environment but also the economic and social development of the country, human habitat and health.

Burning coal is the most polluting process compared to other stages of use.

According to the International experience of solving air pollution, it has been decided to replace the use of raw coal with improved briquettes, coal gasification and natural gas.

The United States Environmental Protection Agency lists 189 substances and elements as air pollutions, of which 16 are found in coal. F, Mn, P, Be, Cl, Cr, Co, Ni, As, Se, Cd, Sb, Hg, Pb, U, Th.

Nitrogen (H_2SO_4) and Sulfur Oxides (HNO_3) from coal burning are readily oxidized to higher oxides, which react with water vapor and form very small droplets of nitric acid. When it falls as acid rain, it causes significant damage to plants, animals, soil, water, buildings, architecture and cultural heritage.

The average Sulfur content of improved briquettes is 0.85% and the average Sulfur content of Energy enriched coal or transitional is 0.9 %. The average sulfur content of Baganuur primary coal is 0.35 %, which is 2.4 times higher than that of transitional products. Depending on this, the amount of sulfur gas released into the air from burning increases and there is a need to reduce it.

Since 1978, in the USA there has been a requirement to install flue gas desulphurization devices or Scrubbers in Power Stations. A Scrubber is placed in the smoke path between the boiler and the chimney of the Power Station. The principle of Scrubber is to convert SO2 into CaSO4 or gypsum by spraying alkaline materials such as lime, limestone…ets, dry or as a paste in the opposite direction of the smoke flow. Dolomite was chosen to absorb sulfur to neutralize the sulfurous gases produced by fuel burning. Theoretically, it takes 100 grams of limestone or $CaCO_3$ to absorb 1 mole or 32 grams of sulfur, resulting in about 80 % neutralization of the gas. [1]

$$(SO_2 + CaCO_3 + 0.5O_2 = CaSO_4 + CO_2) \quad (1)$$

Burning of fuel made of sequestrants with sulfur neutralization additives reduces sulfur gas emissions by 20-50% compared to current fuel.

It has been found that briquettes made from dolomite and hydrated lime binders can dry out quickly.

Due to the alkaline nature of the binders made of hydrated lime, there is a negative aspect of the need to pay special attention to Labor protection conditions during use.

Research Methodology

Research rationale

China is one of the largest players in the manufacturing market and continuous to be the world's largest consumer of coal in terms of manufacturing.

As the world moves towards green Energy and green economy, leading international banks and financial institutions have announced that they will not invest in coal -fired Power and Thermal Stations.

As for Mongolia, the total registered coal reserves are 34.6 million tons as of 2023, which is 3.2 percent of the world's reserves and it has 304 special licenses for exploitation.

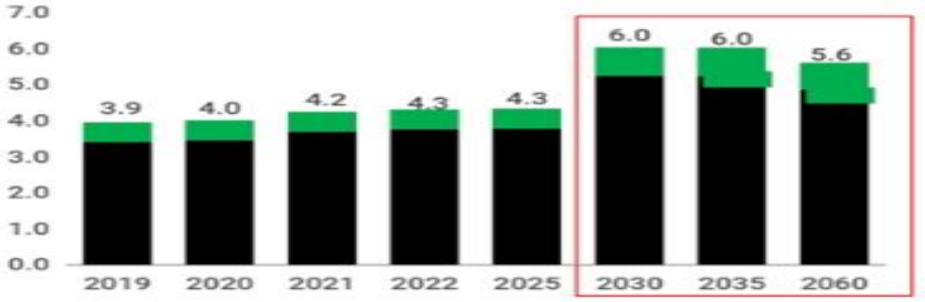

Graph 4. Chine's coal consumption (billion tons) energy coal and coking coal
Source: Sinopec

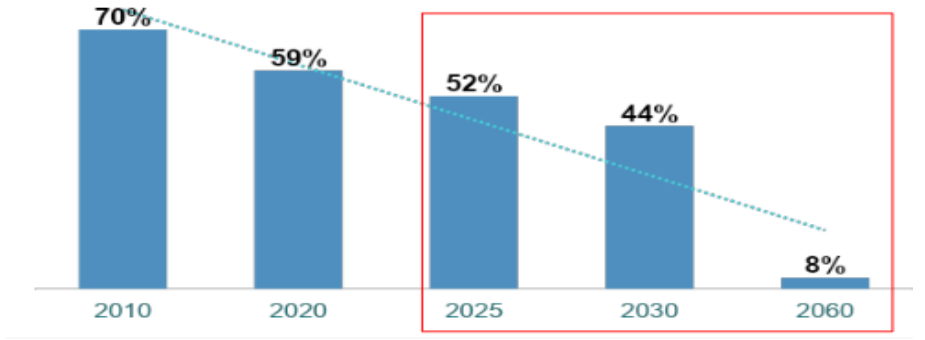

Graph 5. Share of coal in China's Energy production.
Source: CNPC

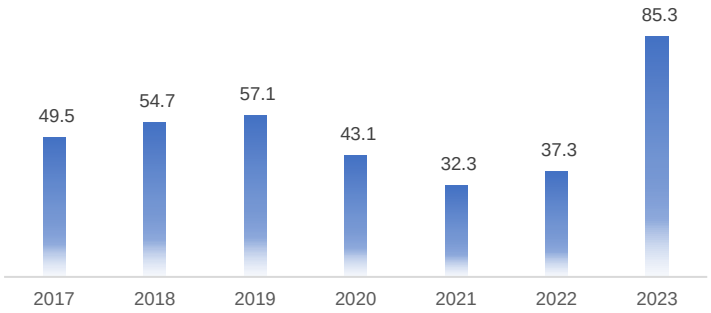

Graph 6. Coal mining in Mongolia (million.ton)

About 80% of mined coal is exported and the remaining 20% is domestic coal consumption.

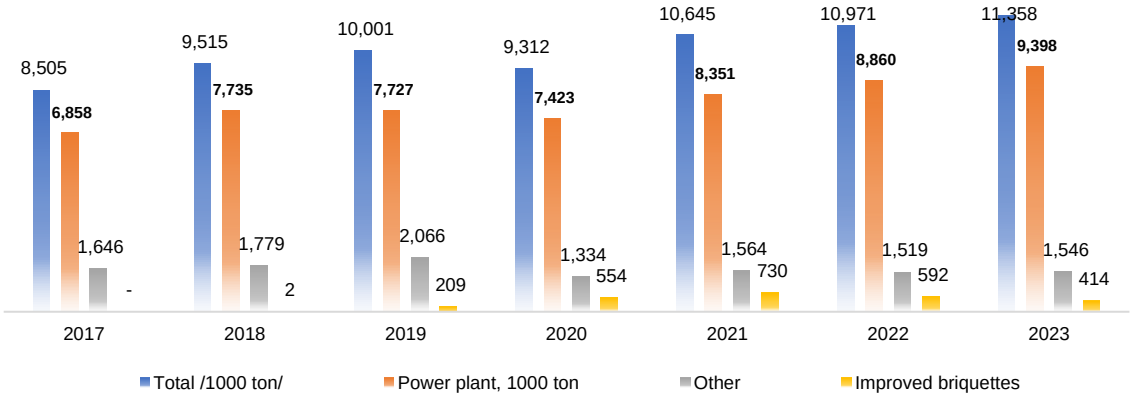

Graph 7. Mongolia's domestic Coal Consumption, (thousand.ton)

Domestic coal consumption has been steadily increasing by 1 million tons annually in recent years, 81% of which is Thermal Power Station, 14 % of households and industries and briquettes have been introduced since 2019 , accounting for 5 percent of Mongolia's coal consumption.

Most of the coal used by households in the ger neighborhood of Ulaanbaatar city was Baganur lignite with high humidity and low warmth and by replacing it with improved briquettes of Tavan Tolgoi coal enrichment, the amount of coal humidity , volatile , substances was reduced by 2 times increased, it was possible to reduce air pollution in the capital city by 50 percent .

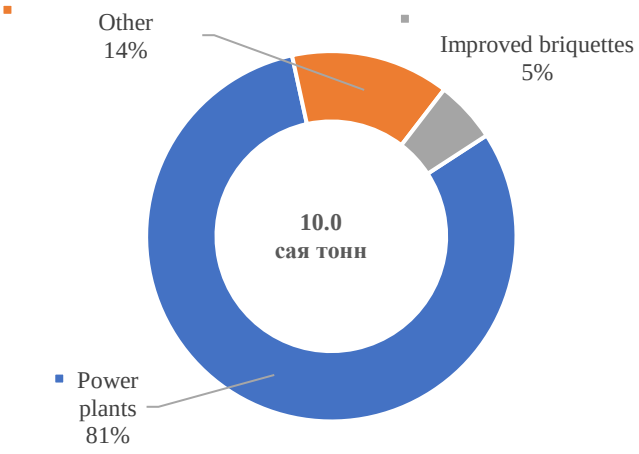

Graph 8. Position of domestic coal consumption

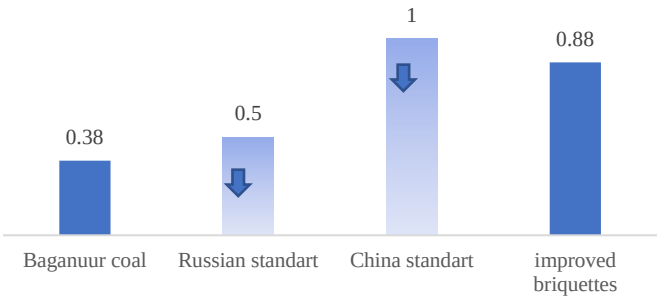

Graph 9. Comparison of percentage of sulfur in coal.

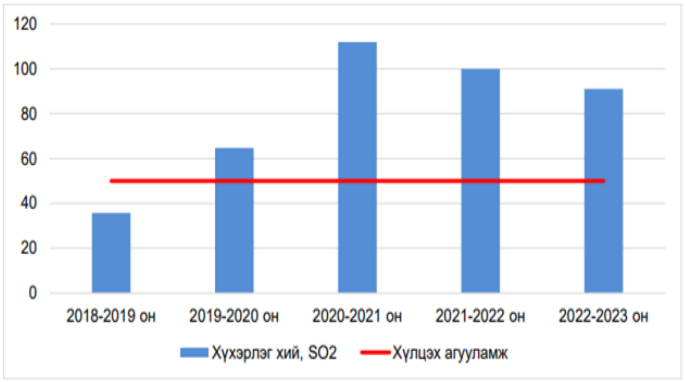

Graph 10. Average content of sulfurous gases in the cold season,2018-2023 (SO_2) мкг/м^3

Although the introduction of compressed fuel improved air quality parameters, the content of sulfur gases released from burning didn't decrease, due to the fact that the amount of sulfur contained in the raw materials or transitional products of the concentrator was 2.5 times higher than that of raw coal.

Since 2019, measures have been taken to reduce the content of sulfurous gases and reduce and neutralize sulfurous gases from burning..

Research Methodology.

In order to reduce the amount of sulfur emitted from the burning of compressed fuel, the neutralization of sulfurous gases is shown in the table below.

Chart 1. The amount of sulfur released from the burning of briquettes.

№	Coal fuel	Total particles (TSP)	Sulfurous gas (SO_2)
		мг/м^3	мг/м^3
1.	Fuel made by Middling	188	808
2.	Fuel with hydrated lime content	117	494
3.	Fuel with Dolomite content	101	289

By using domestic binders containing dolomite:

When burning a fuel made of binders with sulfur neutralization ingredients, sulfur gas emissions are reduced by 40-50 percent compared to the currently used fuel.

It was observed that the fuel made of dolomite and hydrated lime binders can dry quickly.

As the retaining material made of hydrated lime is alkaline, there is a negative aspect of the need to pay special attention to Labor protection conditions during use.

The cost of production was reduced by 30000 MNT per ton.

Analysis of strengths and weaknesses

The SWOT analysis of dolomite binders is shown in the following table.

Chart 2. SWOT analysis

S- Advantages Cheaper than import binders

Reducing the drying process time for the production of binders with dolomite ingredients;
It has an important role in reducing air pollution as it neutralizes sulfur gases released from fuel burning.

W- Weaknesses
Increase the amount of fuel ash;
Import dependence is still 10 percent.

O-Opportunities
Dolomite is a commonly available mineral, and there are many companies that mine it;
This will reduce dependency on binders' imports by 90 percent, while reducing associated transportation, customs and other costs;
Support national binders' production.

T- Threats
Since the import of binders is 10 %, a fall in the exchange rate will increase the price of binders.

After analyzing the advantages and disadvantages, we investigated the possibility of increasing efficiency and reducing losses by using the property that accelerates the drying of fuel.

Computing technology

Briquettes production technology is produced in 2 type: steam and smoke injection and consists of crushing, mixing, molding, and drying. The capacity of the factory is calculated by the capacity of the drying line. Today when entering the drying process, briquettes dry to 2% with 26% humidity, which is 3 times less than the standard.

The theoretical basis for the reduction of fuel drying time is that Carbon dioxide (heat carrier smoke) reacts with moist limestone to form Calcium bicarbonate. In other words, during the drying process, fuel humidity is converted to carbonate, which accelerates fuel drying.

$$CaCO_3+H_2O+CO_2 = Ca(HCO_3)_2 \quad (2)$$

According to Chinese standards, the minimum humidity of briquettes is 8 %.

Group 1 <=8.0
Group 2 >8.0~10.0
Group 3 >10.0~12.0

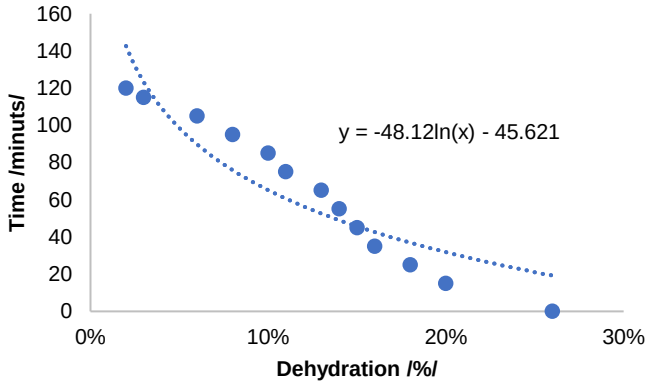

Graph 11. Fuel drying time dependence

According to the cost comparison, if the humidity is increased by 1 percent, the production per day of fuel is 5 percent.

Chart 4. Productivity as a function of humidity.

Cost comparison:

Drying time /minute/	*Percentage of humidity*	*Ratio or increase in productivity compared to the previous time*
56.41	*12%*	*2.13*
60.59	*11%*	*1.98*
65.18	*10%*	*1.84*
70.25	*9%*	*1.71*
75.92	*8%*	*1.58*
82.34	*7%*	*1.46*
89.76	*6%*	*1.34*
98.53	*5%*	*1.22*

Conclusion

The global economy and modern development cannot exist without coal and it is clear that the use of coal will increase in the near future. Therefore, there is a need to develop all processes of coal mining, transportation, use and consumption in an environmentally friendly manner.

A cost reduction study was conducted by studying the advantages of technological quality parameters and reactions by using new types of materials to reduce and neutralize the negative effects of coal during use.

The use of dolomite binders reduces the amount of sulfur gases released from burning by 50%. It is believed that when the humidity is up to 12%, it will not affect the fuel quality. (strength, viscosities.). In other words, excessive heating has occurred.

Therefore, the dependence of the time spent in the drying oven on the mechanical reduction of humidity has been determined and the basis for cost reduction has been derived as a result of the increase in productivity during operation at a reasonable level.

Reference

Dr (Sc.D) J.Narangerel “Fundamentals of Coal Chemistry” 2021

Byamba-Oyu J., Tsedendorj ., “Base and Methodology of the Mining Iindustry Project” UB: 2007

National Statistics Committee Social and Economic Presentation of Mongolia. 2019-2023 “Tavan Tolgoi “ Fuel Joint Stock Company semi- coke fuel report, 2023

Classification and quality requirements of semi-coke GD/T 25211-2023, China

On the result of the introduction of binders with dolomite in the production of improved briquettes, Ministry of Energy. 2023

№10. Academic Council of the Institute of Chemistry and Chemical Technology.

www.mmhi.gov.mn

https://www.statista.com/statistics/265507/global-coal-consumption-in-oil-equivalent/

www.iqair.com

https://www.acanmachine.com/coal-briquetting-history

DIESEL FUEL CONSUMPTION AND IMPACT ON AIR POLLUTION

Alimaa Vanganjal*, Binderiya Taivan

School of Geology and Mining of Geology and Mining, Mongolian University of Science and Technology, MONGOLIA

*Corresponding author: alimaav@must.edu.mn

Abstract

The emissions from diesel engines in dump trucks and hydraulic excavators used in mines are directly influenced by the type and quality of fuel utilized, often failing to meet international emission standards. Introducing the Euro5 fuel standard in Mongolia is poised to mitigate environmental and air pollution. In alignment with international environmental mandates and our commitment to safeguarding the Earth, this article was drafted.

This study centers on the examination of Cummins diesel engines, a globally employed engine manufactured in the United States, specifically focusing on their utilization in Mongolia.

Recently, dump trucks with diesel engines with EGR systems have been introduced and used in the Mongolian mining industry. Most modern vehicles have an EGR valve built into their engine, a device designed to reduce emissions of air pollutants sulfur oxides and nitrogen oxides.

According to international standards, Euro5 standard fuel with 10 ppm should be used for engines with EGR, but in our country, ordinary and Euro 2 ans Euro 3 standard fuel is usually used in the mining sector.

For our country, the diesel fuel standard was updated in 2017 to MNS0216-2017. Diesel fuel Euro (technical conditions), in 2020 MNS 6861:2020 Diesel fuel (technical requirements), MNS 6859:2020 Heavy fraction diesel fuel (technical requirements) standards are approved.

According to Summins Mongolia, a distributor of machinery with internal combustion diesel engines (result of analysis), the amount of sulfur in the air pollutant waste gas emitted during the use of Euro-2 and Euro 3 diesel fuel used throughout Mongolia is approximately 2000-3544 mg/kg (ppm-rarts per million)

In Mongolia, MNS 0216-2017 Diesel Fuel Technical Requirements standard is implemented. According to the above standard MNS 0216-2017, the exhaust gas sulfur content of Euro-5 diesel fuel is 10ppm. However, depending on the quality of the fuel used in our country, the amount of air polluting sulfur is approximately 3544 mg/kg. In other words, it can be seen that the amount of sulfur in air polluting waste gas is 10 ppm or 10 mg/kg, but it is 350 times higher depending on the quality of the fuel used.

Also, one of the main factors affecting the load on the diesel engine is the quality of the fuel, which also affects the reliable operation of the engine.

As you can see, the change in diesel consumption is inevitable, but if it slows down, it will still affect the environment (ozone layer), human health (air pollution, smog), and even mine operations (maintenance systems). The higher the sulfur content, the greater the corrosion of the metal parts of the engine and equipment, the formation of deposits, and the reliable operation of the engine.

Keywords: diesel fuel, air pollution, waste gas, Euro-2, Euro-5

THE REPUTATION OF THE MINING INDUSTRY IN TO THE MONGOLIAN PUBLIC AND THE NEED TO CHANGE PERCEPTIONS

Enkhbat Avirmed

The School of Business Administration and Humanities, Ulaanbaatar 13381, Mongolia

Almost everyone agrees that Mongolia is a mining country whose economy is highly dependent on mining. But it is very interesting that not everyone likes to admit this fact. However, there is no need to further prove this with facts and researches. Today, the main theme of our country's art and literature is about the protection of our land, mountains, and natural resources from foreign mining investors. We come across films, dramas, comics, songs, poems, and literature with such themes almost every day, and our children are growing up in such an environment.

Another problem parallel to this is the "naive perception" of mining in our society. This will be further stimulated by the new generation of film industry in our country. Rumors and gossip spread by word of mouth in urban and rural areas are also responsible. The idea that mining is the only real industry that fulfills the desire to get rich quickly and get a lot of wealth easily is where the "illusion" about mining is created among the public. The belief that “Mining is when you pick up rocks and find solid gold, or shovel coal and sell it across the Chinese border which earns a lot of money in a short period of time” is deeply rooted in our society. In some ways, artists and cultural stars such as singers and wrestlers being sponsored by our mining companies reinforces the above illusion even more.

Although the society doesn't like mining, it has come to see it as an easy way to get rich, but it has created an "artificial fear" of mining. You and I come across a lot of opinions in the online environment that gold is the main cause of landslides and earthquakes, two-headed calves are born due to uranium, mining will exhaust the underground water resources which means there will be no water in the future, and if there is no water, what will we do with only gold?

Hatred of mining, naïve perceptions, illusions, and artificial fears about mining show the need to deliver proper, truthful, and open information about mining to Mongolian society. How

and how to deliver?, Do we have such experience? According to the past history, yes, we have the experience of getting the right understanding about mining as a society. There were also ways of delivery.

Until the beginning of the 20th century, Mongolia's economy was dominated only by traditional animal husbandry. From 1921, Mongolian party and government leaders set the goal of transforming the country from a livestock farming country into an agricultural and industrial country. In the framework of this goal, the work of using natural resources and developing mining has started.

First of all, the party and the government approached the Writers' Union to create songs, poems, and writings to make the public understand the geology and mining industry. As a result, he made artistic films with the meaning of influencing public opinion and made them popular. In 1961, the Mongolian Film Industry collaborated with East German artists to release the film "Altan Urgoo" to the public. Also, in 1962, the Mongolian Film Industry made the film "Tumnii neg" and showed the discovery of Mongolia's natural resources and the need for foreign aid and support in this matter. However, in 1981, the Mongolian Film Industry portrayed the development and production of the mining industry and the life of Mongolian mining engineers with the film "Gerlej Amjaagui Yvna".

These films not only gave the society a positive understanding of geology and mining, but also inspired young people to work in this field. However, today, not only has the policy and planning of this culture been lost, but the anti-idealism of our art industry is being propagated in the society with almost the income from mining.

geomine.must.edu.mn

geomine.must.edu.mn

geomine.must.edu.mn

GEO MINE 2024

BIANNUAL CONFERENCE ON GEOLOGY AND MINING

geomine.must.edu.mn

ISBN 978-991950681-0